DFT STUDY OF TITANIUM CUBANE AND MOLYBDENUM SULPHIDE COMPOUNDS
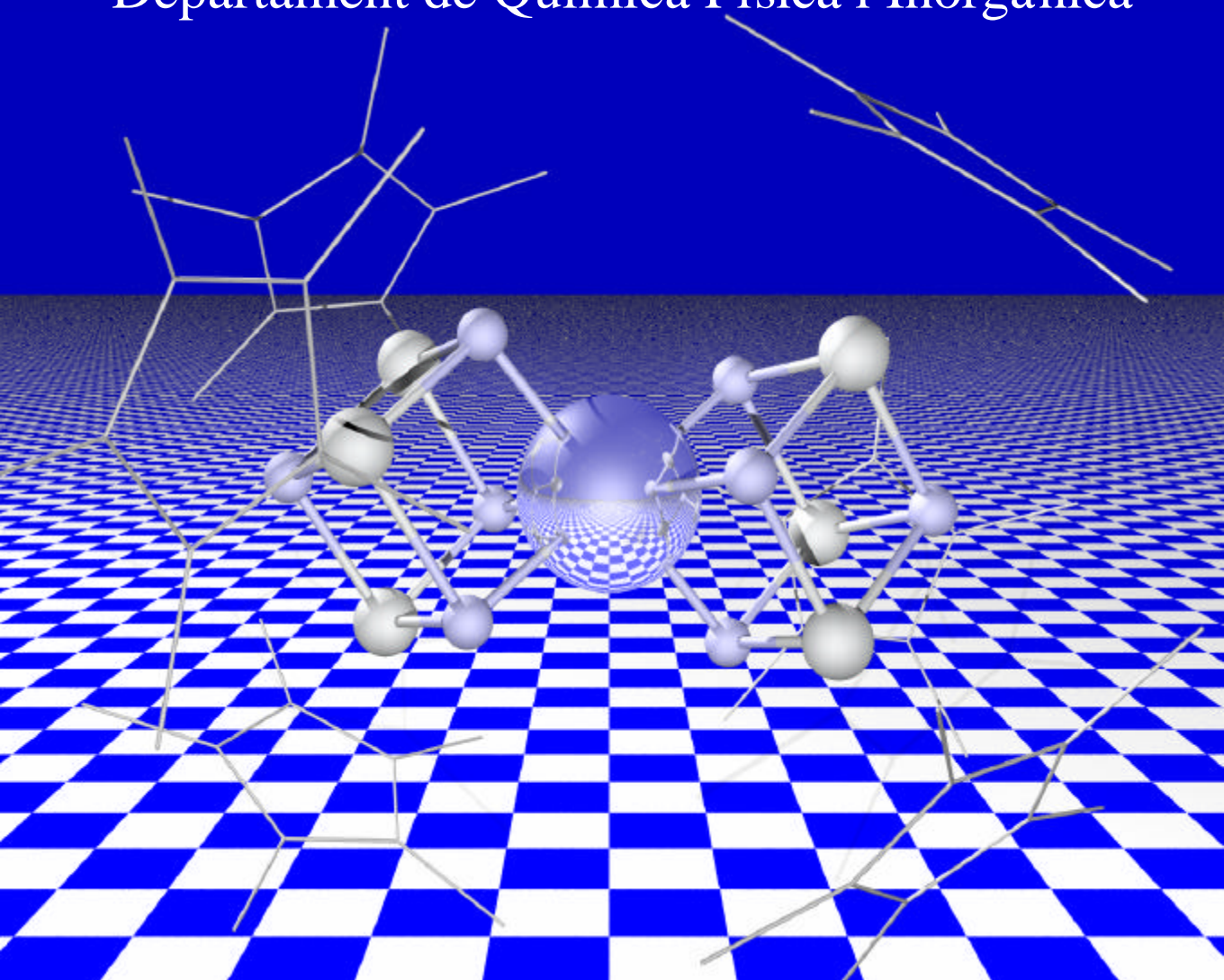
José Gracia Budría
Departament de Química Física i Inorgànica

DFT STUDY OF TITANIUM CUBANE AND MOLYBDENUM SULPHIDE COMPOUNDS

DEPARTAMENT DE QUIMICA FISICA I INORGANICA

José Gracia Budría

Memoria presentada para optar al título de
Doctor en Química

El Dr. Josep Maria Poblet Rius, catedrático de Química Física del departamento de Química Física i Inorgànica de la Universitat Rovira i Virgili; y el Dr. José Pedro Sarasa Solano, profesor titular de Química Física del Departamento de Química Física y Orgánica de la Universidad de Zaragoza

CERTIFICAN:

Que la presente Memoria titulada: "DFT Study of Titanium Cubane and Molybdenum Sulphide Compounds" ha sido realizada en el departamento de Química Física i Inorgànica de la Universitat Rovira i Virgili, por el licenciado en Ciencias Químicas D. José Gracia Budría, bajo nuestra dirección y autorizamos su presentación para obtener el grado de doctor.

Tarragona, 25 de marzo de 2004

Dr. Josep Maria Poblet Rius   Dr. José Pedro Sarasa Solano

DFT STUDY OF TITANIUM CUBANE AND MOLYBDENUM SULPHIDE COMPOUNDS

DEPARTAMENT DE QUIMICA FISICA I INORGANICA

José Gracia Budría

Tesis Doctoral. Tarragona, 2004

Quiero expresar mi agradecimiento:

A todos los miembros del departamento de Química Física i Inorgánica por mantener siempre sus puertas abiertas.

A Jose Ortiz y a Joan Iglesias por su dedicación, trabajo y consejos desde el servicio informático.

A Esther Bordas, Jesús Cabrero, Josep Maria Campanera, Daniel Curulla, Elias Daura, Isabel Gómez, Nuria Queralt, Susana Romo, Engelbert Sans y Ana Valcárcel como compañeros y amigos.

A Alfredo Gil y Xavier López que empezaron remando conmigo en este viaje y espero que los lleve a buen puerto.

A Francisco Ample, más que darle las gracias, forma parte de uno de los apartados que más interés me ha despertado, como colaborador y autor de las pequeñas partes de programación de esta tesis, y por compartir sus ideas y pensamientos durante todo este tiempo.

Al grupo de Química Inorgánica de la Universidad de Alcalá dirigido por el Dr. Mena y también en especial al Dr. Avelino Martín, como colaboradores en los análisis teóricos realizados y autores de todo el trabajo experimental en lo relacionado con los compuestos cubánicos de titanio.

Al catedrático Josep Maria Poblet codirector de esta tesis y una de las personas más razonables que he conocido.

Al Dr. Pedro Sarasa codirector de esta tesis, un ejemplo a seguir, al que ha sido desde antes de acabar la licenciatura mi profesor y amigo.

Por último a mi familia y amigos que siempre han formado y formarán la mitad de mi vida que se mantiene en contacto con el mundo real.

En especial a Raquel porque toda historia tiene dos partes, una que se ve y otra que se siente, y no hay nada más importante que poder sentir.

PRÓLOGO

El extraordinario desarrollo experimentado por la química computacional en las últimas décadas ha motivado un progresivo incremento en el número de estudios basados en un análisis teórico de los sistemas. El optimismo presente no es en vano, sino fruto una creciente experiencia y de la validación de los métodos empleados. A pesar del claro progreso y de las óptimas perspectivas futuras, no se debe olvidar la complejidad de los sistemas reales. En mi opinión, hay que tratar de evitar la sensación de que un estudio computacional ahorra tiempo y dinero a la ciencia.

La posibilidad de un estudio simultaneo y conjunto entre el trabajo experimental en el laboratorio y el análisis teórico es un triunfo presente para química computacional. No obstante, la especial complicación de muchos sistemas reales los hace todavía inabordables computacionalmente en su totalidad. Nos vemos obligados a trabajar con sistemas modelo que nos apartan en cierta medida de la realidad. Estos sistemas modelo pueden reproducir fielmente los sistemas reales, pero se pasa a estar a expensas de poder reproducir los valores experimentales para estar completamente seguro de que el sistema esta correctamente enmarcado.

Nuestro planteamiento para esta memoria implicó desde un principio un trabajo de colaboración conjunta con un grupo experimental, corroborando las suposiciones experimentales y siempre como apoyo a las posibles dudas o sombras que no se pudiesen aclarar fácilmente sin el necesario análisis teórico. En la estructuración de esta tesis se ha intentado presentar lo que ha sido nuestra forma de trabajar durante estos cuatro años, o lo que debería haber sido. La mayoría de los distintos apartados empiezan por un resumen de los datos experimentales de que disponíamos antes de empezar los cálculos; apoyándonos en estos datos, se modelizaban aquellos sistemas que más interés, o dudas, despertaban tanto a nivel experimental como teórico, para así completar su estudio.

Evidentemente la química teórica tiene la ventaja de poder proponer sistemas todavía no sintetizados, y ese podía ser uno de nuestros grandes objetivos, ir más allá de las personas que trabajan en el laboratorio. No obstante, ese no ha sido el objetivo de este trabajo. Prácticamente todos los resultados presentados aquí se basan en sistemas sintetizados, o no

observados, pero de los cuales su síntesis ha sido probada de forma infructuosa, e igualmente se puede estudiar el motivo. Evidentemente, esto supone que sabemos que nos estamos dejando muchos posibles compuestos por tratar.

El resultado del trabajo se presenta realmente fructífero. Por un lado se es capaz de reproducir los sistemas, obteniendo los datos experimentales y partir de ahí aportar otros nuevos. El aporte de información extra es evidentemente bidireccional y nos ayuda a conocer lo que podemos o no tratar. Como ejemplo diré nuestra grata sorpresa en la reproducción de espectros RMN, lo cual nos ha llevado a intentar abrir nuevas vías de trabajo en este campo debido a los buenos resultados obtenidos.

El trabajo multidisciplinar ayuda tanto a ver tus posibilidades como las del resto de grupos implicados, de tal forma que a mí me resulta difícil pensar en otra forma de trabajar más efectiva. Esto significa a su vez, que todavía nos que da mucho trabajo por hacer, los avances no han sido pocos y en muchos casos nos permiten discutir sobre la veracidad de los datos experimentales. No obstante, todavía queda lejos la irrefutabilidad de los datos teóricos. Tratar de que un estudio teórico sea un paso preliminar obligatorio al trabajo en el laboratorio constituye para mí el objetivo ideal y la evolución más lógica de nuestro trabajo.

Tarragona, Marzo 2004   J. Gracia

TABLE OF CONTENTS

1

Introduction and scope

The overall framework of this report aims to summarize the work we have done over the past four years. Conceptually, this thesis is divided into three well differentiated parts. The nucleus is based on a joint project with prof. Mena, of the University of Alcalá (Alcalá de Henares, Spain), whose group is involved in the synthesis and characterization of new aza- and oxo-titanium cubanes. These families of compounds are basically obtained from preorganized titanium tridentate ligands which can incorporate almost all the metals of the periodic table and yield the corresponding heterometallic cubanes. In this respect the theoretical study is based on and adapted from the progress in the laboratory work. Practically every section in this part starts by describing the experimental data available for the specific system studied when we began the analysis. Then we go on to describe the theoretical study and attempt to involve the reader in the problems discussed. As a consequence of the advance in the experimental work, NMR spectra are used to characterize the new compounds. This leads us to initiate studies in the computational simulation of NMR chemical shifts. The most theoretical part of this report is basically an assimilation of these studies. The excellent results obtained for the cubane compounds enabled us to extend the knowledge acquired to other interesting fields and our group has started a study of the NMR shielding tensors in polyoxometalate compounds. The third part of the thesis focuses on some molybdenum-sulphide clusters and their activity as catalysts.

The present chapter introduces the metal aggregates studied and their related chemistry, and describes the general scope of the thesis. The chapter is organized as follows: Section 1.1 gives an overview of the metal aggregates studied, of the computational procedures used and the layout of the thesis. Section 1.2 familiarizes the reader with cubane compounds, the great family of the first compounds studied, titanium cubanes. The important role in catalysis of molybdenum clusters, the second species

Chapter 1

examined, is explained in section 1.3. The scope of the work is reserved for section 1.4.

1.1	**Introduction**
1.2	**Cubic aggregates**
1.3	**Molybdenum catalysts**
1.4	**Scope of the work**

1.1   Introduction

The enormous development of density functional theory (DFT) methods for chemical applications,[1] along with powerful computer hardware during the 1990s, has enabled theory software for modelling real systems to be widely and efficiently used. This parallel evolution has made it possible to deal with more and more complex systems, and the constant progress has meant that computational chemistry is not merely a good tool but an alternative for studying molecules. The objective of the next step was to make a joint theoretical and experimental study.

Molecular metal clusters may provide insight into the mechanism of important processes, and act as potential models for more complicated biological or industrial process.[2] The great variety and versatility of the applications of these compounds has created considerable interest in their theoretical study. The usual size of metal aggregates and the importance of electron correlation means that DFT methods are practically the only reasonable alternative for studying these systems. In these terms, DFT methods have proved to be excellent at treating medium-sized metal aggregates at a good level of approximation. So molecular structures, stability and thermochemistry, chemical reactivity, vibrational frequencies, and magnetic, electric and other important properties have been systematically explored with impressive accuracy.[3,4,5,6]

In the past decade, it has become possible to carry out calculations on NMR chemical shifts[7] with increasing precision. It is fair to state that the use of DFT has been decisive in obtaining accurate computations of NMR parameters in compounds containing heavy elements. The second chapter of

this thesis briefly compares DFT methods with other computational schemes, and goes on to describe the peculiarities of calculating NMR parameters with DFT at greater length. NMR measures are commonly used for characterizing compounds in the laboratory. NMR parameters have only been theoretically computed fairly recently, which has meant that our group has had to make a particular effort to understand the theoretical and practical background. The second chapter reflects our efforts to understand the computation of NMR parameters from the first step, with particular referenced to the projects of our work group.

This report is essentially a theoretical study of two different families of metal clusters. Chapters 3 and 4 are a multidisciplinary study, very closely connected with the experimental part, which focuses on the electronic structure of the new titanium cubane compounds recently synthesized by Mena et al. We work parallel to an experimental group to compare and contrast the theoretical and experimental data, and so establish the base chemistry of these new compounds. In this sense, the various reaction energies were studied, and the compounds and their possible isomers were characterised by means of DFT methods. Particular emphasis is paid to the properties of incomplete Ti_3 core cubane tridentate ligands (precubanes) as bases for obtaining cubanes. The electronic structure, bonding energies, electron transfer processes and reactivity in the titanium Ti_3 core of the metal clusters are studied.

Chapter 5 summarizes the work carried out during a six-month stay in Dr. John E. McGrady's group, which uses density functional theory to explore problems of structure, bonding and reactivity in inorganic compounds. The main focus of the research is metal-metal bonding in cluster compounds. Transition metals have a prominent position in catalysis, both in industrial and biological contexts, and the ultimate goal is to understand the part played by the metal and its ligand environment in facilitating a particular chemical transformation. Chapter 5 studies the electronic structure of the Mo_2S_4 core catalysts and the mechanism of their, unresolved, catalytic activity. The various possible isomers with the generic formula $Cp_2Mo_2S_4$ were studied, and the energy of the electron transfer between the metallic centres and the sulphide ligands, so important in the catalytic process, was investigated in depth. Subsequently, the mechanism of the hydrogen

activation reaction promoted by these bi-molybdenum compounds was studied, and the nature of the different reaction pathways was elucidated.

1.1.1   Computational details

All calculations were carried out by means of DFT calculations including gradient corrections. Most of them were carried out with the ADF package[8] by using the program's standard frozen core TZP basis sets. The basis set includes a triple-z and polarization Slater basis set to describe the upper valence electrons, double-ζ in the subvalence region, and single-ζ in the core region. We used the local spin density approximation, characterized by the electron gas exchange ($X\alpha$ with $\alpha = \frac{2}{3}$) together with Vosko-Wilk-Nusair parameterization[9] for correlation. Becke's nonlocal corrections[10] to the exchange energy and Perdew's nonlocal corrections[11] to the correlation energy were added. Relativistic corrections were made by using the ZORA[12] formalism with corrected core potentials. The relativistic frozen core shells were generated with the auxiliary program DIRAC.[13] DFT-GIAO-based NMR calculations were performed with the auxiliary program NMR.[14] The contributions to the shielding tensor were also analysed with the EPR/NMR program,[15] from single calculations of the previously optimized geometries, but using the PAULI[16] formalism for the relativistic corrections (the ZORA formalism was not implemented). For bi-molybdenum compounds, supplementary calculations using the Gaussian 98[17] program were made with the B3LYP functional.[18] The 6-31G(d) basis set was used for the carbon, while the 6-31G basis set was used for hydrogen. The LANL2DZ[19] basis set and effective core potential were used for molybdenum and sulphur atoms, supplemented with a set of d-polarization[20] functions for the sulphur atoms and f-polarization[21] functions for the metals.

1.2   Cubic aggregates

The molecule from which cubane compounds take their name is the cubic hydrocarbon C_8H_8.[22] This molecule consists of a cube of carbon atoms, which are joined to hydrogen atoms orientated towards the outside (Figure 1.1).

4
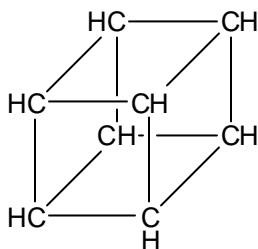
Figure 1.1. *Cubane* C_8H_8

Most cubic aggregates have two types of atoms (M and X) arranged alternately in the vertexes. M_4X_4 cubanes consisting entirely of metal atoms, like the $[Mo\{\boldsymbol{m}_3\text{-HgMo(CO)}_3(\boldsymbol{h}^5\text{-}C_5H_5)\}]_4$ compound, have been characterized.[23] Nevertheless, they typically involve a metal atom ensemble (M_4) and a second group of non-metal atoms (X_4), both of which may have additional ligands in their coordination sphere. The M_4 and X_4 subgroups each form a tetrahedron. The cubic structure can be considered to be the interpenetration of both tetrahedrons (Figure 1.2).
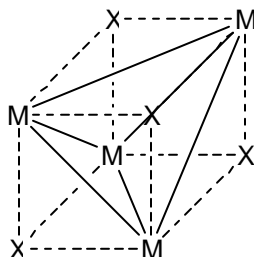
Figure 1.2. *Cubic aggregate as two alternate M_4 and X_4 tetrahedrons*

There are abundant experimental data on the solid state of these compounds. Cubanes generally form a compact packing and one unit has exact or approximate T_d symmetry, which produces an efficient crystalline packing. The distances M-X, X-X and M-M are related;[24] for a given cubane, any attractive interaction between the M atoms increases the X-X distance and vice versa. Additionally, the polyhedron has flat faces only when

5

$M - \widehat{X} - M = X - \widehat{M} - X = 90^{\circ}$, and the relative value of the aforementioned angles is a clear indication of the lengthening of a cubic regular structure due to the difference in size of the M_4 and X_4 tetrahedrons.

1.2.1   Bonding considerations

The structural stability and electronic versatility of these compounds is considerable and they involve many metal and non-metal elements. Depending on the nature of the metal, the non-metal atoms and their respective ligands, there will be a different number of valence electrons and electrons on metal-based orbitals (see Table 1.1).

The electron distribution in these compounds plays a very important role in their rationalisation. In the construction of the complexes, the M-X interactions basically hold the cubane structure. So non-metal and metal elements need to provide the necessary electrons to form the cubane skeleton, along with the electrons required by their respective ligands. Once these requirements have been fulfilled, if the metal atoms have any extra valence electrons, we shall find electrons that can form metal-metal bonds (see Figure 1.3). These last metal electrons are directly involved in the possible structural distortions, redox properties, etc.

For a cubane of general formula $[ML(\boldsymbol{m}_3\text{-X})]_4$ the adapted combinations of T_d symmetry for the metal s and d valence orbitals are

Metal Electrons (M)

- *(n-1)d $\rightarrow$ a₁ + 2e + 2t₁ + 3t₂*
- *ns $\rightarrow$ a₁ + t₂*

where n is the number of the period in the table of the elements. Non metal elements use their np valence electrons, while the nature of the electrons contributed by the metal ligands depends on the type of ligand. Below we show examples with ligand types σ and π.

Non Metal Electrons (X)

- $p \rightarrow a_1 + e + t_1 + 2t_2$

Ligand Electrons (L)

- *Ligand* $s \rightarrow a_1 + t_2$
- *Ligand* $p \rightarrow e + t_1 + t_2$

In the cubane formation, every one of the non-fulfilled orbitals of the metal's ligands (L) combines with an orbital with the same symmetry belonging to the metal, thus forming a metal-ligand bond. In turn, every one of the non-fulfilled orbitals of the non-metal element combines with an orbital with the same symmetry belonging to the metal to form the cube skeleton, while the non-metal fulfilled orbitals go on to form the cube skeleton without requiring any great contribution from the metals. Finally we have to take into account the remaining electrons in the metal orbitals. In this way, the valence orbitals in the cubane cluster are divided into three subgroups, which from smallest to largest energy are usually

i) Orbitals external to the cluster, used, for example, to form p- or s- bonds with the ligands.
ii) Orbitals used by the twelve M-X bonds that form the skeleton of the cube.
iii) Metal-metal orbitals.

Figure 1.3 presents an orbital's interaction diagram for the general case of a cubane $[LM(m_3\text{-}X)]_4$ (L = s- ligand) assuming a hypothetical T_d geometry. With these general orbital interactions, several attempts have been made to try to rationalize the structural properties of the cubanes.[25] We observe the three orbital subgroups: first, a sequence of orbitals corresponds to that of the metal-ligand bond; then, we found the twelve M-X bonding orbitals and finally the orbitals corresponding to the metal-metal bonds. For these last metal-metal orbitals a set of bonding orbitals, a_1, e and t_2, are found to have lower energies than the consequent antibondings, t_1 and t_2, leading to a total metal bond order of 1.0 for clusters with 12 metal electrons. The possible addition of 12 extra electrons would occupy the antibonding orbitals and increase the bond distance, consistent with a metal zero bond order.

Between these two extremes, several types of deformations can be rationalized in terms of a Jahn–Teller distortion, as a function of the partial occupation of the orbitals (see Table 1.1). An extension of this model for all kind of ligands enables us to rationalize the properties of many cubanes.
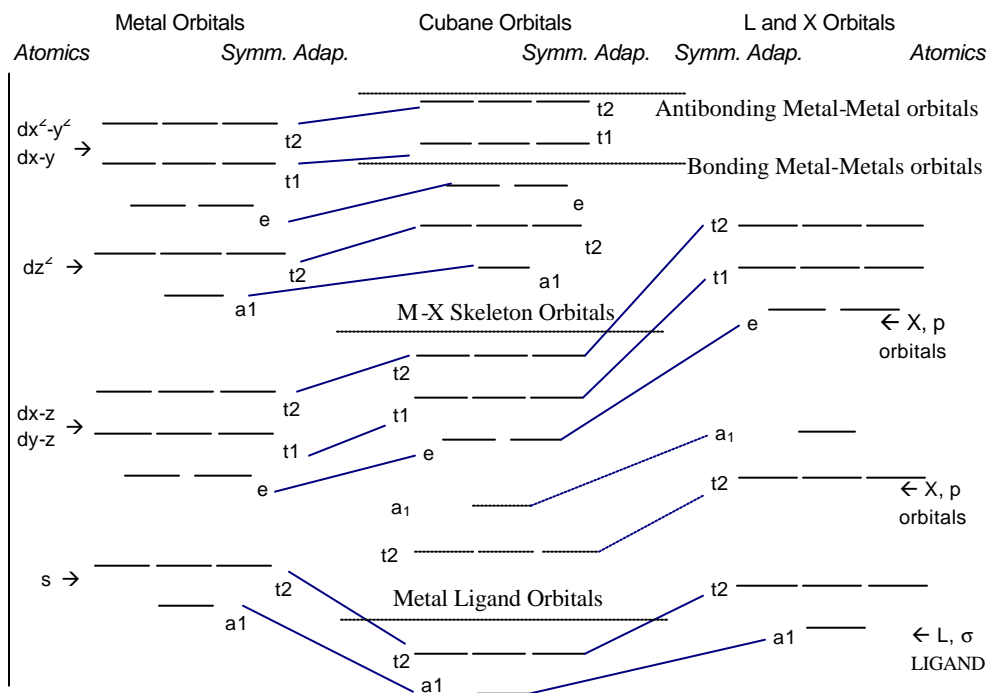
Figure 1.3. *Orbital interaction diagram for a general aggregate $[ML(m_3-X)]_4$ of T_d symmetry without fulfilled metal-metal orbitals*

Notwithstanding, this model cannot rationalize the distortions observed in the complex $[(C_5H_5)CrO]_4$. Green et. al.[26] observed that the electrons in the chrome compound were weakly matched, so the previous model of dislocated electrons proved to be inadequate because the electronic correlation was annulled. A different model with n separated and localised electrons per metal centre can be used to rationalize the structure of the Cr compound.[27] It was established that the energy difference between a

localised and delocalised structure is given by the energy balance between the stabilisation due to the formation of metal-metal (E_{M-M}, delocalisation) and the spin polarisation energy (E_{sp}, localisation). The greater tendency of the heavier metals to form metal-metal links is interpreted simply in terms of a bigger actual overlay. The fact that the orbitals 4d and 5d are large leads to a delocalisation. For the metals with the less diffuse 3d orbitals, however, it is necessary to take into account the associated stability that is the result of the antiferromagnetic coupling in the localized systems.

Table 1.1. *Electron distribution in some cubanes*

Complex	Metal electrons in M-M orbitals
$[PtMe_3(m_3\text{-Cl})]_4$ [28]	24
$[PtMe_3(m_3\text{-OH})]_4$ [29]	24
$[CoCp(m_3\text{-S})]_4$ [30]	24
$[FeCp(m_3\text{-CO})]_4$ [31]	20
$[TiMeCp(m_3\text{-S})]_4$ [32]	4
$[CoCp(m_3\text{-P})]_4$ [33]	20
$[TiCp(m_3\text{-N})]_4$ [34]	0

1.2.2   Metal element

The metal ligands orientated outwards do not form part of the cubane skeleton. However, they make it soluble in organic solvents and also prevent clusters from aggregating to the bulk metal. Non metal elements form the cubane edges by sharing their electrons or ceding a free pair, if its coordinating octet is already complete. On the other hand, the versatility of metal elements means that they are responsible for much of the richness of the structure found. Also, metal electrons are responsible for the interesting catalytic and structural properties of the compounds.

Alkaline and alkaline earth metals only possess s electrons in the valence shell, so they need non-metal elements that can cede electrons to form the

Chapter 1

cubane edges. This is the general case of the cubanes $\left[M(\boldsymbol{m}_3\text{-OYMe}_3)\right]_4$ [35] $M = K$, Rb, or Cs; $Y = C$ or Si, or $\left[BeMe(\boldsymbol{m}_3\text{-OR})\right]_4$.[36] A very interesting case is that of by the electronically-deficient $[Li(\boldsymbol{m}_3\text{-Me})]_4$ [37] cubane; it needs a further 2e for each metal to complete the edges. These alkaline cubanes always lack metal-metal bonding orbitals, because their only s-type electrons are involved in the M-X bonds.

Alcoxides of thallium (I) have been known now for a century. X-ray studies have shown that the constituent molecules of these compounds have a cubic structure.[38] The mere presence of p orbitals means that only very weak metal-metal interactions can be present.[39] Al, Tl, Pb, Sn are the most representative metals of this family in the formation of tetramers. Given the large number of cubane cluster compounds which have been characterized for d-transition metals, it is surprising that more have not been identified for the s- and p- block elements. However, this may reflect the inherent structural preferences of these two branches of inorganic chemistry.

Transition metals use valence occupied d orbitals for the first time. The metal interactions now involve bond distances between metals. The biochemical role of several Fe-S proteins has been discussed and it has been suggested that electrons embody cubane centres $\{Fe_4S_4\}$.[40] Fe-S proteins are an important group of biological materials, which are probably present in all forms of life. The main feature of Fe-S proteins is their ability to transport one or two electrons. The studies on attributable oxidation states for the complexes $[Fe(SR)(\boldsymbol{m}_3\text{-S})]_4$ have been of great value and interest and have established a correspondence between the operative oxidation levels in ferroxines and HiPIP proteins.

The geometry of the cubic structure is sufficiently flexible to accommodate constructions imposed by the bonding and antibonding interactions among the atoms at the vertices of the cubane for a wide range of compounds. For example, complexes containing only the metal atoms $[Ni_8(CO)_8(\boldsymbol{m}_4\text{-PPh})_6]$,[41] $[Mo\{\boldsymbol{m}_3\text{-HgMo(CO)}_3(\boldsymbol{h}^5\text{-C}_5H_5)\}]_4$ have been characterized.[23] A study of the series of compounds $[M(Ph_3Y)X]_4$,[42] where $M = Cu$ or Ag, $Y = P$ or As and $X = Cl$, Br or I, shows the effects of the antibonding interactions on the structure of the cubane. Those tetramers

for which the antibonding interactions on the cubic structure are too big include a chair conformation (Figure 1.4). Several factors influence the relative stability of the structures.[43]

i)   The magnitude of the nonbonding interactions
ii)   The relative stability of the tri- and tetra-coordinated metal
iii)   The relative stability of the atom X in μ_3- or μ_2- coordination
iv)   Interactions of the crystalline packing
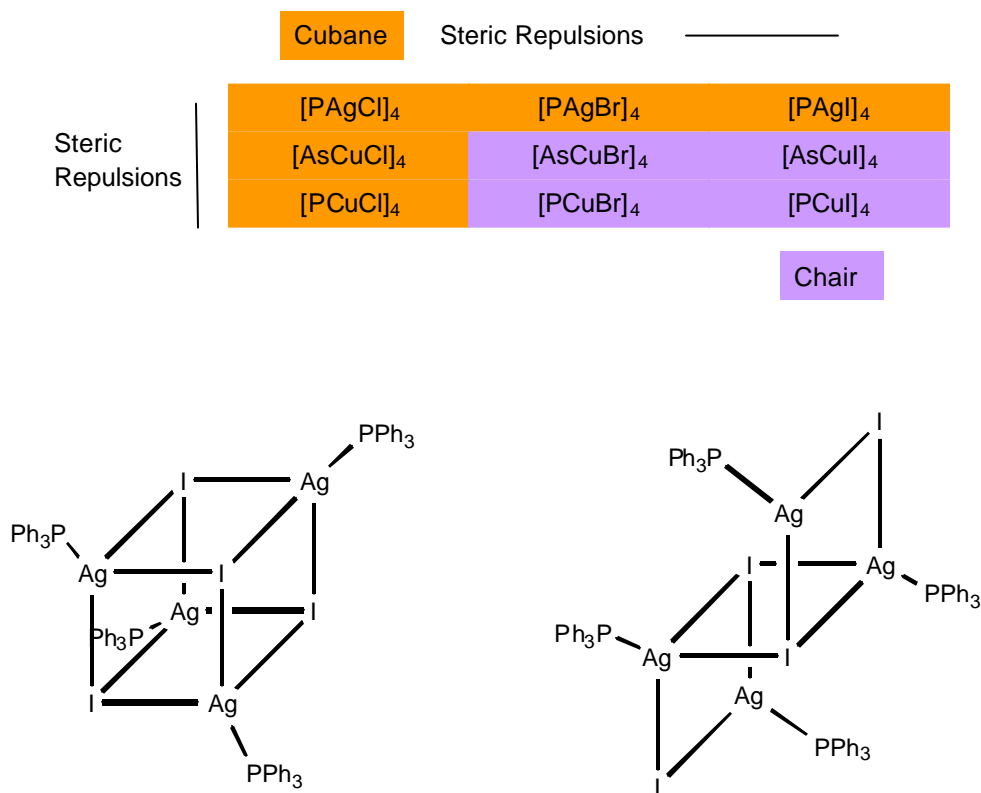
Figure 1.4. *Cubic and chair conformations in terms of the cubane. Examples on* $[Ag(PPh_3)I]_4$[44]

1.2.3   Incomplete cubane structures

The M_3S_4 core ($M = Fe$, Mo) systems were the first time that a metal fragment had been added to preorganized M_3X_4 ligands to form heterometallic cubanes of the $M'M_3S_4$ core.[45] They were to be a reference for subsequent studies on the formation of these monomers. In addition, the Rhenium complex $[Re_3(CO)_9(\boldsymbol{m}\text{-}OH)_3(\boldsymbol{m}_3\text{-}OH)]$ acts as a ligand type in the formation of dicubanes.[48] We are taking the first steps towards a comprehensive understanding of the chemistry of metallic cubane formation, starting from the formation of preorganized organometallic ligands (precubanes) (see Table 1.2) that can incorporate a wide variety of metals in very different oxidation states.

Table 1.2. *Precubane structures*

Precubane	Charge	Metal oxidation state	Nº of metal electrons
$[Fe_3S_4]$[46]	+1	+3	15
$[Cp_3Mo_3S_4]$[47]	+1	+4	9
$[Re_3(CO)_9(\boldsymbol{m}\text{-}OH)_3(\boldsymbol{m}_3\text{-}OH)]$[48]	+1	+4	9
$[Ti_3(\boldsymbol{m}_3\text{-}CR)(\boldsymbol{m}\text{-}O_3)]$[49]	0	+4	0
$[Ti(\boldsymbol{h}^5\text{-}C_5Me_5)(\boldsymbol{m}\text{-}NH)\}_3(\boldsymbol{m}_3\text{-}N)]$[53]	0	+4	0

Titanium nitride is used in a variety of industrial applications because of its important properties.[50] When [TiN] layers are grown, the presence of ammonia is crucial for eliminating significant quantities of carbon from the precursors. Thus the understanding of the reaction of metal nitrides and halides with ammonia proves to be very interesting.[51] In this context, Mena et al. used the ammonolysis of the $[Ti(\boldsymbol{h}^5\text{-}C_5Me_5)Me_3]$ complex to get the aza-compound $[\{Ti(\boldsymbol{h}^5\text{-}C_5Me_5)(\boldsymbol{m}\text{-}NH)\}_3(\boldsymbol{m}_3\text{-}N)]$ (**1**) as a yellow solid,[52] in a similar process to the one used by Roesky et al.[53] (Scheme 1.1).

$$3Cp^*TiMe_3 \ + \ 4NH_3 \ \xrightarrow{} $$

-9 CH$_4$

(**1**)

$[Ti] = TiCp^*$
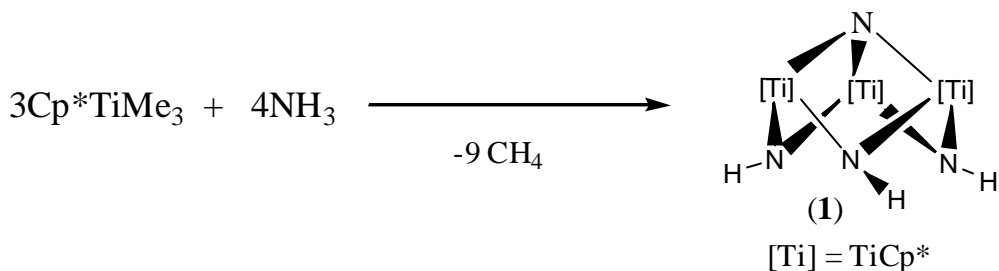
Scheme 1.1. *Reaction of [Ti(h^5-C$_5$Me$_5$)Me$_3$] with NH$_3$*

On the other hand, when a toluene solution of $[Cp^*TiEt(p\text{-}O)]_3$ ($Cp^* = \eta^5\text{-}$ C_5Me_5) was heated at 195 ºC for 12 h (Scheme 1.2), the colour of the solution changed from yellow to dark orange. When the solvent was removed the oxo- compound $[\{TiCp^*(\boldsymbol{m}\text{-}O)\}_3(\boldsymbol{m}_3\text{-}CMe)]$ (**3**) was yielded in quantitative yield and high purity.[54]

Tol/195ºC/12h

-2 C$_2$H$_6$

$[Ti] = TiCp^*$ (**3**)
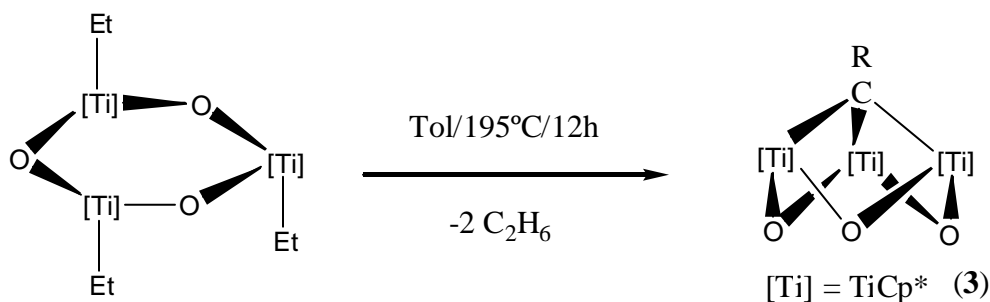
Scheme 1.2. *Formation of the [{TiCp*($\boldsymbol{m}$-O)}$_3$($\boldsymbol{m}_3$-CMe)] compound*

Successive works on the relatively more innovative oxo- Ti_3O_3CR and aza- Ti_3N_4 core systems have expanded their chemistry towards cubane[55] and dicubane[56] compounds. The reaction of the azatitanium compound with some titanium derivatives leads to nitrocubane formation (see Scheme 1.3). This reaction forms a cubane compound by adding the fourth vertex to a structure that becomes a precubane.

Chapter 1
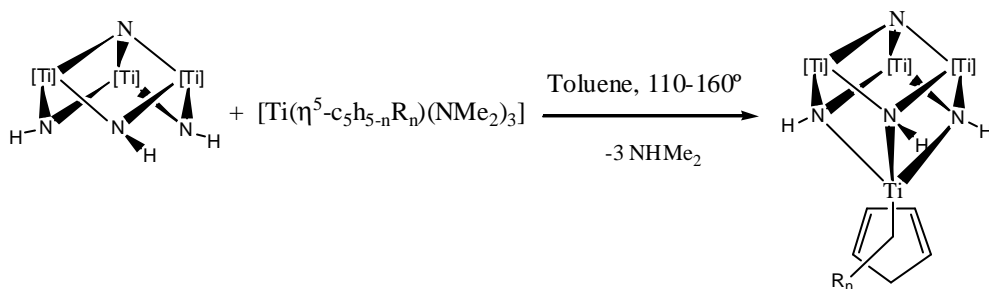
Scheme 1.3. *Reaction of [{Ti($\textbf{h}^5$-C$_5$Me$_5$)($\textbf{m}$-NH)}$_3$($\textbf{m}_3$-N)] with [Ti($\textbf{h}^5$-C$_5$H$_5$R$_n$)(NMe$_2$)$_3$]*

These aza- and oxo- structures can move labile ligands such as carbonyls or methylsilanes, coordinated to group-6 metals, to give the corresponding cubane compounds (Scheme 1.4).[58] Should there be other highly reactive metal ligand bonds, dicubanes may form. Thus dicubanes are obtained from the aggregation of alkaline-metals (Scheme 1.5).[57] Also, [{TiCp*($\textbf{m}$-O)}$_3$($\textbf{m}_3$-CR)] ($R = H$ (**1**), Me (**2**))[55] systems show their coordinating capabilities on unsaturated molecules like carbon monoxide, isocyanates and acetones, or on metal carbonyl hydrides in a chemistry that has no direct metal-metal bond (Scheme 1.6).
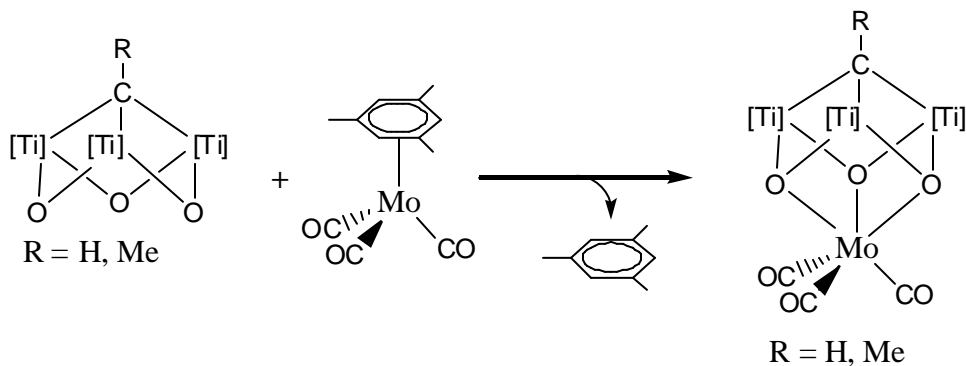
Scheme 1.4. *Synthesis of the heterometallic cubane complexes [Mo(CO)$_3${TiCp*($\textbf{m}$-O)}$_3$($\textbf{m}_3$-CR)] , R = H, Me*

14
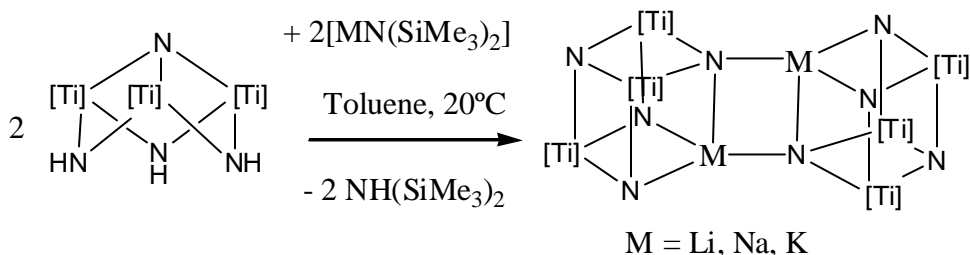
Scheme 1.5. *Synthesis of the edge-linked double azaheterometallocubane complexes [M{TiCp*(**m**-N)}₃(**m**₃-N)]₂ M = Li, Na, K*
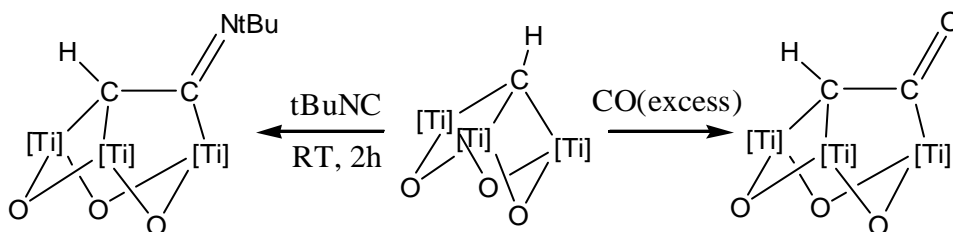
Scheme 1.6. *Reactivity of complex [{TiCp*(**m**-O)}₃(**m**₃-CH)] with tBuNC and CO*

From the electronic point of view, ligands are molecules with non metallic elements that can act as electron donors. It is difficult to establish a universal classification for ligands, because there are two main aspects to emphasize: electronic and structural. When studying ligand complexes it is important to know the number and basicity of their electrons. Structural aspects include the number and arrangement of the donor atoms. Both aspects together, the number of electrons and their arrangement, have considerable repercussions on the final geometry of the complexes. Aza- and oxo precubane compounds have a ligand structure with three electron pairs oriented outwards. Unlike other ligands, they have the peculiarity of possessing empty d-titanium orbitals that can look for a metal-metal connection with the additional metal fragment.

15

A wide range of metal fragments have already been discovered that make good use of one or several interactions to coordinate to the precubane ligands. As the cubanes are being formed, the free electron pairs of the precubane ligand and the interaction with the oxidized titanium atoms mean that electron density is accumulated in the atoms that form the tripod. The fragments incorporated make good use of this electronic density, and there are three possible effects:

a) The incorporated metal fragments look for an electrostatic interaction leading the positive part (central atom) toward the negative charge of the trident (alkaline metals, $C=O$, ...).

b) The empty orbitals of the metal fragment tend to stabilize the free pair electrons of the ligand.

c) The electrons of the fragment are stabilized by interaction with the virtual orbitals of the ligand. The metal may even be oxidised and anionic precubane ligands generated.

Additionally, when studying the direct metal-metal bond, it proves to be impossible not to explore the qualities of the precubane ligands like tridentate donor ligands on metallic fragments in an attempt to find a metal-metal connection among units. In this respect, $[M(CO)_6]$ ($M = Cr$, Mo, W) addition on the oxo- $[Ti_3(m_3\text{-}CR)(m\text{-}O_3)]$ as on the nitro- $[Ti(h^5\text{-}C_5Me_5)(m\text{-}NH)\}_3(m_3\text{-}N)]$ trimmers crystallizes in heterocubanes, where the M-Ti interaction becomes clear. DFT theoretical studies show that they can be useful for this kind of task for examining the interaction in detail.[58]

1.3 Molybdenum catalysts

The original reason for studying the catalytic capabilities of sulphido-bridged dimolybdenum complexes was to develop an understanding of the important yet complex world of heterogeneous catalysis. It was soon evident that valuable insight into the structure and function of heterogeneous catalysts composed of small metal particles could be obtained by using the powerful techniques of X-ray crystallography, NMR spectroscopy, and

other spectroscopic methods for studying the fine details of the structure, bonding, and molecular dynamics of small organic molecules bonded to polynuclear metal centres. However, the complexity of the systems sometimes makes it difficult to elucidate key mechanistic points. More recently, theoretical computational methods have emerged as an efficient and attractive alternative for understanding and solving problems that are difficult to address with experimental methods.

Sulphur-containing compounds have long been known for their strong coordinating and adsorptive properties.[59] Many nonmolecular transition-metal sulphides have intriguing catalytic activity; hydrogenations of unsaturated and aromatic hydrocarbons and hydrogenolysis of molecules with carbon-sulphur, carbon-oxygen, and carbon-nitrogen bonds have been catalyzed. These catalytic properties have been extensively used in fuel processing. The semiconductor properties of metal-sulphide surfaces mean that they also have other catalytic applications:[60] for example, WS_2 has been used as a photocathode and photoanode,[61] and zinc and cadmium sulphides have been extensively studied as photocatalysts.[62] Also in biochemistry, sulphide ligands have been identified in the coordination spheres of the metal centres of several metalloprotein and metalloenzyme systems.[63]

One or more sulphide atoms bonded to a transition metal provide considerable electronic and structural flexibility. This versatile coordination behaviour has been used to develop synthetic routes to metal-sulphur cluster compounds.[64] A large number of molecular transition-metal complexes have been synthesized. As a result of the ability of metal-sulphide complexes to retain their structural integrity, the electron-transfer processes for these complexes often show some degree of reversible character. Moreover, sulphur donor ligands tend to favour the lower oxidation states of metal ions, and the relatively positive reduction potentials of the sulphide complexes provide a favourable situation for the many catalytic reduction reactions that have been characterized. It is also interesting to explore the extent to which this catalytic activity parallels that of non-molecular sulphides or that of biological systems.

The largest sulphide-containing cluster to be studied for its catalytic applications is $[Rh_{17}S_2(CO)_{32}]^{3-}$. This cluster was found to catalyse the reduction of phenylglyoxal to (2-hydroxyethyl)benzene in the presence of hydrogen,[65] or the conversion of CO/H_2 (1:1) to ethylene glycol and

Chapter 1

methanol.[66] Several examples of sulphide clusters and complexes with noble-metal ions have been found to show catalytic activity under hydrogen. Besides, other complexes of groups 8-10 have been used as catalysts for reactions with hydrogen.[67] Iron-sulphur cubane clusters of the general formula $[Fe_4S_4(SR_4)]^{n-}$ have been widely investigated as catalysts for reducing a variety of substrates by hydride or electron donors. Motivation enlarges by the presence of these clusters in the ferrodoxin proteins, which function in many biological electron-transfer processes.[68] Other mixed metal Mo-Fe-S clusters have been compared with the iron-sulphur cubanes.[69]

Of special interest are molybdenum metal sulphides. In the large-scale commercial hydrotreating processes, sulphided molybdenum-cobalt catalysts supported on alumina are generally the systems of choice.[70] Dinuclear cyclopentadienyl molybdenum complexes with bridging sulphide ligands have been found to activate molecular hydrogen. Reaction of $[(CpMo)_2(\mu\text{-}S)_2(\mu\text{-}S_2)]$ with H_2 yields the cleaved hydrogen bond and a product $[(CpMo)(\mu\text{-}S)(\mu\text{-}SH)]_2$ with two hydrosulphido ligands was formed (see Equation 1.1).[71] Additionally, this last compound and the structurally related $[(CpMo(\mu\text{-}S))_2S_2CH_2]$ do not add hydrogen, but they serve as catalysts for the formation of HD from a mixture of hydrogen and deuterium.[72] Hydrogen activation by these neutral derivatives has been found to be useful in the catalytic hydrogenation of organic molecules. For example, the $[(CpMo)(\mu\text{-}S)(\mu\text{-}SH)]_2$ complex catalyzed the hydrogenation of N=N to hydrazines or C=N bonds in imines, isocyanates, and isothiocyanates to form amines, formamides, and thioformamides.

$[(CpMo(\mu\text{-}S))_2(S_2CH_2)]$ promotes the hydrogenation of alkynes to cis alkenes, allenes to alkenes, and ketenes to aldehydes[73] and the hydrogenolysis of carbon disulphide to hydrogen sulphide and thioformaldehide.[74] The mechanisms of hydrogen interaction with these complexes have not been established. It is apparent that the sulphide ligands play a role in hydrogen coordination, and this ligand reactivity was a dominant characteristic throughout the study of these dinuclear molybdenum systems.
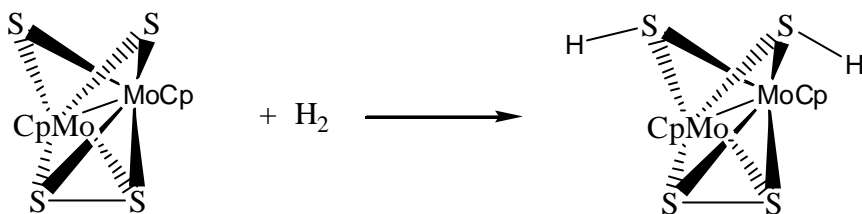
Equation 1.1

The cations $[(CpMo)_2(S_2CH_2)(\mu\text{-}S)(\mu\text{-}SR)]^+$ also undergo an unusual reaction with molecular hydrogen. Final reaction products in these systems have been found to depend on the nature of R.[75] The cation $[(CpMo)_2(S_2CH_2)(\mu\text{-}S)(\mu\text{-}SR)]^+$ undergoes a complex reduction chemistry, both with electron donors and with molecular hydrogen, when R is a electron withdrawing substituent (thiophene $R = C_4H_3S$). When R = Me, the reaction does not reduce the substituent,[76] but to products shown in Equation 1.2.[75a] The synthesis and characterization of the SH compound $[(CpMo)_2(S_2CH_2)(\mu\text{-}SCH_3)(\mu\text{-}SH)]$ have been reported.[77] The obtained SH complex $[(CpMo)_2(S_2CH_2)(\mu\text{-}SCH_3)(\mu\text{-}SH)]$ proved elusive. It is extremely air sensitive and is rapidly oxidized to give the neutral radical $[(CpMo)_2(S_2CH_2)(\mu\text{-}SCH_3)(\mu\text{-}S)]$. In the presence of hydrogen, the solution of this SH complex appears to be quite stable.
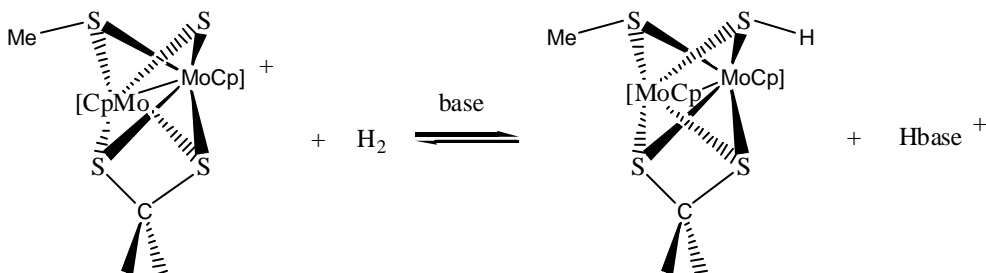
Equation 1.2.

The mechanistics of the hydrogen interaction with these cation complexes have not been established, but it is apparent that the sulphido ligands play a role in the hydrogen coordination. In all cases, it is proposed that hydrogen addition to the cation promoted by base resulted in the formation of a

Chapter 1

reduced SH product (see Equation 1.2). The kinetic data for Equation 1.2 are consistent with the second-order rate law=K[cation][H_2] and suggest that the cations interact directly with the hydrogen. The data also support the conclusion that the reactions of the cations with hydrogen involve an interaction which results in the heterolytic cleavage of H_2.[78] Several possible modes of hydrogen addition to the cations, which are consistent with the kinetic data and with the molecular orbital description of the cation, were considered (see Figure 1.9).[79]
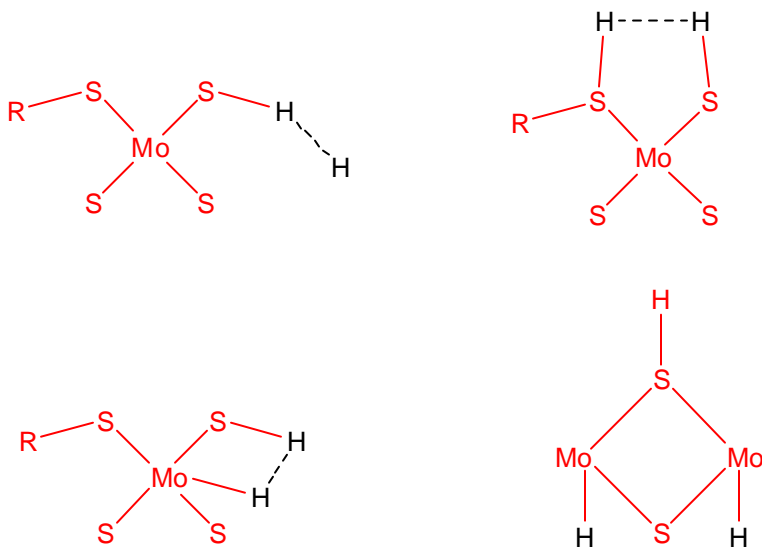
Figure 1.9. *Considered H_2 addition modes to $[(CpMo)_2(S_2CH_2)(m\text{-}S)(m\text{-}SR)]^+$ cations*

Other structures for hydrogen-addition products have been proposed, but reviewers have suggested that they are unlikely.[80] End-on addition of hydrogen to a sulphide ligand in the cation is one potential description of the hydrogen addition process.[81] Addition of H_2 to the sulphur sites would produce a mercaptanbridged structure, which would readily deprotonate in the presence of a base. The analogous reversible addition of ethane to the sulphur sites of an alkanethiolate cation has been characterized recently.[82] An alternative mechanism for the initial interaction of the cation with

hydrogen could be a stepwise addition of hydrogen across a molybdenum-sulphide bond or across a molybdenum-molybdenum bond. Attempts to spectroscopically detect a hydrogen addition product have been unsuccessful.

One indirect method of assessing the relative stabilities of the protonated structures may be to identify the protonation site(s) in related neutral dimers. Protonation studies have provided data to suggest that in most cases molybdenum ions are the most basic sites in these structures. In this sense, the tendency of electron-withdrawing substituents to undergo R-S bond cleavage upon protonation is somewhat unexpected. A rationale for this reactivity suggests that the inductive effect of the substituent may increase electron density in the S and R atoms in the thiolate ligand of the dimer. It is interesting to speculate about whether the site of initial protonation in these systems is therefore altered. However, there is no spectroscopic evidence to suggest that intermediates in the protonolysis reactions have been obtained, and the mechanism of R-S bond protonolysis therefore remains unestablished.

1.4   Scope of the work

This thesis consists of two well differentiated parts: a study of the new family of titanium cubane compounds and a study of the molybdenum-sulphide catalysts. In both cases the main goal is to help to rationalise the chemical properties of the species. The treatment is based on density functional calculations, which have proved to be appropriate for studying metal clusters.

The study of the titanium cubanes is the central core, and the original idea that prompted this thesis. A joint study with synthesis in the laboratory was always the aim. The study of the synthesised species tries to extend the results to new possibilities of laboratory work. The main results are:

- The description of the structural features and the electronic properties of the adducts. The preorganized ligands (precubanes) of general formula $[\{TiCp^*(\mu\text{-}O)\}_3(\mu_3\text{-}CR)]$ and $[\{TiCp^*\}(\mu\text{-}NH)\}_3(\mu\text{-}N)]$ act as macrocyclic tridentate six-electron donor ligands and provide an effective route to

Chapter 1

cubanes with a $[MTi_3(\mu_3\text{-}Y)(\mu\text{-}X)_3]$ core. Fragments of almost all metal groups are expected to interact with these ligands. Changes in the nature of the interaction, ligand behaviour and molecular structure are analysed.

- A study of the stability of the compounds and of the energy processes involved (reaction energies, isomerization processes, etc.). The circumstances that lead to obtaining cubic structures are analysed. The displacement of metal fragment labile ligands by the precubanes, or the activation of ligand proton bonds by interaction with the metallic fragment are examined. Additionally, some compounds show that they have more than one isomer, or experience a dynamic behaviour in solution. These situations are also described.

- The influence of the solvent is also evaluated in some cases because the thermochemistry of the processes in the gas phase is difficult to explain. A continuum model is used to show the effects of the solvent. For a single family of compounds, only in some cases does interaction with precubane ligands lead to the formation of the corresponding cubane compounds, or in very specific conditions. Solvent effects are important factors in obtaining cubanes from alkaline and alkaline earth salts.

- The description of some important chemical properties. The contribution of the nuclear magnetic resonance chemical shift results are decisive for the characterization of the compounds. The peculiarities of calculating the NMR shielding tensors are described in detail, especially for the DFT methods. The activation of the apical carbon proton bond in the oxo ligand $[\{TiCp^*(\mu\text{-}O)\}_3(\mu_3\text{-}CH)]$ during the formation of dimeric structures was followed by ^{13}C NMR spectroscopy. The considerable changes produced in the chemical shift between protonated and unprotonated structures was perfectly described and rationalized by theoretical calculations. As a result of the the description of the NMR values for cubane compounds, these studies have been extended to other topics of interest in our work group. This gives rise to a separate section, included at the end of Chapter 2, on DFT's abilities to compute the NMR shielding tensor of the ^{183}W nucleus in polyoxometalate compounds.

The important catalytic properties of molybdenum-sulphide compounds are studied in the second part of the thesis. The theoretical study attempts to

elucidate some of the aspects of their reaction mechanics that are unclear. Dinuclear cyclopentadienyl molybdenum complexes with bridging sulphide ligands are one of the families that has considerable structural flexibility. The ability of sulphide complexes to activate molecular hydrogen and catalyze substrate reduction by hydrogen is particularly relevant to the chemistry. Those aspects related to the electronic structure of the catalyst and of the reduced substrate are emphasised.

Chapter 1

References and notes

[1] a) L. J. Bartolotti, K. Flurchick, *"Reviews in computational chemistry"* **1995**, Vol. 7; Eds.: KB. Libkowitz, DB. Boyd, Verlag Chemie, New York, 187.
b) R. G. Parr, W. Yang, *"Density functional theory of atoms and molecules"* **1989**. Oxford University Press, New York.

[2] a) *Chem. Rev.* **2000**, Issue number 2.
b) L. N. Lewis, *Chem. Rev.* **1993**, *93*, 2693.
c) K. Herbst, M. Monari, M. Brorson, *Inorg. Chem. (Communication)* **2002**, *41*, 1336.

[3] T. Ziegler, *Chem. Rev.* **1991**, *91*, 649.

[4] G. Frenking, I. Antes, M. Boehme, S Dapprich, A. W. Ehlers, V. Jonas, A. Neuhaus, M. Otto, R. Stegmann, A. Veldkamp, S. F. Vyboishchikov, *Reviews in Computational Chemistry*; Eds. K. B. Lipkowitz, D. B. Boyd; VCH: New York, *Vol. 8*, **1996**, 63.

[5] T. R. Cundari, M. T. Benson, M. L. Lutz, S. O. Sommerer, *Reviews in Computational Chemistry*; Eds. K. B. Lipkowitz, D. B. Boyd; VCH: New York, *Vol. 8*, **1996**, 145.

[6] W. Koch, M. C. Holthausen, *A Chemist's Guide to Density Functional Theory*, Second Edition, Wiley-VCH, **2001**.

[7] a) M. Kaupp, V. G. Malkin, O. L. Malkina, *'NMR of transition metal compounds'*; Ed.: P. von Ragué Schleyer, *'Encyclopedia of Computational Chemistry'*, JohnWiley & Sons, Chichester, **1998** pages 1857–1866.
b) G. Schreckenbach, T. Ziegler, T., *'Density functional calculations of NMR chemical shifts and ESR gtensors'*, *Theor. Chem. Acc.* **1998**, *99*, 71.
c) Bühl, M.; Kaupp, M.; Malkina, O. L.; Malkin, V. G., *'The DFT route to NMR chemical shifts'*, *J. Comput. Chem.* **1999**, *20*, 91.
d) J. Autschbach, T. Ziegler, *'Double perturbation theory: A powerful tool in computational coordination chemistry'*, *Coord. Chem. Rev.* **2003**, *238/239*, 83.
e) J. Autschbach, T. Ziegler, *'Relativistic Computation of NMR shieldings and Spin-spin Coupling Constants'*; Eds: M. D. Grant, R. K. Harris, *'Encyclopedia of Nuclear Magnetic Resonance'*, volume 9, John Wiley & Sons, Chichester, **2002** pages 306–323.

[8] a) G. te Velde, F. M. Bickelhaupt, S. J. A. van Gisbergen, C. Fonseca Guerra, E. J. Baerends, J. G. Snijders, T. Ziegler, *"Chemistry with ADF"*, J. Comput. Chem. **2001**, *22*, 931.
b) C. Fonseca Guerra, J. G. Snijders, G. te Velde, and E. J. Baerends, Theor. Chem. Acc. **1998**, *99*, 391.
c) ADF2002.03, SCM, Theoretical Chemistry, Vrije Universiteit, Amsterdam, The Netherlands, http://www.scm.com.

[9] S. H. Vosko, L. Wilk, M. Nusair, *Can. J. Phys.* **1980**, *58*, 1200.

[10] a) A. D. Becke, *J. Chem. Phys.* **1986**, *84*, 4524.

b) A. D. Becke, *Phys. Rev. A* **1988**, *38*, 3098.

[11] a) J. P. Perdew, *Phys. Rev. B* **1986**, *33*, 8822.

b) J. P. Perdew, *Phys. Rev. B* **1986**, *34*, 7406.

[12] a) E. van Lenthe, E. J. Baerends, J. G. Snijders, *J. Chem. Phys.* **1993**, *99*, 4597.

b) E. van Lenthe, E. J. Baerends, J. G. Snijders, *J. Chem. Phys.* **1994**, *101(11)*, 9783.

c) E. van Lenthe, AE Ehlers, and E. J. Baerends, *J. Chem. Phys.* **1994**, *110*, 8943.

d) E. van Lenthe, J. G. Snijders, and E. J. Baerends, *J. Chem. Phys.* **1996**, *105(15)*, 6505.

e) E. van Lenthe, R. van Leeuwen, E. J. Baerends, J. G. Snijders, *Int. J. Quantum Chem.* **1996**, *57*, 281.

[13] *"Dirac, a relativistic ab initio electronic structure program, Release 3.2 (2000)", written by T. Saue, V. Bakken, T. Enevoldsen, T. Helgaker, H. J. Aa. Jensen, J. K. Laerdahl, K. Ruud, J. Thyssen, and L. Visscher (* http://dirac.chem.sdu.dk*)*

[14] a) G. Schreckenbach, T Ziegler, J. Phys. Chem. **1995**, *99*, 606.

b) G. Schreckenbach, T. Ziegler, *Int. J. Quantum Chem.* **1996**, *60*, 753.

c) G. Schreckenbach, T. Ziegler, *Int. J. Quantum Chem.* **1997**, 61, 899.

d) S. K. Wolff , T. Ziegler, *J. Chem. Phys.* **1998**, *109*, 895.

e) S. K. Wolff, T. Ziegler, E. van Lenthe, E. J. Baerends, *J. Chem. Phys.* **1999,** *110*, 7689.

[15] a) G. Schreckenbach, T. Ziegler, *J. Phys. Chem. A* **1997**, *101*, 3388 (for ESR g-tensor).

b) S. Patchkovskii, T. Ziegler, *J. Phys. Chem. A* **2001**, *105*, 5490 (for high-spin EPR g-tensor).

[16] a) J. G. Snijders, E. J. Baerends, P. Ros, *Mol. Phys.* **1979**, *38*, 1909.

b) P. M. Boerrigter, E. J. Baerends, J. G. Snijders, *Chem. Phys.* **1998**, *122*, 357.

c) T. Ziegler, V. Tschinke, E. J. Baerends, J. G. Snijders, W. Ravenek, *J. Phys. Chem.* **1989**, *93*, 3050.

[17] M. J. Frisch, G. W. Trucks, H. B. Schlegel, G. E. Scuseria, M. A. Robb, J. R. Cheeseman, V. G. Zakrzewski, J. A. Montgomery, R. E. Stratmann, J. C. Burant, S. Dapprich, J. M. Millam, A. D. Daniels, K. N. Kudin, M. C. Strain, O. Farkas,J. Tomasi, V. Barone, M. Cossi, R. Cammi, B. Mennucci, C. Pomelli, C. Adamo, S. Clifford, J. Ochterski, G. A. Petersson, P. Y. Ayala, Q. Cui, K. Morokuma, D. K. Malick, A. D. Rabuck, K. Raghavachari, J. B. Foresman, J. Cioslowski, J. V. Ortiz, B. B. Stefanov, G. Liu, A. Liashenko, P. Piskorz, I. Komaromi, R. Gomperts, R. L. Martin, D. J. Fox, T. Keith, M. A. Al-Laham, C. Y. Peng, A. Nanayakkara, C. Gonzalez, M. Challacombe, P. M. W. Gill, B. G. Johnson, W. Chen, M. W. Wong, J. L. Andres, M. Head-Gordon, E. S. Replogle, J. A. Pople, *Gaussian 9*8, Revision A.7; Gaussian, Inc.: Pittsburgh, PA, **1998**.

Chapter 1

[18] (a) C. Lee, W. Yang, R. G. Parr, *Phys. Rev. B*, 1988, **37**, 785.
(b) A. D. Becke, *J. Chem. Phys.*, 1993, **98**, 5648.

[19] (a) W. R. Wadt, P. J. Hay, *J. Chem. Phys.* 1985, **82**, 284.
(b) T. H. Jr. Dunning, P. J. Hay, *In Modern Theoretical Chemistr*y; Schaefer, H. F. I., Ed.; Plenum: New York, 1976; pp 1-28.

[20] A. W. Ehlers, M. Böhme, S. Dapprich, A. Gobbi, A. Höllwarth, V. Jonas, K. F. Köhler, R. Stegmann, A. Velokamp, G. Frenking, *Chem. Phys. Lett.*, 1993, **208**, 237.

[21] A. W. Ehlers, M. Böhme, S. Dapprich, A. Gobbi, A. Höllwarth, V. Jonas, K. F. Köhler, R. Stegmann, A. Velokamp, G. Frenking, *Chem. Phys. Lett.*, 1993, **208**, 111.

[22] P. E. Eaton, *Angew. Chem. Int. Ed. Engl.* **1992**, *31*, 1421.

[23] J. Deutscher, S. Fadel and M. L. Ziegler, *Angew. Chem. Int. Ed. Engl.* **1977**, *16*, 704.

[24] C. D. Garner, *"Cubane Clusters"*, 265, **1980**, John Wiley & Sons Ltd.

[25] a) F. Bottomley, F. Grein, *Inorg. Chem.* **1982**, *21*, 4170.
b) C. S. Bahn, A. Tan, S. Harris, *Inorg. Chem.* **1998**, *37*, 2770.
c) P. D. Williams, M. D. Curtis, *Inorg. Chem.* **1986**, *25*, 4562.

[26] C. E. Davies, J. C. Green, N. Kaltsoyannis, M. A. MacDonald, J. Qin, T. B. Rauchfuss, C. M. Redfern, G. H. Stringer, M. G. Woolhouse, *Inorg. Chem.* **1992**, *31*, 3779.

[27] J. E. McGrady, *J. Chem. Soc. Dalton Trans.* **1999**, 1393.

[28] R. E. Rundle, J. H. Sturdivant, *J. Amer. Chem. Soc.* **1947**, *69*, 1561.

[29] T. G. Spiro, D. H. Templeton, A. Zalkin, *Inorg. Chem.* **1968**, *7*, 2165.

[30] G. L. Simon, L. F. Dahl, *J. Amer. Chem. Soc.* **1973**, *95*, 2164.

[31] M. A. Neuman, Trinh-Toan and L. F. Dahl, *J. Amer. Chem. Soc.* **1972**, *94*, 3383.

[32] J. Darkwa, J. R. Lockemeyer, P. D. W. Boyd, T. B. Rauchfuss, and A. L. Rheingold, *J. Am. Chem. Soc.* **1988**, *110*, 141.

[33] G. L. Simon and L. F. Dahl, *J. Amer. Chem. Soc.* **1973**, *95*, 2175.

[34] P. Gómez-Sal, A. Martín, M. Mena, C. Yélamos, *J. Chem Soc. Chem. Commun.* **1995**, 2185.

[35] a) E. Weiss, H. Alsdorf, H. Kühr, H.-F. Grützmacher, *Chem. Ber.* **1968,** *101*, 3777.
b) E. Weiss, K. Hoffmann, H.-F. Grützmacher, *Chem. Ber.* **1970**, *103*, 1190.

[36] a) D. Mootz, A. Zinnius, B. Böttcher, *Angew. Chem. Int. Ed. Engl.* **1969**, *8*, 378.
b) N. A. Bell, G. E. Coates, *J. Chem. Soc. (A)* **1966**, 1069.
c) G. E. Coates, M. Tranah, *ibid.* **1967**, 236.

[37] E. Weiss, E. A. Lucken, *J. Organometal. Chem.* **1964**, *2*, 199.

[38] a) L. F. Dahl, G. L. Davis, D. L. Wampler, R. West, *J. Inorg. Nucl. Chem.* **1962,** *24*, 357.
b) V. A. Maroni, T. G. Spiro, *J. Amer. Chem. Soc.* **1967**, *89*, 45.

[39] C. O. Quicksall, T. G. Spiro, *Inorg. Chem.* **1970**, *9*, 1045.

[40] a) E. T. Adman, L. C. Sieker, L. H. Jensen, *J. Biol. Chem.* **1973**, *248*, 3987.
b) E. T. Adman, K. D. Watenpaugh, L. H. Jensen, *Proc. Natl. Acd. Sci. Usa* **1975**, *72*, 4854.
c) E. T. Adman, L. C. Sieker, L. H. Jensen, *J. Biol. Chem.* **1976**, *25*, 3801.

[41] L. D. Lower, L. F. Dahl, *J. Amer. Chem. Soc.* **1976**, *98*, 5046.

[42] B.-K. Teo, J. C. Calabrese, *Inorg. Chem.* **1976**, *15*, 2467.

[43] M. R. Churchil, K. L. Kalra, *Inorg. Chem.* **1974**, *13*, 1899.

[44] B.-K. Teo, J. C. Calabrese, *Inorg. Chem.* **1976**, *15*, 2474.

[45] Some examples:
a) J. N. Butt, F. A. Armstrong, J. Breton, S. J. George, A. J. Thomson, E. C. Hatchikian, *J. Am. Chem. Soc.* **1991**, *113*, 6663.
b) K. K. P. Srivastava, K. K. Surerus, R. C. Conover, M. K. Johnson, J.-B. Park, M. W. W. Adams, E. Münck, *Inorg. Chem.* **1993**, *32*, 927.
c) W. Cen, S. C. Lee, J. Li, F. M. MacDonnell, R. H. Holm, *J. Am. Chem. Soc.* **1993**, *115*, 9515.
d) W. Fu, J. Telser, B. M. Hoffman, E. T. Smith, M. W. W. Adams, M. G. Finnegan, R. C. Conover, M. K. Johnson, *J. Am. Chem. Soc.* **1994**, *116*, 5722.
e) M. G. Finnegan, R. C. Conover, J.-B. Park, Z. H. Zou, M. W. W. Adams, M. K. Johnson, *Inorg. Chem.* **1995**, *34*, 5358.
f) J. Zhou, J. W. Raebiger, C. A. Crawford, R. H. Holm, *J. Am. Chem. Soc.* **1997**, *119*, 6242.
g) G. Sakane, K. Hashimoto, M. Takahashi, M. Takeda, T. Shibahara, *Inorg. Chem.* **1998**, *37*, 4231.
h) R. Hernandez-Molina, V. P. Fedin, M. N. Sokolov, D. M. Saysell, A. G. Sykes, *Inorg. Chem.* **1998**, *37*, 4328.
i) B. Rink, M. Brorson, I. J. Scowen, *Organometallics* **1999**, *18*, 2309.

[46] J. N. Butt, A. Sucheta and F. A. Armstrong, *J. Amer. Chem. Soc.* **1991**, *113*, 8948.

[47] P. J. Vergamini, H. Vahrenkamp and L. F. Dahl, *J. Amer. Chem. Soc.* **1971**, *93*, 6327.

[48] W. A. Herrmann, A. Egli, E. Herdtweck, R. Alberto, F. Baumgärther, *Angew. Chem.* **1996**, *35*, 432.

[49] R. Andrés, M. Galakhov, A. Martín, M. Mena, *J. Chem. Soc. Chem. Commun.* **1995**, 551.

[50] L. E. Toth, *"Transition Metal Carbides and Nitrides"*; Academic Press:New York, 1971.

[51] a) L. Maya, *Inorg. Chem.* **1986**, *25*, 4213.
b) C. H. Winter, T. S. Lewkebandara, M. J. Heeg, J. W. Proscia, A. L. Rheingold, *Inorg. Chem.* **1994**, *33*, 1227.

Chapter 1

[52] A. Abarca, P. Gómez-Sal, A. Martín, M. Mena, J. M. Poblet, C. Yélamos, *Inorg. Chem.* **2000**, *39*, 642.

[53] H. W. Roesky, Y. Bai, M. Noltemeyer, *Angew. Chem. Int. Ed. Engl.* **1989**, *28*, 754.

[54] R. Andrés, M. Galakhov, A. Martín, M. Mena, C. Santamaría, *Organometallics* **1994**, *13*, 2159.

[55] a) M. Galakhov, M. Mena, C. Santamaría, *Chem. Commun.* **1998**, 691.
b) R. Andrés, M. Galakhov, P. Gómez-Sal, A. Martín, M. Mena, C. Santamaría, *Chem. Eur. J.* **1998**, *4*, 1206.

[56] a) M. García-Castro, A. Martín, M. Mena, A. Pérez-Redondo, C. Yélamos, *Chem. Eur. J.* **2000**, *6*, 647.
b) J. Gracia, A. Martín, M. Mena, M. Morales-Varela, J.-M. Poblet, C. Santamaría, *Angew. Chem. Int. Ed.* **2003**, *42*, 927.

[57] A. Abarca, A. Martín, M. Mena, C. Yélamos, *Angew. Chem. Int. Ed. Engl.* **2000**, *39*, 3460.

[58] A. Abarca, M. Galakhov, P. Gómez-Sal, A. Martín, M. Mena, J.-M. Poblet, C. Santamaría, J. P. Sarasa, *Angew. Chem. Int. Ed. Engl.* **2000**, 39, 534.

[59] L. L. Hegedus, R. W. McCabe, *"Catalyst Poisoning";* Marcel Dekker: New York, **1984**.

[60] a) A. J. Bard, *J. Photochem.* **1979**, *10*, 59.
b) A. J. Bard, *J. Phys. Chem.* **1982**, *86*, 172.
c) M. Gratzel, *Acc. Chem. Res.* **1981**, *14*, 376.

[61] a) G. S. Calabrese, M. S. Wrighton, *J. Am. Chem. Soc.* **1981**, *103*, 6273.
b) J. A. Baglio, G. S. Calabrese, D. J. Harrison, E. Kamieniecki, A. J. Ricco, M. S. Wrighton, G. D. Zoski, *J. Am. Chem. Soc.* **1983**, *105,* 2246.

[62] a) A. W. H. Mau, C. B. Huang, N. Kakuta, A. J. Bard, A. Campion, M. A. Fox, J. M. White, S. E. Webber, *J. Am. Chem. Soc.* **1984**, *106,* 6537.
b) S. Yanayida, K. Mizumoto, C. Fac, *J. Am. Chem.* Soc. **1986,** *108*, 647.

[63] a) J. Rawlings, S. K. Shah, J. R. Chisnell, W. J. Brill, R. Zimmerman, E. Munck, W. H. Orme-Johnson, *J. Biol. Chem.* **1978**, *253*, 1001**.**
b) **J.** LeGall, J. G. Maure, H. O. Jr. Peck, A. V. Xavier, *"Iron Sulfur Proteins";* Ed.: T. G. Spiro; Wiley: New York, **1982**; Vol. 4 .
c) S. P. Cramer, *Adv. Inorg. Bioinorg. Mech.* **1983**, *2*, 259.

[64] a) J. Wachter, *J. Coord. Chem.* **1987**, *15*, 219.
b) R. D. Adams, *Polyhedron* **1985**, *4*, 2003.
c) A. Muller, *Polyhedron* **1986**, *5*, 323.

[65] J. L. Vidal, R. A. Fiato, L. A. Cosby, R. L. Pruett, *Inorg. Chem.* **1978**, *17*, 2574.

[66] a) J. L. Vidal, W. E. Walker, *Znorg. Chem.* **1980**, *19*, 896.
b) L. A. Cosby, R. A. Fiato, J. L. Vidal, US. Patent **US. 4**, *115*, 433; *Chem. Abstr.* **1979**, *90,* 103385s.

[67] a) C. P. Kubiak, C. Woodcock, R. Eisenberg, *Inorg. Chem.* **1980**, *19*, 2733.

b) B. Bogdanovic, P. Gottsch, M. Rubach, Z. *Naturforsch. B* **1983**, *38*, 599.

[68] R. H. Holm, *Acc. Chem. Res.* **1977**, *10,* 427.

[69] a) G. Christou, G. D. Garner, F. E. Mabbs, *J. Chem. Soc., Chem. Commun.* **1978**, 740.

b) W. H. Armstrong, P. K. Mascharak, R. H. Holm, *J. Am. Chem. Soc.* **1982**, *104*, 4373.

[70] a) P. Grange, *Catal. Reu.-Sci. Eng.* **1980**, *21*, 135.

b) F. E. Massoth, *Adv. Catal.* **1978**, *27*, 265.

c) H. Topsoe, B. S. Clausen, *Catal. Reu.-Sci. Eng.* **1984**, *26*, 395.

[71] C. J. Casewit, D. E. Coons, L. L. Wright, W. K. Miller, M. Rakowski DuBois, *Organometakics* **1986**, *5*, 951.

[72] M. Rakowski Dubois, M. C. VanDerveer, D. L. DuBois, R. C. Haltiwanger, W. K. Miller, *J. Am. Chem. Soc.* **1980**, *102*, 7456.

[73] M. McKenna, L. L. Wright, D. J. Miller, L. Tanner, R. C. Haltiwanger, M. Rakowski DuBois, *J. Am. Chem. Soc.* **1983**, *105*, 5329.

[74] M. Rakowski DuBois, *J. Am. Chem. Soc.* **1983**, *105*, 3710.

[75] a) R. Weberg, R. C. Haltiwanger, J. C. V. Laurie, M. Rakowski DuBois, M. *J. Am. Chem. Soc.* **1986**, *108*, 6242.

b) D. E. Coons, R. C. Haltiwanger, M. Rakowski DuBois, *Organometallics* **1987**, *6*, 2417.

[76] J. C. V. Laurie, L. Duncan, R. C. Haltiwanger, R. T. Weberg, M. Rakowski DuBois, *J. Am. Chem. Soc.* **1986**, *108*, 6234.

[77] C. J. Casewit, r. C. Haltiwanger, J. Nordic, M. Rakowski DuBois, *Organometallics* **1985**, *4* ,119.

[78] P. J. Brothers, *Prog. Inorg. Chem.* **1980**, *28*, 1.

[79] P. Bernatis, r. C. Haltiwanger, M. Rakowski DuBois, *Organometallics* **1992**, *11*, 2435.

[80] B. R. James, *"In comprehensive Organometallic Chemistry"*; Eds: G. Wilkinson, F. G. A. Stone, E. W. Abel; Pergamon: New York, **1982**; *Vol. 8*, Chapter 51.

[81] K. I. Gell, J. Schwartz, *J. Am. Chem. Soc.* **1978**, *100*, 3246.

[82] J. Birnbaum, R. C. Haltiwanger, C. Teachout, K. Parker, P. Bernatis, M. Rakowski DuBois, *Organometallics* **1991**, *10*, 1779.

Chapter 1

2

Density functional methods.

The calculation of NMR shielding tensors

Current chemistry often seeks support from accurate theoretical predictions. The application of quantum mechanics to chemical problems, such as molecular structure, adduct's stability, species behaviour…, has made enormous progress via the Density Functional Theory (DFT). For instance, speak about theoretical studies of metallic aggregates imply speak about DFT methods. Theoretical studies involve the calculation of important properties like the NMR shielding tensor, one of the observables most frequently used in chemical applications.

This overview makes an effort to present DFT based methods respect other widely employed computational procedures; and additionally, DFT peculiar abilities for the computation of the NMR shielding tensor. In Section 2.1 an introduction to the current situation of DFT based methods and to the calculation of NMR shielding tensors is presented. Dr. John MacGrady of the University of York, during a stay in his group, planted a comparative of DFT methods with the rest of computational schemes in terms of electron correlation; Section 2.2 is an assimilation of this lesson. In Section 2.3, general aspects of the evaluation of the NMR spin-Hamiltonian parameters from the exact electronic wave function are considered, unravelling the physical contributions to the shielding tensor based on Ramsey description. Section 2.4 shows the evaluation of NMR parameters from approximate wave functions, and Section 2.5 reports the particularities for the DFT methods. A resume of the diverse factors that affects the final result in the evaluation of the NMR parameters are exposed in Section 2.6. Finally, Section 2.7 is dedicated to show some example systems treated during the realization of this memory, and studied from the acquired knowledge.

2.1	**Introduction**
2.2	**Electron correlation and DFT**
2.3	**The NMR spin Hamiltonian**
2.4	**Variational perturbation theory for the calculation of NMR parameters**
2.5	**Density functional calculations of NMR chemical shifts**
2.6	**Review of the factors to take into account in the computing of shielding tensors from approximate wave functions**
2.7	**[183]W NMR shielding tensor in polyoxometalate compounds**

2.1   Introduction

Most of our calculations, for the chemical problems planted during this thesis, have been made by means of DFT methods[1,2] with pure functionals. Density functional theory is a tangible and versatile computational method that has been employed successfully to obtain thermochemical data, molecular structures, force fields and frequencies, assignments of NMR, photoelectron, ESR, and UV spectra, transition-state structures, as well as activation barriers, dipole moments, and other electron properties.[3] This suitability motivates an increasing general interest in DFT, founded in the accuracy and computational experience of the method.[4,5]

The computing time in DFT, for a system of many atoms with no geometric symmetries, grows roughly like N_{at}^2 or N_{at}^3. This is much better than traditional methods, where computing time grows as $e^{aN_{at}} (a \simeq 1)$. Favourable scaling yields a computational cost comparable to a self-consistent field (SCF) calculation, with quality of results equalling second-order Moller-Plesset (MP$_2$) calculations[6] in areas ranging from closed-shell geometries of molecules and transition states,[7] heats of formation,[8] spectroscopic properties,[9] and gas-phase acidities.[10]

In this sense, DFT methods allow accurate calculations on systems that cannot be easily treated by standard methods beyond Hartree-Fock. In areas requiring extensive electron correlation, such as structures involving transition metals or open-shell species, the results from DFT calculations are often in better agreement with the available experimental data and highly correlated molecular orbital (MO) calculations than HF or MP$_2$

calculations.[11] This makes DFT an attractive alternative to very costly-coupled cluster (CC)[12] and quadratic configuration interaction (QCI)[13] methods. Another, equally important feature is the inclusion of relativistic effects. Relativistic effects become important for any chemical feature of heavy elements[14] or for light atoms bonded directly to a heavy atom.

Progress in the last five years on modelling such difficult problems, as metal-mediated enzyme kinetics, has been faster than it was imagined because of DFT for large ligand saturated systems is more reliable than could have been expected from results on small unsaturated metal centres.[15] Today, computational transition metal chemistry is almost synonymous with DFT for medium-sized molecules, and is the only viable approach to understanding reactions with realistic ligands.[16]

Not all is good in DFT methods, we should keep in mind that although DFT has a rigorous base, in application is semi-empirical and there is no way to systematically converge to exact results.[17] This contrasts with conventional ab initio approaches, for which we can estimate a priori the quality of a calculation by improving the correlation treatment.

DFT does have some problematic areas,[18] perhaps most notably is a tendency to overestimate delocalisation.[19] This bias is usually quite benign for neutral species, yielding energies of formation 1-2 kcal mol^{-1} too low,[20] as compared to experiment. In some cases, this is enough to overcome a small steric influence; and thus, predict an erroneous geometry as the minimum energy conformer instead of the correct.[21] DFT usually does not treat properly systems with only one electron (exchange correlation energy is different than cero),[22] systems with weak bonds like van der Waals complexes, or charge transfer complexes.[23]

Ab initio calculations of the electronic, magnetic, and optical properties associated with the responses of a molecular electronic system to perturbations such as magnetic and electronic moments have been efficiently considered in recent years. The shielding tensor of nuclear magnetic resonance (NMR) spectroscopy is probably one of the most important second-order properties.[24,25] At the same time, it still represents a test to theoretical methods.

Nuclear magnetic resonance (NMR) shielding tensors are known to be sensitive to everything. On the experimental side, this appears to be the reason that NMR may be considered the single most important spectroscopy technique for chemistry and beyond.[26] Indeed, information regarding, e. g., the molecular structure (geometry), chemical environment, intra- and intermolecular bonding, composition, or dynamic processes is routinely extracted from experimental NMR spectra.

This same sensitivity to everything has considerable challenges for the theoretical chemistry if it attempts to describe NMR parameters based on first principle quantum mechanics. The theoretical description of NMR chemical shifts based on ab initio techniques has seen a tremendous development;[27] thus, in the past two decades it has become possible to carry out accurate NMR shielding calculations routinely.[28]

In particular, the application of density functional theory to the shielding tensor of nuclear magnetic resonance spectroscopy has recently seen a strong interest.[29] The combination of accuracy and speed makes DFT the only available first principle method for the important field of NMR in metal complexes.[30]

The rising interest is also conceptual, motivated because approximate quantum chemical methods need performance tests for their validation. This is particularly true for the modern tools of density functional theory, as the extent of success or failure of a given density functional is hard to estimate beforehand. Experience regarding the performance and reliability of the various flavours of DFT is being accumulated rapidly.[31] The present-day gradient-corrected (GGA) or hybrid functionals are robust enough,[32] structures and energies, as well as vibrational and NMR spectroscopical properties of transition metal complexes can be computed and predicted with reasonable accuracy. Transition-metal NMR chemical shifts have proven to be quite sensitive to the specific density functional employed, and are thus a particularly stringent test for the quality of the latter. Regarding metal complexes, NMR calculations have been done both on light ligand nuclei and on the heavy nuclei proper. Examples in the latter category include studies on the metal NMR shieldings and chemical shifts of compounds containing the chromium (^{53}Cr) and molybdenum (^{95}Mo/^{97}Mo),[33] iron[34] (^{57}Fe), cobalt[35] (^{59}Co), selenium[36] (^{77}Se), zirconium[37] (^{91}Zr), rhodium[38] (^{103}Rh), tellurium[39] (^{125}Te), lead[40] (^{207}Pb) and tungsten

(^{183}W),[41] platinum[42] (^{195}Pt), mercury[43] (^{199}Hg), and uranium[44] (^{235}U) nuclei among others.

Calculations shall be used to rationalize certain trends in the NMR shieldings. This will be achieved by using an analysis of the chemical shift in terms of the calculated electronic structure. The ability to perform such an analysis is one particular strength of theory, and of the DFT-GIAO method in particular.

The direct result of a theoretical NMR calculation is the absolute shielding; the transformation between absolute shieldings and the experimental chemical shifts involves the computation of the shielding of a reference compound for the given nucleus (e.g., tetramethylsilane, for ^{1}H, ^{13}C, and ^{29}Si). Especial attention requires the reference; hence, any error made in the calculation of the reference compound is carried through to the chemical shifts.

2.2   Electron correlation and DFT

The crucial complication in all electronic structure calculations is the presence of the electron-electron potential energy. If we suppose an ideal system of independent electrons that would be obtained if this complicating feature were neglected; the system wave function Ψ° can be solved and is a solution of

$$H^{\circ}\Psi^{\circ}=E^{\circ}\Psi^{\circ}\,;\ \left\{-\frac{\hbar^2}{2m}\sum_a\nabla_a^2-\frac{e^2}{4\pi e_o}\sum_a\frac{z}{r_a}\right\}\Psi^{\circ}=E^{\circ}\Psi^{\circ}\,.$$

This n-electron equation can be separated into n one-electron equations; $H^{\circ}=\sum_{a=1}^{n}h_a$, so we can immediately write Ψ° as a product of one-electron wave functions, the Hartree product,

$$\Psi^{\circ}=\prod_{a=1}^{n}f_a\,.$$

Chapter 2

By using variational theory we can obtain the best solution for the real Hamiltonian, including the electron-electron potential energy, for a given form of the wave function. In the Hartree method,[45] a Hartree product of spin orbitals is proposed as solution for the real Hamiltonian. The best one minimizes the electronic energy

$$E^{\circ} = \sum_a \left\langle f_a^* \left| -\frac{\hbar^2}{2m}\nabla_a^2 - \frac{e^2}{4pe_o}\sum_A \frac{Z_A}{r_{aA}} \right| f_a \right\rangle + \frac{1}{2}\frac{e^2}{4pe_o}\sum_a^N\sum_b^N \left\langle f_a f_a \left| \frac{1}{r_{ab}} \right| f_b f_b \right\rangle ;$$

and the best spin orbital for this equation is solution of the Hartree differential equation

$$h_1 f_a + \frac{e^2}{4pe_o}\sum_{b\neq a}\left[\int dx_2 \left| f_b \right|^2 \frac{1}{r_{12}} \right] f_a = e_a f_a ; \quad \left[h_1 = -\frac{\hbar^2}{2m}\nabla_1^2 - \frac{e^2}{4pe_o}\sum_A \frac{Z_A}{r_{1A}} \right],$$

simplifying

$$\left[h_1 + \sum_{b\neq a} J_b \right] f_a = e_a f_a .$$

Here h_1 includes the electron kinetic energy plus the nucleus electron attractions, and J_b is the Coulomb operator; which represents the classical Coulombic interactions between electrons

$$J_{ab} = \int f_a^*(1) J_b f_a^*(1) dt_1 = \frac{e^2}{4pe_o}\int f_a^*(1)f_b(2)\left(\frac{1}{r_{12}}\right)f_b^*(2)f_a(1)\, dt_1 dt_2 .$$

For the Hartree method, we can identify for all contributions to the energy a classical interpretation of the corresponding implicated interaction, so we associate

$$E_{Hartree} = E_{Classical} .$$

UNIVERSITAT ROVIRA I VIRGILI
DFT STUDY OF TITANIUM CUBANE AND MOLYBDENUM SULPHIDE COMPOUNDS.
Autor: José Manuel Gracia Budria
ISBN: 978-84-690-6751-2 / DL: T.1196-2007

Density functional methods. The calculation of NMR shielding tensors

If we now take into account that the electronic wave function must obey the Pauli principle, from the Hartree products, the overall wavefuntion is the following Slater determinant

$$\Psi^\circ = (n!)^{-\frac{1}{2}} \det \left| \boldsymbol{f}_a(1) \boldsymbol{f}_b(2) ... \boldsymbol{f}_t(n) \right| ;$$

in the Hartree-Fock (H-F) method[46,47] the best n-electron determinantal wave function is sought for the non-independent electronic Schrödinger equation. The Hartree-Fock equation for a spin orbital $\boldsymbol{f}_a$ occupied by electron 1 is

$$\left\{ h_1 + \sum_{b \neq a} (J_b - K_b) \right\} \boldsymbol{f}_a(1) = \boldsymbol{e}_a \boldsymbol{f}_a(1).$$

Relative to the Hartree model appears the exchange operator, K_b

$$K_{ab} = \int \boldsymbol{f}_a^*(1) K_b \boldsymbol{f}_a^*(1) d\boldsymbol{t}_1 = \frac{e^2}{4\boldsymbol{pe}_o} \int \boldsymbol{f}_a^*(1) \boldsymbol{f}_b^*(2) \left(\frac{1}{r_{12}} \right) \boldsymbol{f}_a(2) \boldsymbol{f}_b(1) d\boldsymbol{t}_1 d\boldsymbol{t}_2.$$

This operator takes into account the effects of the spin correlation, a non-classical interaction between same spin electrons.

It will be useful for our analysis to divide the H-F energy into the classical kinetic energy plus coulombic interactions, and the non-classical exchange energy, E_X

$$E_{HF} = E_{Classical} + E_X .$$

Taking as reference the H-F model, Löwdin in 1959[48] defines the correlation energy, E_c, as the difference between the H-F energy and the lowest energy for a full basis set[49]

$$E_C = E_{Exact} - E_{HF} .$$

We now introduce and establish a formal separation of the exact energy, E_{Exact}, like sum of a classical energy term, exchange and correlation contributions

$$E_{Exact} = E_{Classical} + E_X + E_C.$$

This energy description is a useful definition to compare not only same origin molecular quantum methods but Hartree model based methods, Perturbation Theory and DFT methods.

2.2.1 Comparing methods

2.2.1.1 Models based on Hartree method

From Löwdin definition, it is clear that for methods based on Hartree model going beyond H-F method implies treating correlation energy. We can identify two different effects in electron correlation, Sinanoglu, 1964.[50] The first is the influence of other configurations which are low-lying in energy, and that mix strongly with the H-F configuration. This gives rise to the non-dynamical correlation, which can be usually dealt with by multiconfigurational SCF techniques. Non-dynamical correlation is often small in closed-shell molecules near their equilibrium geometry, but increases enormously in importance as a molecule is distorted and bonds are formed or broken. It can also be important in open-shell systems like excited states or transition metals. The second, dynamical correlation arises from the r_{ab}^{-1} term in the Hamiltonian operator. This term is singular as $r_{ab} \to 0$, and mathematical studies of the properties of exact wave functions show that they must contain cusps in r_{ab} to cancel this singularity. Hence treating dynamical correlation requires describing this cusp behaviour.[51]

It should be understood that there is no sharp dividing line between nondynamical and dynamical correlation, and methods for treating one will undoubtedly account in some part for the other; but it is usually most efficient to use different techniques for each, however.

<u>Non-dynamical correlation</u>

Multiconfigurational SCF

There are two popular ways of accounting for non-dynamical correlation. The first is to explicitly include several configurations in the SCF procedure: multiconfigurational SCF (MCSCF) methods.[52] The user selects a set of chemically important active MOs and the MCSCF configurations are defined as a full configuration interaction within that space.

UHF

The second approach is to ignore the spin symmetry of the wave function and use unrestricted Hartree-Fock (UHF) as the single configuration description[53] (the UHF comprises one spin-orbital for each electron).

There is an attractive simplicity about UHF, no active orbitals to identify, and so forth. However, where non-dynamical correlation would be important in an RHF-based treatment, the UHF method will suffer from severe spin-contamination, while where non-dynamical correlation is not important the RHF solution may be lower in energy.

<u>Dynamical correlation</u>

CI

Configuration interaction is probably the oldest treatment for recovering dynamical correlation.[54] We simply generate a list of configurations and use them in a linear variational calculation. A common way of constructing the configurations is to classify them relative the H-F configuration Ψ_o

$$\Psi_{CI} = C_o \Psi_o + \sum_i \sum_a \Psi_i^a C_i^a + \sum_{i>j} \sum_{a>b} \Psi_{ij}^{ab} C_{ij}^{ab},$$

here i, j … index MOs occupied in Ψ_o, while a, b … index MOs unoccupied in Ψ_o, and Ψ_{ij}^{ab} denotes a configuration obtained by exciting two electrons in MOs i and j to MOs a and b.

If all levels of excitation up to N-fold are used for an N-electron system we have a full CI wave function. If this is done for a complete (infinite) one-particle basis we have a complete CI expansion of the exact wave function. In practice the expansion must be truncated.

Perturbation theory

There are several different approaches to the use of perturbation theory in treating dynamical correlation. Møller-Plesset (MP) perturbation theory has been doing dominant.

The simplest level, MP_2, is probably the cheapest available treatment of the dynamical correlation. A comparison between perturbation theory and truncated CI methods is not easy, because the latter include some terms effectively to infinite order, but obviously omit some other terms in lower orders.

Neither MP_2 nor superior MP_3 are entirely satisfactory; these implicitly require the first order wave function, which involves only double excitations. MP_4 is carried out until quadruple excitations. MP_5 and higher orders are lithely to be impractically expensive.

One area in which CI methods appear to be thoroughly superior to perturbation theory is in the treatment of multireference problems: problems with substantial non-dynamical correlation effects.

Coupled-Clusters methods

Coupled-Clusters methods[55] are infinite order nonlinear treatments that can be related to CI methods as follows. We rewrite the CI expansion formally us

$$\Psi_{CI} = (1 + C_1 + C_2 + ...)\Psi_o,$$

employing not the linear formulation, but the following exponential approach

$$\Psi_{CC} = \exp(T)\Psi_o$$

which we can expand as

$$\Psi_{CC} = (1 + T_1 + T_2 + T_1^2 + T_1 T_2 + T_2^2 + T_3 ...) \Psi_o \ .$$

If we employ all levels of excitation, up to N-fold, the wave function is equivalent to a full CI wave function.

The formulation is considerably more complicated because of the nonlinear terms. However, it is more practical to truncate at some finite order. A fixed excitation level of couples cluster treatment is not substantially more expensive than the same excitation level of CI calculation, but the results are generally superior because of the inclusion of the effects of disconnected clusters ($T_1^2, T_1 T_2, T_2^2$, coefficients products of amplitudes of connected clusters).

Coupled-Clusters methods can also be related to perturbation theory, it is possible to obtain MP_2 and MP_3 energies as a by-product of a CCSD calculation (CC including simple and double excitations). For example we note that taken all degrees of excitation in CI and CC, or infinite order of perturbation theory all three approaches will give the same answer.

The CI energy is obtained from a variational calculation and is thus an upper bound to the exact energy. Since neither the perturbation theory energy nor the coupled-cluster energy is variational, neither is an upper bound.

CC treatment of any number of non interacting subsystems of any size will give an answer that is the sum of the subsystems. This is true of perturbation theory too, but it is not generally true of truncated CI. This suggests caution in the application of CI methods to systems with more than a few electrons; the scaling errors grow rapidly.

2.2.1.2 DFT based methods

DFT is a theory, in principle exact, of electronic structure based on the electron distribution, $r(r)$. We shall now sketch the fundamentals of DFT.[56] We limit ourselves here to the simplest class of systems, n

Chapter 2

nonrelativistic, interacting electrons in a nonmagnetic state with Hamiltonian, in atomic units

$$H = T + V + U \;;$$

$$T = -\frac{1}{2}\sum_a \nabla_a^2 \;,\; V = \sum_a v(r_a) \;,\; U = -\frac{1}{2}\sum_{a \neq b}\frac{1}{|r_a - r_b|} \;.$$

The starting point of DFT is the rigorous, simple lemma of Hohenberg and Kohn (HK).[57] The specification of the ground state density, $r(r)$, determines the external potential v(r) uniquely (to within an additive constant (C)

$$r(r) \rightarrow v(r) \;\text{(Unique)}.$$

Since $r(r)$ also determines N by integration, it determines the full Hamiltonian H. With the help of this lemma, a variational principle for the energy as functional of $r(r)$ can be derived. We can express the energy value for an electron and N nuclei system as function of the first order density matrix and of the pair density γ.

$$E_{el} = \int_{r'_1 = r_1}\left(-\frac{1}{2}\nabla^2(1) + v(1)\right)r(r_1, r'_1)dr_1 + \frac{1}{2}\iint \frac{g_2(r_1, r_2)}{|r_1 - r_2|}dr_1 dr_2 \;.$$

The exchange correlation hole $r_{XC}(r_1, r_2)$ it is defined from the expression

$$g_2(r_1, r_2) = r(r_1)r(r_2) + r(r_1)r_{XC}(r_1, r_2),$$

the $r(r_1)r(r_2)$ term is the probably of finding an electron in r_1 and other in r_2, considering the electrons as independent particles, not correlated; $r_{XC}(r_1, r_2)$ is a correction term of the no conditional probability to obtain the conditional one. It is a region around the electron in which the presence of other electrons is more or less excluded.

UNIVERSITAT ROVIRA I VIRGILI
DFT STUDY OF TITANIUM CUBANE AND MOLYBDENUM SULPHIDE COMPOUNDS.
Autor: José Manuel Gracia Budria
ISBN: 978-84-690-6751-2 / DL: T.1196-2007

Density functional methods. The calculation of NMR shielding tensors

The pair density is the sum of four contributions, $\boldsymbol{g}_2\left(r_1,r_2\right)=\boldsymbol{g}_2^{aa}\left(r_1,r_2\right)+\boldsymbol{g}_2^{ab}\left(r_1,r_2\right)+\boldsymbol{g}_2^{ba}\left(r_1,r_2\right)+\boldsymbol{g}_2^{bb}\left(r_1,r_2\right)$, so our exchange correlation hole is also divided in four terms

$$\boldsymbol{g}_2^{aa}\left(r_1,r_2\right)=\boldsymbol{r}^a\left(r_1\right)\boldsymbol{r}^a\left(r_2\right)+\boldsymbol{r}^a\left(r_1\right)\boldsymbol{r}_{XC}^{aa}\left(r_1,r_2\right)$$

$$\boldsymbol{g}_2^{ab}\left(r_1,r_2\right)=\boldsymbol{r}^a\left(r_1\right)\boldsymbol{r}^b\left(r_2\right)+\boldsymbol{r}^a\left(r_1\right)\boldsymbol{r}_{XC}^{ab}\left(r_1,r_2\right)$$

$$\boldsymbol{g}_2^{ba}\left(r_1,r_2\right)=\boldsymbol{r}^b\left(r_1\right)\boldsymbol{r}^a\left(r_2\right)+\boldsymbol{r}^b\left(r_1\right)\boldsymbol{r}_{XC}^{ba}\left(r_1,r_2\right)$$

$$\boldsymbol{g}_2^{bb}\left(r_1,r_2\right)=\boldsymbol{r}^b\left(r_1\right)\boldsymbol{r}^b\left(r_2\right)+\boldsymbol{r}^b\left(r_1\right)\boldsymbol{r}_{XC}^{bb}\left(r_1,r_2\right)$$

where $\boldsymbol{r}_{XC}^{aa}\left(r_1,r_2\right)$ and $\boldsymbol{r}_{XC}^{bb}\left(r_1,r_2\right)$ are the Fermi Hole and represent the space region in which the presence of an electron of the same spin is more or less excluded.

$\boldsymbol{r}_{XC}^{ab}\left(r_1,r_2\right)$ and $\boldsymbol{r}_{XC}^{ba}\left(r_1,r_2\right)$ are the Coulomb holes and they would give us the region in which the presence of a $\boldsymbol{b}$ ($\boldsymbol{a}$) electron is favoured or excluded if we have a reference $\boldsymbol{a}$ ($\boldsymbol{b}$) electron in r_1.

Now we define a variational principle

$$E_{v(r)}[\boldsymbol{r}(r)]\geq E_{v(r)}[\boldsymbol{r}_o(r)]=E$$

where $\boldsymbol{r}_o(r)$ and E are the density and energy of the ground state. We extract the largest and elementary contributions

$$E_{el}=E_{el}^a+E_{el}^b,$$

$$E_{el}^{a(b)}=E_v\left[\boldsymbol{r}^{a(b)}\right]=T\left[\boldsymbol{r}^{a(b)}\right]+\int\boldsymbol{r}^{a(b)}(r)v(r)dr+J\left[\boldsymbol{r}^a,\boldsymbol{r}^b\right]+E_{xc}\left[\boldsymbol{r}^a,\boldsymbol{r}^b\right]$$

$T[\boldsymbol{r}(r)]$ is the kinetic energy,

$\int\boldsymbol{r}(r)v(r)dr$ is the classical interaction with the external potential $v(r)$,

Chapter 2

$J\left[\boldsymbol{r}^a, \boldsymbol{r}^b\right]$ is the classical coulomb repulsion between not correlated electron clouds,

$E_{xc}\left[\boldsymbol{r}^a, \boldsymbol{r}^b\right]$ is the so-called exchange correlation energy.

The system can be transformed into a new set of self-consistent, so-called Kohn-Sham or KS, equations[58] defining $\boldsymbol{r}(r) = \sum_{i=1}^{n} |\boldsymbol{c}_i(r)|^2$

$$(-\frac{1}{2}\nabla^2 + v(r) + \int \frac{\boldsymbol{r}(r')}{|r-r'|} + v_{XC}(r) - \boldsymbol{e}_j)\, \boldsymbol{c}_j(r) = 0$$

$$v_{XC}(r) = \frac{\partial E_{XC}[\boldsymbol{r}(r)]}{\partial \boldsymbol{r}(r)}.$$

The only error in the theory is due to approximations of E_{XC}. The ground state energy is given by

$$E_{el}^{a(b)} = E_v\left[\boldsymbol{r}^{a(b)}\right] = T_S\left[\boldsymbol{r}^{a(b)}\right] + \int \boldsymbol{r}^{a(b)}(r)v(r)\,dr + J\left[\boldsymbol{r}^a, \boldsymbol{r}^b\right] + E_{xc}\left[\boldsymbol{r}^a, \boldsymbol{r}^b\right]$$

where

$$T_s\left[\boldsymbol{r}^{a(b)}\right] = \sum_{i=1}^{n_{a(b)}} \left\langle \boldsymbol{c}_i \left| -\frac{1}{2}\nabla^2 \right| \boldsymbol{c}_i \right\rangle,$$

$$J\left[\boldsymbol{r}^a, \boldsymbol{r}^b\right] = \frac{1}{2}\iint \frac{\boldsymbol{r}^{a(b)}(r_1)\,\boldsymbol{r}^{a(b)}(r_2)}{|r_1 - r_2|}\, dr_1 dr_2 + \frac{1}{2}\iint \frac{\boldsymbol{r}^{a(b)}(r_1)\,\boldsymbol{r}^{b(a)}(r_2)}{|r_1 - r_2|}\, dr_1 dr_2\,,$$

$$E_{XC}\left[\boldsymbol{r}^a, \boldsymbol{r}^b\right] = \frac{1}{2}\int \boldsymbol{r}^{a(b)}(r_1)\,dr_1 \int \frac{\boldsymbol{r}_{XC}^{aa(bb)}(r_1, r_2)}{|r_1 - r_2|}\, dr_1 dr_2 +$$

$$\frac{1}{2}\int \boldsymbol{r}^{a(b)}(r_1)\,dr_1 \int \frac{\boldsymbol{r}_{XC}^{ab(ba)}(r_1, r_2)}{|r_1 - r_2|}\, dr_1 dr_2.$$

It is striking, if E_{XC} is ignored, the physical content of the DFT model becomes identical to that of the Hartree approximation. Continuing the comparison, at H-F level for which the wave function is represented only by one slater determinant

$$r_{XC}^{aa}\left(r_1,r_2\right)=r_{XC}^{bb}\left(r_1,r_2\right)\neq 0 \text{ and } r_{XC}^{ab}\left(r_1,r_2\right)=r_{XC}^{ba}\left(r_1,r_2\right)=0 \,,$$

we do not have electronic correlation between same spin electrons. So we can identify

$$E_X\left[r^{a(b)}\right]=\frac{1}{2}\int r^{a(b)}\left(r_1\right)dr_1\int\frac{r_{XC}^{aa(bb)}\left(r_1,r_2\right)}{\left|r_1-r_2\right|}dr_1dr_2 \,,$$

as the exchange energy, and

$$E_C\left[r^a,r^b\right]=\frac{1}{2}\int r^{a(b)}\left(r_1\right)dr_1\int\frac{r_{XC}^{ab(ba)}\left(r_1,r_2\right)}{\left|r_1-r_2\right|}dr_1dr_2$$

as the correlation energy.

DFT methods take into account, at least in part, the most difficult electron correlation energy

$$E_{Exact}^{DFT}=E_{Classical}^{DFT}+E_X^{DFT}+E_C^{DFT} \,.$$

The approximation is made starting from a singledeterminantal density and adapting the Hamiltonian to obtain the real density, like MP_n or UHF methods. We are including mainly the dynamical term to the correlation energy and the precision depend on the $E_{XC}[r(r)]$ approximation.

The simplest, and at the same time serviceable, $E_{XC}[r(r)]$ approximation, is the LSDA

$$E_{XC}^{LDA}[r(r)]=\int e_{XC}[r(r)]r(r)dr \,,$$

Chapter 2

where e_{XC} is the exchange-energy per particle of a uniform interacting electron gas of density $r(r)$.

The KS orbitals in the LSDA are usually very close to HF orbitals. The severe overbinding character of the LSDA is a disappointing extension of the LSDA. Include local spin-density gradients is the next logical step, the so-called generalized gradient approximations

$$E_{XC}^{GGA} = \int f(r(r), |\nabla r(r)|) dr .$$

To summarize, the LSDA generally gives good molecular structures, vibrational frequencies, and charge densities[59,60] in strongly bound systems. It is not useful, however, for thermo-chemistry. GGA, on the other hand, yield good thermo-chemistry, with average errors of order 6 kcal mol^{-1} in standard thermochemical test.[61] It is at the level of the weakest chemical interactions, namely Vander Waals interactions that GGA apparently fail.[62] Also, both the LSDA and the GGA leave much room for improvement in predicting reactions barrier heights.[63,64]

Exchange energy

The exchange energy takes the simple asymptotic form

$$E_X = \frac{1}{2} \int \frac{r}{r} dr ; \ r \rightarrow \infty .$$

An exchange GGA has been found[65] that exactly reproduce this asymptotic exchange energy behaviour

$$E_X = E_X^{LDA} - b \sum_s \int r_s^{\frac{4}{3}} \frac{c_s^2}{(1 + 6b c_s \sinh^{-1} c_s)} dr$$

$$E_X^{LSDA} = -\frac{3}{2} (\frac{3}{4p})^{\frac{1}{3}} \sum_s \int r_s^{\frac{4}{3}} dr , \ c_s = \frac{|\nabla r_s|}{r_s^{\frac{4}{3}}}$$

b semiempirical fitted parameter.

This functional is effectively an interpolation formula between the small– and large- c limits of the exchange energy density.

Correlation energy

Correlation energy is a very difficult problem; ground state density functional approximations have traditionally made serious errors in the correlation energy for realistic inhomogeneous systems. The LDA approximations overestimates, the correlation energy by 100%. At GGA level, the most popular "dynamical correlation" functionals presently are those of Lee, Yang, and Parr[66], Perdew 1986[67], and Perdew and Wang 1991.[68] Fortunately, the chemical consequences of gradient corrections for correlation are relatively small compared to their exchange counterparts.[69] The specific choice of exchange and correlation functional is much less important than the differences between the LSDA and GGA themselves.

Both the LSDA and the GGA are based on localized model exchange-correlation holes. Only local density information (or local density gradient information) is utilised at each reference point. Ordinary chemical bonds, exchange correlation holes undoubtedly have a small nonlocal component. Proposals to incorporate nonlocality into DFT chemistry[70] have spawned a new class of Hybrid HF/GGA theories with precision surpassing that of pure GGA. They are motivated by the adiabatic connection for the exchange-correlation hole in Kohn-Sham DFT

$$h_{XC}(r,r\acute{}) = \int_{0}^{1} h_{XC}^{l}(r,\acute{r})dl \ .$$

Where the hole generates E_{XC} though the following double integration

$$E_{XC} = \frac{1}{2} \iint \frac{r(r)}{r_{12}} h_{XC}(r,\acute{r})drdr\acute{} .$$

This $h_{XC}^{l}(r,r\acute{})$ equation connects the Kohn-Sham independent-particle reference system ($l = 0$) with the real, fully interacting system ($l = 1$)

Chapter 2

trough a coupling strength parameter l. At $l = 0$ in this independent particle limit, $h_{XC}^{l}(r, r')$ is the pure and exact exchange hole of the Kohn-Sham Slater determinant (no $r(r)$ dependence). This hole is poorly represented by localized LSDA or GGA models in molecular bonds, and hence the small-l region of the coupling strength integration is problematic. A simple but effective cure for the $l = 0$ problem is replacement of the model GGA hole at $l = 0$ with the exact hole, resulting in the following exchange-correlation expression[71]

$$E_{XC} = E_{XC}^{DFT} + a_o (E_X^{EXACT} - E_X^{DFT}),$$

the parameter a_o reflects the importance of nonlocality in the real exchange-correlation hole. In current practice, it is fit to experimental thermochemical data, taking values of 20% or higher depending on the choice of correlation GGA. This kind of exact-exchange mixing reduce average bond energy errors from about 6 kcal mol[1] for pure GGAs to roughly 2 kcal mol[1]. Improvements are particularly striking in nonhydride and multiple bonds, where GGAs suffer overbinding errors as high as 20 kcal mol[1]. Reaction barrier heights are also improved by exact-exchange mixing,[64] thought a thorough study of this important area remains to be undertaken. From the presented overview, DFT is formally exact formulation take into account all the contribution to the energy but into an approximate way that depends on the XC functional.

2.2.2   Comparative table

The real objective of this summary of different methods is to place and to establish a reference for the utilised theoretical schemes. We can compare different procedures if we have common starting points; a knowing of what we are treating in a determinate theoretical procedure respect these common starting points shall let us compare the model with the rest of treatments.

Mostly we are interested into helping to situate DFT based methods respect the other approximations. A comparative scheme between the features included for the different exposed methods is presented in Table 2.1.

Table 2.1. *Comparative table of the treated energy terms for some fundamental theoretical schemes*

Method	$E_{Kinetic}$	$E_{Coulomb}$	E_X	E_C Non-dynamical	Dynamical
Hartree	++	++	-	-	-
ROHF	++	++	++	-	-
UHF	++	++	++	+	-
MCSCF	++	++	++	++	-
CI	++	++	++	+	+
MP_N	++	++	++	+	+
CC	++	++	++	+	+
PURE DFT	++	++	+	+	+
HYBRID DFT	++	++	++	+	+
FCI, CC_∞, MP_∞	++	++	++	++	++

++ Energy term included completely
+ Energy term partially treated
- Not treated

2.3   The NMR spin Hamiltonian

2.3.1   Shielding tensor

At a nucleus is applied an external magnetic field B^{ext}, this is shielded by the electrons moving around the nucleus. The effective field that the nucleus experiences can be written as[72]

$$B^{eff} = B^{ext}\left(1-\overline{\boldsymbol{s}}\right),$$

where $\overline{\boldsymbol{s}}$ is the nuclear magnetic shielding tensor.

The energy levels studied in NMR spectroscopy are the spin eigenstates of chemically bonded nuclei in the presence of an external magnetic field. In

Chapter 2

practice one usually measures the chemical shift $\boldsymbol{d}$, which is related to the resonance frequencies of the sample $\boldsymbol{n}_s$ and of a reference sample $\boldsymbol{n}_{ref}$

$$\frac{\boldsymbol{d}}{ppm} = 10^6 \left(\frac{\boldsymbol{n}_s - \boldsymbol{n}_{ref}}{\boldsymbol{n}_{ref}} \right)$$

The resonance frequencies are determined by the Zeeman splitting caused by the interaction of the B^{eff} with the nuclear magnetic moment. Since a resonance frequency $\boldsymbol{n}$ is linear with $1 - \boldsymbol{s}$, where $\boldsymbol{s}$ is the isotropic shielding $\mathrm{Tr}(\overline{\boldsymbol{s}})/3$, the chemical shift will be, for small shieldings ($\boldsymbol{s} \ll 1$),

$$\frac{\boldsymbol{d}}{ppm} = 10^6 \left(\boldsymbol{s}_{ref} - \boldsymbol{s}_s \right).$$

The molecular properties responsible of the generation of NMR spectra, were identified over 50 years ago by Ramsey.[73,74] The obtained physical contributions to the NMR shielding tensor remaining valid independently of the computational method.

The main features of NMR spectra may be satisfactorily accounted for by the solution of the energy equation of an effective spin-hamiltonian[75] where the electrons do not appear at all, and where the nuclei are represented by their intrinsic spins and their associated magnetic moments

$$H = -\sum_K \boldsymbol{g}_K \hbar B^T \left(1 - \overline{\boldsymbol{s}}_K \right) I_K + \frac{1}{2} \sum_{K \neq L} \boldsymbol{g}_K \boldsymbol{g}_L \hbar^2 I_K^T \left(\overline{D_{KL}} + \overline{K_{KL}} \right) I_L$$

where

$\boldsymbol{g}_K$ = nuclear magnetogyric ratio ;

I_K = nuclear spin operator; nuclear magnetic dipole moment $M_K = \boldsymbol{g}_K \hbar I_K$;

$\overline{\boldsymbol{s}}_K$ = nuclear magnetic shielding tensor, describe the magnetic shielding consequence of the electrons ;

B^T = applied magnetic field (T :: Transpose);

Density functional methods. The calculation of NMR shielding tensors

$\overline{D_{KL}}$ = classical dipolar interactions, describe the direct couplings of the nuclear magnetic dipole moments;

$\overline{K_{KL}}$ = indirect nuclear spin-spin coupling tensor, describe the indirect couplings of the nuclear dipoles, mediated by the surrounding electrons.

For a rapidly tumbling molecule, we must carry on a rotational average of the spin Hamiltonian. Then it turns out that the direct spin-spin coupling constants, $\overline{D_{KL}}$, vanish but that the indirect couplings, $\overline{K_{KL}}$, do not. So for a rotating molecule in an isotropic medium, the NMR spin Hamiltonian may thus be written in the form

$$H_{iso} = -\sum_{K} M_K \left(1 - \boldsymbol{s}_K\right) B + \frac{1}{2} \sum_{K \neq L} M_K M_L K_{KL} \; ;$$

where the nuclear shielding constants $\boldsymbol{s}_K$ and the reduced indirect nuclear spin-spin coupling constants K_{KL} link to the corresponding tensors as $\boldsymbol{s}_K = \frac{1}{3} Tr \overline{\boldsymbol{s}_K}$ and $K_{KL} = \frac{1}{3} Tr \overline{K_{KL}}$. These parameters contain valuable information on the nature of the chemical bonding, and so on. In the experimental work, the numerical values of the shielding and indirect spin-spin coupling constants are determined so that the solutions of the nuclear spin equation with the effective Hamiltonian reproduce as accurately as possible the observed NMR spectrum.

2.3.2 Spin-Hamiltonian parameters as energy derivates

At a more fundamental level, we should be able to determine the nuclear shielding constants ab initio from knowledge of the electronic wave function.

The perturbations introduced in the electronic system by the NMR transitions are exceedingly small; the smallest of the effects permits the application of perturbation theory to the calculation of the NMR parameters from the electronic wave function. We find that the NMR spectrum for a set

51

Chapter 2

of bare nuclei represents transitions of the order of 10^{-8} atomics units. These interactions are indeed small compared with those responsible for chemical bonding, all of which are of the order of unity.

When a molecular electronic system is modified by a perturbation x, its total energy changes

$$E(x) = E^{(0)} + E^{(1)}x + \frac{1}{2}x^T E^{(2)}x + ...$$

The coefficients of this expansion are characteristic of the molecular system in a given quantum state and are known as molecular properties. When the perturbation is static (that is, time-independent, as for the NMR properties studied here for a homogeneous magnetic field) the molecular properties may be calculated by differentiation

$$E^{(1)} = \frac{dE}{dx}\bigg|_{x=0} \quad E^{(2)} = \frac{d^2 E}{dx^2}\bigg|_{x=0}.$$

From the electronic energy of the unperturbed system $E(x) = \langle 0|H|0 \rangle$, in nondegenerate time-independent perturbation theory[76], we have the following expressions for first and second-order molecular properties, where the derivatives are taken at $x=0$,

$$\frac{dE(x)}{dx_i} = \left\langle 0\left|\frac{dH}{dx_i}\right|0\right\rangle, \quad \frac{d^2 E(x)}{dx_i^2} = \left\langle 0\left|\frac{d^2 H}{dx_i dx_j}\right|0\right\rangle - 2\sum_{n\neq0}\frac{\left\langle 0\left|\frac{dH}{dx_i}\right|n\right\rangle\left\langle n\left|\frac{dH}{dx_j}\right|0\right\rangle}{E_n - E_0};$$

the first derivative or the first order property is simply the expectation value of the first order Hamiltonian and requires only knowledge of the unperturbed reference state $|0\rangle$. The second derivate or the second-order property contains an expectation-value term analogous to the first-order

properties but also a sum-over-states contribution form each excited state $|n\rangle$ of energy E_n.

We expand the electronic energy in the magnetic induction B and in the nuclear moments M_K, around zero field and zero magnetic moments

$$E(B,M) = E_0 + E^{(10)}B + \sum_K E_K^{(01)}M_K + \frac{1}{2}B^T E^{(20)}B + \sum_K B^T E_K^{(11)}M_K + \frac{1}{2}\sum_{K \neq L} M_K^T E_{KL}^{(02)}M_L$$

$$M = \{M_K\};$$

$$E^{(10)} = \frac{dE(B,M)}{dB}\bigg|_{B=0,M=0} \quad , \quad E_K^{(01)} = \frac{dE(B,M)}{dM_K}\bigg|_{B=0,M=0} \quad ;$$

$$E^{(20)} = \frac{d^2E(B,M)}{dB^2}\bigg|_{B=0,M=0} \quad , \quad E^{(11)} = \frac{d^2E(B,M)}{dBdM_K}\bigg|_{B=0,M=0} \quad ,$$

$$E_{KL}^{(02)} = \frac{d^2E(B,M)}{dM_K dM_L}\bigg|_{B=0,M=0} \quad ;$$

higher than second-order terms may be neglected due to the smallness of the perturbations.

2.3.3   The molecular electronic Hamiltonian

To arrive at explicit expressions for the nuclear shielding, we must consider the form of the electronic Hamiltonian; its dependence on the magnetic induction, B, and on the nuclear magnetic moments, M_K.

The electrons interact with these perturbations: (1) because of the orbital motion of the electrons and (2) because of the permanent magnetic moment of the electrons, m_i

$$m_i = -g\,\mathbf{m}_B\,s_i = s_i \qquad \left\{ g = 2,\ \mathbf{m}_B = \frac{1}{2},\ in\ atomic\ units \right\}.$$

In the presence of these magnetic perturbations, the non-relativistic molecular electronic Hamiltonian may in atomic units be written in the form

$$H(B,M) = \frac{1}{2}\sum_i \mathbf{p}_i^2 - \sum_i m_i B^{tot}(r_i) - \sum_{ik}\frac{Z_K}{r_{iK}} + \frac{1}{2}\sum_{i\neq j}\frac{1}{r_{ij}}$$

$$+ \frac{1}{2}\sum_{K\neq L}\frac{Z_K Z_L}{R_{KL}} - \sum_K M_K B^{tot}(R_K) + \sum_{K>L} M_K^T D_{KL} M_L.$$

We have introduced the operators for the kinetic momentum $\mathbf{p}_i = -i\nabla_i + A^{tot}(r_i)$, where $A^{tot}(r_i)$ is the vector potential at the position of electron i. The vector potential and the magnetic induction may each be decomposed into one contribution from the external field and one contribution from each nucleus

$$A^{tot}(r_i) = A_o(r_i) + \sum_K A_K(r_i),\ B^{tot}(r_i) = B + \sum_K B_K(r_i).$$

The relation between the magnetic induction and the vector potential is given as for the total potential and field in $B^{tot}(r_i) = \nabla_i \times A^{tot}(r_i)$.

2.3.4   Interaction terms

From the explicit expression of the Hamiltonian, we can derive the first and second-order properties. Beginning from first order properties, for the external magnetic field we find

$$\frac{dH}{dB} = h_B^{orb} + h_B^{spn},\ with\ h_B^{orb} = \frac{1}{2}\sum_i l_{io}\ and\ h_B^{spn} = \sum_i m_i = \sum_i s_i.$$

The first term couples the external field to the orbital motion of the electron by means of the orbital angular-momentum operator

```
UNIVERSITAT ROVIRA I VIRGILI
DFT STUDY OF TITANIUM CUBANE AND MOLYBDENUM SULPHIDE COMPOUNDS.
Autor: José Manuel Gracia Budria
ISBN: 978-84-690-6751-2 / DL: T.1196-2007
```
Density functional methods. The calculation of NMR shielding tensors

$$l_{io} = -ir_{io} \times \nabla_i \text{ (imaginary)};$$

the second term couples the field to the spin angular-momentum operator

$$m_i = -s_i.$$

From these results, we can derive the effect of these operators on a closed-shell wave function

$$h_B^{orb} |0\rangle \rightarrow \text{imaginary singlet,}$$
$$h_B^{spn} |0\rangle \rightarrow \text{vanishes.}$$

For the nuclear magnetic moments, we find three terms

$$\frac{dH}{dM_K} = h_K^{pso} + h_K^{sd} + h_K^{fc};$$

$$h_K^{pso} = a^2 \sum_i \frac{l_{ik}}{r_{ik}^3}, \text{ paramagnetic spin-orbit operator,}$$

h_K^{pso}, couples the nuclear magnetic moments to the orbital motion of the electrons (hyperfine operator),

$$h_K^{sd} = a^2 \sum_i \frac{r_{iK}^2 m_i - 3(m_i r_{iK}) r_{iK}}{r_{iK}^5}, \text{ spin-dipole (SD) operator and}$$

$$h_K^{fc} = \frac{8pa^2}{3} \sum_i d(r_{iK}) m_i, \text{ fermi-contact (FC) operator;}$$

both couple the nuclear magnetic moments to the spin of the electron.

More helpful is to observe the global effect for closed-shell states with total spin zero

$$h_K^{pso} |0\rangle \rightarrow \quad \text{imaginary singlet}$$

55

Chapter 2

$$h_K^{sd}|0\rangle \rightarrow \qquad \text{real triplet}$$

$$h_K^{fc}|0\rangle \rightarrow \qquad \text{real triplet.}$$

At this point, let us comment on the first order magnetic properties of closed-shell systems. The first-order terms, which represent the permanent magnetic moment of the molecule M_{MOL} and the hyperfine coupling tensors A_K of the nuclei, vanish

$$M_{MOL} = -\left\langle 0 \left| \frac{dH}{dB} \right| 0 \right\rangle = 0$$

$$A_K = \left\langle 0 \left| \frac{dH}{dM_K} \right| 0 \right\rangle = 0 \, ;$$

the reason that these terms vanish is now seen to be the absence of real singlet components. So the electronic energy is reduced to

$$E(B,M) = E_0 + \frac{1}{2} B^T E^{(20)} B + \sum_K B^T E_K^{(11)} M_K + \frac{1}{2} \sum_{K \neq L} M_K^T E_{KL}^{(02)} M_L \, .$$

The comparing with the NMR spin-hamiltonian for a rotating molecule in an isotropic medium, the $E^{(20)}$ tensor represents the molecular magnetizability and does not enter the spin-hamiltonian,

$$H_{iso} = -\sum_K M_K (1 - s_K) B + \frac{1}{2} \sum_{K \neq L} M_K M_L K_{KL} \, ,$$

let us identify

$$s_K = 1 + E_K^{(11)} \, .$$

We have reduced the ab initio evaluation of NMR shielding and coupling constants to a special case of the more general problem of evaluating total derivates of molecular electronic energies

$$E_K^{(11)} = \frac{d^2 E(B,M)}{dB dM_K}\bigg|_{B=0,M=0} = \left\langle 0 \left| \frac{d^2 H}{dB dM_K} \right| 0 \right\rangle - 2\sum_{n\neq0} \frac{\left\langle 0 \left| \frac{dH}{dB} \right| n \right\rangle \left\langle n \left| \frac{dH}{dM_K} \right| 0 \right\rangle}{E_n - E_0},$$

$$\frac{d^2 H}{dB dM_K} = -1 + h_{BK}^{dia}; \quad h_{BK}^{dia} = \frac{\boldsymbol{a}^2}{2}\sum_i \frac{(r_{io} r_{iK})1 - r_{iK} r_{io}^{T}}{r_{iK}^3}.$$

Substituting the expressions for the interaction operators, discussed in the preceding sections, into the general expression for second-order properties we obtain Ramsey's expressions for the nuclear shielding tensor

$$\boldsymbol{s}_K = +1\left(-1 + \left\langle 0 \left| h_{BK}^{dia} \right| 0 \right\rangle\right) - 2\sum_{n_s \neq 0} \frac{\left\langle 0 \left| h_B^{orb} \right| n_s \right\rangle \left\langle n_s \left| (h_K^{pso}) \right| 0 \right\rangle}{E_{n_s} - E_0},$$

where $|n_s\rangle$ denotes a singlet excited state.

The expression is divided in a diamagnetic part, which correspond to an expectation value of the unperturbated state, and a paramagnetic part, which represents the relaxation of the wave function in response to the external perturbations.

2.3.5 Physical contributions

For a detailed analysis of the obtained terms in the shielding let us isolate the main physical contributions to the absolute displacement and to the experimental relative displacement $\boldsymbol{d}_K = \boldsymbol{s}_{ref} - \boldsymbol{s}_K$.

Diamagnetic part

$$\left\langle 0 \left| h_{BK}^{dia} \right| 0 \right\rangle \simeq \frac{\boldsymbol{a}^2}{3}\left\langle 0 \left| \sum_i \frac{1}{r_{iK}} \right| 0 \right\rangle \text{ (isolated atom in a } {}^1S \text{ state)}$$

Chapter 2

Inversely proportional to the position of the electrons with respect to the nuclei, represent the classical idea of nucleus shielding by the surrounding electrons. Its specific weight in the chemical shift goes down when the atomic number grows up.

Paramagnetic part

$$-2\sum_{n_s \neq 0} \frac{\left\langle 0 \left| h_B^{orb} \right| n_s \right\rangle \left\langle n_s \left| h_K^{pso} \right| 0 \right\rangle}{E_{n_s} - E_0}$$

main feature is that is inversely proportional to the energy gap between states. The h_B^{orb}

$$\left\langle 0 \left| h_B^{orb} \right| n_s \right\rangle = \left\langle 0 \left| \frac{1}{2} \sum_i l_{io} \right| n_s \right\rangle$$

is common for all atoms in the molecule. It couples the orbital motion of the electrons with the external field. And the h_K^{pso} term

$$\left\langle n_s \left| h_K^{pso} \right| 0 \right\rangle = \left\langle n_s \left| \mathbf{a}^2 \sum_i \frac{l_{iK}}{r_{iK}^3} \right| 0 \right\rangle$$

couples the nuclear magnetic moment to the orbital motion of the electrons. It is inverse proportional to the distance of the electrons to the central nucleus.

A very important general idea can be extracted from this analysis, for the absolute shielding all the electrons and specially the closely placed to the atom (core electrons) mark mainly the shielding value. But the relative shift, if the core electrons keep frozen, is a valence electrons property, and this is very important especially for the theoretical scheme available for computing the electron wave function.

2.3.6 Relativistic effects

The operators that determine the nuclear magnetic shielding and spin-spin coupling constants sample the regions close to the nuclei. For this reason, changes in the electronic structure due to relativistic effects are important for these properties. As an example, we note that the relativistic correction to the hydrogen shielding in hydrogen iodide is about 12 ppm,[77] an effect that exceeds the normal shielding range of protons. For the shielding of heavy elements, the neglect of scalar relativistic effects leads to an underestimation of the tungsten shielding by almost a factor of 3. Thus, in calculations of the shieldings of molecules containing heavy elements, relativistic effects must be taken into account to obtain even qualitative agreement with experimentally observed trends.[78]

Relativistic effects on molecular properties are often classified as *direct* or *indirect*. The direct effects arise directly from relativistic corrections to the electronic structure, at a fixed molecular geometry. The indirect effects, on the other hand, arise from the changes in molecular geometry caused by the changes in the electronic structure when the effects of relativity are taken into account.

In the Breit-Pauli approximation,[27] the dominant relativistic effects on nuclear shielding and spin-spin coupling constants arise from three Hamiltonian corrections. The mass-velocity operator

$$h^{mv} = -\frac{a^2}{8} \sum_i p_i^4 \,,$$

where p_i is the kinetic momentum, the Darwin operator

$$h^{Dar} = \frac{pa^2}{2} \sum_{iN} d\left(r_{iN}\right)$$

and finally the spin-orbit operator

Chapter 2

$$h^{so} = \frac{\mathbf{a}^2}{2}\left(\sum_{iA} Z_A \frac{l_{iA} \cdot s_i}{r_{iA}^3} + \sum_{ij} \frac{l_{ij}\left(s_i + 2s_j \right)}{r_{ij}^3} \right)$$

where we have introduced the two-electron angular momentum operator

$$l_{ij} = r_{ij} \times \mathbf{p}_i .$$

All of these operators yield contributions of second order in $\mathbf{a}$, fine structure constant,[79] to the energy. The different terms have well-established interpretations, with the mass-velocity and Darwin corrections being the main relativistic corrections to the kinetic energy and to the nuclear-attraction energy, respectively. The spin orbit correction describes the coupling between the electron spin and the orbital angular momentum of the electrons.

It is common to refer to effects arising from the mass-velocity and Darwin operators as scalar relativistic effects, as these do not involve the electronic spin. In the vicinity of the nucleus, these scalar relativistic effects dominate. Still, it is difficult to know a priori whether the scalar relativistic corrections or the spin-orbit correction will dominate the relativistic effects on shielding and spin-spin coupling constants.

To investigate the main relativistic corrections to the nuclear shielding starting from a nonrelativistic framework, we may consider the wave function correct to first-order in the mass-velocity, Darwin, and spin-orbit operators

$$\left| y \right\rangle = \left| 0 \right\rangle - \sum_{n_s \neq 0} \frac{\left\langle n_s \left| h^{mv} + h^{Dar} \right| 0 \right\rangle}{E_{n_s} - E_0} \left| n_s \right\rangle - \sum_{n_T} \frac{\left\langle n_T \left| h^{so} \right| 0 \right\rangle}{E_{n_T} - E_0} \left| n_T \right\rangle .$$

Inserting this wave function into the Ramsey equations for the nuclear shielding, we obtain the following equation for the relativistically corrected nuclear shieldings, where, in the spin-orbit contribution, a sum over the spin components should be performed

$$\boldsymbol{s}_K = \left\langle 0 \left| h_{BK}^{dia} \right| 0 \right\rangle - 2 \sum_{n_s \neq 0} \frac{\left\langle 0 \left| h_B^{orb} \right| n_s \right\rangle \left\langle n_s \left| \left(h_K^{pso} \right) \right| 0 \right\rangle}{E_{n_s} - E_0}$$

$$- \sum_{n_s \neq 0} \frac{\left\langle 0 \left| h_{BK}^{dia} \right| n_s \right\rangle \left\langle n_s \left| \left(h^{mv} + h^{Dar} \right) \right| 0 \right\rangle}{E_{n_s} - E_0}$$

$$+ 2 \sum_{n_s, m_s \neq 0} \frac{\left\langle 0 \left| h_B^{orb} \right| m_s \right\rangle \left\langle m_s \left| \left(h_K^{pso} \right)^T \right| n_S \right\rangle \left\langle n_s \left| h^{mv} + h^{Dar} \right| 0 \right\rangle}{\left(E_{n_s} - E_0 \right) \left(E_{m_s} - E_0 \right)}$$

$$+ 2 \sum_{n_s, m_T \neq 0} \frac{\left\langle 0 \left| h_B^{orb} \right| m_s \right\rangle \left\langle m_s \left| \left(h_K^{fc} \right)^T + \left(h_K^{sd} \right)^T \right| m_T \right\rangle \left\langle m_T \left| h^{so} \right| 0 \right\rangle}{\left(E_{n_s} - E_0 \right) \left(E_{m_T} - E_0 \right)}.$$

In this expression, we have included all contributions bilinear in the external magnetic field induction and the nuclear magnetic moments, and we have taken the spin symmetry of the different operators into account when determining the nonvanishing contributions.

As the mass-velocity and Darwin operators can perturb the electronic wave function significantly if heavy elements are present in the molecule, perturbation theory may not be adequate for the study of scalar relativistic effects. In the literature, this potential instability of the perturbation approach has been circumvented in three different ways: (1) using quasi-relativistic effective core potentials (RECP),[80] (2) using the frozen-core approximation,[81] and (3) using the spin-free relativistic Hamiltonian obtained from the no-pair approximation.[82]

In the quasi-relativistic effective core potentials (RECPs), the scalar relativistic effects are included in the effective core potential. However, because NMR parameters depend critically on the electron density in the nuclear regions which may not be accurately modeled by the RECPs, this approach cannot be expected to perform well for the shielding of the heavy atom itself. For this reason, RECPs have been used in molecular calculations to study only the chemical shifts of the ligands.[83]

In the frozen-core approximation, the core density is determined from four-component atomic Dirac-Fock calculations. It is then assumed that the electron density of the core orbitals remains unchanged when the atom is embedded in a molecule, the bonds formed being determined only by the valence electrons. It has been shown that the use of the frozen core approximation performs well for the calculation of nuclear shieldings, and in particular that a relativistic atomic density may be used to investigate scalar relativistic effects of the shieldings of the heavy atoms. Regarding the case of heavy-atom effects on the nuclear shielding of lighter elements, several investigations have shown that these effects are often governed by spin-orbit interactions.[84]

2.4 Variational perturbation theory for the calculation of NMR parameters

Although conceptually important in that they elucidate the different physical mechanisms at work, the Ramsey expressions are not useful for practical calculations since they require an explicit representation of the excited states. We must therefore approach the calculation of the NMR spin-Hamiltonian parameters for the energy functionals of approximate electronic wave functions; we present the general theoretical framework within which NMR parameters are calculated: variational perturbation theory.[85] The principles underlying the calculation of NMR parameters are independent of the wave function model chosen for a particular calculation and their understanding is relevant and useful for the application of existing methods, as well as for further development.

For a variational wave function, we write the electronic energy function in the presence of the magnetic induction B and the nuclear magnetic dipole moments M_K, in the form $E(B,M;l)$, where l is the set of parameters that determine and characterize the wave function. The electronic energy may then be calculated from the expression

$$E(B,M)=E(B,M;l*)$$

Density functional methods. The calculation of NMR shielding tensors

where l^* represents the optimal values of the electronic parameters l and where the optimized energy function $E(B,M;l^*)$ satisfies the variational conditions

$$\frac{\partial E(B,M;l)}{\partial l}\bigg|_{l=l^*} = 0 \text{ , for all values of } B \text{ and } M .$$

To ensure that the variational conditions are always fulfilled, the electronic parameters l must change in a very specific manner with B and M. For the first derivatives, for variational wave functions, we consider the gradient of the electronic energy $E(B,M)$ with respect to the nuclear magnetic moment M_K. Using the chain rule, we obtain

$$\frac{dE(B,M)}{dM_K} = \left[\frac{\partial E(B,M;l)}{\partial M_K} + \frac{\partial E(B,M;l)}{\partial l}\frac{\partial l}{\partial M_K}\right]_{l=l^*} ,$$

combining with $\dfrac{\partial E(B,M;l)}{\partial l}\bigg|_{l=l^*} = 0$, we obtain the following simple expression for the gradient of the electronic energy with respect to the nuclear magnetic moments

$$\frac{dE(B,M)}{dM_K} = \frac{\partial E(B,M;l^*)}{\partial M_K} .$$

We note in passing that for zero field and zero magnetic moments, this last expression corresponds to the hyperfine coupling tensor

$$A_K = \frac{\partial E(B,M;l^*)}{\partial M_K}\bigg|_{B=0,M=0} .$$

Clearly, to obtain the hyperfine coupling tensors, we need not evaluate the response of the wave function $\dfrac{\partial l}{\partial M_K}$. This is an important result which, as we shall shortly see, simplifies the calculation of the shielding tensor. As

Chapter 2

already discussed, the nuclear hyperfine coupling tensor itself vanishes for closed shell systems and is of no interest to us.

An expression for the shielding tensors is obtained by differentiating the gradient $\dfrac{dE(B,M)}{dM_K} = \dfrac{\partial E(B,M;\boldsymbol{l}^*)}{\partial M_K}$ with respect to B

$$\frac{d^2 E(B,M)}{dBdM_K} = \left[\frac{\partial^2 E(B,M;\boldsymbol{l})}{\partial B \partial M_K} + \frac{\partial^2 E(B,M;\boldsymbol{l})}{\partial M_K \partial \boldsymbol{l}} \frac{\partial \boldsymbol{l}}{\partial B} \right]_{\boldsymbol{l}=\boldsymbol{l}^*}.$$

For zero field and zero nuclear magnetic moments, we recover according to $\boldsymbol{s}_K = E_K^{(11)} + 1$ the nuclear shielding tensors

$$\boldsymbol{s}_K = 1 + \left[\frac{\partial^2 E(B,M;\boldsymbol{l})}{\partial B \partial M_K} + \frac{\partial^2 E(B,M;\boldsymbol{l})}{\partial M_K \partial \boldsymbol{l}} \frac{\partial \boldsymbol{l}}{\partial B} \right]_{B=0,M=0,\boldsymbol{l}=\boldsymbol{l}^*}$$

$$= 1 + \frac{\partial^2 E}{\partial B \partial M_K} + \frac{\partial^2 E}{\partial M_K \partial \boldsymbol{l}} \frac{\partial \boldsymbol{l}}{\partial B}$$

in the following, we shall always assume that the derivatives are taken at zero field $B = 0$, for zero magnetic moments $M = 0$, and for the optimized parameters $\boldsymbol{l} = \boldsymbol{l}^*$.

We conclude that, for a fully variational wave function, only the first-order response of the wave function with respect to the external field, $\dfrac{\partial \boldsymbol{l}}{\partial B}$, is required to calculate the nuclear shieldings $\boldsymbol{s}_K$.

At this point, we note that we may derive an expression for the shielding tensor also by differentiation first with respect to B and next with respect to M_K. We then obtain the following alternative expression for the shielding tensor

$$s_K = 1 + \frac{\partial^2 E}{\partial B \partial M_K} + \frac{\partial^2 E}{\partial B \, \partial l} \frac{\partial l}{\partial M_K} \; .$$

Although mathematically equivalent, this expression requires the calculation of three responses for each shielded nucleus, the first one requires the calculation of only three responses, irrespective of the size of the molecule.

Finally, we must consider the evaluation of the first order responses of the wave function. We have already noted that the variational conditions $\left. \dfrac{\partial E(B,M;l)}{\partial l} \right|_{l=l^*} = 0$ determine the dependence of the wave function on B and M . Differentiating these conditions with respect to B and invoking the chain rule, we obtain the conditions

$$\frac{d}{dB} \frac{\partial E}{\partial l} = \frac{\partial^2 E}{\partial B \partial l} + \frac{\partial^2 E}{\partial l^2} \frac{\partial l}{\partial B} = 0$$

which may be written in the form of a set of linear equations:

$$\frac{\partial^2 E}{\partial l^2} \frac{\partial l}{\partial B} = -\frac{\partial^2 E}{\partial l \, \partial B} \; .$$

These equations are known as the response equations since they determine the first derivative (i.e., the first-order response) of the wave function with respect to the applied magnetic field. To determine the response of the wave function to the nuclear magnetic moments, we proceed in the same way obtaining

$$\frac{\partial^2 E}{\partial l^2} \frac{\partial l}{\partial M_K} = -\frac{\partial^2 E}{\partial l \partial M_K} \; .$$

Clearly, the response equations have the same general form for all perturbations the only differences between the linear sets of equations in their right-hand sides.

Chapter 2

The following notation for the electronic gradient and the electronic Hessian of the optimized wave function is used

$$F = \frac{\partial E}{\partial l}, \; G = \frac{\partial^2 E}{\partial l^2}.$$

Naively, one would think that the response equations should be solved by first inverting the electronic Hessian and then obtaining the solutions by simple matrix-vector multiplications according to the expressions

$$s_K = 1 + \frac{\partial^2 E}{\partial B \partial M_K} + \frac{\partial^2 F^T}{\partial M_K} G^{-1} \frac{\partial F}{\partial B}.$$

2.5 Density functional calculations of NMR chemical shifts

In DFT electron correlation effects can be included at a relative low cost, allowing its application to large systems. Instead of the impossibility of systematically improve the results, DFT schemes provide a big versatility in the calculation of NMR chemical shifts thanks to the use of several exchange correlation functionals, frozen core and/or GIAO orbitals. Also, one important feature is the inclusion of relativistic effects that has, so far, been achieved for DFT only. Relativistic effects become important for any chemical feature of heavy elements compounds[86] and NMR and ESR are no exception. The relativistic effects are not only important for the NMR shielding of the heavy atoms themselves but also for light ligands. For the chemical shift of the ligands especially, the spin-orbit coupling turned out to be important.[87]

2.5.1 ZORA relativistic approximation

The one electron Dirac equation may be written as

$$\begin{pmatrix} V & c\boldsymbol{s}\,p \\ c\boldsymbol{s}\,p & V - 2c^2 \end{pmatrix} \begin{pmatrix} \Phi \\ \boldsymbol{c} \end{pmatrix} = E \begin{pmatrix} \Phi \\ \boldsymbol{c} \end{pmatrix},$$

here, V is the electrostatic potential energy, c is the speed of light, $\boldsymbol{s}$ is the three-component Pauli spin matrix, p is the three-component momentum operator, E is the energy, and Φ and $\boldsymbol{c}$ are large and small components. Each of the large and small components are related by $\boldsymbol{c} = X\Phi$ where

$$X = \frac{1}{2c}\left(1+\frac{E-V}{2c^2}\right)^{-1}\boldsymbol{s}\,p\,.$$

Accordingly, the small component can be formally eliminated to give the following eigenequation for the large component

$$\left(V+c\boldsymbol{s}\,pX\right)\Phi = E\Phi\,;$$

however, the Hamiltonian in this equation is not Hermitian, and the resulting eigenfunctions Φ are not normalized. These problems can be circumvented by introducing the Hermitian Hamiltonian which affords normalized states

$$h = \left(1+X*X\right)^{\frac{1}{2}}\left(V+c\boldsymbol{s}\,pX\right)\left(1+X*X\right)^{-\frac{1}{2}}\,.$$

In the familiar relativistic Pauli approximation,[88] to simplify this Hamiltonian, we can assume that $p^2 \ll 4c^2$ and we get the relativistic Pauli approximation

$$h^{Pauli} = V + \frac{p^2}{2} - \frac{p^4}{8c^2} + \frac{\Delta V}{8c^2} + \frac{\boldsymbol{s}\left(\nabla V \times p\right)}{4c^2}\,.$$

This expansion is, however, only valid if the velocity of the electrons is everywhere small compared to the velocity of light $\left(E-V\right) \ll 2mc^2$. This condition is not satisfied for a Coulombic potential like the nuclear potential.[89] This makes all-electrons calculations on heavy systems impossible, because the Pauli Hamiltonian has no lower bound and the necessary tight functions will lead to variational collapse. The quasi-relativistic method can therefore only be applied with a frozen core approximation that avoids variational collapse by the orthogonality

Chapter 2

constraint on the core. In addition the basis set needs to be restricted, in the sense that, in a heavy metal complex for instance, tight functions are to be avoided at the metal nucleus as well as large flexible basis sets on the ligands. Keeping in these restrictions relative displacements have been obtained with similar precision than the newer ZORA relativistic approximation.[90]

An alternative approximation to the above Pauli approximation can be obtained by rewriting $X = \dfrac{1}{2c}(1 + \dfrac{E-V}{2c^2})^{-1}\boldsymbol{s}\,p$ as $X = (\dfrac{c}{2c^2-V})(1 + \dfrac{E}{2c^2-V})^{-1}\boldsymbol{s}\,p$. If we assume $E << (2c^2 - V)$, then the equation can be expanded to zero order in $\dfrac{E}{2c^2-V}$ to give the zero-order regular approximation (ZORA)[91]

$$h^{ZORA} = \boldsymbol{s}\,p\,\frac{K}{2}\,\boldsymbol{s}\,p + V \text{ , where } K = \left[1 - \frac{V}{2c^2}\right]^{-1}.$$

In this case the assumption that $E << (2c^2 - V)$ in the core region remains valid. As a result, the Zora Hamiltonian does not suffer from variational instabilities and can be used in all electrons calculations. Zora orbital energies can be improved further by introducing a simple scale factor.[92] If $h^{ZORA}\Psi_i = E_i\Psi_i$ then the scaled energies $E_i^{scaled} = x_i E_i^{ZORA}$, where

$$x_i = \left(1 + \left\langle \Psi_i \left| \boldsymbol{s}\,p\, \frac{c^2}{(2c^2-V)^2}\,\boldsymbol{s}\,p \right| \Psi_i \right\rangle \right)^{-1}$$

are in much better agreement with the one-electron Dirac energies. For a system the total energy in the scaled Zora formalism is given by

$$E_{Tot}^{Scaled} = \sum_i^{N_{occ}} E_i^{Scaled} - \frac{1}{2}\iint \frac{\boldsymbol{r}(1)\,\boldsymbol{r}(2)}{r_{12}}\,d1d2 + E_{XC}[\boldsymbol{r}] - \int \boldsymbol{r}(1)\frac{dE_{XC}[\boldsymbol{r}]}{d\boldsymbol{r}(1)}\,d1$$

2.5.2 Calculation of NMR parameters

The basic DFT theorem of Hohenberg and Kohn was formulated for a system in the absence of a magnetic field. Taking the latter into account leads to further complications, because the exchange-correlation functional should depend on the magnetic field.[93] Thus, one would need current-dependent (or magnetic-field dependent) exchange-correlation functionals. An implementation of such a current-density[94] functional theory (CDFT) has been carried out by Handy and co-workers.[95] Within the model used, they found that the current dependent contributions to chemical shifts were very small and did not improve the results. Two other models have been suggested, a gradient-corrected current-density functional has recently been suggested by Becke[96] and by Capelle and Gross,[97] but we are not aware of any implementation or results of these new models. More work is needed in this area. Now to find the ZORA NMR shielding tensors, we include the magnetic field in the Hamiltonian by means of minimal substitution

$$h^{ZORA}(\boldsymbol{p}) = \boldsymbol{s}\boldsymbol{p}\frac{K}{2}\boldsymbol{s}\boldsymbol{p} + V \text{ , where}$$

$$\boldsymbol{p} = p + \left(\frac{1}{c}\right)A \text{ , } A \text{ is the magnetic vector,}$$

$$A = A_B + A_m \text{ , } A_B = \frac{1}{2}B \times r \text{ , } A_m = \frac{\left(\boldsymbol{m}_Q - r_Q\right)}{r_Q^3}$$

$\boldsymbol{m}_Q$ is the nuclear magnetic moment attached to nucleus Q at position R_Q, and $r_Q = r - R_Q$.

Via the Hellmann-Feynman[98] theorem, the NMR shielding tensor can be derived from the scaled energy using

$$\partial B_K \partial \boldsymbol{m}_{Q,t}\, E_{Tot}^{Scaled}\Big|_{B=\boldsymbol{m}_Q=0} = \partial B_K \sum_i^{N_{occ}} \left\langle \Psi_i(B) \left| \frac{\partial h^{ZORA}(\boldsymbol{m})}{\partial \boldsymbol{m}_{Q,t}} \right|_{\boldsymbol{m}_Q=0} \Psi_i(B) \right\rangle_{B=0} .$$

It should be noted that when a magnetic field is introduced, the total energy will be a functional of both the density and the current density. In deriving $\partial B_K \partial \boldsymbol{m}_{Q,t} E_{Tot}^{Scaled}\big|_{B=\boldsymbol{m}_Q=0}$ equation, from E_{TOT}^{Scaled}, is assumed that the total energy is independent of the current, and that the first-order change in the density vanish. Thus we are using uncoupled DFT to determine the NMR shieldings.[99]

In order to evaluate the second order property we also need to know the spinors $\Psi_i(B)$ up to first order in the magnetic field. So we first solve the ZORA equation, without magnetic field

$$h^{ZORA}\Psi_i = \left(\boldsymbol{s}\, p \frac{K}{2} \boldsymbol{s}\, p + V \right)\Psi_i = E_i^{ZORA}\Psi_i.$$

This solution can be written in terms of real atomic basis functions $\boldsymbol{j}_n$

$$\Psi_i = \sum_n^N \sum_{g=a,b} d_n^g \boldsymbol{j}_n^g.$$

Next we calculate the solutions of the ZORA equation including the external magnetic field B up to first order

$$h^{ZORA}(B)\boldsymbol{y}_i(B) = E_i(B)\boldsymbol{y}_i(B),$$

where $h^{ZORA}(B)$ up to first order in B is

$$h^{ZORA}(B) = V + \boldsymbol{s}\left(p + \frac{1}{c}A_B\right)\frac{K}{2}\left(p + \frac{1}{c}A_B\right)$$

$$= V + \boldsymbol{s}\, p \frac{K}{2}\boldsymbol{s}\, p + \frac{K}{4c}B(r\times p) + B(r\times p)\frac{K}{4c}$$

$$= \frac{K}{2c}\boldsymbol{s}B + \boldsymbol{s}B\left(r\nabla\frac{K-1}{4c}\right) - \boldsymbol{s}\, r\left(B\nabla\frac{K-1}{4c}\right).$$

2.5.3   DFT shielding tensor

By means of the generalized Hellmann-Feynman[98] theorem we had written

$$\partial B_K \partial m_Q \left. E_{Tot}^{Scaled} \right|_{B=m_Q=0} = \partial B_K \sum_i^{N_{occ}} \left\langle \Psi_i(B) \left| \left. \frac{\partial h^{ZORA}(B,m)}{\partial m_Q} \right|_{m_Q=0} \right| \Psi_i(B) \right\rangle_{B=0}$$

where the Hamiltonian now contains the applied external magnetic field B and the nuclear magnetic moment of the atom under consideration m_Q. $\Psi(B^{ext})$ depends only on the external magnetic field and it is the ground-state eigenfunction of

$$H(B^{ext})\Psi(B^{ext}) = e(B^{ext})\Psi(B^{ext}).$$

Where there is no term dependent on the nuclear magnetic moment on the Hamiltonian.

Making use of the back expressions, the NMR shielding tensor can be written as a sum of three contributions [100]

$$s_{KT} = s_{KT}^d + s_{KT}^p + s_{KT}^{so},$$

the diamagnetic and paramagnetic shieldings match with obtained in the Ramsey expression and as we will show they keep the same physical signification.

Diamagnetic shielding

The diamagnetic shielding depends on the zero-order electronic density only

$$s_{st}^d \propto \frac{1}{2c^2} \sum_i^{occ} n_i \sum_m^N d_{mi} \left\langle y_i \left| \frac{K}{r_N} \right| l_m \right\rangle.$$

Chapter 2

Diamagnetic term is a consequence of produced shielding by the electrons close to the nuclei. It contribution is always positive (shielding) and bigger as many electrons are next around the nuclei. It absolute value grows up with the atomic number, but it relative weight on the chemical shifts goes down. For heavy atoms, the diamagnetic shielding change is really negligible respect the total chemical shift range. This result is readily understandable from the fact that the core MOs, 1s, 2s, in particular, contribute by far the largest part of the diamagnetic shielding. That is a consequence of the localized nature of the NMR shielding/chemical shift. Such core effects are largely independent from the chemical environment of the nucleus. They cancel out in relative chemical shifts. [101,102,103]

Table 2.2 presents ^{1}H NMR shielding constants and chemical shifts, respect to HF that were calculated by Wolff and Ziegler for the hydrogen halides: HF, HCl, HBr, HI.[99] The absolute experimental shielding for the hydrogen of HF is reported in the literature as 28.72 ppm,[104] this value agrees well with the calculated value of 31.5 ppm. From Table 2.2 it is clear that in chemical shifts differences among the hydrogen halides all contributions are significant. Thus, although diamagnetic posses the bigger absolute value, paramagnetic and spin-orbit coupling show bigger relative sensibility to the chemical environment. So for nuclei with higher $\boldsymbol{s}_{st}^{p}$ and $\boldsymbol{s}_{st}^{so}$ tensors in absolute value, these determine the main chemical shift differences between atoms.

Table 2.2. ^{1}H NMR shielding constants and shifts (in ppm)

HX	$\boldsymbol{s}^{p}$	$\boldsymbol{s}^{d}$	$\boldsymbol{s}^{SO}$	$\boldsymbol{s}^{\mathbf{cal}}$	$\boldsymbol{d}^{cal}$	$\boldsymbol{d}^{\exp}$	$\boldsymbol{d}^{\mathbf{cal}}\text{-}\boldsymbol{d}^{\exp}$
HF	8.64	22.74	0.09	**31.47**	0	0	**0**
HCl	2.95	29.22	0.73	**32.90**	-1.43	-2.58	**1.15**
HBr	2.27	29.48	5.06	**36.81**	-5.34	-6.43	**1.09**
HI	1.61	30.53	11.11	**43.26**	-11.79	-15.34	**3.55**

Paramagnetic shielding

The paramagnetic shielding however is determined by the magnetically perturbed MOs. The leading contribution couples occupied and virtual MOs, and one can write, at least approximately

$$ \boldsymbol{s}_{st}^{p} \propto 2\sum_{i}^{occ} n_i \sum_{\boldsymbol{m}}^{N} u_{ai}^{1,s} \left\langle \boldsymbol{y}_i \left| \left[\frac{r_N}{r_N^3} \times p \right] \right|_t \right| \boldsymbol{y}_a \right\rangle $$

$\boldsymbol{y}_a$ and $\boldsymbol{y}_i$ describe virtual and occupied MOs (with occupation number n_i), respectively; r_N is the electronic position operator relative to the NMR nucleus N, and p is the electronic momentum operator. The leading contribution to the first order coefficient $u_{ai}^{1,s}$ is given as

$$ u_{ai}^{1,s} \propto -\frac{1}{\boldsymbol{e}_i^{(0)} - \boldsymbol{e}_a^{(0)}} \left\langle \boldsymbol{y}_i \left| \widehat{M}_S \right| \boldsymbol{y}_a \right\rangle . $$

Paramagnetic shielding contribution depends on the electronic structure and so is sensitive to the XC functional. In the GIAO formulation, see section 2.5.3.1, there are contributions to $\boldsymbol{s}^{p}$ from both occupied-occupied and occupied-virtual couplings. While the former is not negligible, the major contribution of both to $\boldsymbol{s}^{p}$ and to the difference between XC functional stems from the occupied-virtual terms. The coupling between occupied and virtual orbitals is due to the external magnetic field. For an energy gap, the leading contribution stems from integrals of the type

$$ \left\langle l_g \left| \left(-\frac{R_n}{2} \right) \times \nabla \right| l_n \right\rangle . $$

This operator rotates the orbital l_n round its position R_n; e.g., the y component rotates orbitals in the imaginary xz plane, etc. It can be then rationalized in terms of the form of the orbitals

$$ r_n \times \nabla \big|_y \left| p_z \right\rangle \propto \left| p_x \right\rangle . $$

Chapter 2

For instance, the ^{57}Fe NMR shielding and chemical shift in ferrocene, $Fe(C_5H_5)_2$, was studied by Schreckenbach.[105] It is shown that the chemical shift is entirely determined by paramagnetic contributions ($s^p = -4924$) which in turn are dominated by metal based occupied-virtual $d \rightarrow d$ couplings. In particular, the HOMO-1 ($5a_1'$) $s^p_{5a1 \rightarrow 4e2} = -3542$ and the HOMO (e_2') couple with the LUMO ($4e''$). As we can observe in Figure 2.1, operator $\widehat{M}_y$ working on the $4e''$ LUMO result in an orbital, $\widehat{M}_y\left[4e''\right]$, with a strong magnetic interaction, through the common lobes with $5a_1'$.

$$5a_1' \text{ (HOMO-1)} \qquad 4e_1'' \text{ (LUMO)} \qquad \hat{M}_y\,[4e_1'']$$
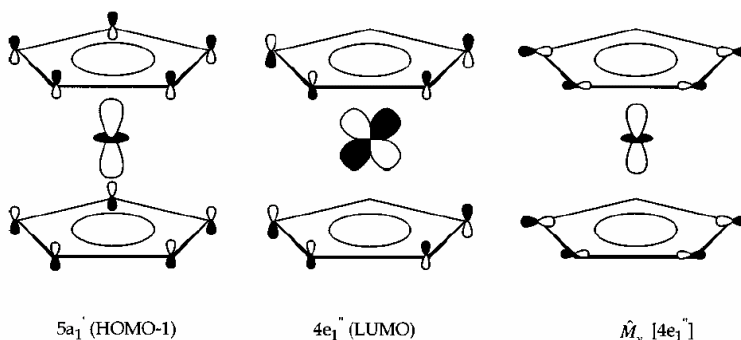
Figure 2.1. *Schematic representation of the $5a_1'$ (HOMO-1) and $4e''$ (LUMO) orbitals. Also shown is the result of the ''magnetic'' operator $\widehat{M}_y$ working on the $4e''$ LUMO. The result is a strong magnetic interaction, through the common lobes in $5a_1'$ and $\widehat{M}_y\left[4e''\right]$*

Similar picture is found for F_2 or CO.[106] For instance in F_2 case, large s^p contribution is essentially due to just one single term, name the $p \rightarrow s*$ transition, out of a whole sum over all possible transitions. As we show in Figure 2.2, the rotation results in a strong interaction between p and $s*$.

Paramagnetic contribution, s^p, is always a leading contribution for heavy atoms. For computed, ^{235}U atoms (Table 2.3),[28] the diamagnetic shielding, s^d, does not vary by more than about 20 ppm. This change is really negligible, given a total calculated shielding range of over 21000 ppm. The

spin-orbit shielding posses a modest although not negligible influence on the chemical shifts; one can see that s^{so} varies within a range of some 1500 ppm, about 6.5% of the total calculated chemical shift range.
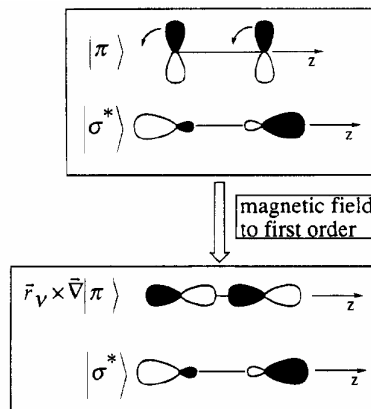
Figure 2.2. *Representation of the* $p \rightarrow s^*$ *coupling for the* F_2 *molecule*

Table 2.3. *Contributions to the* ^{235}*U NMR shifts (in ppm) for* UF_6*,* UF_5Cl *and* $UFCl_5$ *compounds*

Molecule	s^p	$s^{p,oc-vir}$	s^d	s^{so}	s^{total}	d^{cal}
UF_6	-18896	-15380	11610	7964	678	0
UF_5Cl	-21306	-18180	11615	7758	-1934	2612
$UFCl_5$	-29211	-27888	11627	7308	-10275	10954

The largest contribution to the calculated ^{235}U shieldings and chemical shifts is due to the paramagnetic shielding. In Table 2.3 it has been included the calculated values of $s^{p,oc-vir}$. One can perceive that the remaining (occupied-occupied) contribution to s^p is neither small nor negligible, and it can have either sign. Nevertheless, $s^{p,oc-vir}$ is responsible for the largest part of the paramagnetic shielding, as well as for the various trends in the shieldings and chemical shifts. For a qualitative discussion, one can focus on this contribution.

The occupied-virtual paramagnetic contribution grows up from UF_6 to $UFCl_5$ considerably; the occupied-virtual shielding, $\boldsymbol{s}^{p,o\,c-vir}$, is, in turn, dominated by magnetic interactions between uranium 5f-based occupied and virtual orbitals. The strength of the interaction is inversely proportional to the occupied-virtual energy separation and also is sensible to the Uranium 5f-character of the implicated orbitals. Indeed, the first member of the series, UF_6, has a HOMO-LUMO gap that is almost twice as large as for any other molecule. Earlier studies[107] showed that the percentage of f character of the remaining six 5f type virtuals decreases along the fluoride chloride series, from 82.0% for UF_6 to 78.5% for UCl_6. This decrease in virtual f character will be accompanied by an increase in 5f-character for the corresponding occupied MOs. Both factor orbitals energy gap and orbital compositions govern the predisposition of the paramagnetic contribution.

Spin-orbit shielding

The spin-orbit shielding contribution, $\boldsymbol{s}_{ts}^{so}$, is dominated by the Fermi contact that depends on the spin polarization at the NMR nucleus

$$\boldsymbol{s}_{ts}^{so} \propto \boldsymbol{s}_{ts}^{FC} \propto \frac{4\boldsymbol{p}\,g}{3c} \sum_{i}^{occ} \sum_{a}^{vir} u_{ai}^{1,s} \left\langle \boldsymbol{y}_{a} \left| \widehat{S}_{t}\,\boldsymbol{d}\left(r_{N}=0\right) \right| \boldsymbol{y}_{i} \right\rangle$$

where g is the electronic Zeeman g-factor, and $\widehat{S}_{t}$ is a cartesian component of the electronic spin operator.

The spin-orbit contribution arises from the fact that, with the electronic spin-orbit coupling present, the external magnetic field induces an electronic spin density. This spin density then causes nonvanishing shielding contributions by magnetic interactions with the nuclear-spin. The spin-orbit contribution is very sensitive not only to the atomic number of the central nuclei but to the atomic number of the atoms directly coordinated to it. Spin-orbit chemical shifts require strong s-type bonding contributions at the NMR nucleus. This explains why they are found large spin-orbit chemical shifts for the ^{1}H NMR but less so for other nuclei.

Kaupp et al.[78] have presented a simple but general qualitative picture of the mechanism involved. The spin-orbit operators induce spin polarization in the system. This induced spin density interacts with the nuclear magnetic moment of the NMR-active nucleus, by means of a Fermi-contact mechanism, see Figure 2.3. The SO shifts are indicated to be caused by the spin-orbit operator on the heavy atom A, which in the presence of an external magnetic field B_0 leads to a small amount of electronic spin polarization. The latter may now interact with the nuclear magnetic moments (e.g., nucleus B) in the system, mainly via an FC mechanism, and will cause a change in their nuclear shieldings.
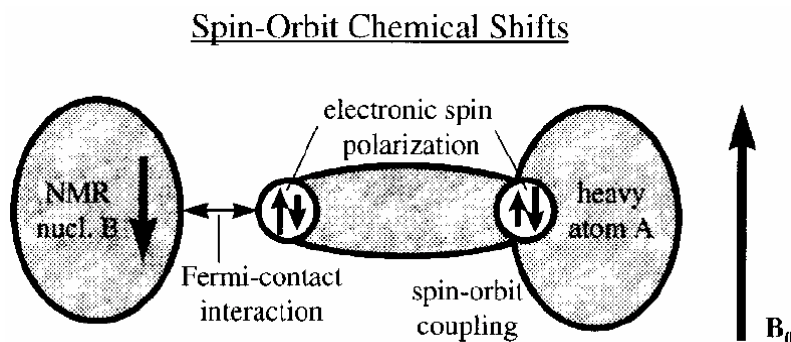
Figure 2.3. *Schematic illustration of the spin-orbit shifts*

That SO shifts will depend strongly on the s-character of the bonding around the atom observed[108] by NMR spectroscopy, as the FC mechanism acts via the spherical part of the density at the nucleus. This dependency on s-character has indeed been demonstrated, and is particularly apparent for SO shifts across one bond; for instance, for the sp^3-, sp^2-, and sp-hybridized *a*-carbon atoms in iodoethane, iodoethylene (iodo-benzene), and iodoacetylene, respectively. The importance of the s-character has far-reaching consequences for SO-induced heavy-atom effects on chemical shifts. Among other things, it explains why chemical shifts of main-group elements in their highest oxidation states exhibit very large SO shifts when attached to halogen or related substituents. The s-character of the bonding to the heavy-atom substituents is large in such cases, and thus there exists an

Chapter 2

efficient FC mechanism that transfers the SO-induced spin polarization to the considered NMR nucleus.

As example of the SO influence of a heavy ligand, mostly over a light atom; Table 2.4 presents ^{13}C NMR shielding constants and shifts calculated[99] for methane and the methyl halides, CH_3Cl, CH_3Br, CH_3I. The shifts are taken with respect to methane. Absolute experimental shieldings for the carbon of methane are reported in the literature: 197.4 ppm, 195.1 ppm.[109] These values agree well with the estimates given in the table. For example, because the SO shifts due to halogen substituents are usually shielding, and their magnitude increases with the atomic number of the halogen, the consequence is a large increase of the nuclear shielding of the central atom when going from Cl to Br to I substituents.

Table 2.4. ^{13}C NMR chemical shifts in ppm, taken with respect to TMS

Molecule	s^p	s^d	s^{FC}	s^{cal}	d^{cal}	d^{exp}	$d^{cal} - d^{exp}$
TMS	-78.8	250.2	0.0	179.5	0.0	0.0	0.0
CH_4	-28.7	222.2	0.0	193.5	-14.0	-9.3	-4.7
CH_3Cl	-67.2	221.8	2.1	156.7	22.8	18.1	4.7
CH_3Br	-58.5	221.5	12.8	175.8	3.7	3.0	0.7
CH_3I	-57.5	233.1	35.2	216.2	-36.7	-27.8	-8.9

Instead for heavy atoms, more than the atomic number of its substituents, the s-character of the bonding in determine an efficient FC mechanism that transfers the SO-induced spin polarization to the ''NMR nucleus.'' In Table 2.5 are presented the computed SO contributions for some Uranium halogens,[28] the SO shielding goes up with the oxidation of the metal and not with atomic number of the ligand.

Table 2.5. *Calculated (computed geometry) and experimental* ^{19}F *NMR shifts, relative to* $CFCl_3$*, (in ppm) for* UF_6*,* UF_5Cl *and* $UFCl_5$ *compounds*

Molecule	s^{so}	d^{cal}	d^{expt}
UF_6	21.2	831.0	764.0
UF_5Cl	19.3	813.3	762.0
$UFCl_5$	7.6	750.8	774.3

2.5.3.1 The Gauge-Origin problem

Exact solutions of the Zora equation are independent of the choice of origin of the vector potential for the external magnetic field. While, in approximate solutions there is a dependency on the gauge of the electrical potential V. Gauge-including atomic orbitals (GIAOs), also called London orbitals,[110] are used to ensure that the calculated results do not depend on the gauge origin of the magnetic vector potential A_B.

For any given magnetic field, there is a considerable freedom in the choice of gauge for the vector potential. In particular, the actual vector potential depends on the arbitrary coordinate origin. Any expectation value can only depend on the values of observable quantities, and the gauge dependence should vanish exactly. This is indeed, the case for exact solutions of; e.g., the KS equations where large (infinite) basis sets are used. For approximate solutions with smaller (finite) basis sets, NMR/ESR properties experiment a strong dependence on the choice of gauge.

Possibly the best solution to the gauge problem is to employ field-dependent GIAOs as basis functions.[111] The basis functions now depend on the external magnetic field as

$$\boldsymbol{j}_m(B,r) = \exp\left[-\left(\frac{i}{2c}\right)(B \times R_m)r\right]\boldsymbol{j}_m(r)$$

Chapter 2

where $j_m(r)$ is the usual field-free basis function (atomic orbital, AO) this is centred at position R_m and $j_m(B,r)$ is the corresponding GIAO. The field-dependent prefactor ensures that only differences of position vectors appear in expectation values. This eliminates any origin-dependence, even for approximate MOs and finite basis sets.

Instead of the GIAO approach, it is also possible to assign similar exponential pre-factor to other entities, e. g., to localized MOs. This is the idea of the IGLO approach.[112] The GIAO approach lends itself ready to an analysis of the calculated shieldings, in terms of the occupied and virtual MOs of the molecule.[113] This analysis constitutes a major advantage of the GIAO method, this is intrinsically impossible for other methods like IGLO-based schemes.

It is convenient to introduce an auxiliary basis set with basis functions Φ_j

$$\Phi_j = \sum_m^N \sum_{g=a,b} d_{mj}^g j_m(B)g, \ \Psi_i(B) = \sum_j^N u_{ji}\Phi_j$$

thus up to first order in the external magnetic field, the solutions of the Zora equation including the external magnetic field $h^{ZORA}(B)y_i(B) = E_i(B)y_i(B)$ are

$$y_i(B) = \Phi_i + \sum_j^N Bu_{ji}^1 \Phi_j$$

2.5.3.2 Frozen core approximation

To save computing time it is often desirable to use frozen core approximation. The MOs close to a nucleus are believed to change only very little in going from a free atom to an atom in a molecule and to have a negligible overlap with each other. With these assumptions we can keep the core AOs frozen during the molecular calculation so that they can be excluded from the matrix equations that are to be solved.

In the frozen-core approximation, the N GIAO basis functions $\{j_m\}$ are split into a core set $\left\{j_m^{core}\right\}_{m=1}^{N_{core}}$ and a valence set $\left\{j_m^{val}\right\}_{m=1}^{N_{val}}$, where $N_{core} + N_{val} = N$. By taking an appropriate combination of core and valence functions, a new set of N_{val} valence basis functions that are orthogonal to the core orbitals are obtained

$$l_m = j_m^{val} + \sum_t^{M_{core}} b_{mt} j_t^{core} \text{, such that } \left\langle l_m \middle| j_t^{core} \right\rangle = 0,$$

here b_{mt} are the core-orthogonalization coefficients.

In addition one can assume that the response of the tightly bound core electrons to the applied magnetic field is negligible. A set of atom centred core orbitals, $\left\{w_a^{core}\right\}_{a=1}^{N_{core}}$, independent to the external magnetic field are then constructed. The new valence functions, l_m^{val}, then become

$$l_m^{val} = j_m^{val} + \sum_t^{M_{core}} b_{mt} w_t^{core} \text{, such that } \left\langle l_m \middle| w_t^{core} \right\rangle = 0.$$

For each nucleus as we have a r_{core}^A independent of the external magnetic field, this fact modifies a little the general view of the shielding tensor. For the diamagnetic shielding we have

$$s_{st}^d = s_{core_{st}}^d + s_{val_{st}}^d,$$

the diamagnetic core contribution, $s_{core_{st}}^d$, is the only core contribution in the total shielding given by r_{core}^A

$$s_{st}^d \propto \frac{1}{2c^2} \sum_A^{N_{nuc}} \int r_{core}^A \frac{K}{r_N} dt.$$

Chapter 2

And the diamagnetic valence part, $\boldsymbol{s}_{val_{st}}^{d}$, is determined by the zeroth-order wave function, but the summation over the occupied orbitals is over the valence orbitals only

$$\boldsymbol{s}_{val_{st}}^{d} \propto \frac{1}{2c^2} \sum_{i}^{val} n_i \sum_{m}^{N} d_{mi} \left\langle \boldsymbol{y}_i \left| \frac{K}{r_N} \right| \boldsymbol{j}_m \right\rangle.$$

The paramagnetic shielding is basically $\boldsymbol{s}_{st}^{p} \simeq \boldsymbol{s}_{st}^{p,val-vir}$, this valence-virtual part is the only most important term since this is the only term that is not a result from the introduction of the GIAOs. There is no contribution from the core orbitals, since it is determined by the wave function in the magnetic field and there was assumed the core orbitals to be independent of the magnetic field. By similar reasons there is also no contribution from the core electrons to the spin-orbit shielding, $\boldsymbol{s}_{st}^{so}$, because the core electrons are excluded to suffer the spin-orbit effect in the initial calculation of the wave function.

2.6   Review of the factors to take into account in the calculation of shielding tensors from approximate wave functions

2.6.1   XC functionals

Existing XC functionals can be roughly divided into three groups, local density approximations (LDAs),[114] generalized gradient approximations (GGAs),[115] and hybrid functionals that incorporate part of the exact Hartree-Fock (HF) exchange.[116]

The general consensus is that the simple LDA is insufficient for chemical shifts.[117,118] The differences between various GGAs seem to be minor and no general trend has emerged. Hybrid functionals have also been tested, they seem to be slightly more accurate than the GGAs for first-row compounds.[119] On the other hand, Kaupp et al.[120], in their study of ^{17}O NMR in transition metal complexes MO_4^{n-}, found that hybrid functionals were inferior to GGAs in this example. Bühl applied hybrid DFT to the

calculation of ^{57}Fe and ^{103}Rh chemical shifts,[121] with quite a dramatic effect, e.g., for ^{57}Fe, by correlating computed with experimental chemical shifts, he obtained linear regression lines with slopes of 0.65 (GGA) and 0.97 (hybrid), respectively, i.e., the hybrid functional is clearly superior in these cases. The reason for these effects is not entirely clear. We conclude, with the words of Kaupp et al.,[122] that "the search for a 'universal' functional is still a challenge".

It is clear that not all functionals designed to reproduce experimental thermochemical data appear to be equally well suited for chemical-shift computations. In transition-metal, in contrast to the situation for chemical shifts of main group nuclei including ligand chemical shifts in transition-metal compounds, any particular DFT method employed for the chemical shift calculations has to be carefully reassessed for every new problem at hand, at least until better functionals (i.e., closer to the elusive, universal one) become available. Most likely, the large sensitivity of the metal shifts to the exchange-correlation potential is related to the largely local types of electronic excitations involved. These are known to be very poorly described by most functionals currently available.[123]

For most of the transition-metal chemical shifts studied so far, the B3LYP hybrid functional performs similar or better than pure density functionals. The latter seem to underestimate proportionally the paramagnetic contributions, $\mathbf{s}^p$, which is apparently corrected for by inclusion of some Hartree-Fock exchange, and of the corresponding, pure HF methods significantly overestimate the chemical shifts.[124] It has yet to be elucidated if the good performance of hybrid functionals is a manifestation of the physical reasoning put forward to motivate the inclusion of HF exchange in density functionals,[125] or simply the result of fortunate error compensation. In any case, the GIAO-B3LYP scheme is not a panacea.

The success of hybrid DFT methods has been analysed[126] and attributed to more diffuse virtual orbitals, coupling due to Hartree-Fock exchange and the increase of the HOMO-LUMO gap relative to that obtained using pure DFT methods. Different generalized gradient approximations, GGA, give similar results whereas hybrid functionals stabilize occupied MOs strongly and destabilize virtual MOs. HOMO-LUMO gaps are nearly doubled as a result.

Chapter 2

Improved functionals without exchange mixing would of course be desirable. The design of new exchange and correlation functionals is a very active field, and so there is some hope that better functionals will eventually become available.

2.6.2 Relativistic effects

Before turning to the current calculations, I would like to qualitatively summarize how relativistic effects manifest themselves in calculated NMR shieldings and chemical shifts; the mechanisms for that are by now well understood.

Sometimes, relativistic effects on some properties like the NMR shielding have been divided into "direct" and "indirect" effects, with the latter arising from the well-known relativistic bond contraction or, more generally, from differences between nonrelativistic and relativistic molecular structures. Here, I will consider fixed, relativistic geometries only and hence will not discuss the "indirect" relativistic effects any further.

The remaining "direct" relativistic effects can be divided into spin-free (scalar) and spin-orbit/Fermi contact effects. The scalar relativistic effects become particularly important when one descends to the sixth period, and thus their inclusion into the calculations is mandatory. Taking only molecules at a given geometry into account there are three major mechanisms in which relativity influences NMR shieldings.

First, relativity contracts the inner-core shells (s and p). This leads to a contraction of the core electronic density which in turn yields a large increase in the diamagnetic shielding. Since this is a core effect, it cancels out in relative chemical shifts.

Second, valence MOs are influenced by relativity as well, since they have to be orthogonal to the compact core MOs. Thus, s- and p-type orbitals are typically contracted and stabilized, while d and f orbitals are more effectively screened from the nuclear charge, and are expanded and destabilized as a consequence. These relativistic changes are reflected in the shieldings and the chemical shifts, primarily through the change in orbital

UNIVERSITAT ROVIRA I VIRGILI
DFT STUDY OF TITANIUM CUBANE AND MOLYBDENUM SULPHIDE COMPOUNDS.
Autor: José Manuel Gracia Budria
ISBN: 978-84-690-6751-2 / DL: T.1196-2007

Density functional methods. The calculation of NMR shielding tensors

energy differences; the strength of the magnetic interaction between different MOs is inversely proportional to their orbital energy differences.

Spin-orbit effects follow a different mechanism. Thus, the relativistic spin-orbit operators, in the presence of a magnetic field, produce spin polarization at the heavy nucleus, even for formally closed-shell systems. This can also be shown rigorously. The spin polarization is transferred through the bond to an NMR nucleus, where it is picked up by means of a Fermi contact mechanism. One important consequence of this picture is that spin-orbit chemical shifts are only relevant if there are strong s-bond contributions at the NMR nucleus.

2.6.3   Frozen-core approximation

It is a common assumption that the NMR chemical shift is a property of the core electronic density near the NMR active nucleus. The fact that the nuclear spin interacts with the electronic movement around the nucleus N, and that this interaction is inversely proportional to r_N^2, is the basis for this assumption. In their attempt to use a relativistic Pauli-type Hamiltonian, Schreckenbach and Ziegler have proposed calculating NMR shieldings using the frozen-core approximation.[127] This method would never work if the above assumption was true, because all core MOs are taken from atomic calculations, kept frozen in subsequent molecular calculations.

The core electronic density is explicitly excluded from contributing to chemical shifts in any way other than through its constant atomic (diamagnetic) contribution; it is not allowed to add to molecular effects in the chemical shift, by coupling with virtual MOs. The valence MOs are, however, orthogonalized against all core MOs; this ensures their correct asymptotic behaviour near the nucleus. Schreckenbach and Ziegler were able to conclude that frozen-core approximation is a useful tool for shielding calculations if the valence space is increased to contain at least the ns, np, (n-1)p, (n-1)d; shells where n is the number of the given period in the periodic table of elements.

It follows clearly that the relative chemical shift is a valence property, and not a core property. More precisely, this is mostly determined by the basis

Chapter 2

set requirements in the very vicinity of the central nucleus due to the mentioned r_N^{-2} dependence.

2.6.4   Geometries of the compounds

Computed geometries determine the electronic structure of the system and so the diverse contributions of the shielding tensors. In a similar way, a change in the structural parameters modifies the shielding tensor.

The dependence of the shielding tensor on the geometry of the system serves us to notify that if the optimized geometry is far from the experimental one, the computed shielding will be far from the experimental one too. Sometimes, it would help the use of experimental parameters for the computation.

Figure 2.4 underlines the dependence of the calculated chemical shifts on the molecular geometry for $HgCl_2$.[43] A change of 0.01 Å in bond length results in a change of approximately 50 ppm for the calculated shifts. The change in the paramagnetic contribution is much larger than the change in the spin–orbit coupling contribution. The diamagnetic contribution is effectively constant and has not been shown in the plot. The relationship is roughly linear with a change of 100 ppm for every 10° change in the bond angle.

Table 2.6 shows ^{199}Hg ZORA NMR shieldings and shifts relative to $HgMe_2$, calculated using optimized geometries. Here the differences between calculated and experimental shifts are disappointingly large because of the deviations between optimized and experimentally determined geometries. For HgI_2 the optimized bond length is 0.08 Å longer that the experimental value, which translates into a difference of 900 ppm between shifts calculated with optimized and experimental structures, respectively, see Table 2.7. The optimized structures for the chloride containing compounds are closer to the experimental estimates with the result that the shifts calculated at these geometries are more similar than for the iodine systems.
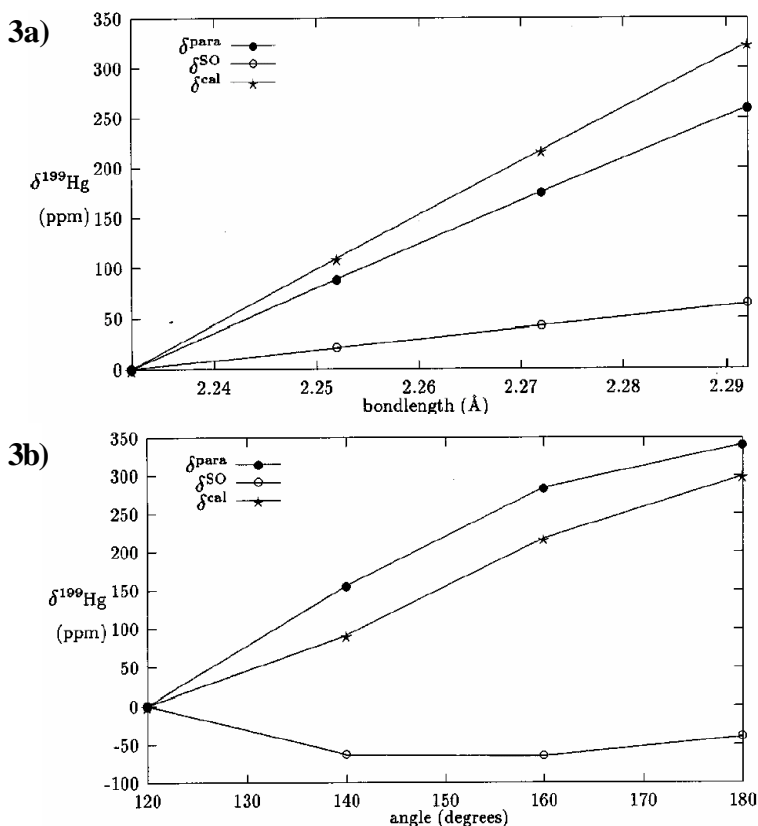
Figure 2.4. *Calculated* ^{199}*Hg NMR shielding changes (in ppm) with change in bond length (in Å) (Fig. 1a) and in* $Cl - Hg - Cl$ *angle (in degrees) (Fig. 1b) for linear* $HgCl_2$

Table 2.6. *Calculated* ^{199}*Hg NMR shielding constants and shifts (in ppm) using computed geometries*

Molecule	r(Hg-L)	s^{cal}	d^{cal}	d^{expt}	$\left| d^{cal} - d^{expt} \right|$
$HgMe_2$	2.101	8091	0	0	0
$HgCl_2$	2.289	9774	-1683	-1519	164
$HgBr_2$	2.438	10952	-2861	-2213	648
HgI_2	2.633	12501	-4409	-3447	962

Chapter 2

Table 2.7. *Calculated* ^{199}Hg *NMR shielding constants and shifts in ppm using experimental geometries*

Molecule	r($Hg-L$)^a	s^{cal}	d^{cal}	d^{expt}	$\lvert d^{cal} - d^{expt} \rvert$
$HgMe_2$	2.083	8020	0	0	0
$HgCl_2$	2.252	9576	-1556	-1519	37
$HgBr_2$	2.410	10704	-2684	-2213	471
HgI_2	2.554	11526	-3506	-3447	59

^{a} *Gas phase*

Using experimental geometries, good qualitative agreement with experiment is obtained, and quantitatively the calculated results deviate from experiment on average by 163 ppm, which is approximately 3% of the total range of ^{199}Hg NMR. In addition, it has been shown, through the mercury NMR shieldings of HgCl₂, how the strong dependence of calculated shifts on the structure puts high demands on the accuracy of optimized geometries if they are to be used in quantitative chemical shift calculations.

2.7 ^{183}W NMR shielding tensor in polyoxometalate compounds

Introduction

Polyoxometalates or polyoxoanions (POMs) are an immense family of compounds made up of transition metal ions in their highest oxidation state usually Mo, W, V and mixtures of these elements and oxo ligands.[128,129,130] The special ability of many POMs to accept one or several electrons with minimal structural changes means that they have potential applications in many fields such as medicine, catalysis, multifunctional materials or chemical analysis.

One of the most powerful methods for characterizing POMs, both in solution and in solids, is NMR.[128] Practically every paper dealing with POMs is accompanied by their NMR spectra. Depending on the complexity

of an anion and on its symmetry, several lines may be observed in the NMR spectra, and sometimes the correct assignment of each line to a particular atom is unclear. The increasing evolution of computational chemistry procedures has made it possible to study a number of molecular properties in the chemistry of polyoxometalates from the electronic structure of the polyoxoanion.[131, 132] The chemical shifts observed in the NMR spectra depend on the electronic and molecular structure of the POM. Finding a correlation between the electronic and molecular structure and the NMR parameters is highly desirable if the role of POMs in many chemical processes is to be understood.

Excellent work by Ziegler and Schreckenbach, who implemented NMR chemical shift calculations in regular DFT procedures, has made it possible to use the modern features of DFT for accurate exchange-correlation (XC) functionals and large basis sets. The interest in reproducing the NMR spectra of POMs is also theoretical. These non-conventional complexes are very suitable models for verifying different theoretical approaches, especially because of the strong dependence of the shielding tensor on variations in the electronic structure of the compounds.

The shielding of the ^{183}W nucleus in Keggin polyoxotungstates has recently been investigated by DFT methods. While there are several examples of calculations of first-row transition metal shifts,[133] the substantial influence of relativistic effects on the second and third row metals hinder the study of polynuclear tungsten complexes.

Ziegler at al. showed how to apply the DFT-GIAO scheme to the calculation of ^{183}W NMR chemical shifts. Pauli and ZORA spin–orbit Hamiltonians (see section 2.5.1) were used to calculate the tungsten series WO_4^{2-}, WO_3S^{2-}, $WO_2S_2^{2-}$, WOS_3^{2-}, WS_4^{2-}, WF_6, WCl_6 and $W(CO)_6$. The authors concluded that the ZORA scheme generally provides chemical shifts in better agreement with the experimental values than the Pauli scheme. Nevertheless, an all-electron basis set of Slater type orbitals was used in the ZORA calculations, while Pauli calculations made use of a similar basis for tungsten atoms but with a frozen core up to 4d. As shown by J. Baerends et. al.,[134] in another revealing work, basis set effects are rather important for obtaining reliable chemical shifts. In this study, the authors used a scalar relativistic scheme to consider all-electron and frozen core calculations. They concluded that it is possible to obtain reliable chemical shifts with a

Chapter 2

frozen core basis set, as long as the valence basis set is sufficiently flexible in the core region to describe the core wiggles of the valence orbitals accurately. In these cases, Zora and Pauli Hamiltonian differences for the chemical shifts are relatively small. The core functions only have to describe the core wiggles of the valence orbitals, not the frozen core orbitals themselves. The latter are taken from separate atomic calculations using very large converged basis sets. Nevertheless, further improvements should include investigating the effects of spin-orbit coupling, exchange correlation functionals and the environment (solvent).

NMR chemical shift computation in POTs

Bagno et al. study the efficacy of effective core potentials (ECPs) in mononuclear tungsten complexes and in $PW_{12}O_{40}^{3-}$ Keggin compound.[135] However, because the paramagnetic contribution depends on integrals containing a r^{3-} dependence, which are very sensitive to the behaviour of molecular orbitals near the nucleus, there is a slight dispersion in chemical shift. In a more recent work, Bagno[136] shows the utility of the DFT-GIAO computational scheme, including relativistic effects for several POTs. The effect of the basis set and of the scalar or spin-orbit relativistic effect are calibrated. A tolerable loss of precision is reported for relativistic scalar and frozen core calculations, but it is pointed out that spin-orbit effects may play a role in determining small shift differences. In a pioneering study, Bagno calibrated the effects of a labile counter anion in the ^{183}W NMR spectra of a Keggin compound.

In this context, we computed chemical shifts for the ^{183}W nucleus using popular DFT methods. We reinvestigated the series of tungstates discussed by Ziegler and co-workers. We also extended our study to some POTs: the most simple of the POTs, the Lindqvist anion, $W_6O_{19}^{2-}$, its nitrosyl derivative $W_6NO_{19}^{3-}$ and the Keggins $BW_{12}O_{40}^{5-}$, $SiW_{12}O_{40}^{4-}$, $PW_{12}O_{40}^{3-}$ and $GeW_{12}O_{40}^{4-}$. NMR chemical shift calculations were performed with the NMR program.[33,43,99,106,127] The atom shift, in terms of the orbitals of the molecule, was also analysed with the EPR program.[33,106,127,137,138] Both of these programs are part of the ADF package.[139] In all cases, shielding values were obtained from an electronic structure computed from pure GGA Becke (exchange) – Perdew (correlation) potential.[65,115a] To evaluate the factors that may affect nuclear shielding, we carried out calculations with several

Density functional methods. The calculation of NMR shielding tensors

basis sets, experimental and optimized gas phase geometries, and scalar and spin-orbit relativistic effects on the ZORA formalism.

Due to the novelty of these studies, the main objectives of the present work are to evaluate the ability of DFT methods to reproduce ^{183}W NMR chemical shifts, and to review the most appropriate way of working in POTs in terms of accuracy and computational cost. In particular, we shall attempt to identify the error sources. We shall also discuss the relationship between the chemical shifts and the electronic structure of the system, by analysing the paramagnetic contributions to the shielding tensor. Subsequently, the utilization of the computational dates to unequivocally characterize the atoms of a compound is a current dare.

All calculations are performed basically at four approximation levels: 1) a scalar relativistic Hamiltonian with two standard ADF TZP basis sets. First a triple-ζ STO basis with one polarization function in the valence shell and a double-ζ in the subvalence shell, and a single-ζ in the core region (up to 4d for tungsten), except for an additional very tight 1s function, with an exponent of ~10^2, in the 5d metals (**fc-sr**). And second, the same frozen core basis, which also includes one steep 1s tight function with ~10^3 exponent (**ae-sr**), for the heteroatoms, and an all-electron basis set with a double-ζ representation in the core region and a triple-ζ representation in the valence area for the tungsten atom. 2) a combination of the spin-orbit Hamiltonian with the same 4d core and all-electron basis sets, denoted as **fc-so** and **ae-so**, respectively. Both basis sets are quite similar but the functions that describe the core wiggles of the valence orbitals in **ae** basis set are tighter and the description of the electronic density close to the nucleus is better.

Optimized geometries have been used in all cases with the exception of the WO_4^{2-} molecule, for which the calculations were performed with the experimental geometry. WO_4^{2-} is used as the reference so that comparisons can be made with the experimental NMR shifts and the previously mentioned study by Ziegler.[40] Test chemical shifts were also obtained from the optimized WO_4^{2-} geometry. Nevertheless, the displacement of the values is inconsistent. The geometries were optimized with the scalar-relativistic (optimization with the spin-orbit Hamiltonian is not implemented in the ADF package) ZORA method for the frozen core basis set; no significant variations are expected in the geometry when the basis set is changed.

Chapter 2

Considering the strong dependence of the NMR shielding on the molecular structure, our discussions assume that the arrangement of our systems is reasonable and that any deviations from experimental NMR values come from an incorrect description of the electronic structure and not from an inappropriate optimized geometry, which obviously is not fully true for all the cases studied.

Table 2.8 shows the NMR chemical shifts computed for the test small molecules together with the absolute shieldings, and the paramagnetic, diamagnetic and spin-orbit contributions. In general, **ae-so** calculations provide chemical shifts that are in better agreement with the experimental ones. Experimental values are almost reproduced for the tetrahedral molecules WO_3S^{2-}, $WO_2S_2^{2-}$, WOS_3^{2-} and WS_4^{2-}. The average absolute deviation is 74 ppm, 1% of the experimental range (7200 ppm) for the [183]W chemical shift of the calculated compounds. Discrepancies were largest for hexacoordinate WCl_6, $W(CO)_6$, and especially WF_6. The average absolute deviation was 445 ppm, 6% of the experimental range. The same problem was observed by Ziegler[40] and Baerends.[134]

The **ae-sr** computed shifts also show a good range of values that are close to those of the **ae-so** calculations. This is because the tungsten compounds considered here make a spin contribution that is small in absolute value. As discussed elsewhere,[78,99] the spin-orbit contribution is important for central atoms if they are coordinated to elements with a large spin-orbit constant (Se, Te, Br, I, etc.) through bonds that contain a significant contribution from the s orbitals in the central atom. Although the spin-orbit contribution to the chemical shifts is not important in absolute value, its contribution is important for distinguishing different chemical environments for a given nucleus. This can be observed perfectly in the tetrahedral molecules WO_4^{2-}, WO_3S^{2-}, WO_2S^{2-}, WOS_3^{2-} and WS_4^{2-}. **ae-sr** calculations show that the relative shifts between the studied molecules are relatively smaller than the experimental values. We obtained an average absolute deviation of 132 ppm with respect to the experimental chemical shifts (see Table 2.8). The introduction of spin-orbit effects provide a proper description of the separation between signals for these molecules. Because the oxygen atom is replaced by the heavier sulphur atoms, the relativistic spin-orbit effects increase to over 20-25 ppm per sulphur atom, which leads to a large gap between molecular signals. So results are more accurate with the average absolute deviation of 74 ppm from the experimental values.

92

Density functional methods. The calculation of NMR shielding tensors

Table 2.8. ^{183}*W NMR signals for simple tungsten molecules*

		EXP.	fc-sr	ae-sr	fc-so	ae-so
WO$_4$$^{2-}$	Chemical Shift	0.0	0.0	0.0	0.0	0.0
	Absolute Shielding		2792.8	617.2	2499.6	193.1
	Paramagnetic		-6871.1	-7976.7	-6901.8	-8067.4
	Diamagnetic		9663.9	8593.8	9664.1	8611.8
	Spin-Orbit				-262.6	-351.3
WO$_3$S^{2-}	Chemical Shift	841	668.3	816.3	628.0	839.7
	Absolute Shielding		2124.5	-199.1	1871.6	-646.6
	Paramagnetic		-7541.0	-8794.0	-7554.6	-8886.2
	Diamagnetic		9665.5	8595.1	9665.7	8612.9
	Spin-Orbit				-239.6	-373.4
WO$_2$S$_2$$^{2-}$	Chemical Shift	1787	1334.7	1636.0	1263.2	1689.7
	Absolute Shielding		1458.1	-1018.8	1236.4	-1496.6
	Paramagnetic		-8208.8	-9614.6	-8204.6	-9709.7
	Diamagnetic		9666.9	8595.8	9667.1	8613.8
	Spin-Orbit				-226.1	-400.7
WOS$_3$$^{2-}$	Chemical Shift	2760	2076.3	2559.6	1971.9	2632.0
	Absolute Shielding		716.5	-1942.4	527.7	-2438.9
	Paramagnetic		-8952.1	-10539.1	-8928.7	-10628.3
	Diamagnetic		9668.6	8596.8	9668.8	8614.7
	Spin-Orbit				-212.4	-425.3
WS$_4$$^{2-}$	Chemical Shift	3769	2924.8	3617.6	2788.6	3701.1
	Absolute Shielding		-132.0	-3000.4	-289.0	-3508.0
	Paramagnetic		-9802.6	-11598.3	-9760.6	-11678.2
	Diamagnetic		9670.6	8597.8	9670.8	8615.7
	Spin-Orbit				-199.2	-445.6
WCl$_6$	Chemical Shift	2181	1862.8	2388.2	1622.8	2306.3
	Absolute Shielding		930.0	-1771.0	876.8	-2113.2
	Paramagnetic		-8744.8	-10373.2	-8715.4	-10452.3
	Diamagnetic		9674.9	8602.2	9675.1	8620.1
	Spin-Orbit				-82.9	-280.9
WF$_6$	Chemical Shift	-1121	-387.5	-344.0	-484.9	-392.4
	Absolute Shielding		3180.3	961.2	2984.5	585.5
	Paramagnetic		-6476.5	-7624.6	-6495.0	-7724.7
	Diamagnetic		9656.9	8585.8	9657.2	8603.8
	Spin-Orbit				-177.6	-293.5
W(CO)$_6$	Chemical Shift	-3446	-3197.6	-3602.3	-3512.9	-3827.1
	Absolute Shielding		5950.4	4219.5	6012.5	4020.2
	Paramagnetic		-3726.7	-4383.8	-3680.7	4445.5
	Diamagnetic		9677.1	8603.3	9667.2	8621.1
	Spin-Orbit				16.0	-155.4

Chapter 2

The values obtained from the frozen core basis set show that the experimental values for the tetrahedral molecules are considerably worse. **fc-so** calculations in this case show an average deviation of 626 ppm (9% of the range). However, for the hexacoordinate molecules the average deviation is 454 ppm (6% of the range), similar to that of the **ae** calculations. The bad results obtained for the tetrahedral molecules can be analysed from the paramagnetic contribution to the shielding. Because oxygen is replaced by the less electromagnetic sulphur atoms, the energy gap between bonding and antibonding orbitals is shorter. The paramagnetic term is increased by the shorter energy gap. So, for the **ae-sr** results, we observe paramagnetic contributions of, -7977, -8794, -9615, -10539 and -11598 ppm for WO_4^{2-}, WO_3S^{2-}, WO_2S^{2-}, WOS_3^{2-} and WS_4^{2-} molecules, respectively. The average separation computed between chemical shifts in the compounds is 908 ppm, while the average experimental separation is 942 ppm. If we now observe some paramagnetic values for the **fc-sr** calculations, we find that this gap has now decreased to an average of 732 ppm. In the absence of spin-orbit effects, there are several possible reasons for this lower value: the core electrons are in fact significantly affected by the external magnetic field, the central nucleus has an excessively big core, or the basis set in the core region is not flexible enough. For this last assumption, Baerends et al. significantly improved their frozen core results by passing from a triple-ζ valence basis set with only a single-ζ description of the core wiggles of the valence orbitals, to a triple-ζ valence basis set with a double-ζ core description. On the other hand, when an extended basis set was used, with a quadruple-ζ valence region and a triple-ζ in the core, results were poorer.[134]

If we now compare the spin-orbit contribution for the tetrahedral molecules, we also observe different trends for the **ae** and **fc** basis sets. While the spin-orbit contribution increases with the number of sulphur atoms for the **ae** set, it decreases for the **fc** set (Table 2.8). The ZORA spin-orbit term is heavily influenced by the relativistic increase in the electron density around the nuclei. Therefore, it is reasonable to expect a strong dependence on the core electrons, and also that an accurate estimation of the spin-orbit contribution to the shielding tensor shall require a flexible basis close to the nucleus.[140] In this respect, the all-electron basis set includes a 1s steep function (~10^3). A more detailed discussion about basis set requirements in the very vicinity of the central nucleus can be found in the literature.[134,140,141]

The results obtained for the sequence of small tungsten molecules show that the **ae-so** calculations are the most accurate, especially for tetrahedral molecules. Otherwise, for hexacoordinate molecules, all-electron and frozen core calculations produce similar errors.

Table 2.9 shows the values obtained for the ^{183}W atom in the Lindqvist $W_6O_{19}^{2-}$ compound (Figure 2.5) for the same four **fc-sr**, **fc-so**, **ae-sr** and **ae-so** approximations. At all levels, the deviations from experimental chemical shifts are considerable. For the Lindqvist structure, all the tungsten atoms are equivalents, showing one signal at 59 ppm. In this case, the **fc-sr** approximation overestimates the signal and obtains 225.8 ppm. The introduction of spin-orbit effects decreases the signal to -33.6 ppm, closer to the experimental value. The explicit treatment of the core electrons in the **ae-sr** approximation yields a value of 350.4 ppm. As in the previous **fc-sr** case, we observe a clear overestimation of the signal. Again the introduction of spin-orbit effects reduces the shift and gives a value of 293.2 ppm, closer to the experimental value but worse than the value for the **fc-so** approximation.
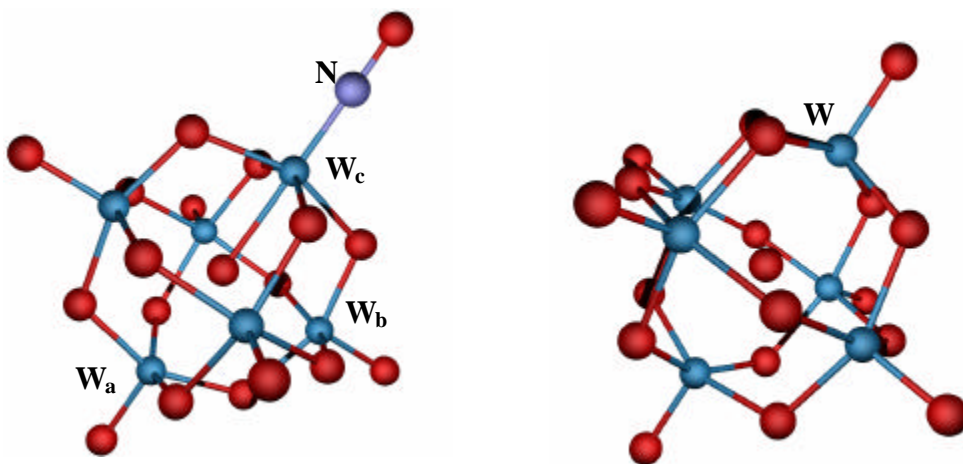

Figure 2.5. *Lindqvist structure (right) and nitrosyl structure (left)*

Chapter 2

Table 2.9. ^{183}W *NMR signals for Lindqvist* $W_6O_{19}^{2-}$ *compound*

$W_6O_{19}^{2-}$	EXP.	fc-sr	ae-sr	fc-so	ae-so
Chemical Shift	59	225.8	350.4	-33.6	293.2
Absolute Shielding		2567.0	266.8	2533.2	-100.1
Paramagnetic		-7091.2	-8318.6	-7062.2	-8399.6
Diamagnetic		9658.2	8585.4	9658.5	8603.4
Spin-Orbit				-63.1	-303.9

Unexpectedly, for this particular molecule the smallest variations in the chemical shifts between computed and experimental values are found for the frozen core calculations. Nevertheless, considerable differences from experimental values are found in all cases. We do not find a precise source of error in the compounds analyzed. While the treatment of tungsten in the tetrahedral molecules shows a logical progress as the theoretical method improves, the behaviour of the calculated shifts for octahedral simple molecules and the $W_6O_{19}^{2-}$ structure is chaotic. So, we opted for the Lindqvist structure as the reference compound in subsequent calculations so that we could extend our study to other similar POTs systems. In an attempt to avoid mistakes caused by different descriptions of the reference compound, we choose a reference compound that is analogous to the structures studied. In any case we try to preclude the observed random behaviour of the methods.

Substituting a terminal oxygen atom in the Lindquist structure for a NO unit leads to a nitrosyl $W_6O_{19}N^{3-}$ structure (Figure 2.5). With reference to the Lindqvist structure, the experimental spectra show signals for three different tungsten atoms. A tungsten atom directly bonded to the nitrogen (W_c) appears at 594 ppm, while the opposite tungsten and the four equatorial ones appear at 58 (W_a) and 109 (W_b) ppm, respectively. The values obtained at the **fc-so** level are 93.8 (W_a), 127.4 (W_b) and 289.9 (W_c) ppm. For purposes of comparison, additional calculations were performed at the best **ae-so** level and chemical shifts of 84.8, 151.5 and 364.0 ppm were obtained for the W_a, W_b and W_c atoms, respectively (Table 2.10). This time the computed values do not show big discrepancies between both approximation levels, and they provide a more consistent image of the methods used. At both levels, the computational values distinguish the three

metals and describe the W_a and W_b tungsten atoms reasonably well, but clearly fail to get the correct signal for W_c nuclei. This nucleus formally represents the substitution of an O^{2-} atom by a reduced nitrosyl NO^{3-} unit, which is a variation in the oxidation state of the tungsten atom directly bonded to the nitrogen. A change in the paramagnetic term by the presence of $\pi_{w\text{-}NO}$ bonding orbitals is explained in detail in the next section. The fact that DFT methods could not properly localize this metal oxygen π interactions could be responsible for the big discrepancies found for this W_c nucleus.

Table 2.10. *Chemical shifts calculations at **fc-so** and **ae-so** levels for the $W_6O_{19}N^{3-}$ structure*

$W_6NO_{19}{}^{3-}$			EXP.	fc-so	ae-so
	W_a	Chemical Shift	58	93.8	84.8
		Absolute Shielding		2439.4	-184.9
		Paramagnetic		-7155.8	-8503.1
		Diamagnetic		9658.8	8603.8
		Spin-Orbit		-63.6	-285.6
	W_b	Chemical Shift	109	127.4	151.5
		Absolute Shielding		2405.8	-251.6
		Paramagnetic		-7190.7	-8553.5
		Diamagnetic		9659.1	8604.0
		Spin-Orbit		-62.7	-302.0
	W_c	Chemical Shift	594	289.9	364.0
		Absolute Shielding		2243.3	-464.1
		Paramagnetic		-7417.5	-8858.5
		Diamagnetic		9664.4	8608.6
		Spin-Orbit		-3.6	-214.2

We observe that expensive **ae** calculations only slightly improve the results, which confirms that there is no need to use current all-electron basis sets in these particular systems, and that the considerable discrepancies between the experimental and computed shifts, like W_c, may come from a non perfect DFT description of the system.

Based on these ideas, we made calculations for the Keggins $BW_{12}O_{40}^{5-}$, $SiW_{12}O_{40}^{4-}$, $PW_{12}O_{40}^{3-}$ and $GeW_{12}O_{40}^{4-}$ at **fc-sr** and **fc-so** levels (see Table 2.11), again taking the Lindqvist structure as reference. **fc-sr** calculations show reasonable values for all the computed atoms with an average deviation from experimental values of 65 ppm. The inclusion of spin-orbit effects considerably improves the results and reduces the average deviation to 19 ppm. These results indicate that **fc-so** is a good method for treating these systems. Nevertheless, variations of a few ppm between metal atoms for different compounds are difficult to reproduce. For example, the experimental tendency that the chemical shift decreases from B to Ge is broken.

Table 2.11. *Relative shifts and shieldings for some Keggin compounds*

		EXP.	fc-sr	fc-so
$BW_{12}O_{40}^{5-}$	Chemical Shift	-190	-235.8	-183.5
	Absolute Shielding		2802.8	2716.7
	Paramagnetic		-6853.7	-6838.6
	Diamagnetic		9656.5	9656.7
	Spin-Orbit			-101.4
$SiW_{12}O_{40}^{4-}$	Chemical Shift	-163	-225.8	-189.0
	Absolute Shielding		2792.8	2722.2
	Paramagnetic		-6864.2	6841.8
	Diamagnetic		9657.0	9657.2
	Spin-Orbit			-93.1
$PW_{12}O_{40}^{3-}$	Chemical Shift	-158	-247.8	-170.2
	Absolute Shielding		2814.8	2703.4
	Paramagnetic		-6842.3	-6830.7
	Diamagnetic		9657.1	9657.3
	Spin-Orbit			-123.2
$GeW_{12}O_{40}^{4-}$	Chemical Shift	-141	-202.0	-172.0
	Absolute Shielding		2769.0	2705.2
	Paramagnetic		-6888.3	-6861.8
	Diamagnetic		9657.3	9657.4
	Spin-Orbit			-90.3

Chemical shift analysis in function of the electronic structure

Rationalising the dependence of the chemical shifts on the electronic structure of the cluster is as important as obtaining precise values of δ. The differences in the ^{13}C chemical shifts are basically due to the paramagnetic tensor in which the major contribution arises from the couplings between the occupied and unoccupied orbitals. The electronic structure of a POM is generally quite simple and consists of a set of doubly occupied orbitals, formally delocalised over the oxo ligands, and an occupied set of d-metal orbitals, both perfectly separated.[129,131] The delocalised nature of the molecular orbitals makes the orbital analysis of the chemical shifts quite difficult because there are no dominant contributions in the occupied-virtual term. Here, we discuss the variations produced in the NMR properties of the Lindqvist complex after a ligand O^{2-} is substituted by a ligand NO^- and the substituted centre is subsequently reduced. In this particular case, the changes in the chemical shifts are more important and the orbital analysis is simpler.

Let us start by analysing the electronic structure of these two complexes. In all fully oxidised polyoxoanions, the lowest metal orbitals are symmetry-adapted d_{xy}-type metal orbitals and the highest occupied orbitals are symmetry adapted p orbitals centred at the oxo ligands. At the present level of theory, the gap between the so-called oxo and tungsten bands appears at 3.24 eV for $W_6O_{19}^{2-}$. The presence of the NO^{3-} modifies this typical situation of a fully oxidised skeleton. The substituted tungsten is reduced to W^{4+} and the two metal electrons reside in a degenerate π_{W-NO} bonding orbital that appears between the oxo and tungsten bands. Figure 2.6 shows the energy levels for several frontier orbitals for $W_6O_{19}^{2-}$ and $W_6NO_{19}^{3-}$. We will show that this localised occupied orbital is responsible for the important changes in the shielding for the reduced tungsten atom.

Table 2.12 compares the shielding tensor and chemical shifts for the two Lindqvist anions. We have already mentioned that the diamagnetic contribution is almost constant and that the NMR properties for heavy atoms depend exclusively on the paramagnetic contribution if the spin-orbit term is not considered. The couplings between the occupied and virtual orbital (the OCC-VIR term) are the dominant contributions to the paramagnetic term and so their analysis may help to understand this observation.

Chapter 2
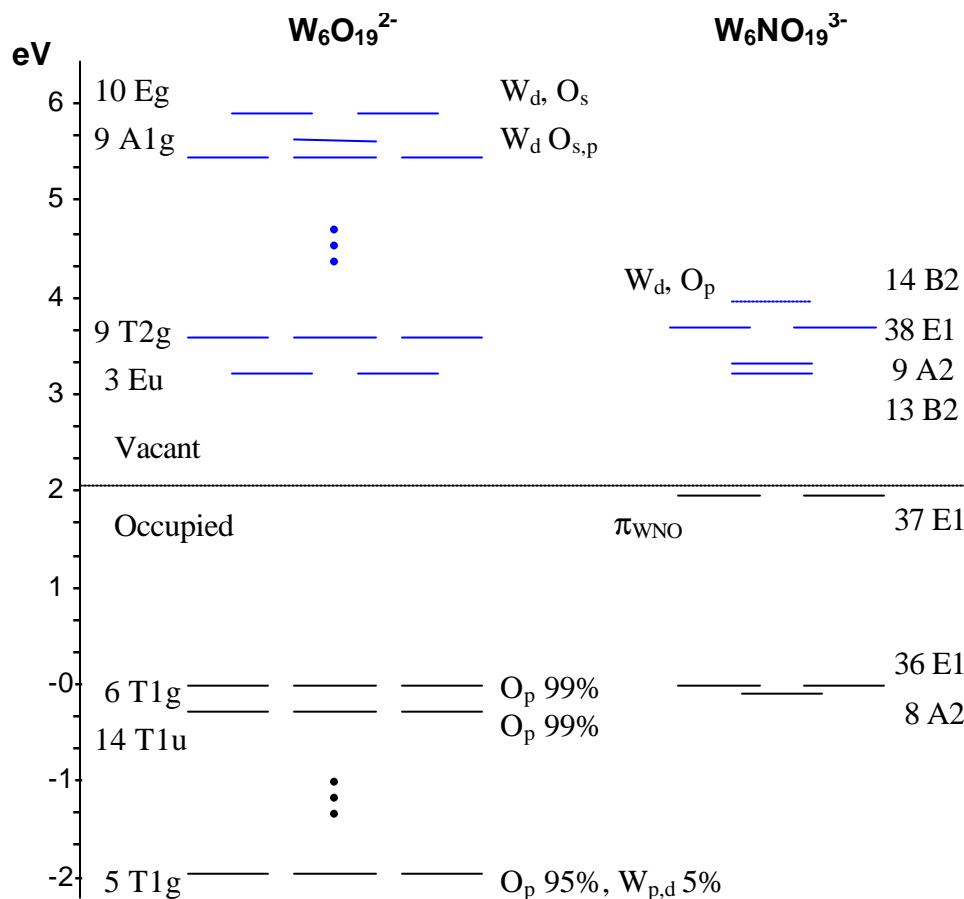
Figure 2.6. *Frontiers orbitals structure for Lindqvist and Nitrosyl adducts*

The change in the ^{183}W chemical shift caused by the substitution of the oxo ligand is considerable in the substituted tungsten (455 ppm), whereas for the other metals the changes are significantly smaller (87 and 125 ppm for the axial and equatorial metals, respectively). The paramagnetic term for the NMR shielding of the single W in the unsubstituted cluster is -7973 ppm. Unfortunately, almost all occupied and virtual orbitals participate to a greater or lesser extent in the paramagnetic term. Only two contributions stand out: the couplings between the occupied orbital 5T1g and the virtual orbitals 9A1g and 10 Eg (15% of total). These orbitals are represented in Figure 2.7 and the main contributions to the paramagnetic term are given in

```
UNIVERSITAT ROVIRA I VIRGILI
DFT STUDY OF TITANIUM CUBANE AND MOLYBDENUM SULPHIDE COMPOUNDS.
Autor: José Manuel Gracia Budria
ISBN: 978-84-690-6751-2 / DL: T.1196-2007
```
Density functional methods. The calculation of NMR shielding tensors

Table 2.13. The substitution of the oxo ligand also increases the value of the OC-VIR term for the unsubstituted metals by ~90 ppm. However, this contribution is not capable of distinguishing between the W_a and W_b metals.

Table 2.12. *Analysis of the main contributions to the Pauli Hamiltonian NMR shielding tensor, by EPR program, for Lindqvist and Nitrosyl adducts*

| | $W_6O_{19}^{2-}$ | | $W_6NO_{19}^{3-}$ | | | | | |
| | | | W_a | | W_b | | W_c | |
	s^a	d^b	s^a	d^b	s^a	d^b	s^a	d^b
Total	1692.0	0.0	1605.0	87.0	1566.8	125.2	1236.5	455.5
Diamagnetic	9665.5	0.0	9666.4	-0.9	9666.7	-1.2	9670.2	-4.7
Paramagnetic	-7973.5	0.0	-8061.5	88.0	-8099.8	126.3	-8433.6	460.1
CORE	-509.8	0.0	-536.2	26.4	-488.4	-21.4	-563.6	53.8
OC-OC	1092.1	0.0	1121.7	-29.6	1030.2	61.9	1291.7	-199.6
OC-VIR	-8555.8	0.0	-8647.0	91.2	-8641.7	85.9	-9168.5	612.7

^{a}*Absolute contribution to the shielding*
^{b}*Shift relative to adduct $W_6O_{19}^{2-}$*

For the substituted W_c, the situation is slightly different because the changes in the paramagnetic term are larger and the extra contribution arises from the coupling between the new $\pi_{W\text{-}NO}$ orbital and the d_{xy}-type orbital $14B_2$. The value of the corresponding coupling integral is -784 ppm. The couplings between occupied and unoccupied orbitals require an appropriate symmetry. This case is quite evident if we consider that the paramagnetic operators $\widehat{M}_x$ and $\widehat{M}_y$ transform the unoccupied orbital $14B_2$ into d_{yz}- and d_{xz}-like orbitals, which have a strong magnetic interaction with 37E, through the common lobes (Figure 2.7). A similar example has been described in section 2.5.3. The relatively small energy gap between the orbital 37E and $14B_2$ also favours the interaction between both. To sum up, this additional interaction means that W_c has the largest paramagnetic term in Table 2.12.

Chapter 2

Table 2.13. *Main contribution to the paramagnetic tensor for Lindqvist tungsten nucleus and Nitrosyl W_c nucleus directly bond to the nitrogen atom*

Compound	Orbitals			Shielding
	OC		VIR	
Lindqvist	5-T1g	→	9-A1g	-599.5
W	5-T1g	→	10-Eg	-678.5
	5-T1g	→	All	-1396.7
	All	→	9 A1g - 10 Eg	-1804.0
Nitrosyl	37-E1	→	14-B2	-783.8
W_c	37 E1	→	All	-2263.8
	All	→	14-B2	-1513.0

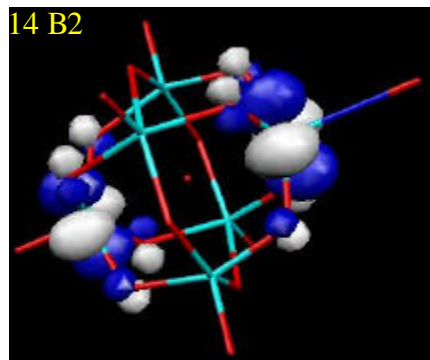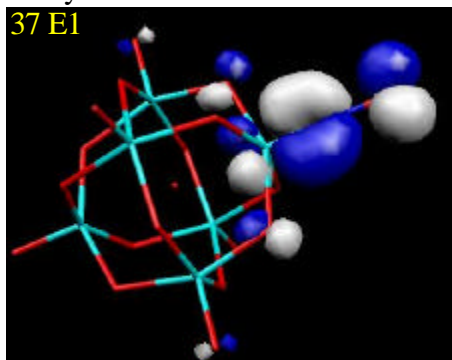Lidqvist orbitals
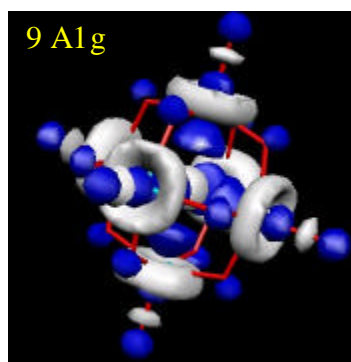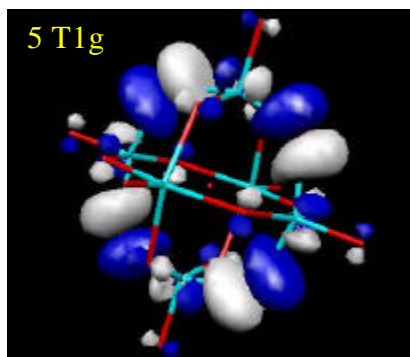
Nitrosyl orbitals

Figure 27. *5-T1g (Lindqvist) and 37-E1 (Nitrosyl) occupied and 9-A1g (Lindqvist) and 14-B2 (Nitrosyl) vacant orbitals. Representation made with the Molekel program, for a contour value of 0.05 [142]*

Density functional methods. The calculation of NMR shielding tensors

Concluding remarks

For big POM systems, frozen core approximation is an important saving in computing time. Previous papers[84,127] have indicated that chemical shifts are a property of valence electrons. The use of the frozen-core approximation to calculate the NMR shielding tensor was validated by a detailed discussion of the consequences of the approximation. So the core electronic density is explicitly excluded from contributing to the chemical shifts in any way other than through its constant atomic (diamagnetic) contribution, and it cannot add molecular effects to the chemical shift by coupling with virtual MOs.

We have applied the GIAO-DFT methods together with standard **ae** and **fc** basis sets at scalar and spin-orbit Hamiltonians for ^{183}W nucleus. At this level, we have some clear problems in obtaining correct chemical shifts from a common reference compound. Changing the reference compound for one that is similar to the systems being studied reduces the experimental range of the signals, and also leads to the methods behaving similarly. At this point, we find that a costly all-electron basis set in the transition metal atoms studied was no improvement on the frozen-core basis set. The results are close to the experimental values: however, it is difficult to reproduce small differences in the chemical shift.

In my opinion, further studies must be carried out into the appropriate conditions for a basis set if the chemical shifts in heavy nuclei are to be properly described. Environmental effects[43] may also have to be included or the DFT XC potentials revised.

Chapter 2

References and notes

[1]   L. J. Bartolotti, K. Flurchick, *"Reviews in computational chemistry"* **1995**, Vol. 7; Eds.: KB. Libkowitz, DB. Boyd, Verlag Chemie, New York, 187.

[2]   R. G. Parr, W. Yang, *"Density functional theory of atoms and molecules"* **1989**. Oxford University Press, New York.

[3]   T. Ziegler, *Chem. Rev.* **1991**, *91,* 651.

[4]   B. B. Laird, R. B. Ross, and T. Ziegler American Chemical Society, *"Chemical Applications of Density Functional Theory"*, ACS Symposium Series 629, American Chemical Society, Washington, D.C., **1996**.

[5]   T. Ziegler, *Can. J. Chem.* **1995**, *73*, 743.

[6]   C. Møller, M. S. Plesset, *Phys. Rev.* **1934**, *46*, 618.

[7]   a) J. Labanowski, J. Andzelm, *"Density Functional Methods in Chemistry"*; Springer-Verlag: New York, **1991**.
      b) O. Wiest, A. K. Black, K. N. Houk, *J. Am. Chem. Soc.* **1994**, *116*, 10336.
      c) T. N. Truong, W. T. Duncan, R. L. Bell, *ACS Symp. Ser.* **1996**, *629*, 85.
      d) J. L. Durant, *Chem. Phys. Lett.* **1996**, *256*, 595.
      e) D. G. Truhlar, *Faraday Discuss.* **1998**, *110*, 362.

[8]   L. A. Curtiss, K. Raghavachari, P. C. Redfern, J. A. Pople, *J. Chem. Phys.* **1997**, *106*, 1063.

[9]   T. Bally, S. Bernhard, S. Matzinger, L. Truttmann, Z. Zhu, J. Roulin, A. Marcinek, J. Gebicki, F. Williams, G. Chen, D. Roth, T. Herbertz, *Chem. Eur. J.* **2000**, *6*, 849.

[10] G. N. Merril, S. R. Kass, *J. Phys. Chem.* **1996**, *100*, 17465.

[11] M. A. Buijse, *"Electron Correlation"* **1991**, Vrije Universiteit, Amsterdam.

[12] a) R. J. Bartlett, G. D. Purvis, *Int. J. Quant. Chem.* **1978**, *14*, 516.
      b) J. A. Pople, R. Krishnan, H. B. Schlegel, J. S. Binkley, *Int. J. Quant. Chem.* **1978**, *XIV*, 545.

[13]   J. A. Pople, M. Head - Gordon, K. Raghavachari, *J. Chem. Phys.* **1987**, *87*, 5968.

[14] P. Pyykkö, *Chem. Rev.* **1998**, *88*, 563.

[15] E. M. Siegbahn, M. R. A. Blomberg, *Chem. Rev.* **2000**, *100*, 421.

[16] S. Nui, M. B. Hall, *Chem. Rev.* **2000**, *100*, 353.

[17] R. J. Bartlett, H. Sekino, *"In Nonlinear Optical Materials: Theory and Modeling"*; Eds.: S. P. Karna, A. T. Yeates; ACS Symposium Series 628; American Chemical Society: Washington, DC, **1996**; Vol. 2, 23.

[18] J. Oxgaard, O. Wiest, *J. Phys. Chem. A* **2001**, *105,* 8236.

[19] V. Hrouda, M. Roeselova, T. Bally, *J. Phys. Chem. A* **1997**, *101*, 3925.

[20] a) A. Karpfen, C. H. Choi, M. Kertesz, *J. Phys. Chem. A* **1997**, *101*, 7426.
      b) Karpfen, A. *J. Phys. Chem. A* **1999**, *103,* 2821.

[21] C. H. Choi, M. Kertesz, *J. Phys. Chem. A* **1997**, *101,* 3823.

UNIVERSITAT ROVIRA I VIRGILI
DFT STUDY OF TITANIUM CUBANE AND MOLYBDENUM SULPHIDE COMPOUNDS.
Autor: José Manuel Gracia Budria
ISBN: 978-84-690-6751-2 / DL: T.1196-2007

Density functional methods. The calculation of NMR shielding tensors

22 T. Bally, G. N. Sastry, *J. Phys. Chem. A* **1997**,*101*, 7923.

23 M. Kamiya, T. Tsuneda, K. Hirao, *J. Chem. Phys.* **2002**, *117*, 6010.

24 H. Fukui, *Magn. Res. Rev.* **1987**, *11*, 205.

25 H. Nakatsuji, *"Nuclear Magnetic Shieldings and Molecular Structure";* NATO ASI C386; Ed.: J. A. Tossell; Kluwer Academic Publishers: Dordrecht, The Netherlands, **1993**.

26 D. M. Grant, R. K. Harris, *"Encyclopedia of Nuclear Magnetic Resonance"* **1996**, John Wiley & Sons: New York.

27 T. Helgaker, M. Jaszunski, K. Ruud, *Chem. Rev.* **1999**, *99*, 293.

28 G. Schreckenbach, S. K. Wolf, T. Ziegler, *J. Phys. Chem. A* **2000**, *104*, 8244.

29 M. Bühl, M. Kaupp, V. G. Malkin, O. L. Malkina, *J. Comput. Chem.* **1999**, *20*, 91.

30 a) J. Autschbach, T. Ziegler, *"Relativistic Computation of NMR shieldings and Spin-spin coupling Constants"*; Eds: D. M. Grant, R. K. Harris, *"Encyclopedia of Nuclear Magnetic resonance"*, *Vol. 9*, John Wiley & Sons, Chichester, **2002** pages 305-323.

    b) J. Autschbach, *"Calculation of heavy-nucleus chemical shifts: Relativistic all electrons methods"*; Eds.: M. Kaupp, M. Bühl, V. G. Malkin, *"Quantum Chemical Calculation of Magnetic Resonance Properties"*, Wiley-VCH, Wienheim. In press

    c) M. Kaupp, *"Relativistic effects on NMR chemical shifts"*; Ed.: P. Schwerdtfeger, "Relativistic electronic structure theory", Vol. 2, Elsevier, Amsterdam. In press.

31 W. Koch, M. C. Holthausen, *"A chemist's guide to density functional theory"* **2000**. Wiley-VCH, Weinheim.

32 E. R. Davidson, *Chem. Rev.* **2000**, *100*, 351.

33 G. Schreckenbach, T. Ziegler, *Int. J. Quantum Chem.* **1997**, *61*, 899.

34 a) M. Bühl, V. G. Malkin, O. L. Malkina, *Helvetica. Chemical. Acta* **1996**, *79*, 742.

    b) M. Bühl, *Chem. Phys. Lett.* **1997**, *267*, 251.

35 a) J. C. C. Chan, S. C. F. Au-Yeung, *J. Phys. Chem. A* **1997**, *101*, 3637.

    b) N. Godbout, E. Oldfield, *J. Am. Chem. Soc.* **1997**, *119*, 8065.

36 a) M. Bühl, W. Thiel, U. Fleischer, W. Kutzelnigg, *J. Phys. Chem.* **1995**, *99*, 4000.

    b) M. Bühl, J. Gauss, J. F. Stanton, *Chem. Phys. Lett.* **1995**, *241*, 248.

    c) G. Schreckenbach, Y. Ruiz-Morales, T. Ziegler, *J. Chem. Phys.* **1996**, *104*, 8605.

37 a) M. Bühl, H.-H. Brintzinger, G. Hopp, *Organometallics* **1996**, *15*, 778.

    b) M. Bühl, *J. Phys. Chem. A* **1997**, *101*, 2514.

38 M. Bühl, *Organometallics* **1997**, *16*, 261.

Chapter 2

[39] Y. Ruiz-Morales, G. Schreckenbach, T. Ziegler, *J. Phys. Chem. A* **1997**, *101*, 4121.

[40] A. Rodríguez - Fortea, P. Alemany, T. Ziegler, *J. Phys. Chem. A* **1999**, *103*, 8288.

[41] A. Bagno, M. Bonchio, A. Sartorel, G. Scorrano, *Eur. J. Inorg. Chem.* **2000**, 17.

[42] T. M. Gilbert, T. Ziegler, *J. Phys. Chem. A* **1999**, *103*, 7535.

[43] S. K. Wolff, T. Ziegler, E. van Lenthe, E. J. Baerends, *J. Chem. Phys.* **1999**, *110*, 7689.

[44] G. Schreckenbach, *Inorg. Chem.* **2002**, *41*, 6560.

[45] D. R. Hartree, *"The wave mechanics of an atom with a non-Coulomb central field"*. *Theory and Methods*. Proc. Cambridge Phil. Soc. 24, 89.

[46] P. W. Atkins, R. S. Friedman, *"Molecular Quantum Mechanism"* **1997**.

[47] a) J. P. Lowe, *"Quantum Chemistry"*; Academic Press: New York, **1978**.
b) I. N. Levine, *"Quantum Chemistry"*, 5th ed.; Prentice Hall : Upper Saddle River, **2000**.

[48] P.-O. Löwin, *Adv. Chem. Phys.* **1959**, *2*, 207.

[49] a) A. Szabo, N. S. Ostlund, *"Modern Quantum Chemistry"*, McGraw-Hill, **1989**.
b) J. Simons, *J. Phys. Chem.* **1991**, *95*, 1017.
c) R. J. Bartlett, *Rev. Comput. Chem.* **1994**, *5*, 65.

[50] O. Sinanoglu, *Adv. Chem. Phys.* **1964**, *6*, 358.

[51] P. E. M. Siegbahn, "The direct CI method", in *Methods in Computational Molecular Physics*; Eds. G. H. F. Diercksen, S. Wilson, D. Reidel, Dordrecht, **1983**.

[52] R. Shepard, *Adv. Chem. Phys.* **1987**, *69*, 63.

[53] W. J. Hehre, L. Radom, P. V. R. Schleyer, J. A. Pople, *"Ab Initio Molecular orbital Theory"*. Wiley-Interscience, New York, **1986**.

[54] I. Shavitt., *"Methods of Electronic Structure Theory"*; Ed.: H. F. Schaefer, Wiley-Interscience, New York, **1986**.

[55] R. J. Bartlett, *J. Phys. Chem.* **1989**, *90*, 4356.

[56] R. M. Dreizler, E. K. V. Gross, *"Density Functional Theory"*; Springer: Berlin, **1990**.

[57] P. Hohenberg, W. Kohn, *Phys. Rev. B* **1964**, *136*, 864.

[58] W. Kohn, L. Sham, *J. Phys. Rev. A* **1965**, *140*, 1133.

[59] a) B. Delley, *J. Chem. Phys.* **1991**, *94*, 7245.
b) J. Andzelm, E. Wimmer, *J. Chem. Phys.* **1992**, *96*, 1280.

[60] B. G. Johnson, P. M. W. Gill, J. A. Pople, *J. Chem. Phys.* **1993**, *98*, 5612.

[61] A. D. Becke, *J. Chem. Phys.* **1992**, *97*, 9173.

[62] a) S. Kristyan, P. Pulay, *Chem. Phys. Lett.* **1994**, *229*, 175.
b) J. M. Perez-Jorda, A. D. Becke, *Chem. Phys. Lett.* **1995**, *233*, 134.

[63] a) L. Fan, T. Ziegler, *J. Am. Chem. Soc* **1992**, *114*, 10890.

Density functional methods. The calculation of NMR shielding tensors

    b) C. Sosa, C. Lee, *J. Chem. Phys*. **1993**, *98*, 8004.

    c) L. Deng, T. Ziegler, L. Fan, *J. Chem. Phys.* **1993**, *99*, 3823.

    d) R. V. Stanton, Jr. K. M. Merz, *J. Chem. Phys.* **1994**, *100*, 434.

    e) B. G. Johnson, C. A. Gonzales, P. M. W. Gill, J. A. Pople, *Chem. Phys. Lett*. **1994**, *221*, 100.

[64]   a) J. Baker, M. Muir, J. Andzelm, *J. Chem. Phys.* **1995**, *102*, 2063.

    b) J. Baker, J. Andzelm, M. Muir, P. R. Taylor, *Chem. Phys. Lett*. **1995**, *237*, 53.

    c) J. Baker, M. Muir, J. Andzelm, A. Scheiner, *ACS Symp. Ser*. **1996**, *629*, 342.

[65]   A. D. Becke, *Phys. Rev .A* **1988**, *38*, 3098.

[66]   C. Lee, W. Yang, R. G. Parr, *Phys. Rev. B* **1988** , *37*, 785.

[67]   J. P. Perdew, *Phys. Rev. B* **1986**, *34*, 7406.

[68]   a) J. P. Perdew, *"In Electronic Structure of Solids"*; Eds.: P. Ziesche, H. Eschrig, Akademie Verlag: Berlin, **1991**.

    b) J. P. Perdew, J. A. Chevary, S. H. Vosko, K. A. Jackson, M. R. Pederson, D. J. Singh, C. Fiolhals, *Phys. Rev. B* **1992**, *46*, 6671.

[69]   A. D. Becke, *J. Chem. Phys.* **1992**, *96*, 2155.

[70]   A. D. Becke, *J. Chem. Phys.* **1996**, *104*, 1040.

[71]   A. D. Becke, *"Modern Electronic Structure Theory"*; Ed.: D. R. Yarkony, World Scientific: Singapore, **1995**.

[72]   J. Mason, *"Multinuclear NMR"*; Plenum: New York, **1987**.

[73]   N. F. Ramsey, *Phys. Rev.* **1950**, *78*, 699.

[74]   N. F. Ramsey, *Phys. Rev.* **1953**, *91*, 303.

[75]   A. Abragam, *"The Principles of Nuclear Magnetic Resonance"* **1961**, Oxford University Press: Oxford.

[76]   R. McWeeny, *"Methods of Molecular Quantum Mechanics"* **1989**, 2nd ed.; Academic Press: New York.

[77]   J. Vaara, K. Ruud, O. Vahtras, H. Gren, J. Jokisaari, *J. Chem. Phys.* **1998**, *109*, 1212.

[78]   M. Kaupp, O. L. Malkina, V. G. Malkin, P. Pyykkö, *Chem. Eur. J.* **1998**, *4*, 118.

[79]   The fine-structure constant is a unitless numerical constant - whose value is approximately equal to: 1/137. In fact the exact value of the fine-structure constant is: 0.007297351 +/- 0.000000006. For additional information see for instance:

    J. K. Webb, M. T. Murphy, V. V. Flambaum, V. A. Dzuba, J. D. Barrow, C. W. Churchill, J. X. Prochaska, A. M. Wolfe, *Phys. Rev. Lett.* **2001**, *87*, 091301.

[80]   M. Kaupp, V. G. Malkin, O. L. Malkina, D. R. Salahub, *J. Am. Chem. Soc.* **1995**, *117*, 1851; (erratum) **1998**, *117*, 8492.

[81]   a) R. P. Hosteny, T. H. Dunning, R. R. Gilman, A. Pipano, I. Shavitt, *J. Chem. Phys.* **1975**, *62*, 4764.

b) V. R. Saunders, J. H. van Lenthe, *Mol. Phys.* **1983**, *48*, 923.

[82]   H. Fukui, T. Baba, *J. Chem. Phys.* **1998**, *108*, 3854.

[83]   M. Kaupp, O. L. Malkina, V. G. Malkin, *"Encyclopedia of Computational Chemistry"*; Ed.: P. v. R. Schleyer; J. Wiley & Sons Ltd.: New York, **1998**.

[84]   P. Pyykkö, A. Görling, N. Rösch, N. *Mol. Phys.* **1987**, *61*, 195.

[85]   a) T. Helgaker, P. Jørgensen, *"Methods in Computational Molecular Physics"*; Eds.: S. Wilson, G. H. F. Diercksen; Plenum Press: New York: **1992**.

b) W. Kutzelnigg, *Theor. Chim. Acta* **1992**, *83*, 263.

[86]   H. Nakatsuji, M. Hada, H. Kaneko, C. C. Ballard, *Chem. Phys. Lett.* **1996**, *255*, 195.

[87]   a) H. Nakatsuji, H. Takashima, M. Hada, *Chem. Phys. Lett.* **1995**, *233*, 95.

b) C. C. Ballard, M. Hada, H. Kaneko, H. Nakatsuji, *Chem. Phys. Lett.* **1996**, *254*, 170.

[88]   a) J. J. Sakurai, *"Advanced Quantum Mechanics"*; Addison-Wesley: Reading MA, **1967**.

b) R. McWeeny, B. T. Suthcliffe, *"Methods of Molecular Quantum Mechanics"*; Academic Press: London, **1976**.

[89]   a) J. D. Morrison, R. Moss, *Mol. Phys.* **1980**, *41*, 491.

b) A. Farazdel, V. H. Jr. Smith, *Int. J. Quantum Chem.* **1986**, *29*, 311.

c) W. Kutzelnigg, *Z. Phys. D* **1989**, *11*, 15.

d) W. Kutzelnigg, *Z. Phys. D* **1990**, *15*, 27.

[90]   R. Bouten, E. J. Baerends, E. van Lenthe, L. Visscher, G. Schreckenbach, T. Ziegler, *J. Phys. Chem. A.* **2000**, *104*, 5600.

[91]   E. van Lenthe, E. J. Baerends, J. G. Snijders, *J. Chem. Phys.* **1993**, *99*, 4597.

[92]   E. van Lenthe, E. J. Baerends, J. G. Snijders, *J. Chem. Phys.* **1994**, *101*, 9783.

[93]   A. K. Rajagopal, J. Callaway, *Phys. Rev. B* **1973**, *7*, 1912.

[94]   G. Vignale, M. Rasolt, *Phys. Rev. B* **1988**, *37*, 10685.

[95]   A. M. Lee, N. C. Handy, S. M. Colwell, *J. Chem. Phys.* **1995**, *103*, 10095.

[96]   A. D. Becke, *Can. J. Chem.* **1996**, *74*, 995.

[97]   K. Capelle, E. K. U. Gross, *Phys. Rev. Lett.* **1997**, *78*, 1872.

[98]   S. T. Epstein, *"The Variational Method in Quantum Chemistry"*; Academic: New York, **1974**.

[99]   S. K. Wolff, T. Ziegler, *J. Chem. Phys.* **1998**, *109*, 895.

[100] G. Schreckenbach, R. M. Dickson, Y. Ruiz-Morales, T. Ziegler, *"Chemical Applications of Density Functional Theory"*; ACS Symposium Series 629; Eds.: B. B. Laird, R. B. Ross, T. Ziegler; American Chemical Society: Washington, DC, **1996**.

[101] G. Schreckenbach, T. Ziegler, *Theor. Chem. Acc.* **1998**, *99*, 71.

UNIVERSITAT ROVIRA I VIRGILI
DFT STUDY OF TITANIUM CUBANE AND MOLYBDENUM SULPHIDE COMPOUNDS.
Autor: José Manuel Gracia Budria
ISBN: 978-84-690-6751-2 / DL: T.1196-2007

Density functional methods. The calculation of NMR shielding tensors

[102] Y. Ruiz-Morales, G. Schreckenbach, T. Ziegler, *J. Phys. Chem.* **1996**, *100*, 3359.

[103] Y. Ruiz-Morales, T. Ziegler, *J. Phys. Chem. A* **1998**, *102*, 3970.

[104] D. B. Chesnut, *"Annual Reports on NMR Spectroscopy"*; Ed.: G. A. Webb; Academic: New York, **1994**, Vol. 29.

[105] G. Schreckenbach, *J. Chem. Phys.* **1999**, *110*, 11936.

[106] G. Schreckenbach, T. Ziegler, *J. Phys. Chem.* **1995**, *99*, 606.

[107] G. Schreckenbach, *Inorg. Chem.* **2000**, *39*, 1265.

[108] M. Bühl, M. Kaupp, V. G. Malkin, and O. L. Malkina, *J. Comput. Chem.* **1999**, *20*, 91.

[109] A. K. Jameson, C. J. Jameson, *Chem. Phys. Lett.* **1987**, *134*, 461.

[110] a) F. London, *J. Phys. Radium* **1937**, *8*, 397.
b) R. Ditchfield, *Mol. Phys.* **1974**, *27*, 789.

[111] K. Wolinski, J. F. Hinton, P. Pulny, *J. Am. Chem. Soc.* **1990**, *112*, 8251.

[112] a) W. Kutzelnigg, U. Fleischer, M. Schindler, *"NMR ± basic principles and progress"* **1990**, vol. 23. Springer, Berlin Heidelberg New York.
b) W. Kutzelnigg, *Isr. J. Chem.* **1980**, *19*, 193.
c) M. Schindler, W. Kutzelnigg, *J. Chem. Phys.* **1982**, *76*, 1919.

[113] a) Y. Ruiz-Morales, G. Schreckenbach, T. Ziegler, *Organometallics* **1996**, *15*, 3920.
b) A. W. Ehlers, Y. Ruiz-Morales, E. J. Baerends, T. Ziegler, *Inorg. Chem.* **1997**, *36*, 5031.

[114] S. H. Vosko, L. Wilk, M. Nusair, Can. J. Phys. **1980**, *58*, 1200.

[115] a) J. Perdew, *Phys. Rev. B* **1986**, *33*, 8822.
b) J. Perdew, Y. Wang, *Phys. Rev. B* **1992**, *45*, 13244.

[116] a) A. D. Becke, *J. Chem. Phys.* **1993**, *98*, 1372.
b) P. J. Stephens, F. J. Devlin, C. F. Chabalowski, M. J. Frisch, *J. Phys. Chem.* **1994**, *98*, 11623.
c) V. Barone, *Chem. Phys. Lett.* **1994**, *226*. 392.

[117] a) V. G. Malkin, O. L. Malkina, D. R. Salahub, *Chem. Phys. Lett.* **1993**, *204*, 80.
b) V. G. Malkin, O. L. Malkina, D. R. Salahub, *Chem. Phys. Lett.* **1993**, *204*, 87.
c) V. G. Malkin, O. L. Malkina, M. E. Casida, D. R. Salahub, *J. Am. Chem. Soc*. **1994**, *116*, 5898.
e) P. Politzer, J. M. Seminario, *"Modern density functional theory: a tool for chemistry"*. Elsevier, Amsterdam.

[118] G. Rauhut, S. Puyear, K. Wolinski, P. Pulay, *J. Phys. Chem.* **1996**, *100*, 6310.

[119] J. R. Cheeseman, G. W. Trucks, T. A. Keith, M. J. Frisch, *J. Chem. Phys.* **1996**, *104*, 5497.

Chapter 2

[120] R. Salzmann, M. Kaupp, M. T. McMahon, E. Oldfield, *J. Am. Chem. Soc.* **1998**, *120*, 4771.

[121] M. Bühl, *Chem. Phys. Lett.* **1997**, *267*, 251.

[122] M. Kaupp, O. L. Malkina, V. G. Malkin, *J. Chem. Phys.* **1997**, *106*, 9201.

[123] a) T. Ziegler, J. Li, *Can. J. Chem.* **1993**, *72*, 783.
b) R. Fournier, *J. Chem. Phys.* **1993**, *99*, 1801.
c) M. C. Holthausen, C. Heinemann, H. H. Cornehl, W. Koch, H. Schwarz, *J. Chem. Phys.* **1995**, *102*, 4931.

[124] M. Bühl, *Chem. Phys. Lett.* **1997**, *267*, 251.

[125] A. D. Becke, *J. Chem. Phys.* **1993**, *98*, 5648.

[126] P. J. Wilson, D. J. Tozer, *J. Chem. Phys.* **2002**, *116*, 10139.

[127] G. Schreckenbach, T. Ziegler, *Int. J. Quantum Chem.* **1996**, *60*, 753.

[128] M. T. Pope, *"Heteropoly and Isopoly Oxometalates"*; Springer-Verlag, Berlin **1983**.

[129] Special issue on Polyoxometalate compounds; Ed.: C. L. Hill, *Chem. Rev.* **1998**, *98*, 390.

[130] H. T. Pope, A. Müller, *Angew. Chem., Int. Ed. Eng.* **1991**, *30*, 34.

[131] J.-M. Poblet, C. Bo, X. Lopez, *Chem. Soc. Rev.* **2003**, *32*, 297.

[132] Special issue on *"Computacional Transition Metal Chemistry"*, E. R. Davidson, *Chem. Rev.* **2000**, *100*, 531.

[133] a) C. J. Jamenson, *Annu. Rev. Phys. Chem.* **1996**, *47*, 135.
b) D. B. Chesnut, *Reviews in Computational Chemistry*; Eds: K. B. Lipkowitz, D. B. Boyd, VCH, New York, **1996**.
c) A. C. De Dios, *Prog. Nucl. Magn. Reson.* **1996**, *29*, 229.
d) J. C. C. Chan, S. C. F. Au-Yeung, P J. Wilson, G. A. Webb, *J. Mol. Struct. (Theochem)* **1996**, *365*, 125.

[134] R. Bouten, E. J. Baerends, E. van Lenthe, L. Visscher, *J. Phys. Chem. A* **2000**, *104*, 5600.

[135] A. Bagno, M. Bonchio, *Chem. Phys. Letters* **2000**, *317*, 123.

[136] A. Bagno, M. Bonchio, A. Sartorel, G. Scorrano, *CHEMPHYSCHEM* **2003**, *4*, 517.

[137] G. Schreckenbach, T. Ziegle r, *J. Phys. Chem. A* **1997**, *101*, 3388.

[138] S. Patchkovskii, T. Ziegler, *J. Phys. Chem. A* **2001**, *105*, 5490.

[139] a) G. te Velde, F.M. Bickelhaupt, S.J.A. van Gisbergen, C. Fonseca Guerra, E. J. Baerends, J. G. Snijders, T. Ziegler, *"Chemistry with ADF"*, *J. Comput. Chem.* **2001**, *22*, 931.
b) C. Fonseca Guerra, J. G. Snijders, G. te Velde, E. J. Baerends, *Theor. Chem. Acc.* **1998**, *99*, 391.
c) ADF2002.03, SCM, Theoretical Chemistry, Vrije Universiteit, Amsterdam, The Netherlands, http://www.scm.com.

[140] J. Jokisaari, S. Järvinen, *J. Phys. Chem. A* **2002**, *106*, 9313.

[141] a) J. Autschbach, T. Ziegler, *J. Chem. Phys.* **2000**, *113*, 936.
b) J. Autschbach, T. Ziegler, *J. Am. Chem. Soc.* **2001**, *123*, 3341.

[142] *MOLEKEL 4.0,* P. Flükiger, H.P. Lüthi, S. Portmann, J. Weber, *Swiss Center for Scientific Computing,* Manno (Switzerland), **2000**.

Chapter 2

3

Azametallocubanes

The search for new ligand frameworks that can promote new reactivity pathways is currently underway in organometallic chemistry. In this context, nitrogen donor ligands proved to be versatile since they allow suitable combinations of electronic and stereo chemical properties. New catalysts for olefin polymerization,[1,2] the activation of N_2 and P_4 bonds,[3] and the stabilization of reactive unsupported early-late bonds[4] are relevant examples of new reactivity patterns supported by such ligands. Several types of polyfunctional ligands have been reported,[5] including functionalized 1,4,7-triazacyclononane (tacn) and other saturated nitrogen macrocycles with anionic nitrogen moieties.[6] In recent years investigation into the synthesis and reactivity of nitro- complexes of titanium (IV) with the ligand pentamethylcyclopentadienyl ($Cp^* = \mathbf{h}^5 - C_5Me_5$) has revealed the versatility of trimmer* $\left[\left\{ Ti\left(\mathbf{h}^5 - C_5Me_5\right)\left(\mathbf{m}_3 - NH\right)\right\}_3 \left(\mathbf{m}_3 - N\right)\right]$. The chemistry related to this Aza ligand and scopes is introduced in Section 3.1. Sections 3.2 - 3.7 present our theoretical contributions to the study of this tridentate ligand chemistry.*

3.1   Introduction

The discovery that cations and anions form stable complexes with macrocyclic polyethers and polyamines has opened the door to several broad and fruitful areas of chemical investigation.[7] Interest in these macrocycles was stimulated when it was found that some of them formed stable complexes with alkali and alkaline earth metal ions and that preferential cation complexation resulted when the relative sizes of the cation and ligand cavity were matched.[8]

What is more, the structure and reactions of these synthetic ligands are similar to those of many naturally occurring compounds of the macrocyclic type which are known to exhibit selective cation complexation.[9] A large number of these ligands have been synthesized and studied. Interpreting the cation and anion binding data in terms of the observed selectivity and solvation characteristics of the ligands under various experimental conditions has presented a considerable challenge.

Macrocyclic ligands have been used successfully for such processes as separation of ions by transport through artificial and natural membranes, liquid-liquid or solid-liquid phase-transfer reactions, dissolution in apolar solvents of metal and organic salts, preparation of ion-selective electrodes and isotope separations. They have also been used to further understanding of some natural processes through mimicry of metalloenzymes.[10] In addition, attention must be paid to the various parameters involved in ion-macrocycle interaction such as relative cation/anion and ligand cavity sizes, the number and stereochemical arrangement of ligand binding sites, substitution on the macrocyclic ring, solvent effects, macrocyclic effects, and type of bonding. Oxygen donor macrocycles like crown ethers are noted for their success in metal separation processes; however the use of nitrogen donor macrocycles may introduce another variable into the complexation chemistry.[11] Nitrogen donor macrocycles can produce a better match with some metals because of their softer Lewis base nitrogen donor capabilities.

Roesky et al. described the imido-nitrido complex $\left[\left\{Ti\left(\boldsymbol{h}^5-C_5Me_5\right)\left(\boldsymbol{m}_3-NH\right)\right\}_3\left(\boldsymbol{m}_3-N\right)\right]$ (1) obtained by the ammonolysis

of $\left[\left\{Ti\left(\boldsymbol{h}^5 - C_5Me_5\right)\right\}Me_3\right]$.[12] This complex combines the coordinating capability of a tridentate nitrogen macrocycle ligand with the presence of empty d orbitals from totally oxidised Ti metals.

The trinuclear titanium complex **1** has considerable possibilities as a fac-coordinating ligand. Heterometallic cubanes can easily be synthesized by reaction of the organometallic complex **1** with appropriate metal molecules; to our knowledge, these results are the first examples of an unprecedented family of cubane clusters containing Ti_3M heterometallic cores. Just before work began on this thesis, it was found that **1** was capable of displacing labile ligands coordinated to group 4[13] and 6[14] metals. Nowadays, the family has been extended and it has been shown that group 1, 2, 4-6, 8, 9 and 13-14 metal fragments have been included. Moreover, if other highly reactive metal-ligand bonds are present in the incorporated metal, N-H bond activation occurs in **1** to give corner-shared double cube complexes.[15]

Although theoretically **1** may be able to produce cubanes and dicubanes from all metal groups, we shall focus only on previously synthesized compounds.[16] Our aim is to contribute to the understanding of this new family of cube-type nitrido titanium (IV) derivatives. Particular attention will be paid to the tridentate ligand $\left[\left\{Ti\left(\boldsymbol{h}^5 - C_5Me_5\right)\left(\boldsymbol{m}_3 - NH\right)\right\}_3\left(\boldsymbol{m}_3 - N\right)\right]$ as precursor of these new cube type structures; its abilities as a ligand will be studied and compared with those of other tridentate ligands. Attention will also be paid to the incorporated metal fragment, and possible interaction between the metal fragment and the ligand d^n-d^0 orbitals.

3.2   Group 1 complexes: azaheterometallocubanes from alkaline monohalides

The complexing ability of alkali metals is weaker than that of the more commonly studied transition metal ions. It used to be thought that the coordination chemistry of alkali and alkaline earth cations was simple and could be discerned merely with the help of the ionic model.[17] This delayed interest in the coordination chemistry of these metals. The importance of understanding the interactive principles of these metals, however, becomes

apparent when attempting to understand the vital roles that Na, K, Mg and Ca metals play in biological systems.[18]   The ability of some ligands to selectively complex alkali and alkaline earth metal cations is related to the mechanism of active transport of cations through membranes.[19]

Coordination differences between alkali metals are shown by differences in the sizes of their unipositive ions, all of which are large except the Li^+ (see Table 3.1). The smallest in fact has greater polarization power; so the greater Lewis acidity of lithium produces stronger metal-ligand interactions. Lithium halides, and to a lesser extent sodium halides, form stable solid complexes with some nitrogen ligands, like NH_3 or p,p'-methylenedianiline. The complexing ability of the metal is not the only important thing. Lithium flouride is much less soluble in water than other alkaline salts, because of its high lattice energy.[20]

**Table 3.1.** *Atomic radii of the alkali metals in pm and absolute electronegativities in eV*[21]

	Li	**Na**	**K**	**Rb**	**Cs**
Ionic M^{1+} radius	78	98	133	149	165
Electronegativity	3.01	2.85	2.42	2.34	2.18

The purpose of this section is to describe some of the properties of $\left[\left\{ Ti\left(h^5 - C_5H_5\right)\left(m_3 - NH\right)\right\}_3 \left(m_3 - N\right)\right]$ (**1**) ligand complexation with a variety of alkaline salts. From this analysis, as well as the description of a new family of compounds, we will obtain the first image of **1** as a neutral polydentate ligand.

3.2.1   Experimental data

The reaction of ligand **1** with one equivalent of group 1 monohalides MX afforded   the   azaheterometallocubane   complexes $\left[XM\left\{ Ti\left(h^5 - C_5Me_5\right)\left(m_3 - NH\right)\right\}_3 \left(m_3 - N\right)\right]$ [M = Li, X = Br, I; M = Na, X

= I] (see Scheme 3.1). Attempts to obtain other monohalide cubanes were unsuccessful.[22]
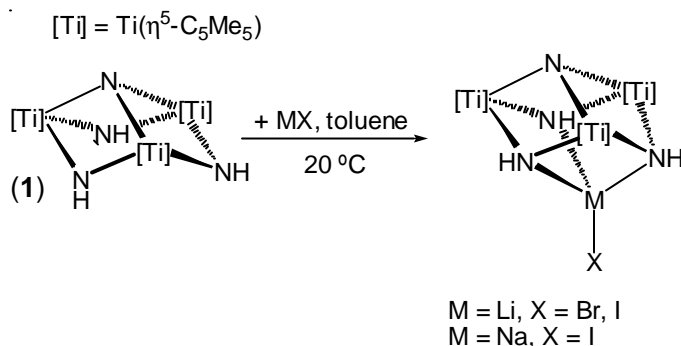

Scheme 3.1. *Formation of alkali halide azaheterometallocubane complexes from **1** and alkali halide salts in solvent*

Complexes 1-MX were characterized by spectral and analytical techniques. The mass spectra obtained for 1-LiBr and 1-NaI suggest a monomeric formulation in the gas phase. IR spectra of 1-MX show one $\boldsymbol{n}_{NH}$ vibration between 3349 and 3337 cm^{-1}, similar to that determined for **1**, 3352 cm^{-1}, and other azaheterometallocubane derivatives.[13,14,15,23] ^{1}H and ^{13}C NMR spectra in [D$_6$]benzene at room temperature show resonances for equivalent NH and C$_5$Me$_5$ groups, suggesting a highly symmetrical structure or the existence of low energy exchange processes in solution.

Alkali metal cyclopentadienide complexes [M($\boldsymbol{h}^5$-C$_5$H$_5$)] are also able to react with ligand **1** in toluene to form the $\left[(\boldsymbol{h}^5\text{-C}_5\text{H}_5)M\left\{Ti\left(\boldsymbol{h}^5-C_5Me_5\right)\left(\boldsymbol{m}_3-NH\right)\right\}_3\left(\boldsymbol{m}_3-N\right)\right]$ [M = Li; Na] adducts (Scheme 3.2); cubane formation for the biggest alkali metals was not observed. The molecular structure of complex 1-NaCp has been characterized by X-ray studies; the crystal structure shows an azaheterometallocubane core [MTi$_3$N$_4$] by coordination of the three NH groups to the sodium centre (see Figure 3.1 and Table 3.3). The identification of the disposition of compound 1-NaCp together with

117

spectroscopic data serve to propose structures with metal pseudo tetrahedral coordination for the remaining compounds too (Figure 3.1).
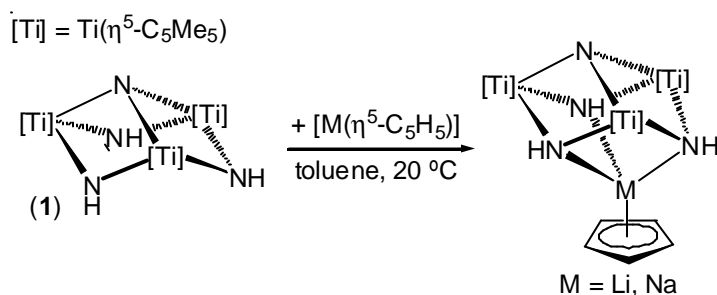
Scheme 3.2. *Formation of alkali metal cyclopentadienide complexes* $\left[(\boldsymbol{h}^5\text{-}C_5H_5)M \left\{ Ti\left(\boldsymbol{h}^5 - C_5Me_5\right)\left(\boldsymbol{m}_3 - NH\right)\right\}_3 \left(\boldsymbol{m}_3 - N\right)\right]$ *[M = Li; Na]*

3.2.2 Results

Optimized geometries under C_{3v} symmetry restrictions were calculated for model complexes $\left[XM \left\{ Ti\left(\boldsymbol{h}^5 - C_5H_5\right)\left(\boldsymbol{m}_3 - NH\right)\right\}_3 \left(\boldsymbol{m}_3 - N\right)\right]$, 1'-MX, [M = Li, Na, K, Rb, Cs, X = F, Cl, Br, I]. Under Cs symmetry restrictions they were calculated for cyclopentadienide complexes $\left[(\boldsymbol{h}^5\text{-}C_5H_5)M \left\{ Ti\left(\boldsymbol{h}^5 - C_5H_5\right)\left(\boldsymbol{m}_3 - NH\right)\right\}_3 \left(\boldsymbol{m}_3 - N\right)\right]$ [M = Li, Na].

Table 3.3 shows main selected structural parameters for computed molecules together with the crystal structure of ligand **1** and the compound 1-NaCp. For purposes of comparison, the table also includes the experimental parameters for related alkali metal halide complexes with N-donor ligands with similar alkali metal tetrahedral dispositions; tris(3,5dimethylpyridine)-LiX[24] [X = Cl, Br, and I] and tris(triphenylphosphineimine)-NaI.[25] A scheme of these compounds can be seen in Figure 3.2.
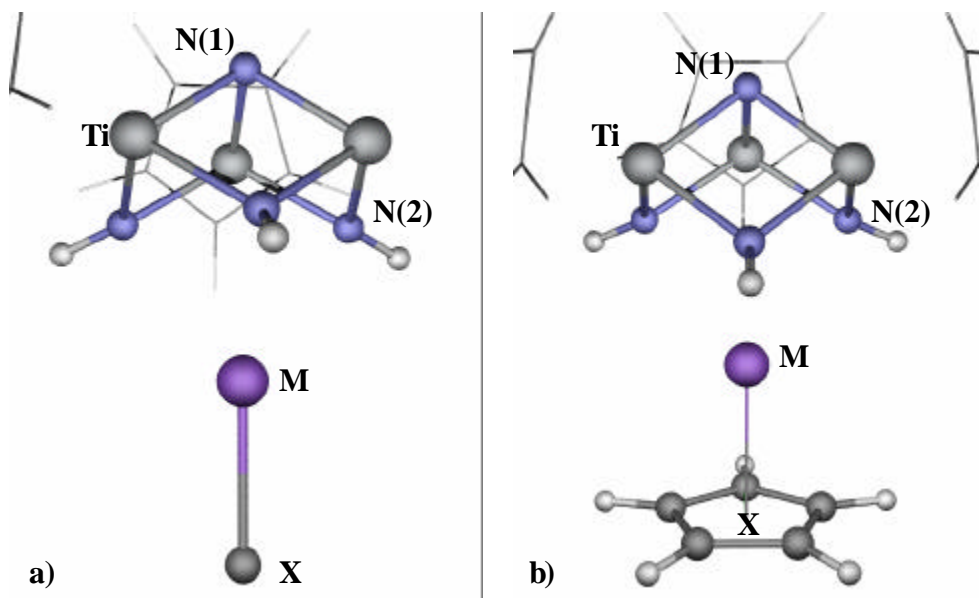
Figure 3.1. *3D representation of 1-MX, a); and 1-MCp structures, b)*

Computed data perfectly match the experimental data available for the isolated ligand **1** and compound 1-NaCp, and confirm the predicted tetrahedral metal environment. The structural data clearly show that the tridentate ligand is hardly modified after coordination to the alkali metal. The small changes observed for ligand **1** confirm the considerable rigidness of the ligand.

In view of the result computed for the X-ray determined compound 1-NaCp, the calculated distances are expected to be slightly higher than the experimental ones; metal-ligand nitrogen computed data (2.716 Å) are about 0.1 Å longer than the experimental data (2.614 Å), an acceptable discrepancy if we consider the crystal packing effects and the inexact theoretical method. The discrepancy is bigger in the experimental distances for the molecules tris(3,5-dimethylpyridine)-LiX and tris(triphenylphosphineimine)-NaI. The metal-ligand nitrogen distances are about 0.25 Å bigger when the ligand is **1** than when it is 3,5-dimethylpyridine or triphenylphosphineimine. This discrepancy is partly due to the rigidity of the ligand. Complexation is dependent on the flexibility of the ligands. Table 3.3 shows that the metal-ligand nitrogen

angle (N_2-M-N'_2) is much smaller for ligand **1** than is normally accepted for a tetrahedral coordination, which does not favour spatial accommodation of the ligand electrons.
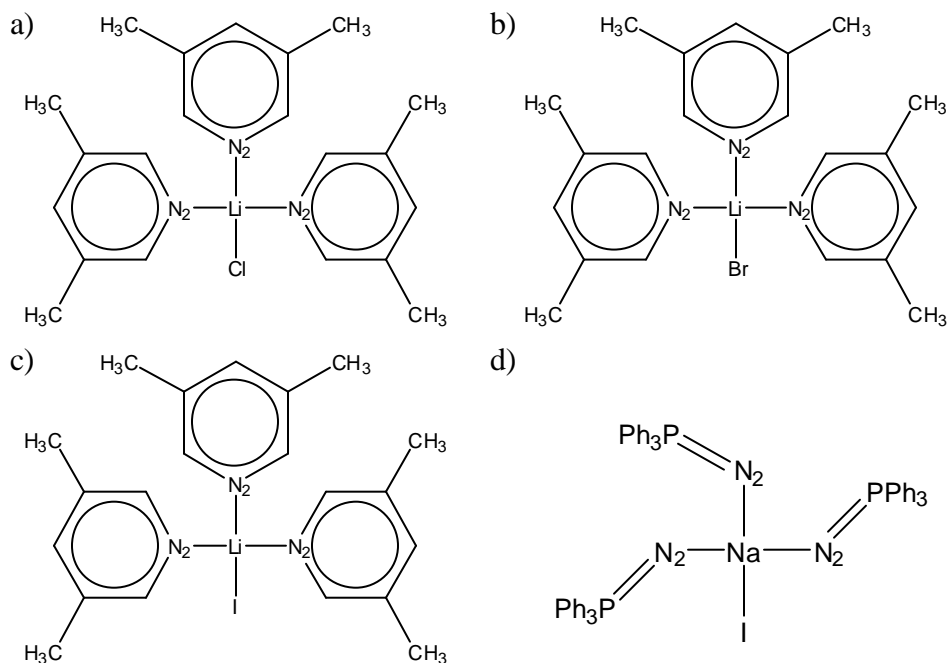

Figure 3.2. *Schematic structure of X-tris(3,5-dimethylpyridine)-lithium [X = Cl (a), $C_{21}H_{27}N_3LiCl$; Br (b), $C_{21}H_{27}N_3LiBr$ and I (c), $C_{21}H_{27}N_3LI$] and Iodo-tris(triphenylphosphineimine)-sodium (d), $C_{54}H_{48}P_3N_3NaI$*

Computed ligand - metal fragment separation, indicated by the alkali metal-ligand donor nitrogen bond lengths, changes from about 3.3 Å in the biggest Rb atom to about 2.3 Å in the Li atom. For the metal atom, changes in the halogen atom hardly modify the metal-ligand distance, although there is a clear tendency for the separation to reduce as you move down the halogen group. On the other hand, introducing a Cp ligand instead of the halogen atom considerably increases the metal-ligand distance to about 0.14 Å (see Table 3.3).

The tendency for the metal-ligand distance to decrease going from F to I is related to the tendency for the alkali metal-halogen to increase. Table 3.2 presents the experimental and calculated distances for the alkali monohalides molecules isolated and after complexation with **1**. As we can observe, after complexation the metal-halogen distance increases. Curiously for the same alkali metal this increment is also bigger going from F to I, in correspondence with the lowest metal fragment-ligand separation.

Table 3.2. *Experimental and computed M-X distances in the gas phase, for isolated monohalides and monohalide cubanes*

	Li-F	Li-Cl	Li-Br	Li-I	Na-I	K-I
M – X experimental[26]	1.564	2.021	2.170	2.392	2.711	3.048
1'-MX computed	1.655	2.141	2.326	2.574	2.863	3.217
M-X computed	1.615	2.084	2.230	2.461	2.745	3.091
% Variation*	2.4	2.7	4.1	4.4	4.1	3.9

** % of computed M-X length increase after complexation with **1***

The charge rearrangement caused by the net bonding contributions between **1'** and MX fragments can be seen in the electron density difference maps for 1'-LiX (X = Cl, I) and 1'-MI (M = Na, K) complexes (Figure 3.3). We will use these maps to make a preliminary analysis of the changes in the electronic distribution of the fragments during complexation and, therefore, of the derived energy terms.

```
UNIVERSITAT ROVIRA I VIRGILI
DFT STUDY OF TITANIUM CUBANE AND MOLYBDENUM SULPHIDE COMPOUNDS.
Autor: José Manuel Gracia Budria
ISBN: 978-84-690-6751-2 / DL: T.1196-2007
```
Chapter 3

Table 3.3. *Calculated and experimental bond lengths (Å) and angles (º) for selected N-donor ligand alkali metal complexes*

Compound	N_2-M	M-X	N_1-Ti	N_2-Ti	Ti-Ti	M-Ti
1			1.921	1.944	2.827	
[exp]**(1)**[27]			(1.912)	(1.933)	(2.803)	
1-LiF	2.309	1.655	1.921	1.947	2.837	2.984
1-LiCl	2.303	2.141	1.921	1.951	2.843	2.974
1-LiBr	2.287	2.326	1.923	1.945	2.832	2.967
1-LiI	2.274	2.574	1.924	1.949	2.835	2.955
1-LiCp	2.434	1.930[a]	1.919	1.943	2.833	3.157
1-NaI	2.651	2.863	1.922	1.950	2.835	3.360
1-NaCp	2.716	2.340[a]	1.922	1.946	2.833	3.394
[exp]**(1-NaCp)**[22]	(2.614)	(2.350)[a]	(1.919)	(1.930)		
1-KI	3.031	3.217	1.920	1.950	2.834	3.773
1-RbI	3.297	3.405	1.919	1.947	2.826	4.051
$(C_{21}H_{27}N_3)$-LiCl	2.054	2.320				
$(C_{21}H_{27}N_3)$-LiBr	2.072	2.517				
$(C_{21}H_{27}N_3)$-LiI	2.057	2.795				
$(C_{54}H_{48}P_3N_3)$NaI	2.388	3.159				

	N_2-M-N_2	N_2-M-X	Ti-N_1-Ti	Ti-N_2-Ti	N_1-N_2-H	Ti-N_2-M
1			94.7	93.3	151.0	
(1)[exp]			(94.2)	(92.9)		
1-LiF	81.2	131.3	95.2	93.5	157.0	88.6
1-LiCl	81.7	131.0	95.4	93.5	157.6	88.3
1-LiBr	81.6	131.0	94.9	93.4	157.2	88.6
1-LiI	82.3	130.6	94.9	93.4	157.6	88.5
1-LiCp	74.2	135.0[a]	95.0	93.7	156.3	89.5
1-NaI	70.2	138.4	95.0	93.2	152.6	92.6
1-NaCp	69.7	138.3[a]	94.9	93.4	154.3	93.2
(1-NaCp)[exp]	(70.9)	(139.9)[a]	(94.0)	(94.0)		(92.3)
1-KI	68.8	144.2	95.1	93.2	150.3	96.1
1-RbI	55.7	147.4	94.8	93.0	149.0	97.8
$(C_{21}H_{27}N_3)$-LiCl	106.4	112.4				
$(C_{21}H_{27}N_3)$-LiBr	108.9	110.1				
$(C_{21}H_{27}N_3)$-LiI	110.3	108.7				
$(C_{54}H_{48}P_3N_3)$NaI	107.5	111.3				

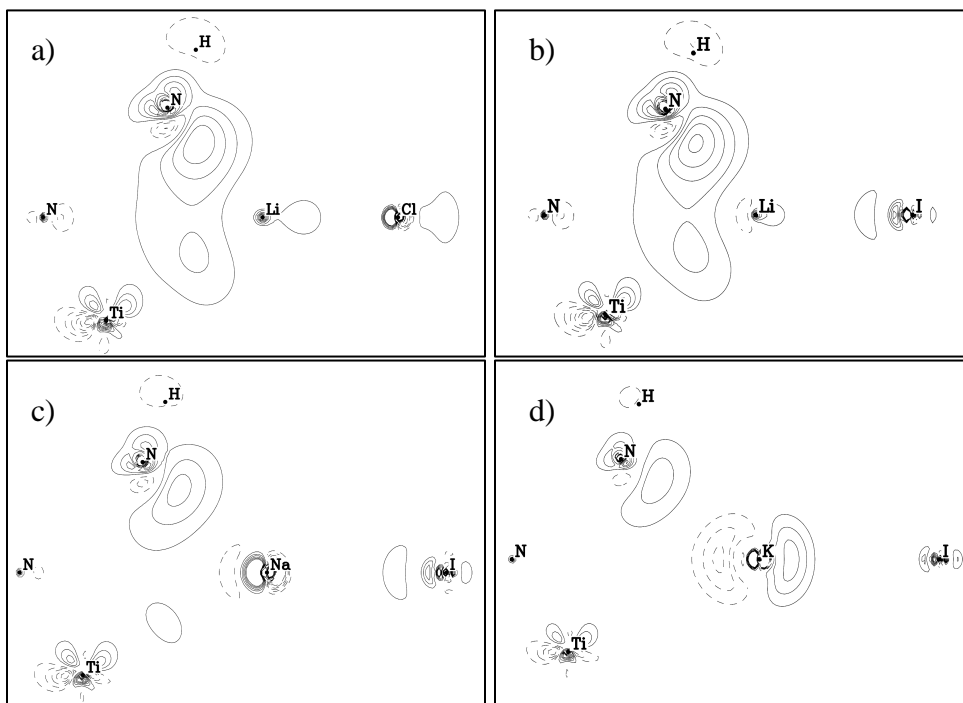[a] *Parameters obtained from the centroid of the cyclopentadienide ligand*

Figure 3.3. *Electron density deformation maps (EDPs) for complexes 1'-LiCl (a), 1'-LiI (b), 1'-NaI (c), 1'-KI (d). The EDP maps are computed as the difference between the density of the fragment 1'-MX and **1'** and MX, at the geometry of the optimized cluster. The EDPs are shown in the plane containing the fragment MX and a NH of **1** (C_{3v} symmetry plane). The maps are contoured linearly. Negative contours are dashed*

The formation of the M-N bonds induces a polarization of the electronic distribution in the M-X fragment and a charge density accumulation along the M-N bonds. So the formation of 1'-MX complexes results in the creation of three M-N bonds, while the polarization of the metal fragment weakens the metal halide bond, which clarifies the increment in the M-X distance. EDPs show that the greatest accumulation of electron density is between **1'** and MX for the smallest alkali metals. The accumulation of charge density is greater for Li-I than for K-I, which is logical if we consider the polarization power of the alkali metal. In a similar way, for the same alkali atom, the accumulated electron density decreases slightly going from I to Cl (see, Figure 3.3a and 3.3b). We can extract some ideas about

123

Chapter 3

the complexation. Only heterocubanes were obtained for the smallest alkali metals, because of their greater polarization power (Lewis acidity). However, they were only obtained for the least electronegative halogens.

Table 3.4 shows the calculated reaction energies in the gas phase for alkali metal halides M-X and metal cyclopentadienide species with **1'**. The processes were largely exothermic with reaction energies between -23 and -162 kJ mol^{-1}. There was a clear increase in the reaction energy going from Cs to Li and from Cp to F to I (see Figure 3.4 and Table 3.4). In view of the charges for the metal fragments, also included in Table 3.4, the observed trend in the increment of the reaction energy does not seem to correspond to an increment in the electrostatic interaction between fragments.

To examine the different energy terms involved in the complexation, we studied the decomposition of the interaction energy between fragments for the representative molecules $[XM\{Ti(\boldsymbol{h}^5 - C_5H_5)(\boldsymbol{m}_3 - NH)\}_3(\boldsymbol{m}_3 - N)]$ [M = Li, X = Cl, I, Cp; M = Na, K, X = I]. The difference between the interaction energy and the reaction energy lies in the energy that the reagents require to go from the vacuum to the interior of the complex. The analysis was made taking ligand **1'** and alkali halide as fragments and following Ziegler and Rouk's extension[28] to Morokuma's well-known decomposition scheme.[29] The total energy is decomposed into two terms: SR + OI The SR (steric repulsion) consists of two components: the classical electrostatic interaction (EI) between two unperturbed charge distributions of the two interacting fragments and the so-called exchange repulsion or Pauli repulsion (PR). In addition to the steric repulsions, there are orbital interactions (OI). This term represents the stabilization produced when the electron densities are allowed to relax and accounts for the charge-transfer between fragments and the mutual polarization of each fragment.

The analysis of the bond formation in terms of the energy decomposition from the two contact fragments made it possible to identify the nature of the interaction (see Table 3.5). The interaction energy, as was observed in the reaction energy, is highly exothermic. As the radii of the alkali atoms decrease, there is a rapid increase in the charge density of the cations, which leads to a greater Lewis acidity of the complexes. So for one halogen, the lithium atom has more effective electrostatic interactions. Its greater Lewis acidity also leads to greater electrostatic interactions and, finally, its small

radius increases the Pauli repulsions. Overall the main electrostatic and orbital contributions favour the smaller and more acid alkali atoms in the interaction with electron donor ligand **1'**.

For an alkali metal, iodine halides make bigger orbital and electrostatic contributions. This contrasts with the fact that the F atom is more electronegative than I and it polarizes the alkali metal more. To explain this the halogen and ligand properties must be taken into account. Furthermore, the fact that the nucleophilicity of F or Cl is bigger than that of Br and I produces stronger electrostatic repulsions with ligand donor electrons, as can be observed in Table 3.5. Also, fluorine and chlorine alkali bonds are less polarizable, more rigid and more ionic than bromide or iodine ones, so orbital interaction with the ligand is expected to be lower.

Table 3.4. *Calculated reaction energies (kJ mol^{-1}) in the gas phase for* $[XM\{Ti(\boldsymbol{h}^5 - C_5H_5)(\boldsymbol{m}_3 - NH)\}_3(\boldsymbol{m}_3 - N)]$ *[M = Li, Na, K, Rb, Cs, X = Cp, F, Cl, Br, I]compounds, together with Mulliken charges*

M-X	React.	Charges M	Charges X	M-X	React.	Charges M	Charges X
Li-Cp*	-52.0	0.31	-0.46	K-Cp*	-35.4	1.01	-0.90
Li-F	-126.3	0.64	-0.83	K-F	-64.6	0.93	-0.85
Li-Cl	-149.4	0.39	-0.61	K-Cl	-81.0	0.93	-0.86
Li-Br	-151.3	0.43	-0.67	K-Br	-83.9	0.96	-0.89
Li-I	-161.9	0.34	-0.59	K-I	-92.6	0.94	-0.87
Na-Cp*	-54.4	0.69	-0.65	Rb-Cl	-74.5	0.96	-0.87
Na-F	-100.3	0.83	-0.82	Rb-Br	-75.3	0.98	-0.90
Na-Cl	-111.9	0.73	-0.72	Rb-I	-80.3	0.96	-0.88
Na-Br	-113.8	0.77	-0.77	Cs-Cp*	-23.5	1.05	-0.85
Na-I	-117.7	0.69	-0.68	Cs-F	-54.8	0.98	-0.84
				Cs-Cl	-63.8	0.98	-0.89
				Cs-Br	-65.0	1.00	-0.91
				Cs-I	-70.2	0.99	-0.90

* Charges calculated from the addition of all the carbon and hydrogen ones

Chapter 3

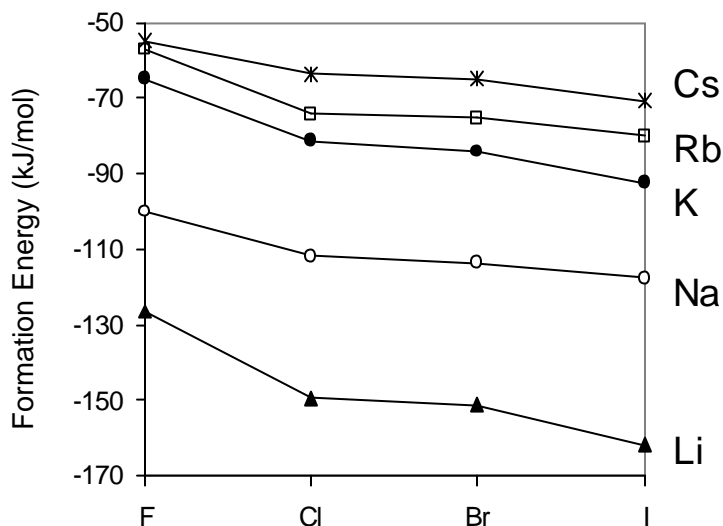**Figure 3.4.** *Formation energies for alkali halides*

Table 3.5. *Bonding energy decomposition in kJ mol^{-1} for* $\left[XM\left\{ Ti\left(\boldsymbol{h}^5 - C_5H_5\right)\left(\boldsymbol{m}_3 - NH\right)\right\}_3 \left(\boldsymbol{m}_3 - N\right)\right]$ *[M = Li , X = Cl , I , Cp; M = Na , K , X = I]*

	1-LiCp	1-LiCl	1-LiI	1-NaI	1-KI
Pauli	71.8	69.0	78.9	63.1	60.2
Electrostatic	-126.8	-143.1	-156.9	-132.4	-110.3
Steric	-55.0	-74.1	-78.0	-69.3	-50.1
Orbital	-49.1	-81.2	-92.4	-52.1	-45.3
Total	**-104.1**	**-155.3**	**-170.4**	**-121.4**	**-95.4**

126

These overall energy reactions between ligand and substrate can be classified as a function of the nature of the ligand.[30] Ligands can act as electron donors (Lewis base) for the cation, and as proton donors (Lewis acid) for the anion, in our case, Lewis base ligand to the cation. On this basis, ligands can be divided into two categories:

i) Simple Ligands. These ligands stabilize only the cation, and not its counteranion. In the case of complexation of a salt by a main ligand in a solvent, they usually produce ion-paired complexes. Salts represent a crystal structure formed by ion pairs interacting at a finite distance, and complexation and solution represents ion pairs at an infinite distance. Although these ligands do not complex a cation via its charge separation, charge separation of the complexing salt may be a consequence of complexation.

The following tendencies should be noted:

- Complexation increases as the charge density difference of the constituting ions increases. For a given anion, solvation of a cation is in the order:

$Li > Na > K > Rb > Cs$

The coordinative characteristics of a cation during interaction with a multidentate ligand become increasingly detectable as the cavity size of the polydentate ligand exceeds the cation size. Under these conditions cation-ligand complexation becomes increasingly dependent on the flexibility of the species. Thus, the conformation energy should be:

$Cs > Rb > K > Na > Li$

ii) Double action ligands. These ligands are capable of stabilizing a cation and an anion simultaneously. For a given cation complexation is hampered as the nucleophilicity of the counteranion increases. The complexation of a cation increases in general from F to I. It frequently causes charge separation of an ion pair. Under these conditions both cation and anion stabilization are facilitated. This contrasts with the behaviour of the group i) ligands, the efficiency of which for a given cation enhances as the nucleophilicity of the counter anion increases.

In summary **1'** acts as a simple tridentate ligand. We find ion paired complexes in which the metal size is not a determining factor in the stability of the compounds, so the interaction energy increases with the Lewis acidity of the metal, $Li > Na > K > Rb > Cs$, and with the decrease in the nucleophilicity of the counter anion, $I > Br > Cl > F > Cp$.

Solvent effects

Present DFT-calculated reaction energies in the gas phase reproduce the experimental trends for obtaining complexes 1-MX but they cannot explain the experimental results. All the reactions between **1'** and MX salts proved to be exothermic (Table 3.4) but no reaction was observed between **1** and a large number of metal halides.

From the data obtained in the gas phase, we can see that the reaction energy is not (nearly) enough to counteract the energy of sublimation to diatomic gas molecules from the solid salts MX (Table 3.6), and the $MX_{(solid)} + \mathbf{1}_{(gas)}$ -> 1-MX $_{(gas)}$ processes should be endothermic.

Table 3.6. *The molar enthalpy of sublimation (kJ mol^{-1}) for MX salts [M = Li, Na, K, Rb, Cs, X = F, Cl, Br, I]^{31}*

	Li	Na	K	Rb	Cs
F	276	282	242	226	194
Cl	213	235	223	207	203
Br	197	218	214	-	197
I	189	208	206	-	195

Reactions were carried out from the halides in the solid state but in a solvent. To explain how a main ligand contributes to the solubilization process of a crystal in a solvent, the salt ion pair-ligand complexation, the lattice energy of the salt and the dielectric constant of the solvent are of basic importance.[32] The alkali metal has a pronounced affinity for the halogen and gives an ion pair.[33] In the solid state the contact of ion pairs

forms the crystal, and the dissolution of the crystal involves the separation of the ion pairs in the solvent. So the complexation energy in the solvent, ΔE_F, must be greater than the dissolution energy, ΔE_D, of the salt.

A simple thermodynamic cycle can be constructed using experimental and theoretical values to estimate the dissolution energy. Figure 3.5 shows the thermodynamic cycle. The experimental condensation energy, ΔE_C, represents the total energy that passes from the molecules in the gas phase, MX(g), to the crystal, MX(s). This energy is the sum of two energies: the first step is to a liquid phase in a solvent, the computed solvation energy of which is ΔE_S; and the second step is from liquid to solid, the precipitation energy of which is ΔE_P. Precipitation energy is the same as dissolution energy, ΔE_D, but defined in the opposite sense. So we can estimate the dissolution energy as:

$$\Delta E_D = \Delta E_S - \Delta E_C$$

Now the dissolution energy can be compared with the reaction energy in the solvent, which is the energy required if complexation is to take place.

At present, it is still not possible for a quantum chemistry study to take into account all the factors that have an effect on chemical reactions in solution. However, a first-order approximation for dilute solutions is to model the solvent effects with a polarizable continuum.[34] The 1'-MX formation energies with toluene and dichloromethane as solvents were computed for several lithium halides (Figure 3.6).

Although the reaction energies have the same trends as in the gas phase, they are significantly smaller. Apparently, complexation energy values suggest that polar solvents do not directly favour the complexation of **1'** and MX in solution because the MX dipole is relatively more stable in polar solvents than the cubane structures. But now these complexation energies in solvent have to be compared with the dissolution energies obtained. In general the decrease in the complex formation energy is less than the decrease caused by the change from condensation energy to dissolution energy. So the overall process is clearly favoured if the solvent is taken into

Chapter 3

account (see Table 3.7 for a detailed analysis of the energies involved for the lithium metal).
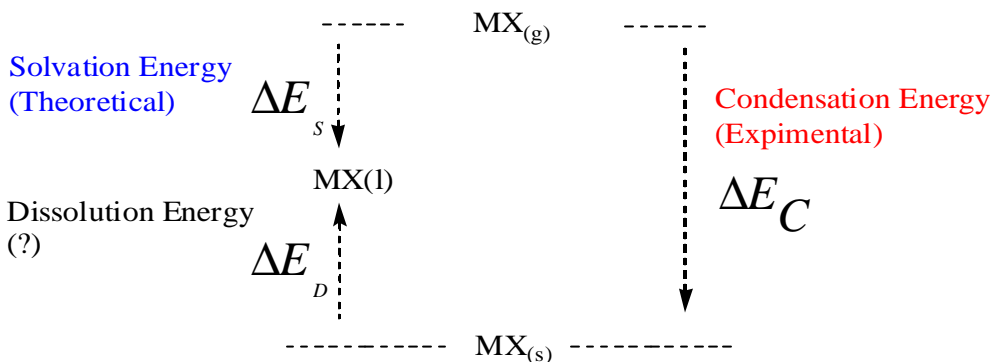

Figure 3.5. Thermodynamic cycle used to estimate the solution energies in the solvents

Figure 3.6 and Table 3.7 show how the dissolution energy of LiX in solvent decreases in the halogen group. The salt lattice energies mean that this result is only to be expected. Therefore, LiI is the easiest salt to dissolve. At the same time, iodine salts have the largest reaction energy, which means that 1'-LiI formation is the most favourable. The LiI complexation process is slightly endothermic by 8 kJ mol^{-1} in toluene and exothermic by 14 kJ mol^{-1} in dichloromethane. Only the energy of the iodine salt becomes exothermic. However, for the other halogens, the energy values are much nearer than in the gas phase.

As far as the two solvents are concerned, the values of dichloromethane, the more polar solvent, are the most favourable. The dissolution energies are clearly lower than those for toluene, while formation energies decrease the least. So, the formation of these kinds of complexes is favoured by more polar solvents.

We can conclude that the complexation of alkaline halides with ligand **1** is clearly favourable. The nature of the ligand determines the interaction energy with the salt ion pairs. This energy increases as the Lewis acidity of the metal increases and as the nucleophilicity of the counteranion decreases.

130

But these arguments cannot explain why experimentally the energetically less favoured cyclopentadiene Li and Na salts were found and not the Li and Na chlorine salts. To complete the view it is necessary to take into account both the lattice energy of the salt and the solvent effects, which overall generate the dissolution energy of the salt. In view of the results, it is this dissolution energy that really determines the complexation process and, therefore, the salt lattice energy.

Table 3.7. *Computed and estimated energies (kJ mol^{-1}) for several steps in the formation of 1-LiX in toluene and dichloromethane*

Step	Energy	Method	Halogen			
			F	Cl	Br	I
			Toluene			
1(l)+LiX(l) → 1-LiX(l)	ΔE_L	DFT+SOLVENT	-94.0	-92.1	-107.4	-117.8
LiX(g) → LiX(l)	ΔE_S	DFT+SOLVENT	-74.7	-73.1	-66.6	-63.6
LiX(s) → LiX(l)	ΔE_D	Expt [a]	201.3	139.9	130.4	125.4
1(l)+LiX(s) → 1-LiX(l)	ΔE_F	$\Delta E_L + \Delta E_D$	110.5	47.5	22.9	7.6
			Dichloromethane			
1(l)+LiX(l) → 1-LiX(l)	ΔE_L	DFT+SOLVENT	-69.9	-77.7	-73.8	-83.7
LiX(g) → LiX(l)	ΔE_S	DFT+SOLVENT	-126.0	-130.5	-122.2	-119.0
LiX(s) → LiX(l)	ΔE_D	Expt [a]	150.0	82.5	74.8	70.0
1(l)+LiX(s) → 1-LiX(l)	ΔE_F	$\Delta E_L + \Delta E_D$	80.1	4.8	1.0	-13.7

a) The dissolution energies of the solid ($\boldsymbol{DE}_D$) are estimated from the experimental energies of condensation (LiX(g)? LiX(s)), ($\boldsymbol{DE}_C$) taken from reference 31) and from the computed solvation energy of the gas($\boldsymbol{DE}_S$)

131

Chapter 3

Toluene

kJ mol^{-1}

	F	Cl	Br	I
◆ LiX Prec.	-201.3	-139.87	-130.45	-125.36
■ NaX Prec.	-208.35	-170.39	-159.96	-157.62
▲ NaX Reac.	-76.94	-85.58	-84.52	-89
✕ LiX Reac.	-94.0377	-92.1331	-107.349	-117.837

CH$_2$Cl$_2$

kJ mol^{-1}

	F	Cl	Br	I
◆ LiX Prec.	-149.55	-82.52	-74.76	-69.78
■ NaX Prec.	-156.52	-119.39	-111.9	-113.26
▲ NaX Reac.	-58.06	-63.74	-62.44	-66.17
✕ LiX Reac.	-69.8645	-77.7376	-73.8203	-83.681
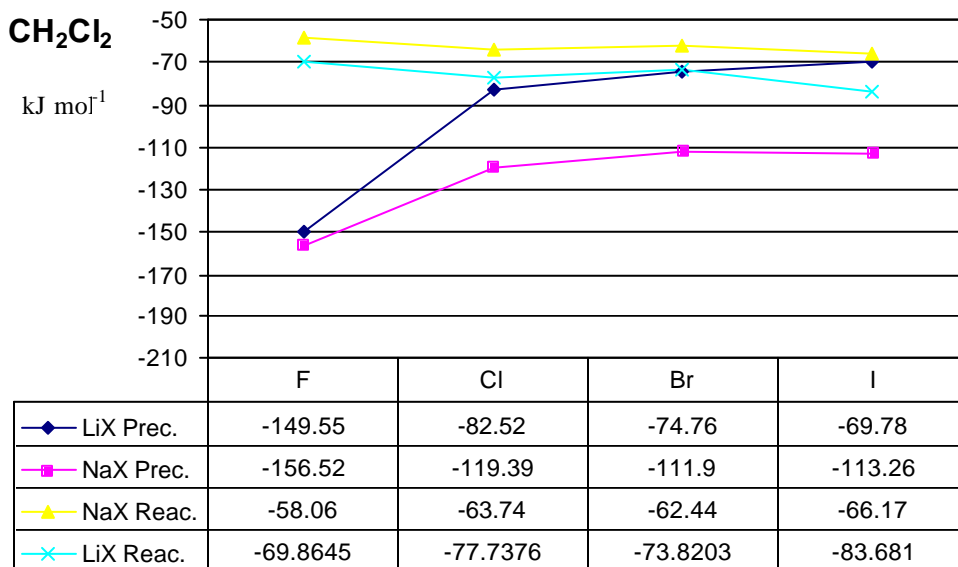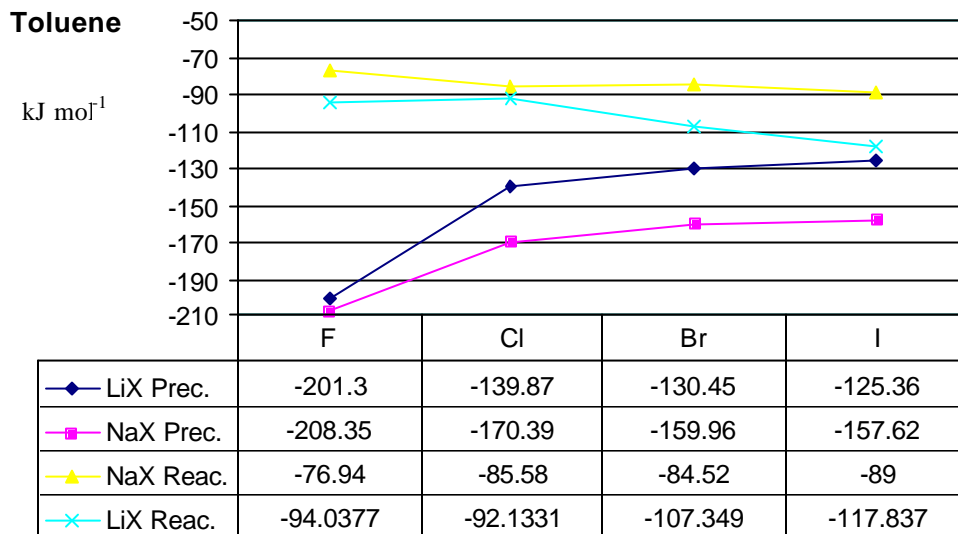
Figure 3.6. *Calculated reaction energies (kJ mol^{-1}) for processes **1'** + MX (M = Li , Na ; X = F , Cl , Br , I) in toluene and (CH$_2$Cl$_2$), compared with the energy change from MX (solution) to solid phase (kJ mol^{-1})*

132

3.3   Group 2 compounds: alkaline earth dihalide adducts

Transition metals support a rich variety of ligand systems.[35] Such richness is much less common among main group compounds, especially those containing the highly electropositive s-block elements, group 1 and 2, the complexes of which are characteristically ionic species. However, ligands are often found to be present as neutral bases, esters and amines.

Far from being simple ionic ns compounds, alkaline earth halides are one the most intriguing and best studied groups.[36] In fact their structural characteristics cannot be explained by ns valence electrons. Several studies have suggested that as much attention should be paid to the d orbitals of alkaline earth metals as to the orbitals of transition metals.[37]

The properties of alkaline earth complexes depend on the degree of metal acidity, which varies substantially from Be to Ba because of the increasing ionic radii (see Table 3.8). Beryllium stands apart from the other members of the group. The effective nuclear charge on a 2s electron in Be is much greater than in the other elements of the group, so the atom is small and the first ionization energy is large. The extreme smallness of the Be^{2+} ion makes it so strongly polarising that Be^{II} compounds are almost entirely covalent. The elements Ca to Ra, however, have low polarising power (see Table 3.8), and the compounds are predominantly ionic. The Mg^{2+} ion, on the other hand, has properties that are between Be^{2+} and Ca^{2+}.

The modification observed in the electronic structure, when going from Be and Mg compounds to Ca, Sr, and Ba compounds, provides both challenges and opportunities with regard to computational methodology, interpretations, and the practical consequences for organometallic and bioinorganic alkaline earth chemistry. The changing features of their interaction with the ligands means that sometimes it is the ligand which determines the stability of the adduct.

We shall now go on to show the result of the interaction of $\left[\left\{Ti\left(h^5 - C_5Me_5\right)\left(m_3 - NH\right)\right\}_3 \left(m_3 - N\right)\right]$ (**1**) ligand with alkaline earth halides. First we shall describe the experimental conditions and observed products and then we shall make a detailed analysis of the compounds and their stabilities. Special attention is obviously given to the nature of the

133

Chapter 3

metal ligand interaction. Because the chemistry of the alkaline earth metals does not increase gradually from Be to Ba, important conclusions about the nature of the ligand can be drawn from their complexation behaviour.

Table 3.8. *Atomic radii of alkaline earth metals in pm and absolute electronegativities in eV[21]*

	Be^{2+}	Mg^{2+}	Ca^{2+}	Sr^{2+}	Ba^{2+}
Ionic M^{2+} radius	34	79	106	127	143
Electronegativity	4.9	3.75	2.2	2.0	2.4

Observed products

Treatment of alkaline earth diiodides MI_2 with **1** in dichloromethane at room temperature gives the corresponding adducts $\left[I_2 M \left\{ Ti \left(h^5 - C_5 Me_5 \right) \left(m_3 - NH \right) \right\}_3 \left(m_3 - N \right) \right]$ [M = Mg; M = Ca; M = Sr] as yellow solids (Scheme 3.3).
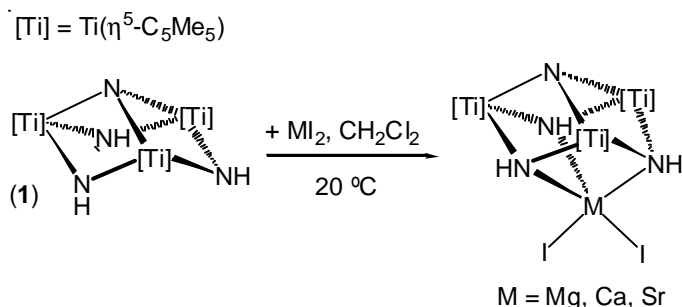
Scheme 3.3. $\left[I_2 M \left\{ Ti \left(h^5 - C_5 Me_5 \right) \left(m_3 - NH \right) \right\}_3 \left(m_3 - N \right) \right]$ *[M = Mg, Ca, Sr] adduct formation*

The 1-MX_2 complexes were characterized by spectral and analytical techniques. IR spectra reveal two absorptions in the range 3343-3236 cm^{-1} for the NH groups of the molecule. ^1H and ^{13}C NMR spectra in

134

[D$_1$]chloroform at room temperature show equivalents NH and η^5-C$_5$Me$_5$ groups on the NMR time scale. The NMR data are consistent with the complexes being fluxional in solution.

For the preparation of dihalide derivatives, alkaline earth iodides were used to prepare the 1-MX$_2$ adducts since, for instance, CaCl$_2$ does not react under the same conditions.

Analysis

The spectroscopic data suggest that there are two possible isomers, both with Cs symmetry and, a priori, with the alkali earth metal coordinated to the NH ligands in a tripodal fashion. In one, the five co-ordinated metal centres would adopt trigonal bipyramidal geometry, with the NH ligands occupying two equatorial positions and one axial (Figure 3.7a). In the other, the metal is inside a square pyramid with the NH ligand occupying the cusp and two equatorial positions (Figure 3.7b).
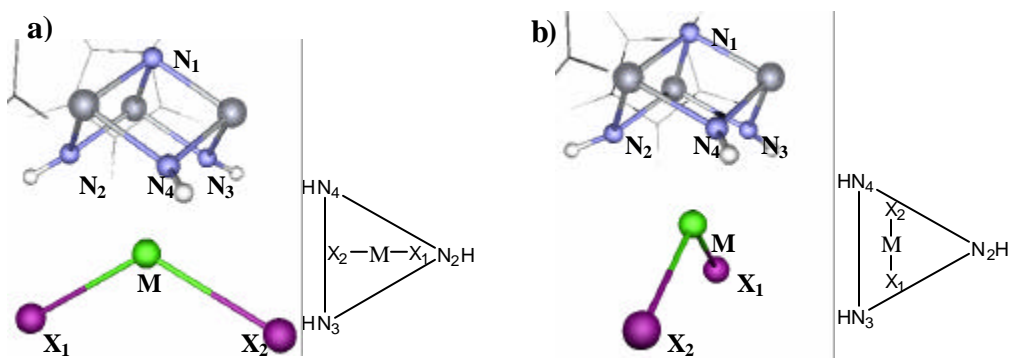
Figure 3.7. *Possible* $\left[X_2 M \left\{ Ti \left(h^5 - C_5 Me_5 \right) \left(m_3 - NH \right) \right\}_3 \left(m_3 - N \right) \right]$ *species. a) Trigonal bipyramidal coordination, b) Square pyramidal coordination*

Chapter 3

Both possible isomers were initially computed for model iodine molecules and also the model $CaCl_2$ complex, $\left[X_2 M\left\{Ti\left(h^5 - C_5H_5\right)\left(m_3 - NH\right)\right\}_3 \left(m_3 - N\right)\right]$, 1'-MX₂, [M = Ca, X = Cl; M = Mg, Ca, Sr, X = I].

Table 3.9. *Energy differences in kJ mol^{-1} for computed* $\left[X_2 M\left\{Ti\left(h^5 - C_5H_5\right)\left(m_3 - NH\right)\right\}_3 \left(m_3 - N\right)\right]$ *[M = Ca, X = Cl; M = Mg, Ca, Sr; X = I] square pyramidal and trigonal bipyramidal isomers*

	1'-CaCl₂	1'-MgI₂	1'-CaI₂	1'-SrI₂
Square Pyramid	0.0	0.0	0.0	0.0
Trigonal Bipyramid	5.7	1.0	1.8	1.8

In all cases, model complexes with a square pyramidal structure were slightly more stable and the energy differences were always smaller than 6.0 kJ mol^{-1}. Table 3.9 shows the computed energy differences. The trigonal bipyramidal structure can be regarded as the eclipsed structure of the staggered square pyramid. Figure 3.7 shows that the change from one structure to the other is only a 30° rotation of the metal fragment around a hypothetical axis that goes from the apical cubane N_1 atom to the alkaline earth metal. A physical barrier to the rotation is not expected. Together with the small energy differences found for the interchange of structures, this explains the experimental findings of the compounds' fluxional behaviour.

Structures and reaction energies were calculated, on the basis of the square pyramidal conformation, for the whole family of model alkaline earth halide compounds $\left[X_2 M\left\{Ti\left(h^5 - C_5H_5\right)\left(m_3 - NH\right)\right\}_3 \left(m_3 - N\right)\right]$, (M = Be, Mg, Ca, Sr; X = F, Cl, Br, I). Table 3.10 shows selected structural data for the compounds, and Table 3.11 shows the computed reaction energies.

136

Table 3.10. *Computed structural data for square pyramidal model isomers* $\left[X_2M\left\{ Ti\left(\mathbf{h}^5 - C_5Me_5\right)\left(\mathbf{m}_3 - NH\right)\right\}_3 \left(\mathbf{m}_3 - N\right)\right]$ *[M = Ca, X = Cl; M = Mg, Ca, Sr; X = I], except when indicated*

	$N_2 - M$	$N_3 - M$	$M - X_1$	$X_1 - M - X_2$	$N_2 - M - X_2$
$BeF_2^{\ Trig}$	1.754	3.356	1.478	128.9	115.2
$BeCl_2^{\ Tetra}$	3.203	1.921	1.967	116.7	71.4
$BeCl_2^{\ Trig}$	1.719	3.336	1.939	123.2	118.0
$BeBr_2^{\ Trig}$	1.728	3.384	2.107	121.5	118.8
$BeI_2^{\ Trig}$	1.692	3.391	2.328	120.4	119.4
$MgF_2^{\ Trig}$	2.140	3.280	1.814	140.7	109.3
$MgCl_2$	2.290	2.537	2.302	115.9	111.1
$MgBr_2$	2.210	2.541	2.487	115.5	111.7
MgI_2	2.255	2.478	2.726	111.7	111.5
$MgI_2^{\ Bypi}$	2.500	2.323	2.724	111.3	81.2
CaF_2	2.688	2.751	2.055	125.2	114.5
$CaCl_2$	2.541	2.681	2.581	127.3	107.0
$CaCl_2^{\ Bypi}$	2.619	2.606	2.564	126.6	82.8
$CaBr_2$	2.583	2.686	2.721	116.7	116.4
CaI_2	2.539	2.596	3.026	122.5	108.5
$CaI_2^{\ Bypi}$	2.584	2.553	3.012	121.7	80.2
SrF_2	2.786	2.966	2.221	131.5	106.5
$SrCl_2$	2.729	2.831	2.741	137.2	104.9
$SrBr_2$	2.747	2.823	2.900	133.7	106.8
SrI_2	2.772	2.825	3.293	128.3	108.7
$SrI_2^{\ Bypi}$	2.834	2.839	3.262	133.4	72.2

^{Tetra} *Tetrahedral metal environment*
^{Trig} *Trigonal planar metal environment*
^{Bypi} *Trigonal bipyramidal structure*

Because of the large size of the metals, Ca and Sr compounds have three-coordinate metal centres. The metal-nitrogen distances from the ligand are similar but the distances from the equatorial nitrogens are slightly larger. For one halogen, a change in the metal logically means that the distance will vary with the radius of the metal. On the other hand, for the same metal centre a change in the halogen has no particular effect.

Beryllium metal compounds have the peculiar structural characteristics that can be deduced from their small size. Compounds present one short metal – nitrogen distance at about 1.7 Å corresponding to the axial nitrogen, and two longer distances over 3.35 Å for the equatorial positions. The overall geometry is similar to that of one coordinate compounds with the metal adopting a trigonal planar geometry (Figure 3.8 b).

Be complexes usually involve sp^3 hybrid orbitals, which give the four bonds over the Be atom a tetrahedral disposition. A tetragonal structure was computed by placing the $BeCl_2$ molecule between two imido nitrogen atoms (Figure 3.8 a). Surprisingly a pseudo tetrahedral metal disposition appeared at about 6.6 kJ mol^{-1} over the initial trigonal planar structure. The selected parameters can be seen in Table 3.10.
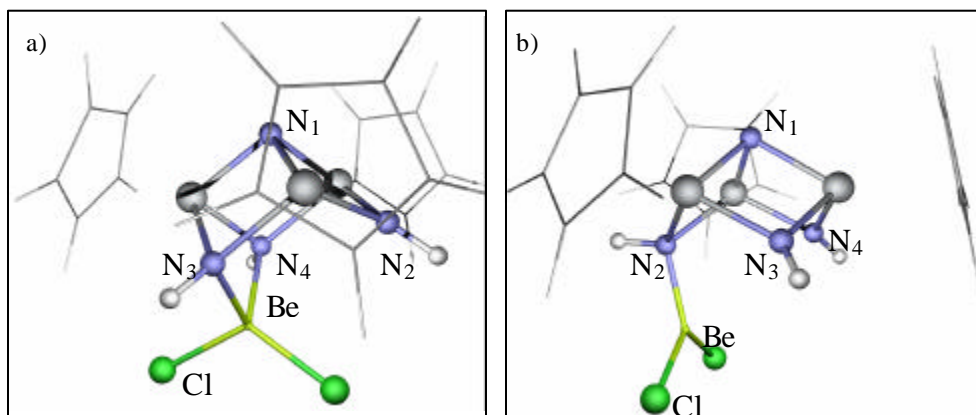
Figure 3.8. Trigonal planar, a), and tetrahedral, b), isomers for the beryllium compounds $\left[Cl_2Be\left\{ Ti\left(h^5 - C_5Me_5\right)\left(m_3 - NH\right)\right\}_3 \left(m_3 - N\right)\right]$

Finally, let us discuss Mg^{2+} atom adducts. Their characteristics are somewhere between those of Be^{2+} and Ca^{2+} and can be observed extremely well. The 1'-MgF_2 complex has a clear one-coordinate metal with the ligand and moves toward the three-coordinated structure as you move down the halogen group. In this case, the MgI_2 complex has smaller metal-ligand nitrogen bond differences for the equatorial and axial imido nitrogens, 2.255 Å, and 2.596 Å, respectively.

Table 3.11 shows the reaction energies between alkaline earth dihalides MX_2 and **1'**. The nature of the bond can be analysed in terms of the Lewis acidity of the metal centre, and the effective accommodation of the ligand electrons. For the clear three-coordinated Ca and Sr adducts, the reaction energy increases with the acidity of the metal for one halogen atom, while for a metal, the change in the halogen favours the complexation as we go down the group. In previous sections we have pointed out that the simple nature of the ligand favours complexation as the nucleophilicity of the halogen decreases.

Mg complexes have lower reaction energies than Ca and Sr adducts. The atom size makes the accommodation of the ligand electrons more difficult and the steric effects increase. While Cl, Br and I complexes remain three-coordinated, F complexes become one-coordinated. This change is also observed in a reduction of the reaction energy of about 30 kJ mol^{-1} for the F compound.

The Be atom has a more homogeneous energy picture. The reaction energies are the lowest and similar for all the halogens. Its considerably reduced size increases the steric effects and all the compounds remain one-coordinated. No particular trend is observed when the halogen changes, probably because of the compromise between the acidity of the metal and the steric repulsions. To illustrate this, Table 3.11 shows the Mulliken charges for the atoms involved. The BeF_2 fragment has the greatest polarization, which leads to greater electrostatic interaction with the ligand. In turn, the high nucleophilicity of the F atoms increase the steric repulsions. In this way, the interaction energy is greatest for the $BeBr_2$ molecule that is halfway between the attracting electrostatic interactions and the repulsing steric interactions.

Chapter 3

Table 3.11. *Reaction energies in kJ mol^{-1} and Mulliken charges for the computed $\left[X_2 M \left\{ Ti \left(h^5 - C_5 Me_5 \right) \left(m_3 - NH \right) \right\}_3 \left(m_3 - N \right) \right]$ model isomers*

	Reaction Energy	Mulliken Charges			
		M	X_{1-2}	N_2	N_{3-4}
BeF_2	-133.8	0.920	-0.659	-0.792	-0.62
$BeCl_2$	-128.4	0.236	-0.325	-0.733	-0.619
$BeBr_2$	-134.9	0.304	-0.361	-0.734	-0.622
BeI_2	-132.8	0.12	-0.284	-0.703	-0.622
MgF_2	-133.7	1.421	-0.797	-0.936	-0.64
$MgCl_2$	-158.9	0.952	-0.570	-0.817	-0.740
$MgBr_2$	-159.3	0.842	-0.556	-0.789	-0.704
MgI_2	-164.4	0.699	-0.429	-0.777	-0.714
CaF_2	-185.3	1.484	-0.747	-0.791	-0.731
$CaCl_2$	-207.6	1.685	-0.793	-0.862	-0.762
$CaBr_2$	-244.3	1.393	-0.727	-0.836	-0.760
CaI_2	-240.8	1.425	-0.669	-0.859	-0.826
SrF_2	-156.7	1.555	-0.780	-0.816	-0.733
$SrCl_2$	-183.3	1.409	-0.718	-0.825	-0.757
$SrBr_2$	-180.2	1.463	-0.754	-0.820	-0.763
SrI_2	-196.6	1.575	-0.734	-0.857	-0.812

To sum up, the order of the binding strengths for the interaction of alkaline earth metals with ligand **1'** suggests that the strongest bond is not originated for the most intensely charged ions. But Mg^{2+} and Be^{2+} ions may deviate because their small radius does not allow efficient "packing of all necessary chelating sites". Apparently steric oversaturations are the reason why no more than one of certain large ligands can be accommodated on group 2

metal centres. For instance, attempts to form the metallocene $BeCp*_2$ by halide metathesis have been unsuccessful:[38]

$$2\,NaCp^* + BeCl2 \;\nrightarrow\; BeCp^*_2 + 2NaCl$$
$$\rightarrow Cp^*BeCl + NaCl + NaCp^*$$
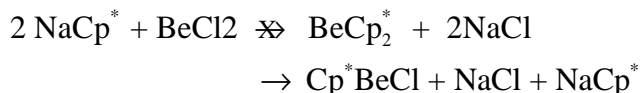
For the same reason the Be complexes distort from a tripodal coordination to a lower coordinated structure. A characteristic feature of organoalkaline-earth complexes is the formation of a variety of adducts with Lewis bases. In the formation of adducts, the coordination number of the metal increases with the radius:

$Be^{2+} < Mg^{2+} < Ca^{2+} < Sr^{2+} < Ba^{2+}$

This tendency is the same with ligands that completely envelop the metal centre. The corresponding steric oversaturation explains the stability of the compounds. However, the inherent acidity of the metal centre must also be a determining factor in the stability of acid/base adducts, and the acidity varies in the order:

$Be^{2+} > Mg^{2+} > Ca^{2+} > Sr^{2+} > Ba^{2+}$
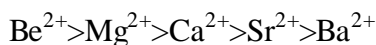
As these two trends pull in opposite directions, it is often the ligands that determine the stability of these adducts. These aspects complete the view of our compounds and provide important information about our ligand and possible secondary applications. They also provide us with an image of the steric size of our ligand and give a short guide for distinguishing cations.

Although the exothermic reaction energies are not small, the corresponding $\left[X_2M\left\{Ti\left(h^5 - C_5Me_5\right)\left(\mu_3 - NH\right)\right\}_3\left(\mu_3 - N\right)\right]$ adduct does not form in some cases. As in Group 1 halides, the initial reaction comes from the solid salts and the ligand in solution, so to treat the reaction in the solvent; we must take into account the dissolution energy. All the thermodynamic values for the sublimation energies (Table 3.12) are much greater than the estimated reaction energies, so no heterocubanes are formed. What is clear,

Chapter 3

however, is that for these compounds the energy gap is lower as we move down the halogen group.

Table 3.12. *The molar enthalpy of sublimation (kJ mol^{-1}) for MX_2 salts, [M = Be, Mg, Ca, Sr; X = F, Cl, Br, I]*[31]

	Be	Mg	Ca	Sr
F	233	400	438	452
Cl	136	241	324	343
Br	126	215	285	308
I	125	192	261	286

Our results were improved if the salvation influence was included. Because of the expense, only calculations for the complexation of **1'** with MgI_2 were performed. The reaction energy, which is exothermic in the gas phase by –164.4 kJ mol^{-1}, is reduced in solution (CH_2Cl_2) to –83.9 kJ mol^{-1}, but the solvent interaction also reduces the energy required to remove a salt molecule from the crystal by –134.0 kJ mol^{-1}. So the effect of the overall reaction is favourable. These results are exported to the remaining dihalides and clearly expose our conclusions for the formation of heterometallocubanes.

3.4 Titanium and zirconium cubanes

Extensive research efforts have recently focused on transition-metal complexes that enclose multiply bonded ligands.[39] Complexes containing metal-nitrogen multiple bonds are ubiquitous in transition-metal chemistry.[40] Especially important is the growing number of group IV imido complexes. Group IV imido complexes participate in imine metathesis[41] and catalyze the hydroamination of alkynes to enamines.[42]

A wide range of ancillary ligand environments for the M=NR functional group has been explored. Much of the recent activity in group 4 imido

142

chemistry has centred on reactions of the M=NR functional group itself, although the role of imides as supporting ligands also continues to be developed.[43]

Part of this current interest has been attracted by titanium imido compounds[44] (for instance, their role as transient intermediates in the conversion of other titanium-nitrogen compounds to titanium nitride TiN, a material with several important uses). A number of titanium imides have been isolated and tested as single-source CVD (chemical vapour deposition) precursors to TiN.[45]

Titanium nitride, TiN, displays an interesting combination of properties.[46] For instance, the optical properties of TiN resemble those of gold, yet it is harder than all elemental metals and sapphire, Al_2O_3, and almost as hard as diamond. Its melting point is almost 3000 ºC, which is higher than that of most materials, and it is inert to most solvents except aqua regia, which dissolves it slowly, and HF. Titanium nitride is a better electrical conductor than titanium metal. Because of their unique properties, TiN thin films have been used for several technological applications. For example, they are widely used as wear-resistant coatings on machine tools and as decorative (gold-coloured) coatings on watches and jewellery. Possible applications of TiN films include their use as diffusion barriers or as electrical connections in microelectronics and solar cells. Titanium nitride can also be used as a solar control coating on windows in warm climates.

In this section we shall not attempt to explain titanium nitride applications. As in previous sections, however, we shall try to describe the formation of some titanium imido adducts with $\left[\left\{Ti\left(\boldsymbol{h}^5 - C_5Me_5\right)\left(\boldsymbol{m}_3 - NH\right)\right\}_3\left(\boldsymbol{m}_3 - N\right)\right]$ precubane, the nature of the interaction and the electronic structure of the new compounds.

In this special case, the addition of titanium metal fragments leads us to homometal titanium cubane compounds. We shall first describe the monomer species, and go on to introduce corner shared cubanic dimers, extending their ligand capabilities through sandwich type complexes.

Chapter 3

3.4.1 Titanium monomers

The reaction of complex $\left[\{Ti(\boldsymbol{h}^5\text{-}C_5Me_5)(\boldsymbol{m}\text{-}NH)\}_3(\boldsymbol{m}_3\text{-}N)\right]$ (1) with the d^0 imidotitanium complexes $\left[Ti(NR)Cl_2(py)_3\right]$ (R = Ar and tBu) in toluene at room temperature affords brown crystals of $\left[\{Cl_2(RN)Ti\}(\boldsymbol{m}_3\text{-}NH)_3\{Ti_3(\boldsymbol{h}^5\text{-}C_5Me_5)_3(\boldsymbol{m}_3\text{-}N)\}\right]$ (R = Ar and tBu) and $\left[\{Cl_2Ti\}(\boldsymbol{m}_3\text{-}N)_2(\boldsymbol{m}_3\text{-}NH)\{Ti_3(\boldsymbol{h}^5\text{-}C_5Me_5)_3(\boldsymbol{m}_3\text{-}N)\}\right]$ (3.1) green solid, respectively (Scheme 3.4).
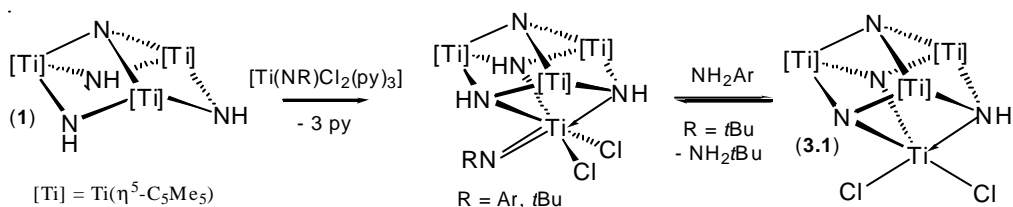
Scheme 3.4. *Reaction of* $\left[\{Ti(\boldsymbol{h}^5\text{-}C_5Me_5)(\boldsymbol{m}\text{-}NH)\}_3(\boldsymbol{m}_3\text{-}N)\right]$ *(1) with imidotitanium(IV) complexes*

The reaction between 1 and $\left[Ti(NtBu)Cl_2(py)_3\right]$ in dichloromethane was monitored by NMR spectroscopy. NMR spectra showed the evolution of 1-Ti(NtBu)Cl₂ to give 3.1 and tert-butylamine at room temperature.

Compounds 1-Ti(NAr)Cl₂ and 3.1 were characterized by ^{1}H and ^{13}C NMR spectroscopy, infrared spectroscopy, microanalysis and X-ray structure determination for 1-Ti(NAr)Cl₂. The solid state structure revealed a distorted [Ti$_4$N$_4$] cube core, in which the imido-bonded titanium atom shows a six-coordinated geometry with three *fac*-sites being occupied by the $\left[\{Ti(\boldsymbol{h}^5\text{-}C_5Me_5)(\boldsymbol{m}\text{-}NH)\}_3(\boldsymbol{m}_3\text{-}N)\right]$ organometallic ligand, and the rest of the coordination sphere being completed by two chlorines and one arylimido group. The structural trans-effect (STE)[47] of this ligand results in a longer

titanium-nitrogen *trans* distance (Ti-N_{trans}, 2.602 Å) than those in the *cis* positions (Ti-N_{cis}, 2.284 Å) (see Table 3.14).

The 1-Ti(NR)Cl_2 complexes show fluxional behaviour on the NMR time scale. The ^{1}H-NMR spectrum obtained for 1-Ti(NAr)Cl_2 in a 500 MHz spectrometer in toluene at room temperature showed equivalent NH and h^5-C_5Me_5 ligands. After cooling at –70 °C, the spectrum revealed two types of m_3-NH and h^5-C_5Me_5 ligands (2:1 ratio), consistent with the solid-state structure.

The fluxional process in complex 1-Ti(NAr)Cl_2 can be visualized as rotation (octahedron-trigonal prism-octahedron) of the organometallic ligand around the $\left[TiCl_2NAr\right]$ fragment (Figure 3.9), analogous to that of $\left[Ti(NR)(Me_3tach)Cl_2\right]$ (Me_3tach = 1,3,5-trimethyl-1,3,5-triazacyclohexane ; R = tBu or 2,6-iPr$_2C_6H_3$) complexes , previously described by Mountford et al. [48]

The kinetic parameters of the dynamic behaviour in these compounds (see Table 3.13), which were calculated on the basis of H-DNMR data by line shape analysis of the h^5-C_5Me_5 resonances, are in good agreement with an intramolecular process (log A = 12.5-14.0) and support a non-dissociative mechanism ($\Delta S^{\neq}$ = (-4.4)-(+4.6) e.u.).

Table 3.13. *Activation parameters for the h^5-C_5Me_5 group exchange in the 1-Ti(NR)Cl2 complexes*

Compound	Log A	E_a [kcal/mol]	$\Delta H^{\neq}$ [kcal/mol]	$\Delta S^{\neq}$ [e.u.]	$\Delta G^{\neq \ 298 \ K}$ [kcal/mol]
1-Ti(NR)Cl_2	14.00±0.45	14.45±0.50	13.95±0.50	+3.9±2.0	12.8
	R = 0.997		r = 0.997		

Chapter 3
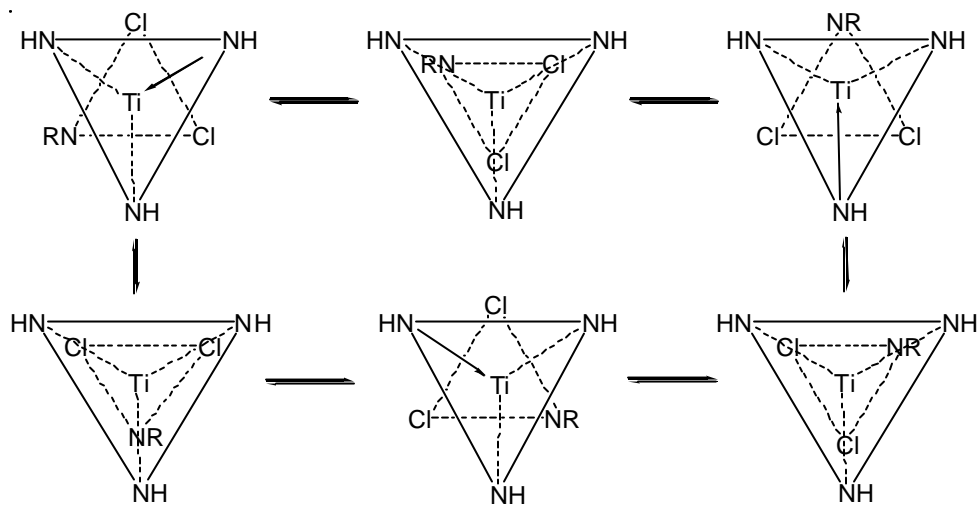
Figure 3.9. *Proposed fluxional process for the 1-Ti(NR)Cl₂ complexes*

The ^{1}H and ^{13}C NMR spectra of **3.1** in chloroform-d$_1$ at room temperature revealed resonances for two different h^5-C$_5$Me$_5$ ligands (1:2 ratio). The limited solubility and the low value of the n_{NH} vibration in the IR spectrum could indicate strong inter/intramolecular N-H···Cl interactions in this complex.[49]

First, density functional theory based calculations were carried out on $\left[\{Cl_2(NAr)Ti\}(m_3\text{-NH})_3\{Ti_3(h^5\text{-}C_5H_5)_3(m_3\text{-N})\}\right]$ 1'-Ti(NAr)Cl$_2$ and $\left[\{Cl_2(MeN)Ti\}(m_3\text{-NH})_3\{Ti_3(h^5\text{-}C_5H_5)_3(m_3\text{-N})\}\right]$ 1'-Ti(NMe)Cl$_2$ model compounds. The geometrical parameters selected are given in Table 3.14. Theoretical calculations on model compound 1'-Ti(NAr)Cl$_2$ reproduce the experimental geometry well and the calculated trans-effect (STE)[50] of the imido ligand (elongation = 0.33 Å) is also similar to the one observed experimentally (0.32 Å). These data are consistent with the large trans-effect (STE) found in the solid state structure of 1-Ti(NAr)Cl$_2$ and its dynamic behaviour in solution. The difference in the electronic energy between the prismatic and octahedral environment for compound model 1'-Ti(NAr)Cl$_2$ was estimated by calculations in 44 kJ·mol^{-1}.

146

Table 3.14. *Computed selected bond lengths (Å) and angles (°) for 1'-Ti(NAr)Cl$_2$ and 1'-Ti(NMe)Cl$_2$. Also experimental data for complex 1-Ti(NAr)Cl$_2$*

	1'-Ti(NAr)Cl$_2$	1'-Ti(NMe)Cl$_2$	1-Ti(NAr)Cl$_2$
Ti-N$_{ax}$	2.63	2.60	2.60
Ti-N$_{eq}$	2.30	2.31	2.28
Ti-NR	1.73	1.70	1.70
Ti-Cl	2.39	2.41	2.37
N$_{ax}$-Ti-N$_{eq}$	76.3	76.6	75.3
N$_{eq}$-Ti-N$_{eq}$	76.6	76.5	76.5
N$_{ax}$-Ti-NR	178.2	177.5	173.6
N$_{eq}$-Ti-NR	102.4	101.5	100.9
Cl-Ti-Cl	105.8	106.9	98.3

The reaction energy of ligand **1'** and the [TiCl$_2$NAr] fragment to give the 1'-Ti(NAr)Cl$_2$ is -203 kJ·mol^{-1}, whereas the fragment interaction energy between the same fragments is –289 kJ·mol^{-1}. We should point out that dissociation and fragment interaction energies are interconnected by the deformation energy necessary to transform the fragments from their optimal structure to the geometry adopted in the final compound.

A correlation diagram for 1'-Ti(NAr)Cl$_2$ is presented in Figure 3.10. It should be noted that the formation of these complexes is not accompanied by changes in the oxidation state of the metal centres, Ti(IV), and arises from the stabilization of the lone pair electrons of the tripodal ligand **1'**. It should also be observed that the energy of the HOMO orbital in complex 1'-Ti(NAr)Cl$_2$, in essence an orbital of the [TiCl$_2$NAr] fragment which formally corresponds to the ***p*** bond between the metal and the phenylimido ligand, increases during the formation of complex 1'-Ti(NAr)Cl$_2$. Its destabilization is due to the increasing antibonding character between the Cl orbital contribution and the other orbitals. There is a change in the

Chapter 3

N-Ti-Cl angle, from 111.6° in the isolated [TiCl$_2$NPh] fragment to 103.6° in the complex 1'-Ti(NAr)Cl$_2$.

The special capabilities of our organometallic ligand can best be described by comparing its interaction energy with several metal fragments. Table 3.15 shows the dissociation energies computed for several aza metallocubane complexes [(L$_n$M)(μ_3-NH)$_3${Ti$_3$(η^5-C$_5$H$_5$)$_3$(μ_3-N)}]. The values in this table clearly indicate that there is a relationship between the dissociation energy and the number of d-electrons in the heterometal. This is a consequence of the non-negligible mixing between the d-orbitals of the metal center and the d-titanium orbitals of the Ti$_3$N$_3$ core. The heterometal shares its d-electrons with the three titanium atoms. In complex 1'-Ti(NAr)Cl$_2$, the heterometal is a Ti(IV) with no d electrons, so the bonding energy is only caused by metal-ligand interactions with the total absence of metal couplings. Thus, this complex has the lowest dissociation energy.
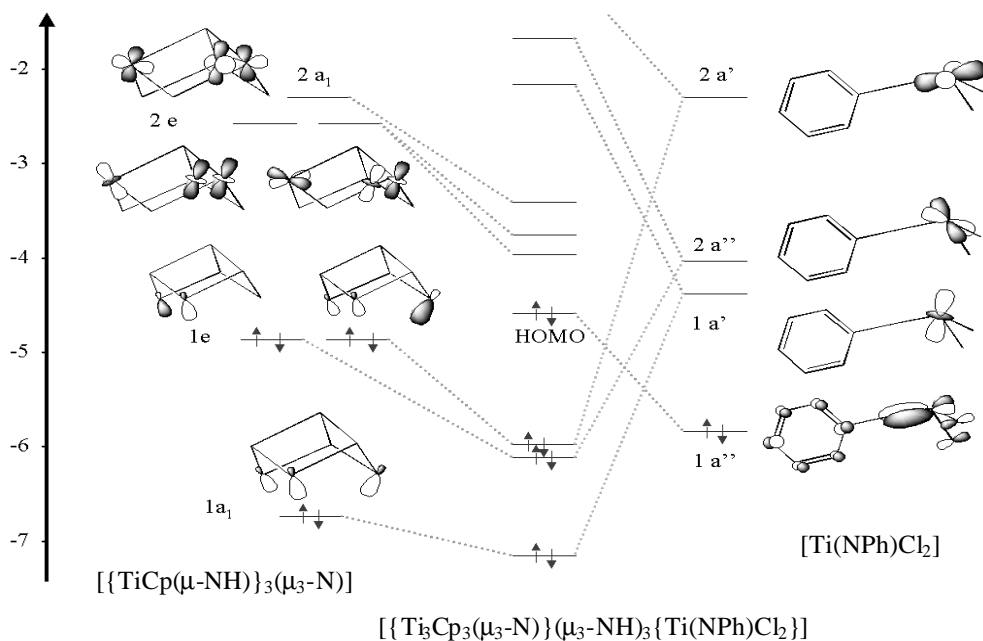
Figure 3.10. *Interaction orbital diagram for the complex [{Cl$_2$(NAr)Ti}(μ_3-NH)$_3${Ti$_3$(η^5-C$_5$H$_5$)$_3$(μ_3-N)}]*

148

Table 3.15. *Dissociation energy (ΔE_{Dis}) for azaheterometallocubane complexes $[(L_nM)(m_3\text{-}NH)_3\{Ti_3(h^5\text{-}C_5H_5)_3(m_3\text{-}N)\}]$*

Complex	M	ΔE_{Dis}(kJ·mol^{-1})
$\left[\{Cl_2(PhN)Ti\}(m_3\text{-}NH)_3\{Ti_3(h^5\text{-}C_5H_5)_3(m_3\text{-}N)\}\right]$	**Ti(d^0)** [51]	203
	Cr(d^6) [14]	376
$\left[\{(CO)_3M\}(m_3\text{-}NH)_3\{Ti_3(h^5\text{-}C_5H_5)_3(m_3\text{-}N)\}\right]$	**Mo(d^6)** [14]	351
	W(d^6) [14]	445
$\left[\{(COD)M\}(m_3\text{-}NH)_3\{Ti_3(h^5\text{-}C_5H_5)_3(m_3\text{-}N)\}\right]^+$	**Rh(d^8)** [52]	378
	Ir(d^8) [52]	445

The elements Ti and Zr have a strong tendency to exhibit the group's maximum charge number, +4, almost to the exclusion of lower oxidation states. This is particularly true of Zr. Metal(II) dihalides can be obtained by reducing tetrahalides and keeping them apart from oxidants. Another way of obtaining metal (IV) dihalides is to substitute two halogens in TiCl$_4$ by some similar ligands. For example, if TiCl$_4$ is treated with C_5H_5Na, bis(cyclopentadienyl) titanium dichloride, $(C_5H_5)_2TiCl_2$, is obtained. Similarly, our imido titanium compounds evolve to a titanium dihalide cubane compound **3.1** through the activation of two basal imido protons, with no change metal oxidation state. Two aspects are significant in this process: the reactivity of the M=NR functional group and the polyfunctionality of ligand **1**.

Calculations were carried out to establish the structure for the model complex $\left[\{Cl_2Ti\}(m_3\text{-}N)_2(m_3\text{-}NH)\{Ti_3(h^5\text{-}C_5H_5)_3(m_3\text{-}N)\}\right]$ **3.1'.** The structure has two azatitanocubanes connected by symmetrical chloro bridges, in a C_{2h} symmetry (Figure 3.11). In this way the titanium atoms adopt octahedral surroundings where the axial positions are occupied by the imido group >NH and the terminal chlorine atom. The energy difference calculated between the dimeric and monomeric structures is 74 kJ·mol^{-1}.

Chapter 3

The calculated bond distances and angles are similar to those found in the literature for complexes containing the structural unit $ClTi(\textbf{\textit{m}}\text{-}Cl)_2TiCl$.[53]
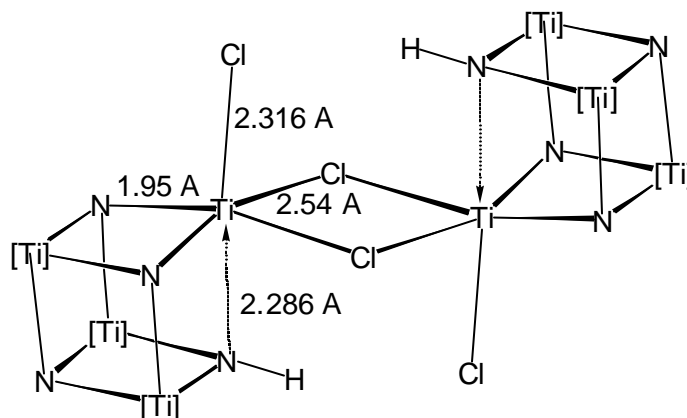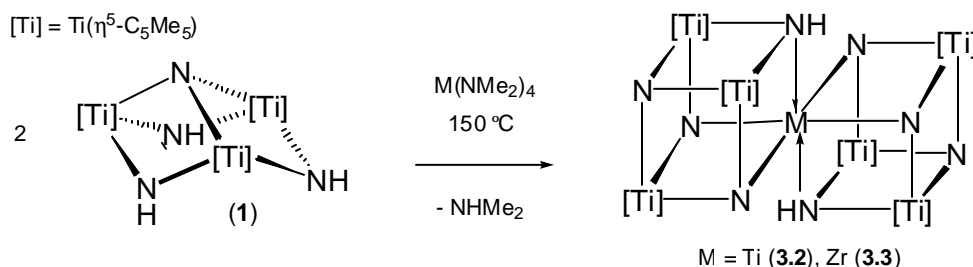

Figure 3.11. *Proposed structure for the complex* **3.1'**. *[* Ti *] = Ti(* $\textbf{\textit{h}}^5$ *-* C_5H_5 *)*

3.4.2   Dimers

Treatment of **1** with 0.5 equivalents of $\left[M(NMe_2)_4\right]$ (M = Ti[54], Zr[55]) in toluene at 150 °C afforded the corner-shared double cube complexes $\left[M\{(\textbf{\textit{m}}_3\text{-}N)_2(\textbf{\textit{m}}_3\text{-}NH)\}_2\{Ti_3(\textbf{\textit{h}}^5\text{-}C_5Me_5)_3(\textbf{\textit{m}}_3\text{-}N)\}_2\right]$ [M = Ti (**3.2**), Zr (**3.3**)] (Scheme 3.5).

Scheme 3.5.   *Reaction   of* $\left[\{Ti(\textbf{\textit{h}}^5\text{-}C_5Me_5)(\textbf{\textit{m}}\text{-}NH)\}_3(\textbf{\textit{m}}_3\text{-}N)\right]$ *(1)   with homoleptic early transition metal amido complexes*
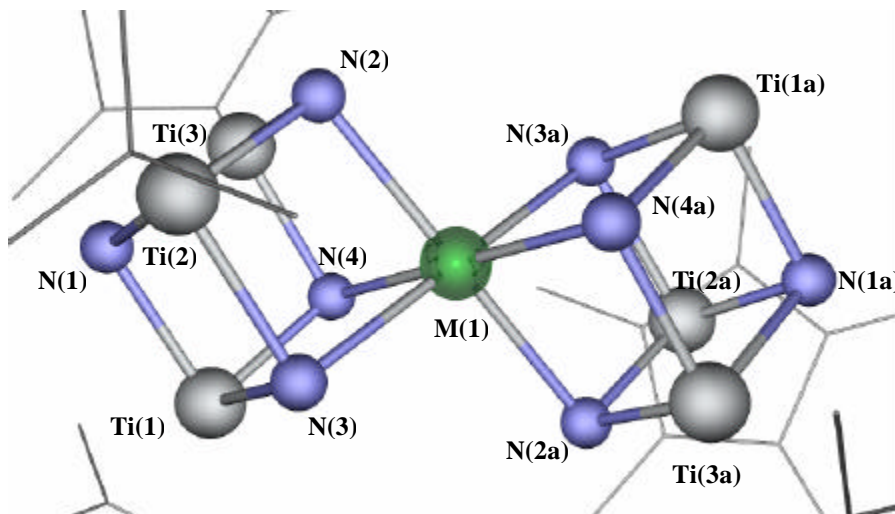
Figure 3.12. *Structure of complexes* **3.2-3.3**

Complexes **3.2**-**3.3** were characterized by infrared spectroscopy and C, H, N microanalysis, as well as by an X-ray crystal structure determination. None of the double cube complexes is soluble in common organic solvents; therefore, it was not possible to obtain their NMR spectra. The IR spectra showed one absorption in the range 3356-3345 cm^{-1} attributable to the ν_{NH} vibrations, and several very strong bands between 805-590 cm^{-1} for the ν_{MN} vibrations in the molecule.

3.2 and **3.3** structures show two cubes with a common titanium/zirconium vertex. The perspective view and most important structural data are in Table 3.16 and Figure 3.12. This metal center has a six-coordinate geometry, in which the nitrogen atoms lie at the vertices of a trigonal antiprism. The two $\left[Ti_3(\boldsymbol{h}^5\text{-}C_5Me_5)_3\,(\boldsymbol{m}\text{-}N)_2\,(\boldsymbol{m}NH)(\boldsymbol{m}_3\text{-}N)\right]^{2-}$ ligands adopt a mutually staggered conformation which may correspond to the minimization of the steric repulsion of the bulky pentamethylcyclopentadienyl ligands.[15] The relative location of the imido protons between both ligands is impossible to determine, so they are not mentioned in Figure 3.12.

151

Chapter 3

Table 3.16. Selected bonds (Å) and angles (°) for $\left[M\{(\boldsymbol{m}_3\text{-}N)_2(\boldsymbol{m}_3\text{-}NH)\}_2\{Ti_3(\boldsymbol{h}^5\text{-}C_5Me_5)_3(\boldsymbol{m}_3\text{-}N)\}_2 \right]$ [M = Ti (**3.2**), Zr (**3.3**)]

	3.2	**3.3**
$M(1) - N(2)$	2.125	2.233
$M(1) - N(3)$	2.122	2.234
$Ti(1) - N(1)$	1.931	1.940
$M(1) - Ti(1)$	2.948	3.072
$Ti(1) - Ti(2)$	2.800	2.802
$N(2) - M(1) - N(3a)$	99.0	102.2
$N(3) - M(1) - N(4)$	81.3	77.8

In order to determine the positions of the imido groups >NH in the $\left[MTi_6N_8 \right]$ (M = Ti, Zr) core of structures **3.2** and **3.3**, calculations were carried out on the model complexes $\left[Ti\{(\boldsymbol{m}_3\text{-}N)_2(\boldsymbol{m}_3\text{-}NH)\}_2\{Ti_3(\boldsymbol{h}^5\text{-}C_5H_5)_3(\boldsymbol{m}_3\text{-}N)\}_2 \right]$ (**3.2'**) and $\left[Zr\{(\boldsymbol{m}_3\text{-}N)_2(\boldsymbol{m}_3\text{-}NH)\}_2\{Ti_3(\boldsymbol{h}^5\text{-}C_5H_5)_3(\boldsymbol{m}_3\text{-}N)\}_2 \right]$ (**3.3'**). Accepting that each cube has one >NH group, two structures are possible: one of C_{2h} symmetry with the two >NH in a *trans* position and the other of C_2 symmetry, in which the two >NH are in a *cis* position (Figure 3.13).
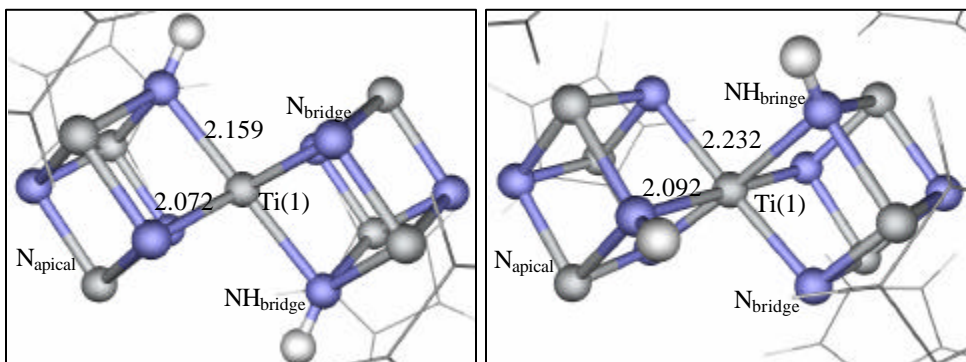
Figure 3.13. Cis and Trans conformers for complex **3.2'**

For species **3.2'**, both structures were optimized and the most important result is that their energies were similar. The computed difference is lower than 3 kJ·mol^{-1}. Another feature that should be pointed out is that in both cases the $Ti_{central}$-NH bond lengths are longer than the $Ti_{central}$-N (see Figure 3.13). A similar result is observed for model compound **3.3'**$_{C2h}$. However, this result seems to contradict the crystal determination for the complexes **3.2-3.3**, where all the metal$_{central}$-nitrogen distances are the same in each compound. This discrepancy might be attributed to the steric effects induced by the pentamethylcyclopentadienyl ligands in the real complexes, but the incorporation of the methyl groups in the calculations only generates a slight lengthening of all the bonds around the central metal (~0.02Å). Another option is to consider a dynamic process of interchange between both structures, which leads to an average M(1)-N distance. The computed average distances range between 2.126 Å for the protonated nitrogens and 2.152 Å for the single nitrogens, compared to the experimental distances of 2.125 Å and 2.122 Å for (3.2).

Because of the M(1)-N distances were found similar, a last option could be to replace the protons in the apical nitrogens of a D$_3$d structure (see Figure 3.14). Calculations on this more symmetric structure were performed for model compound **3.2'**, and this specie turned out to be slightly lower in energy than the C$_2$h structure by only 3.4 kJ mol^{-1}. Now the computed M(1)-N distances are all equal to 2.089 Å.
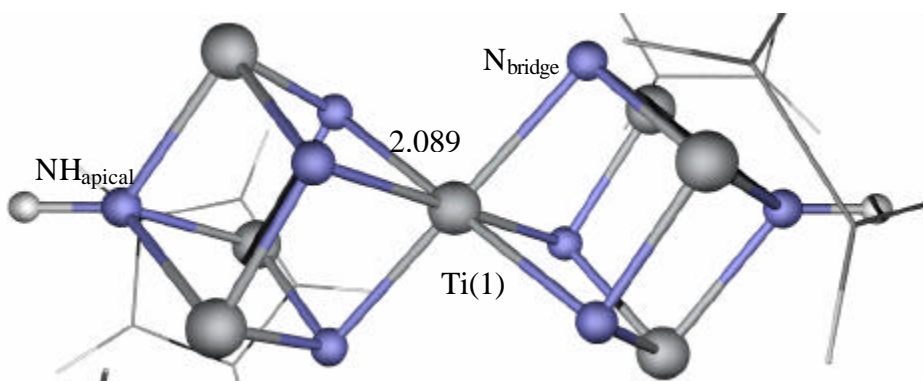

Figure 3.14. *Computed D$_3$D structure for compound* **3.2'**

Chapter 3

We were a little surprised that the lowest energy was that of the symmetric D_3d structure. This made us ask the following question: is the model anionic precubane ligand most stable when the proton is over the apical nitrogen $\left[Ti_3(\boldsymbol{h}^5\text{-}C_5H_5)_3(\boldsymbol{m_3}\text{-}N)_3(\boldsymbol{m_3}\text{-}NH)\right]^{2-}$ (C_3v structure) or over the bridge nitrogen $\left[Ti_3(\boldsymbol{h}^5\text{-}C_5H_5)_3(\boldsymbol{m_3}\text{-}N)_2(\boldsymbol{m}\text{-}NH)(\boldsymbol{m_3}\text{-}N)\right]^{2-}$ (C_s structure)? The model ligand with the C_s structure was 49.1 kJ mol^{-1} more stable than the C3v, which means that the D_3D dimer is more stable than the less symmetric ones by other reasons. This must be due to the presence of three pairs of unpaired electrons in the C_3v ligand, which are stabilized by the metal in the dimer formation. Instead, the C_s ligand has only two pairs of unpaired electrons, which means that the stabilization energy is lower.

Finally, ^{15}N nuclear magnetic resonance spectra could be useful for clarifying the proton situation. In the absence of experimental data, the computed absolute nitrogen NMR shieldings are shown in Table 3.17 for D_3d and C_2h **3.2'** model dimmers.

Table 3.17. *Nitrogen NMR shieldings (in ppm) for D_3d and C_2h 3.2' isomers*

	D$_3$d structure		C$_2$h structure		
	N$_{bridge}$	NH$_{apical}$	N$_{bridge}$	NH$_{bridge}$	N$_{apical}$
Paramagnetic	-920.8	-481.8	-931.2	-489.6	-958.3
Diamagnetic	342.1	320.5	340.2	325.2	341.8
Total	-578.7	-161.2	-591.0	-164.4	-616.5
Relative	**417.5**	**0.0**	**426.6**	**0.0**	**452.1**

3.5 Rh and Ir COD species

Transition metal-mediated oxidation of olefins by environmentally friendly oxidants H_2O_2 or O_2 (air) is of great industrial importance.[56] It has been shown that rhodium has homogeneous catalytic activity in the oxidation of olefins. The selective oxidation of linear olefins to ketones by O_2, H_2O_2 or

tBuOOH[57] and the oxidation of tetramethylethylene to the epoxide by tBuOOH have been reported.[58]

To understand the mechanistic features of the oxidation the reaction intermediates must be isolated. One of the latest developments in synthetic organometallic chemistry has been the preparation of a number of metallaoxetanes of transition metals.[59] The oxidation of olefins bonded to rhodium with fac-coordinating triaza ligands gave a rhodaoxetane, which can be isolated.[60] 1-oxa-2-metallacyclobutanes have been proposed as intermediates in such synthetic conversions as the Rh-catalysed catalytic rearrangement of epoxides to ketones,[61] and the Rh-catalysed asymmetric hydrogenolysis of epoxides.[62] For iridium metal, the oxidation of [(cyclic triamine) (1,5-cyclooctadiene)iridium]$^+$ cations by hydrogen peroxide forms metallaoxetanes, iridaoxetane intermediates stable enough to detect or isolate before rearrangement to some other species.

The comprehensive study of rhodium-iridium cyclooctadiene complexes with tridentate ligands $\left[\{Ti(h^5\text{-}C_5Me_5)(m\text{-}NH)\}_3(m_3\text{-}N)\right]$ is presented below. The electrochemical oxidation and oxygenation by H_2O_2 and O_2 have been investigated for five-coordinate cyclooctadiene (COD) complexes[63] ['N3'Rh(COD)]+ ('N3' = tridentate cyclic triamine or podal pyridine-amine-pyridine ligand). The σ-donor capacity of ligand 'N3' strongly influences the electrochemical oxidation potential and ^{13}C chemical shift of the COD double band. So the ligand coordinating capabilities expand the Rh and Ir chemistry and give new results. For purposes of comparison, we also add data about the complexation of metal cyclooctadiene fragments with well known neutral and anionic ligands.
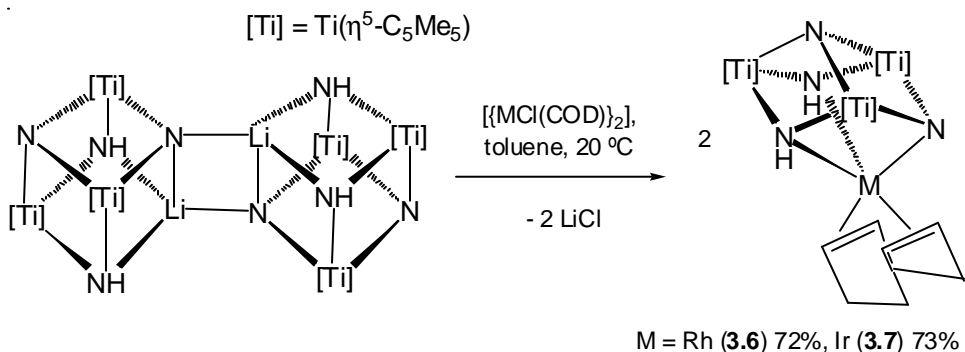
3.5.1 Experimental data

The ionic heterocubanes $\left[M(COD)(m_3\text{-}NH)_3Ti_3(h^5\text{-}C_5Me_5)(m_3\text{-}N)\right]Cl$ [M = Rh (**3.4**), Ir (**3.5**)] (Scheme 3.6) and neutral $\left[M(COD)(m_3\text{-}NH)_2(m_3\text{-}N)Ti_3(h^5\text{-}C_5Me_5)(m_3\text{-}N)\right]$ [M = Rh (**3.6**), Ir (**3.7**)][52] were synthesized (Scheme 3.7).

Chapter 3

M = Rh (**3.4**) 69%, Ir (**3.5**) 75%
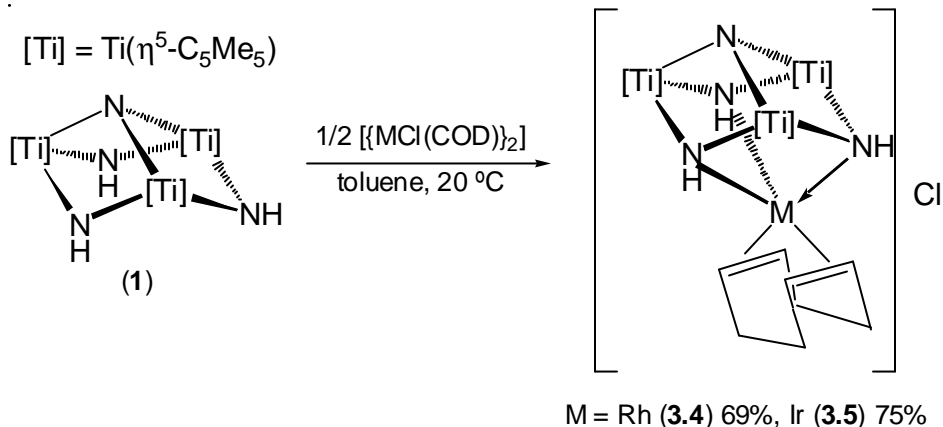
Scheme 3.6. *Formation of the ionic cubanes*
$\left[M(COD)(\mathbf{m}_3\text{-}NH)_3Ti_3(\mathbf{h}^5\text{-}C_5Me_5)(\mathbf{m}_3\text{-}N) \right]Cl$ *[M = Rh (3.4), Ir (3.5)]*

M = Rh (**3.6**) 72%, Ir (**3.7**) 73%

Scheme 3.7. *Formation of the neutral cubanes*
$\left[M(COD)(\mathbf{m}_3\text{-}NH)_2(\mathbf{m}_3\text{-}N)Ti_3(\mathbf{h}^5\text{-}C_5Me_5)(\mathbf{m}_3\text{-}N) \right]$ *[M = Rh (3.6), Ir (3.7)]*

In all cases, the spectroscopic data show tridentate ligands coordinated to the metal in a tripodal fashion, forming a trigonal bipyramidal environment that occupies ligand nitrogen atoms, two equatorials and one axial position (Figure 3.15).

156

For both the ionic and neutral compounds, the metal is in a state of oxidation (I), so the metallic fragment in all cases supports a formal charge (+1). For the neutral cubanes, it is shown that the precubane behaves like an anionic ligand (-1).
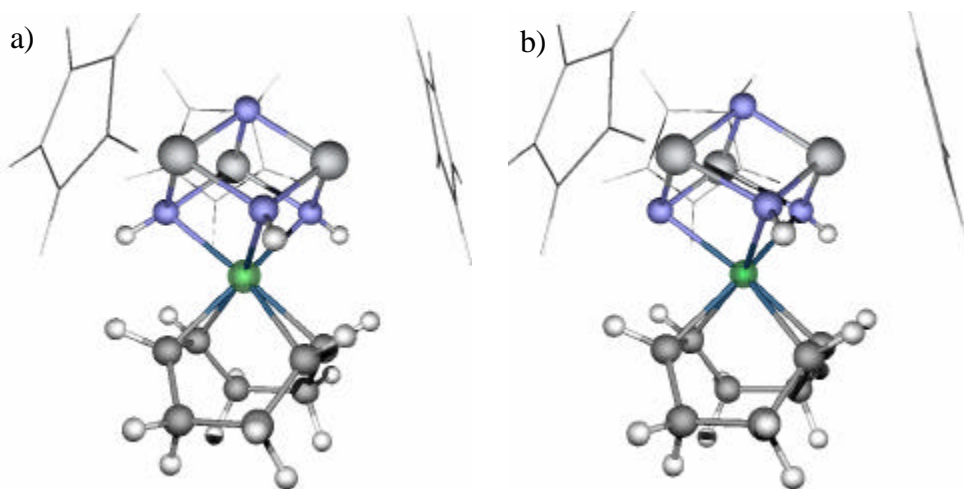

Figure 3.15. *3D view of the ionic structures* $\left[M(COD)(\boldsymbol{m}_3\text{-NH})_3Ti_3(\boldsymbol{h}^5\text{-}C_5Me_5)(\boldsymbol{m}_3\text{-N})\right]Cl$ *(a) [M = Rh (**3.4**), Ir (**3.5**)]* *and the neutral* $\left[M(COD)(\boldsymbol{m}_3\text{-NH})_2(\boldsymbol{m}_3\text{-N})Ti_3(\boldsymbol{h}^5\text{-}C_5Me_5)(\boldsymbol{m}_3\text{-N})\right]$ *(b)*

3.5.2 Theoretical study

When we studied these compounds, we modelled the ionic cubanes $\left[M(COD)(\boldsymbol{m}_3\text{-NH})_3Ti_3(\boldsymbol{h}^5\text{-}C_5H_5)(\boldsymbol{m}_3\text{-N})\right]Cl$ [M = Rh (**3.4'**), Ir (**3.5'**)] and the neutral cubanes $\left[M(COD)(\boldsymbol{m}_3\text{-NH})_2(\boldsymbol{m}_3\text{-N})Ti_3(\boldsymbol{h}^5\text{-}C_5H_5)(\boldsymbol{m}_3\text{-N})\right]$ [M = Rh (**3.6'**), Ir (**3.7'**)]. Rh and Ir adducts show that these metals can coordinate with donor tridentate ligands with six electrons, like the ligands $\left[\text{Hydrotris(pyrazolyl)borate}\right]^{64}$, $\{HB(pz)_3\}$ and $\left[\text{Tris(pyrazolyl)methane}\right]^{65}$, $\{HC(pz)_3\}$, or of cyclic triamine ligands, $\{Cn\}$.[63,66] These coordinating

Chapter 3

properties make Rh and Ir metallic fragments ideal systems for coordinating with our more complex, precubane ligand. For purposes of comparison, calculations were not only carried out for the cubane aggregates but also for such well-known ligands as $\{HC(pz)_3\}$ ($[M(COD)\{HC(pz)_3\}]^+$ [M = Rh, Ir]), $\{Cn\}$ ($[M(COD)\{Cn\}]^+$ [M = Rh, Ir]) and $\{HB(pz)_3\}^-$ ($[M(COD)\{HB(pz)_3\}]$ [M = Rh, Ir]) (Figure 3.16).
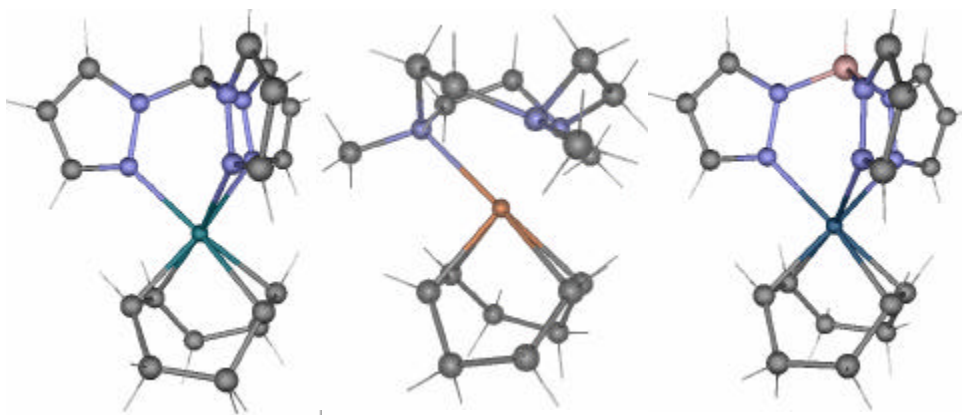

Figure 3.16. *From left to right compounds* $[M(COD)\{HC(pz)_3\}]^+$, $[M(COD)\{Cn\}]^+$, $[M(COD)\{HB(pz)_3\}]$; *M = Rh, Ir*

The calculated geometric parameters show good concordance with the experimental values for cubane and non cubane structures. Table 3.18 compares the most important values.

158

Table 3.18. *Comparison of distances for tridentate ligands and metallic (* MCOD *) type fragment aggregates*

Compound	M-N_{AX}	M-N_{EQ}	M-C_{AX}	M-C_{EQ}
3.4'	2.115	2.299	2.199	2.128
3.5[52]	(2.106)	(2.302)$_{av.}$	(2.180)$_{av.}$	(2.102)$_{av.}$
3.5'	2.092	2.211	2.156	2.073
3.6'	2.160	2.253	2.166	2.120
3.7'	2.110	2.175	2.139	2.067
$([Rh(COD)\{HC(pz)_3\}]^+)_{exp.}$[67]	(2.095)	(2.267)$_{av.}$	(2.136)$_{av.}$	(2.076)$_{av.}$
$[Rh(COD)\{HC(pz)_3\}]^+$	2.126	3.308	2.166	2.091
$[Ir(COD)\{HC(pz)_3\}]^+$	2.124	2.281	2.162	2.091
$([Ir(COD)\{Cn\}]^+)_{exp.}$[63]	(2.200)	(2.339)$_{av.}$	(2.162)$_{av.}$	(2.080)$_{av.}$
$[Rh(COD)\{Cn\}]^+$	2.160	2.357	2.178	2.097
$[Ir(COD)\{Cn\}]^+$	2.159	2.340	2.165	2.095
$[Rh(COD)\{HB(pz)_3\}]$	2.122	2.284	2.157	2.087
$([Ir(COD)\{HB(pz)_3\}])_{exp.}$[68]	(2.087)	(2.230)$_{av.}$	(2.126)$_{av.}$	(2.047)$_{av.}$
$[Ir(COD)\{HB(pz)_3\}]$	2.124	2.245	2.156	2.091

Both the Rh and Ir neutral compounds show shorter distances than the ionic compounds because of major electrostatic compacting effects. To get an idea of the type of interactions between the fragments, it is very useful to decompose the interaction energies between the precubane and the metallic fragment (Table 3.19).

Table 3.19. *Decomposition of the interaction energies for complexes* **3.4'-3.7'**, $[M(COD)\{HC(pz)_3\}]^+$ *and* $[M(COD)\{HB(pz)_3\}]$ *(in kJ mol^{-1})*

	3.4'	3.5'	3.6'	3.7'	$[M(COD)\{HC(pz)_3\}]^+$		$[M(COD)\{HB(pz)_3\}]$	
					Rh	*Ir*	*Rh*	*Ir*
PR[a)]	942.4	1267.8	1000.2	1341.9	676.9	929.7	754.4	1036.7
EI[b)]	-767.4	-999.4	-1101	-1341	-643.6	-769.5	-986.9	-1125.5
SR[c)]	175.0	286.4	-100.5	0.9	58.4	131.9	-233.2	-159.4
OI[d)]	-586.2	-756.1	-656.5	-835.3	-417.4	-551.8	-508.7	-658.8
FIE[e)]	**-411.2**	**-487.7**	**-757.0**	**-834.4**	**-359.1**	**-420.0**	**-741.9**	**-818.2**

a) *PR = Pauli Repulsion*
b) *EI = Electrostatic Interaction*
c) *SR = Steric Repulsion (PR+EI)*
d) *OI = Orbital Interaction*
e) *FIE = Fragment Interaction Energy*

The interaction energy of the neutral cubanes is about 350 kJ mol^{-1} greater than that of the ionics, ranging from -411.2 kJ mol^{-1} and -487.7 kJ mol^{-1} for the ionic clusters of Rh and Ir, respectively, to -757 kJ mol^{-1} and -834.4 kJ mol^{-1} for the neutrals. The total Mulliken charge for the metallic fragment in the Rh^{+1} cubane is +0.90 e-, and for the precubane it is +0.10 e-. The neutral cubane, on the other hand, has charges of +0.66 e- for the metallic fragment and -0.66 e- for the precubane. The neutral compounds do not have to support a +1 charge, which creates a greater charge separation, and this in turn creates greater electrostatic interaction.

Table 3.20. *Description of HOMO, LUMO and some occupied molecular orbitals with important mixings between d^8 metal and Ti_3 d-orbitals in clusters* **3.4'** *and* **3.5'***. The highest MO with an important participation of $d_{x^2-y^2}$ rhodium (or iridium) orbital is also included* [a]

Orbital	E.(eV)	$[(\mu_3\text{-NH})_3\text{Ti}_3(\eta^5\text{-}C_5H_5)_3(\mu_3\text{-N})]$			MCOD				
3.4'		**Ti**(d)	**N**(p)	**C**(p)	**M** (d_z^2	d_{xz}	d_{yz}	$d_{x^2-y^2}$)	**C**(p)
57 a' LUMO	-6.12	82.0							
56 a' HOMO	-8.04	12.2			62.7				
41 a''	-8.16	7.5	19.6			11.6	18.7		18.1
55 a'	-8.65		9.7	27.9				36.4	
40 a''	-8.80	7.8	14.4		39.4	16.4			8.4
3.5'									
61 a' LUMO	-6.08	81.9							
60 a' HOMO	-8.04	16.1			57.7				
44 a''	-8.22	10.6	17.9			11.5	15.4		21.0
59 a'	-8.64		10.0	20.7				49.6	
43 a''	-8.85	8.8	15.4		33.3	13.2			10.6

[a] The atomic d_{xy} orbitals for Rh and Ir do not appear in the occupied molecular orbitals, which highlights the d^8 nature of the complexes. Non negligible percentages of d_{xz}, d_{yz} and d_{x2-y2} Rh and Ir orbitals appear in lower molecular occupied orbitals, which are not included in this Table. Only contributions > 7% are reported.

It is observed that the interactions for the Rh compounds is about 75 kJ·mol^{-1} lower than those for Ir. As far as the description of the molecular orbitals is concerned (Table 3.20), it can be seen that the relatively bigger d orbital of the Ir participates more in the molecular orbitals, which in turn generates a greater charge transfer between fragments and a greater delocalization that causes a greater interaction energy. At the same time, we can observe that

Chapter 3

the $\left[M(COD)\{HC(pz)_3\}\right]^+$ and $\left[M(COD)\{HB(pz)_3\}\right]$ adducts follow the same rules as for the ionic and neutral structures, and Rh, Ir metals. Comparing the cubane structures with the non-cubane ones, we observed that the lack of empty d-metallic orbitals in the non organometallic ligands decreases the FIE. This difference was about 50 kJ mol^{-1} in the ionic compounds and about 15 kJ mol^{-1} in the neutral ones. This decrease was attributed to the increase in the height of the common electrostatic effects. These FIE differences clearly show that the ligand's d-orbitals participate more in the cubane formation than the non-organometallic ligands and supplementary chelating strengths.

3.6   In and Tl monohalides

Coordination compounds derived from the elements of group 13 are an important feature of main group chemistry. In the present case, the indium (III) halides and pseudo halides give rise to large numbers of neutral compounds and anionic species.[69]

Indium (III) halide complexes of the type InX_3L_n where L = monodentate ligand [N, O, P-donor] have attracted considerable interest recently. Certain bonding characteristics, in particular relative binding energies, and variations in coordination numbers and geometries have increasingly been linked with their possible commercial exploitation as precursors for Metallo - Organic Chemical Vapor Deposition (MOCVD) processes, e. g. indium nitride films.[70,71]

Indium and thallium both have the ns^2np^1 configuration and ^2P ground state found in boron, aluminium and gallium. Mono- or three-substituted halides can be found for indium and thallium, as well as for other ligands. Indium tends to retain the $5s^2$ shell. With thallium the $6s^2$ shell is very stable and the Tl^+ ion appears in many well-characterised salts. The stability of the M^I state increases further down the subgroup, but the stability of the M^{III} state decreases.

In oxidation states (I) and (III), tetrahedral coordination dominates the organometallic chemistry of group 13 metals,[72] but in recent years it has been seen that there is an increase in the number of five- and six-coordinate

compounds.[73] If we compare the relative stability of the group III elements in similar compounds, thallium is an even weaker acceptor than indium.[74] The In and Tl atomic and ionic radii are close and increase little as the atomic number increases (Table 3.21). Despite the slight differences between In and Tl already mentioned, their complexes do not behave in the same way; although complexes of indium (III) halides have been characterised as six coordinated, $InX_3 \cdot 3L$,[75] the corresponding thallium halides[76] are five coordinated, $TlX_3 \cdot 2L$.

Table 3.21. *Atomic radii of the group 13 elements in pm and absolute electronegativities in eV[21]*

	B	**Al**	**Ga**	**In**	**Tl**
Ionic M^{1+} radius			113	132	149
Ionic M^{3+} radius	23	57	62	92	105
Electronegativity	4.29	3.23	3.2	3.1	3.2

In this section we study ligand **1** complexation with $In^{(I)}$ and $Tl^{(I)}$ halides and cyclopentadienide adducts. The theoretical aspects of their complexation will be compared in both the gas and solvent phase, and particular attention will be paid to the complexation energy, the coordination sphere of the metal and the ligand performance in the different adducts.

3.6.1   Experimental frame

Reaction of **1** with indium and thallium iodides in dichloromethane affords $\left[IM \left\{ Ti \left(\mathbf{h}^5 - C_5 Me_5 \right) \left(\mathbf{m}_3 - NH \right) \right\}_3 \left(\mathbf{m}_3 - N \right) \right]$ [M = In, Tl] as brown and yellow solids, respectively (Scheme 3.8).

Chapter 3
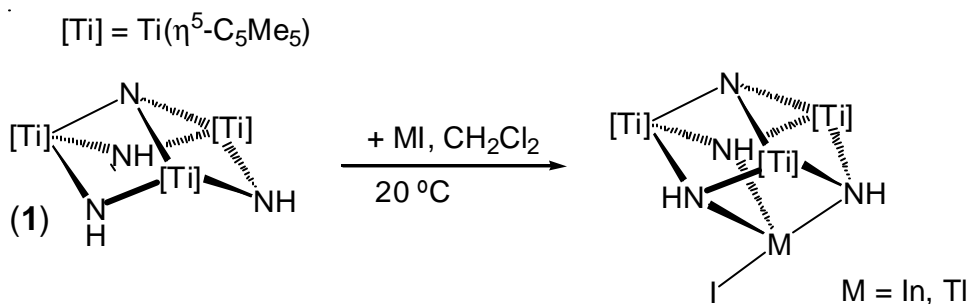
Scheme 3.8. $\left[IM\left\{ Ti\left(\boldsymbol{h}^5 - C_5Me_5 \right)\left(\boldsymbol{m}_3 - NH \right)\right\}_3 \left(\boldsymbol{m}_3 - N \right)\right]$ $[M = In, Tl]$ *formation*

The corresponding InCl adduct $\left[ClIn(\boldsymbol{m}_3\text{-}NH)_3Ti_3(\boldsymbol{h}^5\text{-}C_5Me_5)_3(\boldsymbol{m}_3\text{-}N)\right]$ was characterized by NMR spectroscopy in $[D_6]$benzene solutions.[77] However, ^{1}H NMR spectroscopy monitoring of a $[D_6]$benzene solution of 1-InCl in a flame-sealed tube for several days showed that the initial NH and C_5Me_5 resonances were moving towards those of **1**, and a gray solid was deposited in the tube. TlCl did not react in the same conditions.

Complexes 1-MI were characterized by spectral and analytical techniques. The IR spectra of 1-InI and 1-TlI reveal two absorptions in the range 3352-3246 cm^{-1} for the NH groups of the molecules. ^{1}H and ^{13}C NMR spectra in $[D_6]$benzene at room temperature of 1-MI show resonances for equivalent NH and C_5Me_5 groups, suggesting a highly symmetrical structure or the existence of low energy exchange processes in solution. The data led us to propose cube-type structures for the 1-MI complexes, whereas indium 1-InI and thallium 1-TlI centres may show trigonal bipyramidal geometries with a missing vertex where the metal lone pair resides.

The analogous reaction of **1** with thallium cyclopentadiene in toluene affords $\left[\left(\boldsymbol{h}^5 - C_5Me_5 \right) Tl\left\{ Ti\left(\boldsymbol{h}^5 - C_5Me_5 \right)\left(\boldsymbol{m}_3 - NH \right)\right\}_3 \left(\boldsymbol{m}_3 - N \right)\right]$ as a red solid (Scheme 3.9). Complex 1-TlCp is soluble in toluene and from these solutions single-crystals suitable for X-ray diffraction studies of 1-TlCp can be grown.

$[Ti] = Ti(\eta^5\text{-}C_5Me_5)$

Scheme 3.9. $\left[\left(h^5 - C_5Me_5\right)Tl\left\{Ti\left(h^5 - C_5Me_5\right)\left(m_3 - NH\right)\right\}_3\left(m_3 - N\right)\right]$

formation
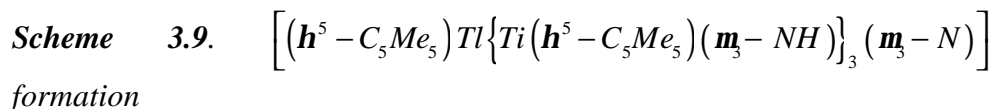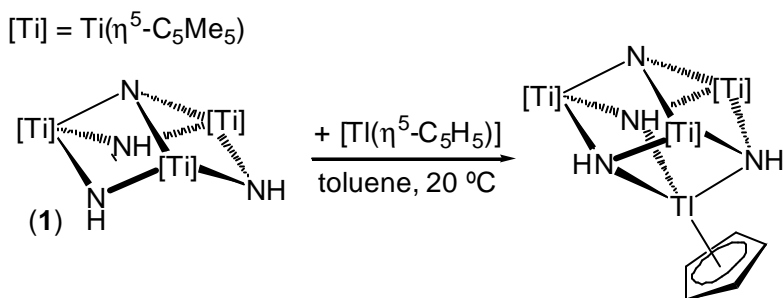
Complex 1-TlCp was characterized by analytical and spectroscopic methods, as well as by X-ray crystal structure determinations. IR spectra only showed one n_{NH} absorption at 3345 cm^{-1}. The ^{1}H and ^{13}C NMR spectra in [D$_6$]benzene at room temperature reveal resonances due to equivalents NH, h^5-C$_5$Me$_5$ and h^5-C$_5$H$_5$ groups at chemical shifts.
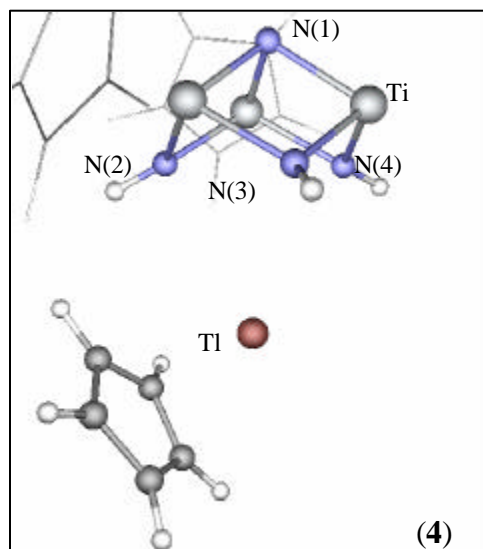
Figure 3.17. *Perspective view of the 1-TlCp compound*

Chapter 3

The solid-state structure reveals tridentate coordination of the neutral ligand **1** to the metal cyclopentadienyl fragments. Selected bond lengths and angles are given in Table 3.22, and the perspective view is presented in Figure 3.17. The molecular structure of 1-TlCp consists of a distorted $[\text{TlTi}_3\text{N}_4]$ cube-type core. Thallium is bound to one $\boldsymbol{h}^5$-cyclopentadienyl ligand and three imido groups of the incomplete cube core $[\text{Ti}_3(\boldsymbol{m}\text{-NH})_3(\boldsymbol{m}_3\text{-N})]$. If the centroid of the cyclopentadienyl ligand is considered, the coordination sphere about the thallium atom may be described as distorted trigonal bipyramid with a "missing vertex" which corresponds to the lone pair on the thallium (I) center.

In this geometry, the neutral ligand $[(\boldsymbol{m}\text{-NH})_3\text{Ti}_3(\boldsymbol{h}^5\text{-C}_5\text{Me}_5)_3(\boldsymbol{m}_3\text{-N})]$ coordinates in a tripodal fashion, occupying one axial and two equatorial coordination sites, whereas the $\boldsymbol{h}^5$-C$_5$H$_5$ ligand and the lone pair are in the remaining equatorial and axial positions, respectively. The resulting structural disposition may explain why the thallium-axial nitrogen (2) (2.868 Å) is shorter than the ones found for Tl-N(3) equatioral, 3.190(1) Å, and Tl-N (4) equatorial, 3.152(1) Å, which are in front of the cyclopentadienyl ligand. The thallium-nitrogen bond lengths compare well with those found in the literature for other structures bearing weak Tl-N interactions and are within the sum (3.47 Å) of the Van der Waals radii of thallium and nitrogen.[78] The cyclopentadienyl ligand is bound in a $\boldsymbol{h}^5$ fashion to thallium with a Tl(1)-Cp (centroid) distance of 2.687 Å, well within the range observed for other crystalline cyclopentadienyl-containing Tl complexes.[79] Within the neutral ligand moiety $[(\boldsymbol{m}\text{-NH})_3\text{Ti}_3(\boldsymbol{h}^5\text{-C}_5\text{Me}_5)_3(\boldsymbol{m}_3\text{-N})]$ there is no important distortion in bond lengths and angles when compared with **1**.

3.6.2 Theoretical study

Two optimal C$_s$ geometries were modelled in response to the expected structure, in which alternatively an axial (a) or equatorial (b) position of the pseudo trigonal bipyramidal centre is "missing" (see Scheme 3.10). In both cases, $[\text{IIn}\{\text{Ti}(\boldsymbol{h}^5\text{-C}_5H_5)(\boldsymbol{m}\text{-NH})\}_3(\boldsymbol{m}_3\text{-N})]$, 1'-InI and 1'-TlI model

compounds, the C_s structure with the lone pair occupying the axial position is the most stable by 3.1 and 20.6 kJ mol^{-1}, respectively. The relatively small energy differences between these isomers also suggest fluxional behaviour, the origin of only one resonance signal for NH and C_5Me_5 groups in the NMR spectra.

Scheme 3.10. *Optimal C_s geometries for the In, Tl compounds* $\left[IM(\boldsymbol{m}_3\text{-}NH)_3Ti_3(\boldsymbol{h}^5\text{-}C_5H_5)_3(\boldsymbol{m}_3\text{-}N) \right]$, *in which alternatively an axial, (a), or equatorial position, (b), of the pseudo trigonal bipyramid is missing*

For the established geometry, In(I) and Tl(I) model complexes $\left[XM(\boldsymbol{m}_3\text{-}NH)_3Ti_3(\boldsymbol{h}^5\text{-}C_5H_5)_3(\boldsymbol{m}_3\text{-}N) \right]$ [M = In, Tl; X = F, Cl, Br, I, Cp] were calculated. Results prove that both metals have similar coordination structures. The computed data agree with the experimental values, when they are available; metal-ligand nitrogen lengths are slightly higher than experimental ones and they present normal distance adaptation with the change in metal. At the same time, no clear tendency is observed with the change in halogen.

Table 3.22. *Calculated and experimental bond lengths (Å) and angles (º) for selected N-donor ligand 1 In and Tl complexes*

Compound	N_2-M	N_3-M	N_2-Ti	H-X_1	M-X_1
1			1.944		
(1)^{exp}			(1.930) av.		
1-InF	2.986	3.094	1.923	2.022	2.134
1-InCl	2.602	3.252	1.953	2.417	2.636
1-InBr	2.595	3.218	1.953	2.541	2.804
1-InI	2.584	3.094	1.953	2.724	3.074
1-InCp	2.991	3.446	1.945		2.490
1-TlF	2.817	3.098	1.923	1.672	2.322
1-TlCl	2.926	3.032	1.929	2.372	2.759
1-TlBr	2.906	3.035	1.931	2.518	2.900
1-TlI	2.931	3.002	1.932	2.745	3.161
1-TlCp	3.138	3.324	1.936		2.610
(1-TlCp)^{exp}	(2.868)	(3.171)av.	(1.936)av.		(2.687)

	N_2-M-N_3	N_3-M-N_4	N_2-Ti-N_3	N_1-N_2-H	N_2-M-X_1
1			106.6	151.0	
(1)^{exp}			(107.5)av.		
1-InF	60.3	58.8	103.9	179.5	64.4
1-InCl	61.6	56.1	103.2	157.7	75.0
1-InBr	62.0	56.8	102.9	157.0	75.8
1-InI	63.7	59.3	102.1	156.5	76.1
1-InCp	56.3	53.1	104.3	154.8	105.4
1-TlF	62.0	59.6	103.7	179.4	59.9
1-TlCl	61.6	61.0	103.3	170.1	68.0
1-TlBr	61.8	60.9	103.3	167.9	69.9
1-TlI	61.9	61.7	103.2	165.8	71.1
1-TlCp	56.5	55.1	104.3	159.0	97.7
(1-TlCp)^{exp}	(60.7)av.	(57.8)	(96.4)av.	(93.6)	(107.1)

[a] *Parameter obtained from the centroid of the cyclopentadienide ligand*

Table 3.23. *Reaction energies for In(I) and Tl(I) model complexes* $\left[XM(\mu_3\text{-}NH)_3Ti_3(\eta^5\text{-}C_5H_5)_3(\mu_3\text{-}N) \right]$ *[M= In, Tl; X= F, Cl, Br, I, Cp]*

	Cp	F	Cl	Br	I
In	-17.9	-53.1	-62.9	-64.9	-71.0
Tl	-23.4	-63.4	-61.1	-62.2	-65.1

The complexation processes were favourable in all cases. In principle, Cp ligands have the smallest reaction energies, and the interaction increases from F to I. It is noteworthy that indium metal has the strongest interactions for the least nucleophilic I, Br and Cl species, in this order. Tl adducts, however, undergo a sudden jump in their stability, going from I to F. As we mention in the Introduction, the Lewis acidity of indium is slightly higher than that of thallium, but as we observed in previous sections this is not the only feature to take into account for the stability of compounds; ligand conduct and steric repulsions are also important. A compromise among opposite tendencies determines the overall stability of the compounds. Although all indium compounds are more stable than the respective Tl compounds, fluorine adducts are an exception.

Indium and thallium monohalides make it possible to observe alternative ligand **1** behaviours. The reaction energies for the indium monohalides also tend to become more stable as the nucleophilicity of their substituents decreases, behaving as a simple ligand. But for the thallium compounds this trend is interrupted in favour of fluorine halides. If we compare the structural parameters of the various metal halides, there is a considerable reduction of the distance from the halogen atom to the nearest imido proton, H-X_1, from F to I (see Table 3.22).

If the nucleophilicity of the halogen is increased, there is a corresponding increase in the interaction with the imido-proton. This was most noticeable in the case of the most polarizable Tl metal and the most nucleophilic fluorine, where the proton-fluorine distance was short, only 1.672 Å. To illustrate this fact, Figure 3.18 shows the density Laplacian maps for Tl halides. It is clearly observed that in the case of fluorine the halogen atom is directly bonded to the imido proton, and that this interaction decreases as we

move towards the iodine atom. In summary, the triaza ligand is acting as a double-action ligand; the cation and anion of the salt are stabilized simultaneously, specially for the polar TlF halogen.
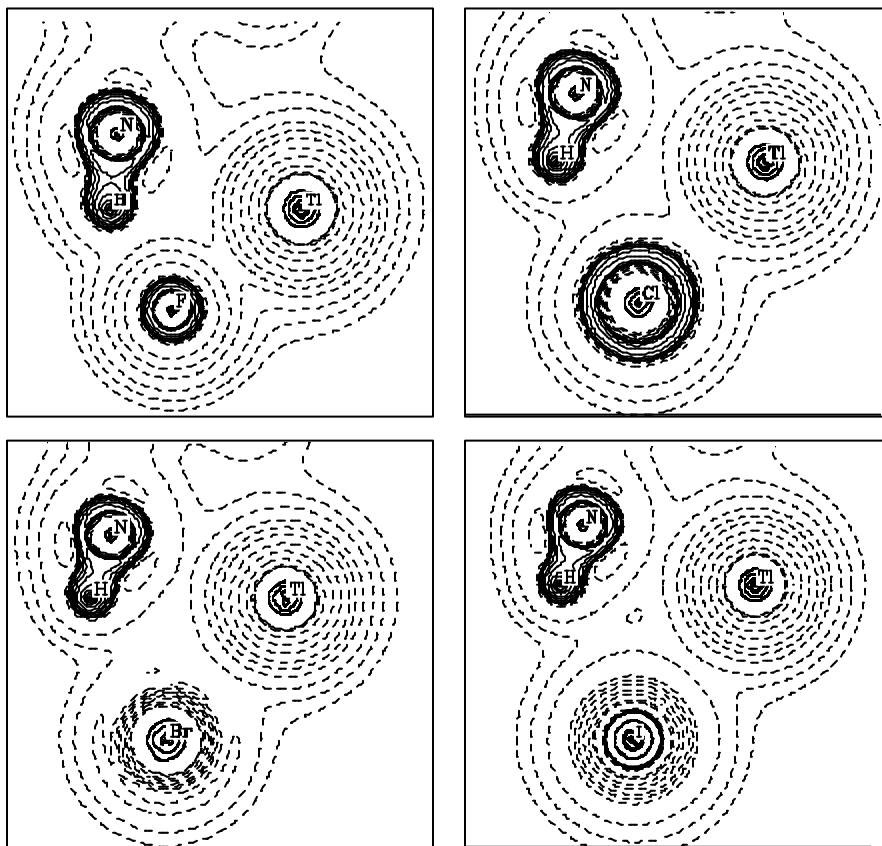

Figure 3.18. *Density Laplacian maps for thallium halide heterocubanes*

Also interesting is how the solvent affects complexation. As in group 1 and group 2 halogens, the reaction is only produced for some metal counteranions and in a particular solvent. Simple considerations of energy reactions in the gas phase clearly fail to explain the formation of the energetically disfavoured TlCp adduct.

170

Table 3.24. *Reaction and solvation energies in kJ mol^{-1} for the In, Tl* $\left[IM(\textbf{\textit{m}}_3\text{-}NH)_3 Ti_3(\textbf{\textit{h}}^5\text{-}C_5H_5)_3(\textbf{\textit{m}}_3\text{-}N) \right]$ *compounds*

	Toluene		Dichloromethane	
	In	*Tl*	*In*	*Tl*
Solvation Energy	-36.7	-42.4	-97.0	-118.3
Reaction Energy	54.2	54.7	-19.9	-17.2

Lattice energy is the principal factor that affects the reaction. Complexation is only produced for the salts with low lattice energy and, even then, only under certain conditions. The solvent is also important. It plays an important role in the overall process and has two contrasting effects: it reduces the solvation energy required to remove the salt molecules from the crystal; but at the same time, the solvent reduces the interaction energy. The reaction energy for the experimentally observed Tl-I and In-I derivatives is about 65-70 kJ mol^{-1} in the gas phase; in CH_2Cl_2 (dipolar moment 8.93) solvent, the reaction energy is reduced to 17-20 kJ mol^{-1}. The least polar toluene solvent (dipolar moment 2.38) is particularly unfavourable because of the change in the reaction energy from exothermic to endothermic, 54-55 kJ mol^{-1} (see Table 3.24).

Although the solvation energy is a considerable reduction in the energy necessary for complexation, the lattice energy of the most ionic halogen salts is still too high for the complexes to be seen. So although iodine and cyclopentadienide salts have smaller interaction energies, the small lattice energy allows complexation to occur in the most polar solvent.

3.7   Tin and lead halides

Tin and lead resemble carbon and silicon because they have the ns^2np^2 electron configuration, and they form the tetrahedral bonds associated with sp^3 hybridisation. But going down group 14 there is an increasing tendency to form an inert pair ion instead. So in its most stable salts, lead preserves an ns^2 core.

The presence of both a lone pair and an empty orbital in the valence shell of dihalides suggests that such species have the potential to function both as electron acceptors and donors.[80] However, the inductive effect of the halogens enhances the acceptor capability of the metal and restrict its donor capacity. One example of a tin (II) compound that acts as an electron donor is $Sn(C_5H_5)_2$, which lacks the aforementioned inductive effect.[81] On the other hand, when they coordinate to a Lewis base the lone pairs put electron density back on the metal and improve its donating ability.

Tin (II) halides form both 1:1 and 1:2 adducts with a small Lewis base such us trimethylamine.[82] The 1:2 adducts were found to be less stable than the 1:1 adducts and the order of stability for both the 1:1 and 1:2 species was $SnF_2 > SnCl_2 > SnBr_2 > SnI_2$. Here we describe the incorporation of tin (II) and lead (II) dihalides into the $[(\eta_3\text{-}NH)_3Ti_3(\eta^5\text{-}C_5Me_5)_3(\eta_3\text{-}N)]$ nitrogen donor ligand. The structural and electronic description of the compounds, as well as stability of the compounds, will be analysed.

3.7.1   Experimental data

The reaction of **1** with tin (II) and lead (II) chlorides in toluene or dichloromethane affords $[Cl_2M(\eta_3\text{-}NH)_3Ti_3(\eta^5\text{-}C_5Me_5)_3(\eta_3\text{-}N)]$ [M = Sn; M = Pb] as orange or yellow solids (Scheme 3.11). Complexes 1-MCl_2 were characterized by spectral and analytical techniques. IR spectra reveal two absorptions in the range 3343-3236 cm^{-1} for the NH groups of the molecules for complex 1-$SnCl_2$, whereas a broad band was observed for the lead 1-$PbCl_2$ derivative approximately in the middle of that range, at 3301 cm^{-1}.

^1H and ^{13}C NMR spectra in chloroform at room temperature show equivalent NH and η^5-C_5Me_5 groups on the NMR time scale. The NMR data are consistent with the complexes being fluxional in solution in a similar fashion to the previously presented rhodium and iridium derivatives.[52] The X-ray structure over the 1-$SnCl_2$ complex reveals that these compounds do not contain five-coordinated tin and lead centres, but three-coordinated metal centres with the metal lone pair occupying the four position (for selected structural data, see Table 3.25).
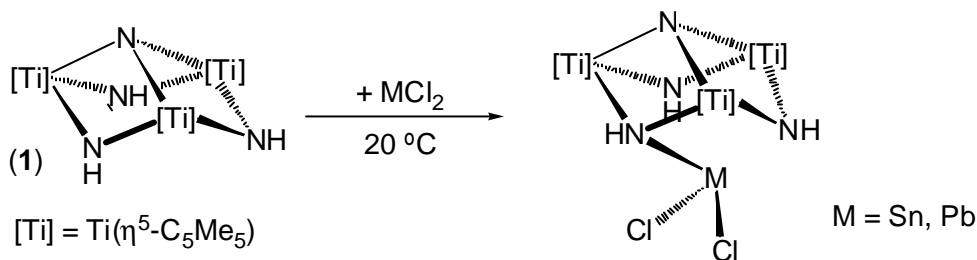
Scheme 3.11. $\left[Cl_2M(\mathbf{m}_3\text{-}NH)_3Ti_3(\mathbf{h}^5\text{-}C_5Me_5)_3(\mathbf{m}_3\text{-}N) \right]$ *[M = Sn; M = Pb]*
formation

3.7.2   Theoretical study

Like the experimental three coordinated metal centres and their fluxional behavior, two Cs symmetry model structures were computed for tin metal halides (Figure 3.19). The most stable conformation was for a pseudo tetrahedral coordination of the metal with one of the positions occupied by the metal lone pair (Figure 3.19a). A pseudo trigonal prismatic structure was observed between 2.5-10 kJ mol^{-1} (depending on the metal halide) above the most stable geometry (Figure 3.19b). Formally this can be represented as the eclipsed structure of the most stable alternate tetrahedral species. A big energetic barrier is not expected for the interchange between both isomers, so fluxional behaviour appears to be energetically accessible.

F to I tin and lead dihalide cubanes were computed for the pseudo tetrahedral structure. Table 3.25 shows some selected parameters. We can observe that the theoretical data for the 1'-SnCl$_2$ pseudo tetrahedral structure reproduce the experimental data. However, the distances computed for M(1)-N(3-4) are still too long. The structural differences found are probably due to low costing solid packing effects or to the steric effects of the *Cp** ligands and the metal fragment. There are no significant changes in the structures when the halogen atoms are changed, apart from the logical variation in the distance when the metal changes.

Chapter 3
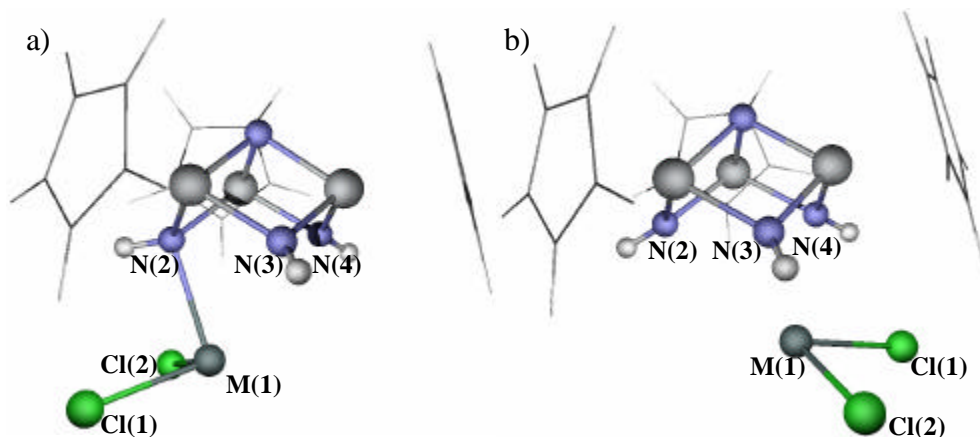
Figure 3.19. Two main conformation structures found for the $\left[Cl_2M(\mathbf{m}_3\text{-}NH)_3Ti_3(\mathbf{h}^5\text{-}C_5Me_5)_3(\mathbf{m}_3\text{-}N)\right]$ *1'-MCl$_2$ species. a) Pseudo octahedral coordination of the metal with one of the positions occupied by the lone pair, b) trigonal bipyramidal structure*

In order to show the compound's tetrahedral coordination, Figure 3.20 presents density Laplacian maps for the model compound of 1'-SnCl$_2$, in two molecular planes. The first plane contains Sn(1)-N(1)-N(2) atoms, and the Sn-N(2) bond can be seen clearly (Figure 3.20a). The second plane contains Sn(1)-N(3)-N(4) atoms, and confirms the non-bonding interaction between metal and N(3-4) ligand donors (Figure 3.20b).

It was a little surprising that the metal lone pair cannot be observed in the density laplacian map of the Sn(1)-N(1)-N(2) plane. Instead there appears what seems to be a very diffuse density zone. In an attempt to localize the lone pair, we made a small FORTRAN program to compute not the electronic density Laplacian maps but the electrostatic potential Laplacians from DFT calculations. In principle, electrostatic potential Laplacian maps and molecular charge distribution have a structural homeomorphism,[83] but the topography of the MESP does, in general, show enhanced features as compared to that of electronic density, particularly, the minima due to lone-pair electrons and π electrons, which are conspicuously absent in the topography of the charge distribution.[84] Figure 3.21 shows the electrostatic

potential Laplacian map for the Sn(1)-N(1)-N(2) plane in the model compound 1'-SnCl$_2$. Initially, no special improvement respect to electronic density maps is observed. In both cases, we conclude that a detail analysis of the topography of the charge density and the molecular electrostatic potential is necessary. The different kinds of critical points must be identified and their occurrences discussed.

Table 3.25. *Structural parameters for tin and lead model compounds, and experimental 1-SnCl$_2$ cubane. Distances in Å and angles in º*

	M-N$_2$	M-N$_3$	M-Cl	N$_2$-M-Cl	N$_2$-M-N$_3$	Cl-M-Cl
1'-SnF$_2$	2.371	3.723	2.034	85.8	55.8	94.2
1'-SnCl$_2$	2.395	3.338	2.524	90.1	61.5	96.9
(1-SnCl$_2$)*	(2.300)*	(3.000)*	(2.544)*	(96.0)*	(65.0)*	(90.0)*
1'-SnBr$_2$	2.388	3.354	2.690	92.0	61.4	97.1
1'-SnI$_2$	2.398	3.145	2.942	94.4	64.3	98.5
1'-PbF$_2$	2.558	2.981	2.144	79.3	65.4	93.2
1'-PbCl$_2$	2.595	3.013	2.619	86.1	62.1	99.6
1'-PbBr$_2$	2.573	3.047	2.774	88.3	64.4	98.7
1'-PbI$_2$	2.619	2.992	3.017	91.3	64.8	99.9

* Average distances from the crystallographic structure

Sn and Pb dihalide addition reactions are exothermic in all cases (see Table 3.26). In this case tin and lead clearly have opposite trends: while tin interaction energy increases as you go down the halogen group, lead does exactly the opposite. The nature of the bond and energy interaction is regarded as being the same as in previous cases: a compromise between metal acidity and steric repulsions. This shows that, for the smallest Sn atom, the steric repulsions caused by the nucleophilicity of the halogen dominate the interaction but that, for the larger lead atom, the acidity of the metal is still the main factor.

Chapter 3
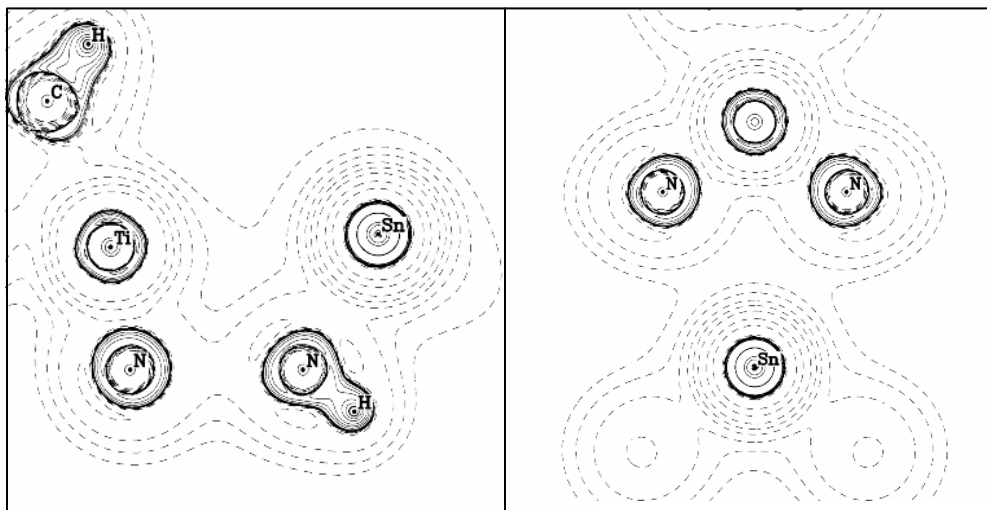
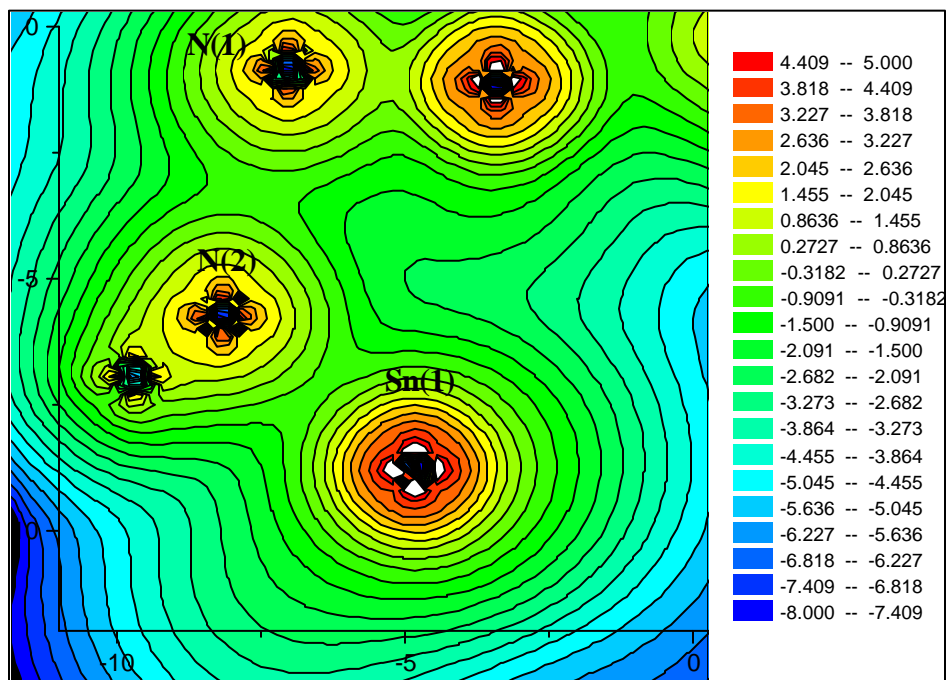**Figure 3.20**. *Electronic density Laplacian maps for 1'-SnCl$_2$; plane N(1)-N(2)-Sn(1) Figure a), plane N(3)-Sn(1)-N(4) Figure b)*

Figure 3.21. *Electrostatic potential Laplacian maps for 1'-SnCl$_2$; plane N(1)-N(2)-Sn(1)*

The fact that the behaviour of Sn and Pb is similar to that of halogens from other groups means that their reaction energy in solution need not be studied; the observation of the Cl compounds is, therefore, the result of a compromise between the solvation energies and the reaction energies.

Table 3.26. *Reaction energies (in kJ mol^{-1}) computed for the 1-MX$_2$ (M = Sn, Pb ; X = F , Cl , Br , I) formation*

MX$_2$	F	Cl	Br	I
Sn	-95.7	-104.9	-102.1	-106.2
Pb	-110.6	-110.0	-106.6	-104.7

Chapter 3

References and notes

1   Y. Yoshida, J. Saito, M. Mitani, Y. Takagi, S. Matsui, S. Ishii, T. Nakano, N. Kashiwa, T. Fujita, *J. Chem. Soc., Chem. Comun.* **2002**, 1298.

2   R. R. Schrock, R. Baumann, S. M. Reid, J. T. Goodman, R. Stumpf, W. M. Davis, *Organometallics* **1999**, *18*, 3649.

3   a) C. C. Cummins, *Prog. Inorg. Chem.* **1998**, *47*, 685.
    b) G. R. Weisman, S. C. H. Ho, Van Johnson, *Tetrahedron Lett.* **1980**, *21*, 335.
    c) M. D. Fryzuk, S. A. Johnson, *Coord. Chem. Rev.* **2000**, *335*, 200.

4   L. H. Gade, M. Schubart, B. Findeis, S. Frade, I. Bezougli, M. Lutz, I. J. Scowen, M. McPartlin, *Inorg. Chem.* **1999**, *38*, 5282.

5   a) R. R. Kempe, *Angew. Chem., Int. Ed.* **2000**, *39*, 468.
    b) L. H. Gade, *J. Chem. Soc., Chem. Commun.* **2000**, 173.

6   A. R. Dias, A. M. Martins, J. R. Ascenso, H. Ferreira, M T. Duarte, R. T. Henriques, *Inorg. Chem.* **2003**, *42*, 2675.

7   a) C. J. Pedersen, *J. Am. Chem. Soc.* **1967**, *89*, 2495.
    b) C. J. Pedersen, *J. Am. Chem. Soc.* **1967**, *89*, 7017.
    c) C. J. Pedersen, *"Synthetic Multidentate Macrocyclic Compounds"*, Eds: R. M. Izatt, J. J. Christensen, Academic Press: New York, **1978**.

8   J. D. Lamb, R. M. Izatt, J. J. Christensen, D. J. Eatough, *"Coordination Chemistry of Macrocyclic Compounds"*; Ed: G. A. Melson, Plenum Press: New York, **1979**; pp 145.

9   Y. A. Ovchinnikov, V. T. Ivanov, A. M. Shkrob, *"Membrane-Active Complexes"*; Elsevier: Amsterdam, **1974.**

10 F. Vogtle, *"Topics in Current Chemistry"*; Springer-Verlag: New York, **1982.**

11 R. D. Hancock, H. Okawa, N. Matsumoto, M. Koikawa, S. Kida, *J. Chem. Soc., Dalton Trans.* **1991**, 1657.

12 H. W. Roesky, Y. Bai, M. Noltemeyer, *Angew. Chem. Int. Ed. Engl.* **1989**, *28*, 754.

13 A. Abarca, P. Gómez-Sal, A. Martín, M. Mena, J.-M. Poblet, C. Yélamos *Inorg. Chem.* **2000**, *39*, 4.

14 A. Abarca, M. Galakhov, P. Gómez-Sal, A. Martín, M. Mena, J. M. Poblet, C. Santamaría, J. P. Sarasa, *Angew. Chem. Int. Ed.* **2000**, *39*, 534.

15 A. Abarca, A. Martín, M. Mena, C. Yélamos, *Angew. Chem. Int. Ed.* **2000**, *39*, 3460.

16 This work was originally planned as a collaborate work with Mena et al. inorganic chemistry group of the University of Alkala.

17 C. S. G. Phillips, R. J. P. Williams, *"Inorganic Chemistry"*, Vol. 2, Oxford University Press, Oxford, **1966**, Chapter 20.

18 a) E. E. Bittar, *"Membranes and Ion Transport"*, Vol. 1, Wiley-lnter-science, London, **1970**.

b) A. Kotyk, K. Janacek, *"Cell Membrane Transport"*, Plenum Press, London, **1970**.

c) D. R. Williams, *"Metals of Life"*, Van Nostrand Reinhold, New York, **1971**.

d) M. N. Hughes, *"The inorganic Chemistry of Biological Systems"*, Wiley, New York, **1972**.

e) S. Gershon, Shopsin, Eds., *"Lithium: Its Role in Psychiatric Research and Treatment"*, Plenum, New York, **1973**.

f) C. J. Duncan, *"Calcium in Biological Systems"*, Cambridge University Press, Cambridge, England, **1976**.

g) G. Eisenman, *"Membranes-A Series of Advances"*, Vol. 1-3, Marcel Dekker, New York, **1973-1975**.

h) D. A. Phipps, *"Metals and Metabolism"*, Oxford University Press, **1977**.

i) J. L. Hall, D. A. Baker, *"Cell Membranes and Ion Transport: Integrated Themes in Biology"*, Longmans, Harlow, U. K., **1977**.

[19] a) N. P. Marullo, J. F. Allen, G. T. Cochran, A. Lloyd, *Inorg. Chem.* **1974**, *13*, 115.

b) L. A. Duvall, D. P. Miller, *Inorg. Chem.* **1974**, *13*, 120.

[20] G. Sandrone, D. A. Dixon, *J. Phys. Chem. A* **1998**, *102*, 10310.

[21] J. Emsley, *"The elements"* Third edition, Oxford **1998**.

[22] M. García-Castro, J. Gracia, A. Martín, M. Mena, J. P. Sarasa, J.-M. Poblet, C. Yélamos, In press.

[23] M. García-Castro, A. Martín, M. Mena, A. Pérez-Redondo, C. Yélamos, *Chem. Eur. J.* **2001**, *7*, 647.

[24] C. L. Raston, C. R. Whitaker, A. H. White, *J. Chem. Soc., Dalton Trans.* **1988**, 991.

[25] T. Grob, C. Muller, W. Massa, T. Miekisch, G. Seybert, K. Harms, K. Dehnicke, *Z. Anorg. Alig. Chem.* **2001**, *627*, 2191.

[26] M. Hargittai, *Chem. Rev.* **2000**, *100*, 2233.

[27] H. W. Roesky, Y. Bai, M. Noltemeyer, *Angew. Chem. Int. Ed. Engl.* **1989**, *28*, 754

[28] a) T. Ziegler, A. Rauk, *Teor. Chim. Acta* **1977**, *46*, 1.

b) T. Ziegler, A. Rauk, *Inorg. Chem.* **1979**, *18*, 1558.

[29] a) K. Morokuma, *J. Chem. Phys.* **1971**, *55*, 1236.

b) K. Kitaura, K. Morokuma, *Int. J. Quantum. Chem.* **1976**, *10*, 325.

[30] N. Poonia, A. V. Bajaj, *Chemical Reviews* **1979**, *79*, 389.

[31] G. Aylward, T. Findlay, *"SI Chemical Data"* 4th Edition, John Wiley & Sons **1998**.

[32] J. Strong, T. R. Tuttle, *J. Phys. Chem.* **1973**, *77*, 533.

[33] L. Brewer, E. Brackett, *Chem. Rev.* **1961**, *61*, 425.

[34] N. S. Hush, J. R. Reimers, *Chem. Rev.* **2000,** *100, 775.*

Chapter 3

[35] J. P. Collman, L. S. Hegedus, J. R. Norton, R. G. Finke, *"Principles and Applications of Organotrasition Metal Chemistry"*, University Science books, Mill Valley, CA, **1987**.

[36] a) I. Eliezer, A. Reger, *Coord. Chem. Rev.* **1972**/**1973**, *9*, 189.
b) M. Spoliti, G. De Maria, L. D'Alessio, M. Maltese, *J. Mol. Struct.* **1980**, *67*, 159.

[37] L. Seijo, Z. Barandiarán, S. Huzinaga, *J. Chem. Phys.* **1991**, *113*, 3762.

[38] C. J. Burns, R. A. Anderson, *J. Organomet. Chem.* **1987**, *325*, 31.

[39] W. A. Nugent, J. A. Mayer, *"Metal-Ligand Multiple Bonds"*, Wiley-Interscience: New York, **1988**.

[40] a) W. A. Nugent, B. L. Haymore, *Coord. Chem. Rev.* **1980**, *31*, 123.
b) P. Mountford, *Chem. Commun.* **1997**, 2127.
c) D. E. Wigley, *Prog. Inorg. Chem.* **1994**, *42*, 239.

[41] a) K. E. Meyer, P. J. Walsh, R. G. Bergman, *J. Am. Chem. Soc.* **1995**, *117*, 974.
b) K. E. Meyer, P. J. Walsh, R. G. Bergman, *J. Am. Chem. Soc.* **1994**, *116*, 2669.

[42] a) P. J. Walsh, A. M. Baranger, R. G. Bergman, *J. Am. Chem. Soc.* **1992**, *114*, 1708.
b) K. A. Brown-Wensley, S. L. Buchwald, L. Cannizzo, L. Clawson, S. Ho, D. Meinhardt, J. R. Stille, D. Straus, R. H. Grubbs, *Pure Appl. Chem.* **1983**, *55*, 1733.

[43] a) J. L. Bennett, P. T. Wolczanski, *Inorg. Chem.* **1993**, *32*, 131.
b) J. L. Polse, R. A. Andersen, R. G. Bergman, *J. Am. Chem. Soc.* **1998**, *120*, 13405.
c) R. E. Blake, D. M. Antonelli, L. M. Henling, W. P. Schaefer, K. I. Hardcastle, J. E. Bercaw, *Organometallics* **1998**, *17*, 718.

[44] a) C. H. Winter, P. H. Sheridan, T. S. Lewkebandara, M. J. Heeg, J. W. Proscia, *J. Am. Chem. Soc.* **1992**, *114*, 1095.
b) D. M. Hoffman, *Polyhedron* **1994**, *13*, 1169.

[45] a) C. J. Carmalt, S. R. Whaley, P. S. Lall, A. H. Cowley, R. A. Jones, B. G. McBurnett, J. G. Ekerdt, *J. Chem. Soc., Dalton Trans.* **1998**, 553.
b) T. S. Lewkebranka, P. H. Sheridan, M. J. Heeg, A. L. Rheingold, C. H. Winter, *Inorg. Chem.* **1994**, *33*, 5879.
c) P. J. McKarns, G. P. A. Yap, A. L. Rheingold, C. H. Winter, *Inorg. Chem.* **1996**, *35*, 5968.

[46] J. L. Margrave, *"Refractory Materials"*, Academic Press: New York, **1971**.

[47] B. J. Coe, S. J. Glenwright, *Coord. Chem. Rev.* **2000**, *203*, 5.

[48] a) P. J. Wilson, P. A. Cooke, A. J. Blake, P. Mountford, M. Schröder, *New. J. Chem.* **1999**, 271.
b) P. J. Wilson, A. J. Blake, P. Mountford, M. Schröder, *J. Organomet. Chem.* **2000**, *600*, 71.

[49] a) C. H. Winter, T. S. Lewkebandara, M. J. Heeg, J. W. Proscia, A. L. Rheingold, *Inorg. Chem.* **1994**, *33*, 1227.
b) N. Adams, A. R. Cowley, S. R. Dubberley, A. J. Sealey, M. E. G. Skinner, P. Mountford, *Chem. Commun.* **2001**, 2738.

[50] N. Kaltsoyannis, Philip Mountford, *J. Chem. Soc., Dalton Trans.* **1999**, 781.

[51] A.Abarca, M. V. Galakhov, J. Gracia, A. Martín, M. Mena, J.-M. Poblet, J. P. Sarasa, C. Yelamos, *Chem. Eur. J.* **2003**, *9*, 2337.

[52] K. Freitag, J. Gracia, A. Martín, M. Mena, J.-M. Poblet, J. P. Sarasa, C. Yelamos, *Chem. Eur. J.* **2001**, *7*, 3644.

[53] a) A. Mommertz, R. Leo, W. Massa, K. Dehnicke, *Z. Naturforsch, Teil B* **1998**, *53*, 887.
b) A. J. Nielson, M.W. Glenny, C. E. F. Rickard, *J. Chem. Soc., Dalton. Trans.* **2001**, 232.

[54] D. C. Bradley, I. M. Thomas, *J. Chem. Soc.* **1960**, 3857.

[55] M. H. Chisholm, C. E. Hammond, J. C. Huffman, *Polyhedron* **1988**, *7*, 2515.

[56] a) R. S. Drago, *Coord. Chem. Rev.* **1992**, *117*, 185.
b) R. S. Drago, R. H. Beer, *Inorg. Chim. Act.* **1992**, *359*, 198.
c) R. H. Holm, *Chem. Rev.* **1987**, *87*, 1401.

[57] a) R. S. Dickson, *"Homogeneous Catalisis with Compounds of Rhodium and Iridium"*, D. Reidel Publishing Company, Dordrecht Holland, **1985**.
b) E. D. Nyberg, D. C. Pribich, R. S. Drago, *J. Am. Chem. Soc.* **1983**, *105*, 3538.
c) R. S. Drago, A. Zuzich, E. D. Nyberg, *J. Am. Chem. Soc.* **1985**, *107*, 2898.

[58] P. Muller, H. Idmoumaz, *J. Organomet. Chem.* **1971**, *26*, 417.

[59] a) K. A. Jorgensen, B. Schiott, *Chem. Rev.* **1990**, *90*, 1483.
b) A. A. Zlota, F. Frolow, D. Milstein, *J. Am. Chem. Soc.* **1990**, *112*, 6411.
c) M. J. Calhorda, A. M. Galvao, C. Unaleroglu, A. A. Zlota, F. Frolow, D. Milstein, *Organometallics* **1993**, *12*, 3316.
d) J. C. Hartwig, R. G. Bergman, R. A. Andersen, *Organometallics* **1991**, *10*, 3344.
e) J. C. Hartwig, R. G. Bergman, R. A. Andersen, *J. Am. Chem. Soc.* **1990**, *112*, 3234.

[60] B. de Bruin, M. J. Boerakker, J. J. J. M. Donners, B. E. C. Christiaans, P. P. J. Schlebos, R. de Gelder, J. M. M . Smits, A. L. Spek, A. W. Gal, *Angew. Chem., Int. Ed. Engl.* **1997**, *36*, 2064.

[61] J. Blum, B. Zinder, D. Milstein, O. Buchman, *J. Org. Chem.* **1978**, *43*, 2961.

[62] J. Bakos, A. Orosz, S. Cscrepi, I. Coth, D. Sinou, *J. Mol. Catal. A: Chem.* **1997**, *116*, 85.

[63] B. de Bruin, J. A. Brands, J. Donners, R. de Gelder, J. Smits, A. Gal, A. Spek, *Chem. Eur. J.* **1999**, *5*, 2921.

[64] a) S. Trifomenko, *Chem. Rev.* **1993**, *93*, 943.

Chapter 3

b) M.-C. Nicasio, M. Paneque, P. J. Pérez, A. Pizzano, M. L. Poveda, L. Rey, S. Sirol, S. Taboada, M. Trujillo, A. Monge, C. Ruiz, E. Carmona, *Inorg. Chem.* **2000**, *39*, 180.

[65] J. C. Jeffery, P. A. Jellis, V. N. Lebedev, F. Gordon, A. Stone, *Organometallics* **1996**, *15*, 4737.

[66] a) T. C. Flood, M. Limura, J. M. Perotti, A. L. Rheingold, T. E. Concolino, *Chem. Commun.* **2000**, 1681.

[67] M. A. Esteruelas, L. A. Oro, M. C. Apreda, C. Foces-Foces, F. H. Cano, R. M. Claramunt, C. Lopez, J. Elguero, M. Begtrup, *J. Organomet, Chem.* **1988**, *344*, 93.

[68] A. Albinati, M. Bovens, H. Rüegger, L. M. Venanzi, *Inorg. Chem.* **1997**, *36*, 5991.

[69] A. J. Downs, Ed., *"The chemistry of Aluminium, Gallium and Thallium"*, Blackie, London, **1993**.

[70] a) J. Kim, S. G. Bott, D. M. Hoffman, *Inorg. Chem.* **1998**, *37*, 3835.

[71] a) D. M. Hoffman, *Polyhedron* **1994**, *13*, 1169.

b) S. Strite, M. E. Lin, H. Morkoc, *"Thin Solid Films"* **1993**, *231*, 197.

c) D. A. Neumayer, J. G. Ekerdt, *Chem. Mater.* **1996**, *8*, 9.

[72] G. Wilkinson, F. G. A. Stone, E. W. Abel, Eds., *"In Comprehensive Organometallic Chemistry"*, Pergamon Press: Oxford, England, **1983**, Vol. 1.

[73] a) R. A. Walton, *Inorg. Chem.* **1968**, *7*, 640.

b) J. T. Leman, H. A. Roman, A. R. Barron, *Organometallics* **1993**, *12*, 1986.

[74] F. G. A. Stone, *Chem. Rev.* **1958**, *58*, 101.

[75] a) L. P. Bicelli, *Ann. Chim.* **1958**, *48*, 749.

b) B. N. Ivanov, Ya I. Rabovik, *Zh. Neorgan khim.* **1959**, *4*, 2228.

[76] a) F. A. Cotton, B. F. G. Johson, R. M. Wing, *Inorg Chem.* **1965**, *4*, 502.

b) B. F. G Johnson, A. Walton, *Inorg. Chem.* **1966**, *5*, 49.

[77] NMR data for **17**: ^{1}H NMR (300 MHz, C_6D_6, 20 °C, TMS): $\boldsymbol{d}$ = 13.60 (s br., 3 H ; NH), 2.00 (s, 45 H ; C_5Me_5); ^{13}C{^{1}H} NMR (75 MHz, C_6D_6, 20 °C, TMS): $\boldsymbol{d}$ = 117.6 (C_5Me_5), 11.9 (C_5Me_5).

[78] G. B. Deacon, E. E. Delbridge, C. M. Forsyth, B. W. Skelton, A. H. White, *J. Chem. Soc., Dalton Trans.* **2000**, 745.

[79] a) G. Lin, W-T. Wong, *J. Organomet. Chem.* **1995**, *495*, 203.

b) P. Jutzi, *Adv. Organomet. Chem.* **1986**, *26*, 217.

[80] C. C. Hsu, R. A. Geanangel, *Inorg. Chem.* **1980**, *19*, 110.

[81] P. G. Harrison, J. A. Richards, *J. Organomet. Chem.* **1976**, *108*, 35.

[82] C. C. Hsu, R. A. Geanangel, *Inorg. Chem.* **1977**, *16*, 2529.

[83] a) Y. tal, R. F. W. bader, J. Erkku, *Phys. Rev.* **1979**, *21*, 1.

b) S. R. Grade, R. D. Bendale, *Chem. Phys. Lett.* **1986**, *130*, 575.

[84] S. R. Grade, S. A. Kulkarni, I. H. Shrivastava, *J. Chem. Phys.* **1992**, *96*, 5253.

4

Oxometallocubanes

Oxotitanium $[\{Ti(\mathbf{h}^5 - C_5Me_5)(\mathbf{m}-O)\}_3(\mathbf{m}_3 - CR)]$ *(R = H, Me) ligands, with the same tripodal structure as the Azatitanium* $[\{Ti(\mathbf{h}^5 - C_5Me_5)(\mathbf{m}-NH)\}_3(\mathbf{m}_3 - N)]$*, also serve as possible base for the formation of oxometallocubane compounds. Species with oxometallocubane structure constitute an interesting building block in inorganic solids,[1] and provide molecular models for heterogeneous catalysis as deduced from organometallic complexes adsorbed at metal oxide surfaces.[2]*

The present chapter is divided into the following sections: Section 4.1 introduces the $[\{Ti(\mathbf{h}^5 - C_5Me_5)(\mathbf{m}-O)\}_3(\mathbf{m}_3 - CR)]$ *ligands, previous studies and describes the present scope. Section 4.2 discusses the interactions of the oxotitanium ligands with alkaline metals. Finally, Section 4.3 is dedicated to the special chemistry that takes place on the* $[(\mathbf{m}_3 - ethylidyne)]$ *alkylidine unit in complex* $[\{Ti(\mathbf{h}^5 - C_5Me_5)(\mathbf{m}-O)\}_3(\mathbf{m}_3 - CMe)]$ *when it is treated with cationic metal fragments (metal support for vinylidene-acetylidene species).*

Chapter 4

4.1 Introduction

This chapter discusses oxotitanium complexes, which contain a tetrahedral Ti_3CR unit supported by oxygen atoms and pentamethylcyclopentadienyl (Cp^*) ligands, $[\{TiCp^*(\mu\text{-}O)\}_3(\mu_3\text{-}CR)]$ (R = H (**2**), Me (**3**)). X-ray crystallographic studies of these complexes suggest that the apical carbon atom can be regarded as a saturated sp^3 alkylidyne carbon incorporated in the Ti_3O_3 ligand core.[3] This point of view is similar to that of Chisholm et. al. for the early transition metal clusters $[M_3(\mu_3\text{-}CR')(OR)_9]$ (M = Mo, W).[4]

In general, the chemistry of the μ_3-alkylidyne_trimetal clusters has been extensively explored.[5,6] However, to our knowledge, the $[\{CrCp(\mu\text{-}Cl)\}_3(\mu_3\text{-}CH)]$[7] ($Cp = \eta^5\text{-}C_5H_5$), $[\{TiCp^*(\mu\text{-}O)\}_3(\mu_3\text{-}CR)]$ and $[\{TiCp^*\}_4(\mu_3\text{-}CH)_4]$[8] complexes are the only reported examples of μ_3-alkylidyne units supported on trinuclear cores without metal-metal bonds, and their reactivity is as yet practically unknown.[9] Interestingly, the μ_3-alkylidyne and, in particular, the μ_3-ethylidyne groups are not exclusive to polynuclear organometallic complexes. They have also been identified on numerous metal surfaces, thus providing evidence of a close relationship between organometallic and solid surface systems.[10,11] The chemistry of these d^0 μ_3-alkylidyne compounds is different to that of mononuclear hydrocarbyl complexes which contain metals in the highest oxidation state. Cooperative effects between the metals centres imitate the behaviour of the alkylidine groups attached to metal or metal oxide surfaces. In our case, the Ti_3O_3 core in these complexes exhibits chemical and geometrical flexibility, which stabilises unexpected complexes. So unsaturated molecules such as CO or isocyanides, have been incorporated into the Ti_3O_3 core by been inserted into the alkylidyne units in a quite specific manner and under mild reactions conditions.[12]

It has also been reported that these oxotitanium complexes can act as macrocyclic, tridentate six-electron donor ligands and thus provide an effective route to heterocubanes with a $[MTi_3(\mu_3\text{-}CR)(\mu\text{-}O)_3]$ core. This core could be invaluable as a discrete and ideal model of oxide-supported metal carbonyl complexes, for studying the catalyst-support interaction.[13] The heterometallic cubanes $[\{Ti_3Cp_3^*(\mu_3\text{-}CR)\}(\mu_3\text{-}O)_3\{Mo(CO)_3\}]$ (R = H, Me) has been formed from $[Mo(CO)_3\text{-}(1,3,5\text{-}Me_3C_6H_3)]$ and $[\{Ti_3Cp_3^*(\mu_3\text{-}CR)\}(\mu\text{-}O)_3]$ (R = H (**2**), Me (**3**)) compounds.[14] The alkylidine complexes **2** and **3** act as preorganized ligands that donate electron density to the added

molybdenum atom through the three electron-rich bridging oxygen atoms to give the heterometallic cubane core. Theoretical results confirm that the formation of the cluster is not accompanied by the oxidation of the molybdenum centre and, as in the precubane precursors; the oxidation state of the titanium atoms is still 4+. Nevertheless, the Mo atom shares electron density by means of metal-metal coupling with the Ti_3 unit. Harris et al.[15] reported similar charge delocalization in the cubane-type clusters $[MMo_3S_4]$ (M = Ni, Pd, Co).

Cyclic polyethers, known collectively as crown ethers, are probably the best known oxygen donor preorganized ligands. The studies into these ligands have been partly motivated by the complexation of a wide variety of cations. The discussion of the chemical and physical properties of metal polyethers has focused on the question of accommodating of the metal ion in the ligand cavity size. Moreover, size alone is clearly not the sole determining factor that determines the stability of adduct formation.[16] Multidentate $[\{Ti(h^5-C_5Me_5)(m-O)\}_3(m_3-CR)]$ ligands are an opportunity for adding new cation selectivity to the rich oxo-ligand chemistry. The observation that the oxo-systems $[\{Ti(h^5-C_5Me_5)(m-O)\}_3(m_3-CR)]$ (R = H(**2**), Me(**3**))[3,9,17] may be involved directly as macrocyclic tridentate six-electron donor ligands in the encapsulation processes of several metals means that it is interesting to study them to determine which metal fragments can be incorporated.

The structural and electronic similarity of $[\{Ti(h^5-C_5Me_5)(m-O)\}_3(m_3-CR)]$ ligands to $[\{Ti(h^5-C_5Me_5)(m-NH)\}_3(m_3-N)]$ (**1**) makes comparisons inevitable. Nevertheless some differences are noteworthy: the lack of basic protons over the donor oxygen atoms in **2** and **3** a priori makes it impossible for them to work as double action ligands[18] and these proton bonds cannot be activated to act as anionic ligand. In contrast, as we will see, the apical carbon – proton bond can be activated to give rise to a tripodal anionic ligand from **2**.

Figure 4.1 shows the orbital diagrams of the aza- **1** and oxo- **2** ligands. Qualitatively there are few differences in the electronic structure between aza- **1** and oxo- **2**, **3** compounds. It should be noted only that the relative

Chapter 4

energy level of the oxygen-free pairs is more stable than that of the nitrogen-free pairs by over 2.0 eV, which means that they have a harder basicity.

Here we will study the potential incorporation of alkali metal halides to **2**. It is interesting to compare these compounds with the relative aza-ones, because of the differences in their complexation. We will also study the formation of alkali dicubane clusters, which lead us to the first examples of apical carbon-proton bond activation. Finally, we will do a little chemistry and study the vinylidene-acetylidene isomerization process that occurs over the oxygen titanium surface in the (μ_3-ethylidine) unit of ligand **3**.
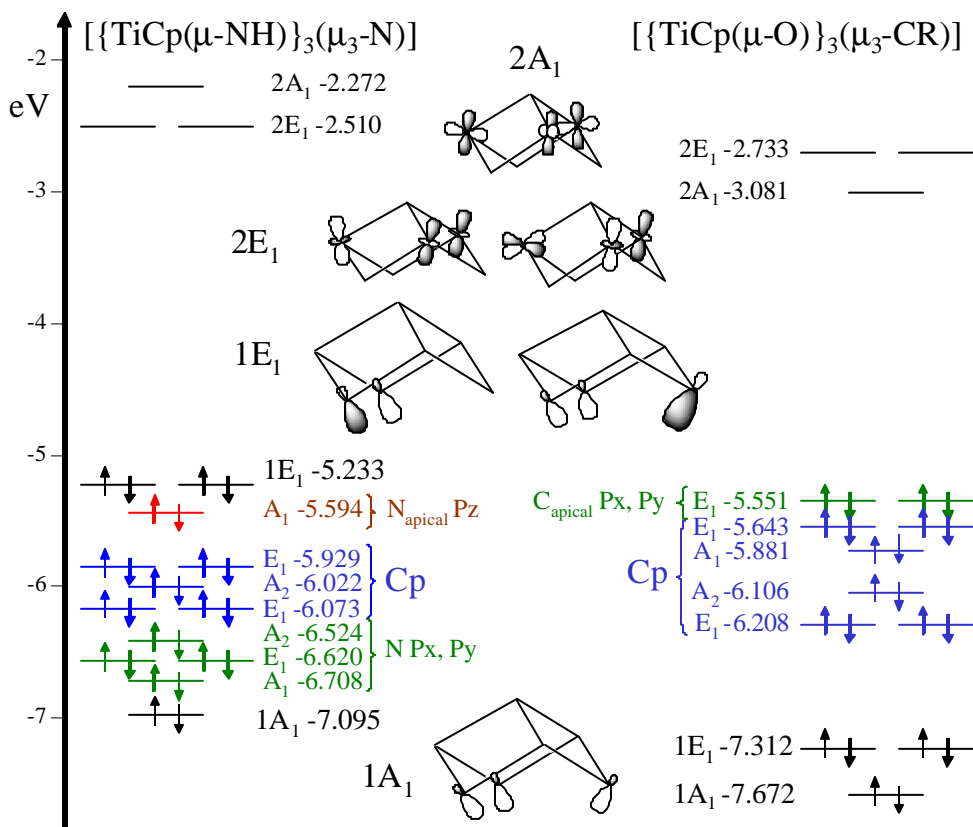
Figure 4.1. *Comparative diagram of orbitals for aza-**1** and oxo-**2** ligands*

4.2   Alkali oxometallocubanes

It has been presented the precubane $[\{Ti(h^5 - C_5Me_5)(m - NH)\}_3(m_3 - N)]$ (**1**) by direct reaction with the salts M-X (M = Li, Na, K, Rb, Cs; X = F, Cl, Br, I) yields 1-MX heterocubanes only in some cases.[19] We showed that the obtaining of adducts depends on whether the interaction energy between salt and ligand is enough to compensate the salt lattice energy in a solvent. For the oxo-ligands the corresponding oxo-heterocubane formation starting from the solid salts is not observed in any case. Nevertheless, related alkali oxo-cubane complexes are obtained by treating of the alkylidine ligands with different alkali-metal alkyls and amides.

Calculations were made for the $[\{Ti_3Cp_3(\mu_3\text{-}CR)\}(\mu_3\text{-}O)_3\{LiX\}]$, ($Cp = \eta^5$-$C_5H_5$), 2-LiX, (X = F, Cl, Br, I and CH_3) compounds under C_3v symmetry restrictions. As well as the halogen counteranions, the CH_3 unit was chosen as an example of an alkyl substituent for the alkali metal. In all cases, the compounds have short Li-O distances between 2.4 and 2.2 Å (see Table 4.1). There is a clear tendency for the lithium – bridging oxygen atom distance to increase from I to F. The Li-O distance of the alkyl CH_3 substituent is similar to that of the Cl counteranion. Complexation is also accompanied by a logical slight enlargement of the Li-X bond (see Table 4.1).

Table 4.1. *Selected bond lengths in Å for 2-LiX and LiX (X = F, Cl, Br, I, CH_3) compounds*

	2-LiF	2-LiCl	2-LiBr	2-LiI	2-LiCH$_3$
Li-X	1.642	2.108	2.292	2.509	2.093
Li-O	2.371	2.311	2.215	2.192	2.197

	LiF	LiCl	LiBr	LiI	LiCH$_3$
Li-X	1.615	2.084	2.230	2.461	1.999
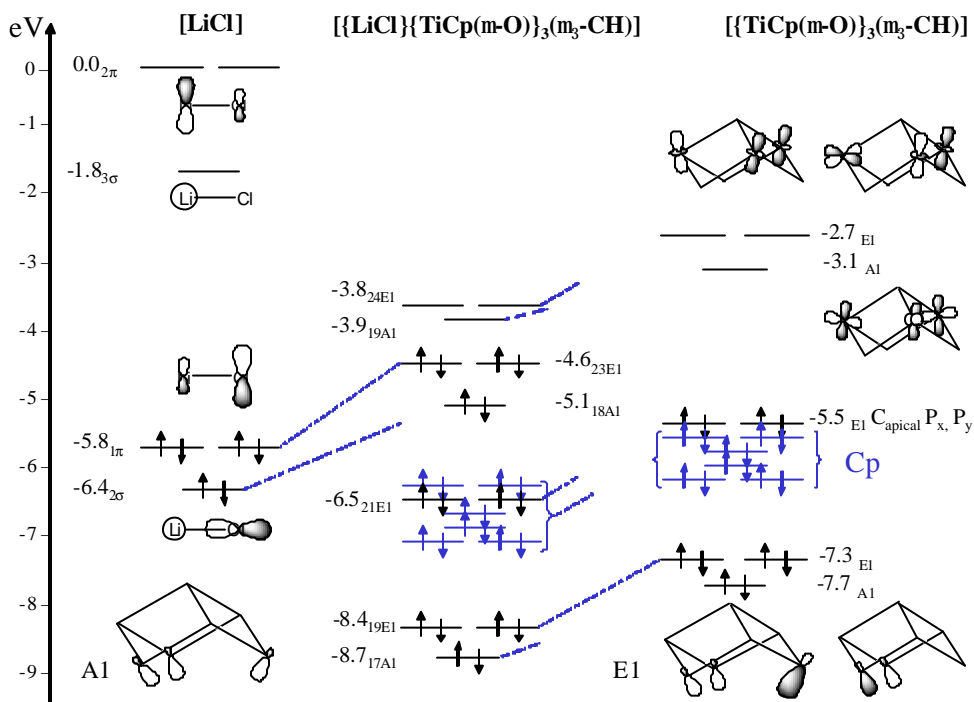
Figure 4.2. *Fragment interaction diagram between the* $\left[\left\{Ti\left(h^5 - Cp\right)\left(m-O\right)\right\}_3 \left(m_3 - CH\right)\right]$ *precubane and* $\left[LiCl\right]$ *molecule*

Table 4.2 shows the decomposition of the interaction energy with **2** and LiX as fragments. The nature of the interaction between the metal and ligand fragments can be understood in the same terms as for the alkali aza-cubanes. An important electrostatic attraction between fragments, increasing from F to I, is the main stabilising interaction for halogens, so this last I atom has the biggest interaction energy. The orbital interaction energy is also important, partly because the fragments are polarised by the electrostatic attraction, and so increase from F to I. Again the interaction energy of the CH_3 substituent is close to that of chlorine atom, but a clear change is observed: the importance of electrostatic interaction energy is reduced in favour of the orbital interaction energy. Figure 4.2 shows and orbital interaction diagram between **2** and the LiCl molecule. It can be seen that there is an overall stabilization of the frontier orbitals of the ligand, related to the important electrostatic interaction with the incorporated metallic

188

fragment. At the same time, the simple nature of the ligand is revealed by the destabilization of the frontier orbitals of the alkali metal fragment when interacting with the ligand.

In comparison to the aza ligand **1**, there is a considerable reduction in the complexation energy, mainly because of the approximate 70 kJ mol^{-1} reduction in the electrostatic attractive energy due to the presence of more basic oxygen free pairs. Similar analyses and comparisons were made between oxo and aza ligands for the addition of $[M(CO)_3]$ (M = group-6 element), metal fragments.[14]

Table 4.2. *Energy decomposition for the 2-LiX (X = F, Cl, Br, I, CH$_3$), compounds with **2** and LiX as fragments*

	2-LiF	2-LiCl	2-LiBr	2-LiI	2-LiCH$_3$
Pauli	35.2	43.0	57.6	67.1	80.2
Electrostatic	-72.0	-79.1	-88.9	-97.0	-85.2
Orbital	-52.0	-67.8	-77.4	-86.0	-96.5
Interaction Energy	**-88.8**	**-103.9**	**-108.7**	**-115.9**	**-101.5**
Reaction Energy	-63.3	-78.7	-98.3	-105.4	-65.9

Of particular interest is the weakening of the M-X bond when the salt is inserted into the ligand (see Table 4.3). The interaction with the ligand produces a slight mixing of the last occupied orbitals of the ligand with the unoccupied antibonding orbitals of the M-X fragments. This leads to a certain occupation of these antibonding orbitals and consequently a weakening and an enlargement of the M-X bond. The greater the mix between ligand-occupied orbitals and metal antibonding orbitals, the weaker this bond will be. In the next section we will see the importance of this weakening for the formation of dimer complexes.

```
UNIVERSITAT ROVIRA I VIRGILI
DFT STUDY OF TITANIUM CUBANE AND MOLYBDENUM SULPHIDE COMPOUNDS.
Autor: José Manuel Gracia Budria
ISBN: 978-84-690-6751-2 / DL: T.1196-2007
```
Chapter 4

Table 4.3. *Li-X (X = F, Cl, Br, I, CH_3) bond energies, in kJ mol^{-1}, for the LiX free molecules and for the $[\{LiX\}\{Ti(h^5-Cp)(m-O)\}_3(m_3-CH)]$ adducts*

	LiX	2-LiX	% Variation
Li-F	-594.0	-448.3	25
Li-Cl	-443.5	-313.2	29
Li-Br	-400.2	-290.0	28
Li-I	-340.2	-236.6	30
Li-CH_3	-187.1	-44.0	76

Oxoheterometallodicubanes

An one-pot reaction of the tripodal starting material $[\{Ti(h^5-C_5Me_5)(m-O)\}_3(m_3-CH)]$ with MR (M = Li, R = CH_2SiMe_3, CH_2CMe_3, Bu^n; M = Na, R = Bu^n; M = K, R = Bu^n, CH_2Ph) in a double layer of toluene/hexane at room temperature yields the heterometallodicubanes $[M(m_3-O)_3\{Ti_3(h^5-C_5Me_5)_3(m_3-C)\}]_2$ (M = Li(**4.1**), Na(**4.2**), K(**4.3**)) in good yields.[20] Repeating the synthesis with $MN(SiMe_3)_2$ (M = Li, Na, K) in toluene or hexane at 60ºC affords the same oxometallodicubane complexes **4.1**-**4.3** (see Scheme 4.1).
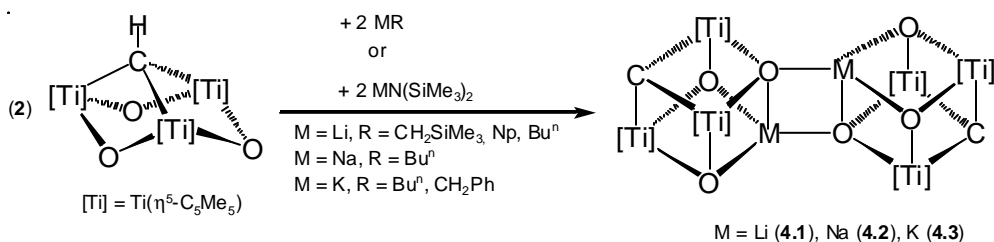
M = Li (**4.1**), Na (**4.2**), K (**4.3**)

Scheme 4.1. *Synthesis of the herometal dicubane-type complexes $[M(m_3-O)_3\{Ti_3(h^5-C_5Me_5)_3(m_3-C)\}]_2$ (M = Li (**4.1**), Na (**4.2**), K (**4.3**))*

Some solid compounds were spectroscopically characterized. The ^{13}C NMR data display resonances with their corresponding multiplicity for Cp*, as well as a singlet for the apical methylidyne carbon (δ = 586.7 (**4.2**) and 582 ppm (**4.3**)), much larger than the δ = 383.2 ppm for the parent methylidyne complex **2**. These data show that the proton of the apical μ_3 − methylidyne fragment has been removed and that the diamagnetic compounds $[M(\mu_3\text{-O})_3\{Ti_3(\eta^5\text{-}C_5Me_5)_3(\mu_3\text{-C})\}]_2$ (M = Li, Na, K) have been formed. Recently, Mountford et al. characterized a naked sp^3 carbanion by reacting $[Ti(NtBu)\{HC(Mepz)_3\}Cl_2]$ with LiMe.[21]

Crystallization of **4.1** gave crystals suitable for an X-ray diffraction study. The molecular structure of **4.1** is shown in Figure 4.3 and a selection of bond lengths and angles are shown in Table 4.4. This latter table reveals an edge-linked double cube[22] with two μ_4-O-to-Li bridges in a rhombic Li_2O_2 arrangement. Each edge is shared between two four-coordinate Li centres, with a central planar rhombic fragment, whereas the rhombic moieties in each cubane-like unit show a non planar arrangement necessary to adopt a cube-type geometry, analogously to that found for $[M(\mu_3\text{-N})(\mu_3\text{-NH})_2\{Ti_3(\eta^5\text{-}C_5Me_5)_3(\mu_3\text{-N})\}]_2$ (M = Li, Na).[23]
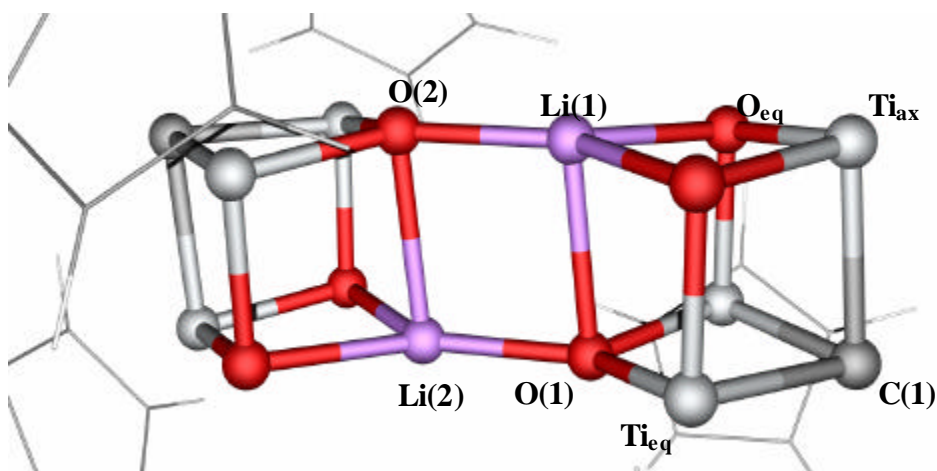
Figure 4.3. *X-ray molecular structure for compound* $[Li(\mu_3\text{-O})_3\{Ti_3(\eta^5\text{-}C_5Me_5)_3(\mu_3\text{-C})\}]_2$ *(4.1)*

Chapter 4

The Ti_3O_3C subunits of **4.1** have several structural differences with respect to the parent **2** and relative **3** compounds. **2** and **3** selected parameters can also be analysed in Table 4.6. The Ti-O-Ti (95.4° av.) and O-Ti-O (96.4° av.) angles are smaller than those found for $[\{Ti(h^5 - C_5Me_5)(m-O)\}_3(m_3 - CR)]$ (R = H(**2**), Me(**3**); Ti-O-Ti = 100°, O-Ti-O = 104°, average).[3] The average distance from the titanium atoms to the methylidyne carbon is 2.055 Å, clearly shorter than that shown in **2** (Ti-C(1) = 2.10 Å av.),[9] **3** (Ti-C(1) = 2.12 Å av.; Ti-C(1)-Ti 83.5°).[3] The Ti-Ti distances, 2.79 Å (av.), compare well with those found for **2** and **3** (Ti-Ti distances, 2.82 Å).

DFT calculations reproduce the X-ray geometry found for dimer **4.1** quite well (see Table 4.4). However, for the central rhombic unit the optimization process yielded a structure with two short and two long Li-O bonds of 1.858 and 2.213 Å, respectively. Whereas the short bonds compare very well with the experimental distance (1.892 Å) the discrepancy (0.173 Å) in the long bonds seems excessive. It should be pointed out here that dicubane **4.1** is quite fluxional. We found that the energy difference between the complex that was optimised by keeping the central parallelepiped fixed at the experimental geometry and the fully optimised complex is only 12 kJ mol^{-1}.

Table 4.4. *Selected calculated and experimental structural data for* $[Li(m_3-O)_3\{Ti_3(h^5-C_5Me_5)_3(m_3-C)\}]_2$ *(4.1) dimer. Distances in Å and angles in °*

	C(1)-Ti$_{ax}$	C(1)-Ti$_{eq}$	Ti$_{ax}$-Ti$_{eq}$	O$_{eq}$-Li	O(1)-Li(1)	O(1)-Li(2)	Li-Li
4.1	1.969	1.952	2.777	2.062	2.213	1.858	2.764
(4.1)*	(2.046)	(2.059)	(2.802)	(2.057)	(2.386)	(1.892)	(2.612)

	Li(1)-O(1)-Li(2)	O(1)-Li(1)-O(2)	Li(1)-O$_{eq}$-Ti$_{ax}$	O(1)-Ti$_{eq}$-C(1)
4.1	85.1	94.9	87.5	87.4
(4.1)*	(74.3)	(105.7)	(86.8)	(90.8)

* Average experimental data
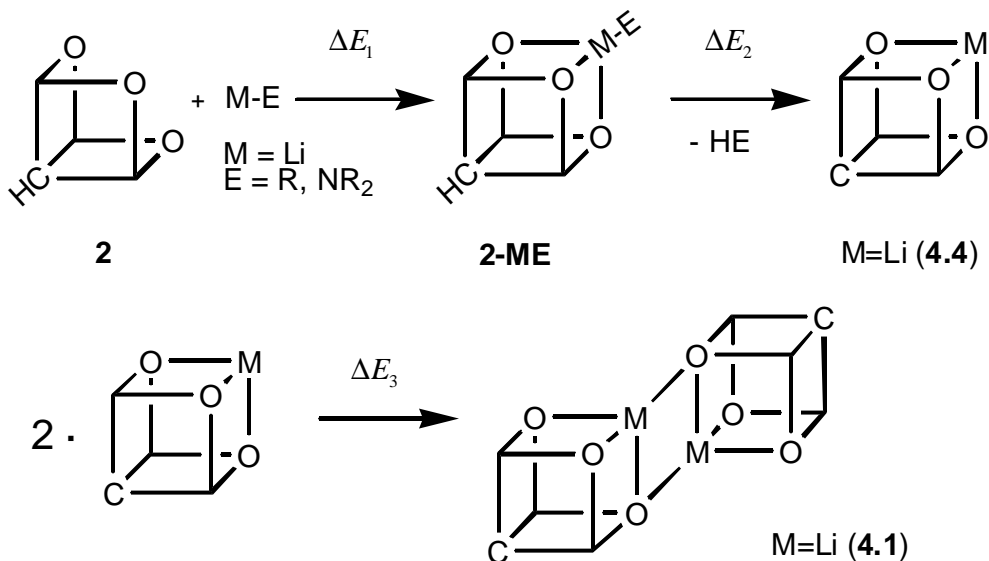
Scheme 4.2. *Proposed mechanism for the formation of the heterometal dicubane-type complexes **4.1**-**4.3***

Calculations were initially made to determine the energy of the proposed mechanism for the formation of the heterometallodicubanes **4.1**-**4.3** from $[\{Ti(\boldsymbol{h}^5-C_5Me_5)(\boldsymbol{m}-O)\}_3(\boldsymbol{m}_3-CH)]$ and M-E fragments, where M = Li and E = CH_3, NH_2 and Cl (see Scheme 4.2). Table 4.5 shows the computed energies for the adduct formation (ΔE_1), the breaking of $C-H$ and $M-E$ bonds and subsequent formation of the $C[Ti]_3O_3M$ monomer **4.4** and $H-E$ molecule (ΔE_2), and finally the energy associated to the building of the dimer, (ΔE_3). The energy corresponding to the global process $2HC[Ti]_3O_3 + 2M-E \rightarrow (C[Ti]_3O_3M)_2 + 2HE$ (ΔE) is also given in Table 4.5. Table 4.6 shows the main geometrical parameters for structures involved in Scheme 4.2.

Chapter 4

Table 4.5. *Computed energies in kJ mol^{-1} for the reaction steps shown in Scheme 4.2*

	ΔE_1	ΔE_2	ΔE_3	ΔE [a)]
CH_3	-65.9	-141.8	-136.0	-551.4
NH_2	-62.4	-61.7	-136.0	-384.2
Cl	-78.7	140.9	-136.0	-11.6

[a)] $\Delta E = 2\Delta E_1 + 2\Delta E_2 + \Delta E_3$

Table 4.6. *Selected calculated and experimental structural data (Distances in Å and angles in º) for compounds involved in Scheme 4.2*

	C(1)-Ti	Ti-Ti	Ti-O	Li-O	C(1)-Ti-O	Ti-O-Ti	O-Ti-O	Ti-O-Li
2	2.101	2.823	1.838	-	86.4	100.8	102.8	-
3	2.121	2.829	1.836	-	86.9	100.8	102.8	-
(3)*	(2.121)	(2.823)	(1.830)	-	(87.0)	(100.8)	(104.2)	-
2-LiCH₃	2.097	2.833	1.859	2.197	87.4	99.3	98.3	90.2
4.4	1.964	2.773	1.900	2.027	88.1	93.7	96.2	87.6

* Average experimental data

The $HC[Ti]_3O_3$-ME adduct is assembled via the interaction between the three oxo atoms and the alkaline metal. The adduct formation is accompanied by a charge transfer from the alkali metal unit to the $HC[Ti]_3O_3$ fragment. This transfer, 0.35 electrons, is more clearly perceptible in the electron density deformation map computed for the $HC[Ti]_3O_3$-LiCH$_3$ adduct with respect to a promolecule composed of the no interacting fragments $HC[Ti]_3O_3$ and Li-CH$_3$ (Figure 4.4). Figure 4.4 shows that there is a general depopulation in the Li-CH$_3$ subunit: the electron density is transferred to the oxo ligands and titanium orbitals, and there is a considerable accumulation of charge density in the region between the oxo ligands and the lithium. Similar but less pronounced depopulation in the Li-X subunit was observed and analysed for the complexation of alkaline halogen salts with oxo- and aza- precubane compounds. Alkali metal alkyls

have the biggest depopulation because, in comparison to the halogens, the nucleophilicity of the alkyl moiety is lower and the polarizability of the metal alkyl bond is bigger.

The process of cubane formation is exothermic: $\Delta E_1 = $ -66 kJ mol^{-1}, -62 kJ mol^{-1} and -79 kJ mol^{-1} for Li-CH_3, Li-NH_2 and Li-Cl respectively. The second step, which consists of the formation of CH_4, NH_3 or HCl molecules and monomer $C[Ti]_3O_3$-Li (**4.4**), via the breaking of the $C-H$ bond in $HC[Ti]_3O_3$-LiCH$_3$, is also an exothermic reaction with an energy exchange of -142 kJ mol^{-1} and -62 kJ mol^{-1} for CH_3 and NH_2 respectively. For chlorine, however, it is endothermic, 141 kJ mol^{-1}. As consequence of a greater electrostatic interaction, the debilitation of alkaline metal – halogen bonds in their complexation with **2** is lower; in that case the dimers formation is disfavoured.

Finally, the formation of heterometallodicubane **4.1** generates two new ionic Li-O bonds, a process that has an associated energy reaction that is quite significant ($\Delta E_3 = $ -136 kJ mol^{-1}). To analyse the bonding nature of the interaction between the two monomers that gives dimer **4.1**, a decomposition based on Morokuma scheme was done.[24] The overall interaction energy for the monomers is quite exothermic, -194.7 kJ mol^{-1}, and the electrostatic interaction is the dominating contribution, -229.3 kJ mol^{-1}. The Pauli repulsion represents 160 kJ mol^{-1} and the other contribution in the total energy is OI (-125.9 kJ mol^{-1}). The quite significant orbital interaction energy indicates that the formation of the cluster is accompanied by an important electronic reorganization, which plays a significant role in the stabilization of the cluster.

The overall reaction $2\cdot(\mathbf{2}) + 2\cdot(M\text{-}E) \rightarrow \mathbf{4.1} + 2\cdot EH$ is a strongly exothermic process for E = CH_3 (ΔE = -551 kJ mol^{-1}). For E = NH_2 (ΔE = -384 kJ mol^{-1}), the reaction is also exothermic but the energy involved is considerably lower for E = Cl (ΔE = -12 kJ mol^{-1}). These energy results are consistent with the observed formation and the significant stability of clusters **4.1**-**4.3** from alkyls and amides.
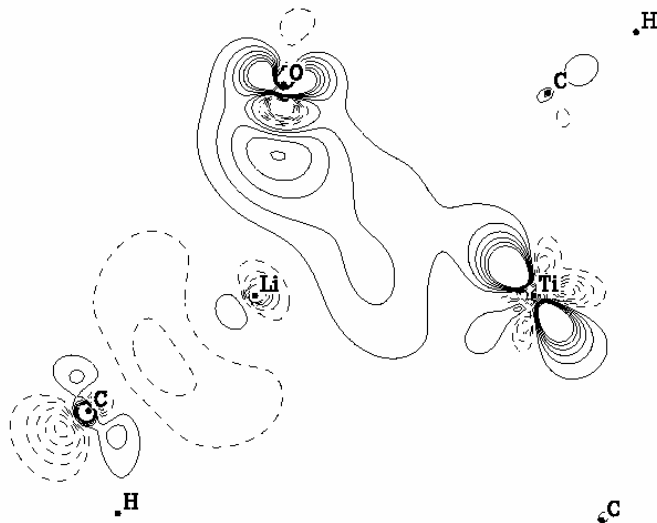
Chapter 4

Figure 4.4. *Density deformation map computed for the $HC[Ti]_3O_3$-$LiCH_3$ adduct 4.4 as $r_{[HCT_iO_3]\cdot[ME]} - (r_{[HCT_iO_3]} + r_{[ME]})$. The plane shown contains the lithium carbon bond, one hydrogen of the methyl group, one titanium, one oxygen atom and two CHs. Solid lines are used for zero and positive contours (relative charge accumulations) and dashed lines for negative contours (relative charge depletion)*

The NMR shielding tensor was calculated in the framework of gauge including atomic orbitals (GIAO). The calculation took into account the relativistic effects,[25,26] and made it possible to compare the calculated and observed NMR spectra. This may help to identify of new species. We computed the carbon chemical shift for the apical methylidyne carbon in the precursor tridentate ligand **2**, in adduct 2-LiCH₃, in monomer **4.4** and finally in dimer **4.1** (see Table 4.7). The theoretical shift computed for the apical carbon in **2** was 385.3 ppm, very close to the observed value in the ^{13}C NMR spectrum (δ = 383.2 ppm). There is a small shift to 400.6 ppm after the complexation of the LiCH₃ unit, and the elimination of the proton significantly enlarges δ to 572.2 ppm. The shift computed for the methylidyne carbon in **4.1** (δ = 572.2 ppm) fully agrees with the corresponding experimental values observed for dimers **4.2** (δ = 586.7 ppm) and **4.3** (δ = 582 ppm). These theoretical results corroborate that the

hydrogen bonded to the apical carbon is removed in the transformation process from **2** to **4.1-4.3**.

Table 4.7. *Calculated and experimental ^{13}C shielding constants*

Adduct	Chemical Shift [a]		Shielding			Charge	
	d (expt.)	d (DFT)	σ_p [b]	σ_d [c]	σ_T [d]	C [e]	M [e]
LiCH$_3$							0.219
2	383.2	385.3	-444.2	241.2	-203.0	-0.544	
2-LiCH$_3$		400.6	-461.3	243.0	-218.3	-0.537	0.345
4.4		572.2	-644.1	254.2	-389.9	-0.689	0.432
4.1		572.5	-646.6	256.4	-390.2	-0.712	0.360
4.2	586.7						
4.3	582.0						

[a] *Shift in ppm relative to tetramethylsilane, TMS . Chemical shift is equal to $d=s(TMS)-(s_d+s_p)$, where computed $s(TMS)$ is 182.3 ppm.*
[b] *Paramagnetic shielding*
[c] *Diamagnetic shielding*
[d] *Absolute shielding tensor*
[e] *Net charge associated to the methylidyne carbon and to the alkaline metal determined from Mulliken analysis*

Table 4.7 shows the diamagnetic and paramagnetic contributions to the shielding tensors for the different structures. The major electronic difference between protonated **2** and 2-LiCH$_3$ compounds, and unprotonated **4.1**-**4.4** adducts is that the lack of the apical proton in the latter produce a relative destabilization of the carbon p_z electrons. Indeed, in unprotonated compounds the last occupied orbital (HOMO ~ -4.9 eV) (Figure 4.5a) is essentially the apical carbon p_z atomic orbital, while similar molecular orbital for protonated compounds appear deeper in energy (~ -8.0 eV). HOMO orbital in the latter corresponds basically to the degenerate apical carbon p_x and p_y – titanium d bonding orbitals (Figure 4.5b). At the same time, that a destabilization of the carbon p_z – titanium d bonding orbital is

Chapter 4

produced, a stabilization of the corresponding carbon p_z – titanium d antibonding orbital is observed with the removing of the proton. Latter orbital (Figure 4.5c) (~ -1.8 eV) appears energy close respect lowest empty titanium-titanium bonding orbitals (Figure 4.5d) (~ -3.0 - -1.9 eV).
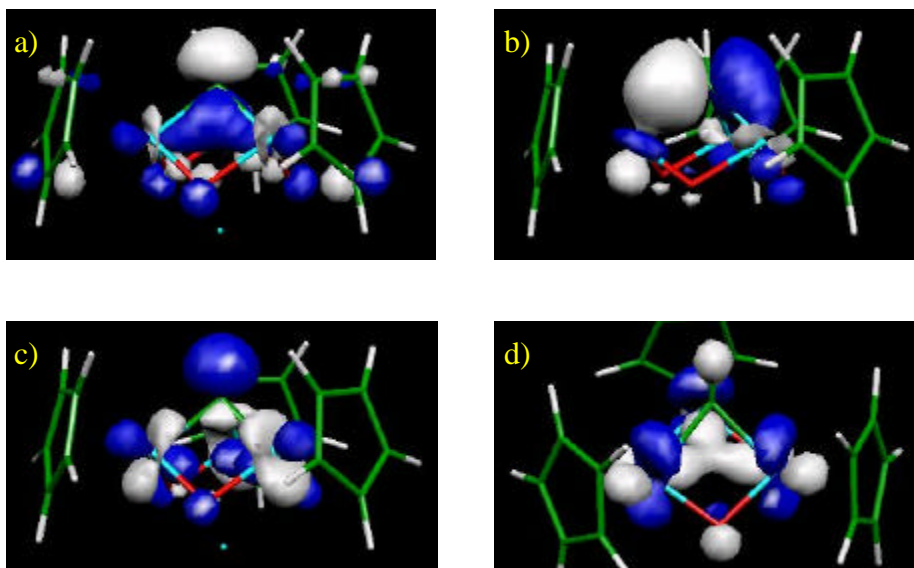

Figure 4.5. *Frontier orbitals for compound* **2**

Difference in the chemical shift for the apical carbon between species is primarily given by the paramagnetic contribution to the shielding tensor, σ_p (see Table 4.7). Paramagnetic contribution results over 200 ppm, in absolute value, bigger in unprotonated species than in the protonated ones. This leads to the chemical shift differences between compounds. The analysis of the paramagnetic tensor can be performed in function of the molecular orbitals of the compounds, in Scheme 4.3 is shown a comparative diagram of the frontier orbitals for protonated and unprotonated compounds. From this analysis we observe how this greater chemical shift in unprotonated compounds can be attributed to two main factors: first to a greater coupling between the high p_z carbon lone pair and the close unoccupied orbitals (+50 ppm), and second, to the diverse couplings of the occupied orbitals with the

relative low in energy vacant antibonding carbon p_z orbital (+80 ppm). This yields to the increment of the paramagnetic contribution respect protonated species.

Protonated especies   Unprotonated especies
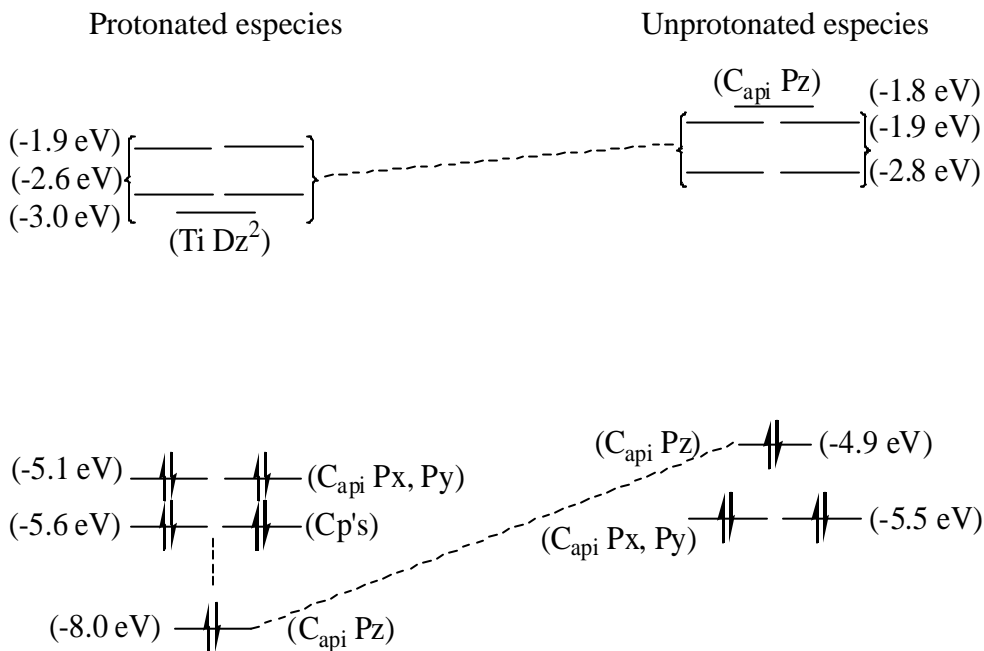
Scheme 4.3. *Orbitals diagram for protonated and unprotonated structures*

4.3   Addition of alkaline earth bis-amides

Alkaline amides and alkyls are often used as selective proton abstraction reagents in organic[27] and metallorganic chemistry.[28] This time the reactions take place on the μ_3-ethylidyne compound $[\{TiCp^*(\mu\text{-}O)\}_3(\mu_3\text{-}CMe)]$ (**3**), where the α-ethylidyne group deprotonation promotes μ-vinylidine – μ-acetylene species. The overall sequence μ-alkylidyne $\rightarrow$ μ-vinylidene $\leftrightarrow$ μ-acetylene has received considerable attention, because it is a model for hydrocarbon rearrangements on metal surfaces.[29]

Chapter 4

The reactivity of unsaturated hydrocarbons on transition metal centers is currently a topic of considerable interest in both homogeneous and heterogeneous catalysis. In particular, the acetylene-vinylidene rearrangement in the coordination sphere of a transition metal has attracted much interest from both experimental and theoretical point of view.[30] While the formation of vinylidene from free acetylene molecules is a strongly endothermic process (184-196 kJ mol^{-1}), the relative energies of the respective isomers change dramatically in the coordination sphere of one or several transition metals. The stabilization of transient species by coordination to transition metals has enabled their chemistry to be studied and their behavior as intermediates to be modeled and understood. This modeling has also been extended to surface chemistry. So the chemistry of unsaturated carbenes, such as vinylidene, allenylidene, and their derivatives, coordinated to one or more metal atoms, has been explored.[31]

Here, we will discuss the peculiar chemical behaviour exhibited by the μ_3-ethylidyne [{TiCp*(μ-O)}$_3$(μ_3-CMe)] (**3**) complex against alkaline earth metal amides and alkyls. We shall study the bonding and structural characteristics of molecular heterometallic oxide cubanes that have a vinylidene-acetylene moiety in one of the corners. Special attention will be paid to the reproduction of the experimental ^{13}C NMR spectra, with the main goal of validating the experimental structures.

Preparation and characterization of oxoheterometallocubane derivatives of alkaline earth metals

The group of Mena has observed very recently that the treatment of the μ_3-ethylidine complex [{TiCp*(μ-O)}$_3$(μ_3-CMe)] (**3**), Cp* = η^5-C$_5$Me$_5$) with alkaline earth bis-amides [M{N(SiMe$_3$)$_2$}$_2$·(thf)$_2$] (M = Mg, Ca, Sr) (thf = tetrahydrofurane) promotes the stepwise deprotonation of the alkylidine moiety μ_3-CCH$_3$ supported by the three titanium atoms; an anion **3$^-$** has been isolated and the ^{13}C NMR spectra determined. Formed incomplete cubane structure [{TiCp*(μ-O)}$_3$(μ_n-C$_2$H$_2$)] (**3$^-$**) leads to the metallic amide to be incorporated at the free vertex of the ligand to give the μ_3-vinylidene and μ_3-acetylene oxoheterometallocubane derivatives [{MN(SiMe$_3$)$_2$(thf)$_x$}{TiCp*(μ-O)}$_3$(μ_n-C$_2$H$_2$)] (M = Mg (x = 0), Ca (x = 1), Sr (x = 1).

When the μ_3-ethyliyne complex [{TiCp*(μ_3-O)}$_3$(μ_3-CMe)] (**3**) reacts with [Mg{N(SiMe$_3$)$_2$}$_2$·(thf)$_2$] (1:1 ratio) in hexane at 180º led to a mixture of the [{Mg(N(SiMe$_3$)$_2$)}{TiCp*(μ_3-CCH$_2$)}] vinylidene (**4.5vin**) and [{Mg(N(SiMe$_3$)$_2$)}{TiCp*(μ_3-HCCH)}] acetylene (**4.5ace**) in a 55:45 ratio, respectively (Scheme 4.4). Under these conditions, both species co-crystallize as red crystals. Attempts to displace the equilibrium and obtain these compounds separately were unsuccessful.

Compounds **4.5** were characterised by standard analytical/spectroscopic techniques. The most notable feature in the ^{1}H and ^{13}C NMR spectra are resonances for the vinylidene-acetylene groups. The ^{13}C NMR spectra reveals a NMR signal for the (μ_3-C$_\alpha$C$_\beta$H$_2$) vinylidene carbons of C$_\alpha$= 385.5 ppm and C$_\beta$= 84.9 ppm, and a second acetylene isomer (μ_3-C$_\alpha$HC$_\beta$H), with signals close to 200 ppm for both carbons.

In addition, treatment of compounds **4.5** with hydrogenated ligands CpH and Ph$_3$COH deprotonates the latter and substitutes the amide ligands (see Scheme 4.4). In the case of the CpH molecule, [{MgCp}{TiCp*(μ-O)}$_3$(μ_3-CCH$_2$)] (**4.6vin**) and [{MgCp}{TiCp*(μ-O)}$_3$(μ_3-CHCH)] (**4.6ace**) adducts were found, in a 62:38 ratio for vinylidene and acetylene species, respectively. The addition of Ph$_3$COH leads to vinylidene [{MgCp}{TiCp*(μ-O)}$_3$(μ_3-CCH$_2$)] (**4.7vin**) and acetylene [{MgCp}{TiCp*(μ-O)}$_3$(μ_3-CHCH)] (**4.7ace**) tautomers, also in a 62:38 ratio.

Mena and co-workers in their systematic preparation of oxoheterometallocubanes observed that the reaction of **3** with the bis-amide [M{N(SiMe$_3$)$_2$}$_2$·(thf)$_2$] (M = Ca, Sr) (1:1 ratio) leads to the formation of complexes [{MN(SiMe$_3$)$_2$(thf)}{TiCp*(μ-O)}$_3$(μ_3-CCH$_2$)] (M = Ca, Sr), for which only the vinylidene isomer is detected. Spectroscopic features of these adducts are resonances at δ = 380.1 ppm and 377.3 ppm for C$_\alpha$, and 82.3 ppm and 81.2 ppm for C$_\beta$, in the ^{13}C NMR spectra for M = Ca and Sr, respectively. The crystal structure of the calcium derivative [{CaN(SiMe$_3$)$_2$(thf)}{TiCp*(μ-O)}$_3$(μ_3-CCH$_2$)] (**4.9vin**) was solved by X-ray diffraction. It revealed a heterometallic cubane structure in which the calcium amide moiety and one tetrahydrofurane molecule are linked to the μ_3-vinylidyne fragment through the three bridging oxygen atoms (see Scheme 4.5).

Chapter 4
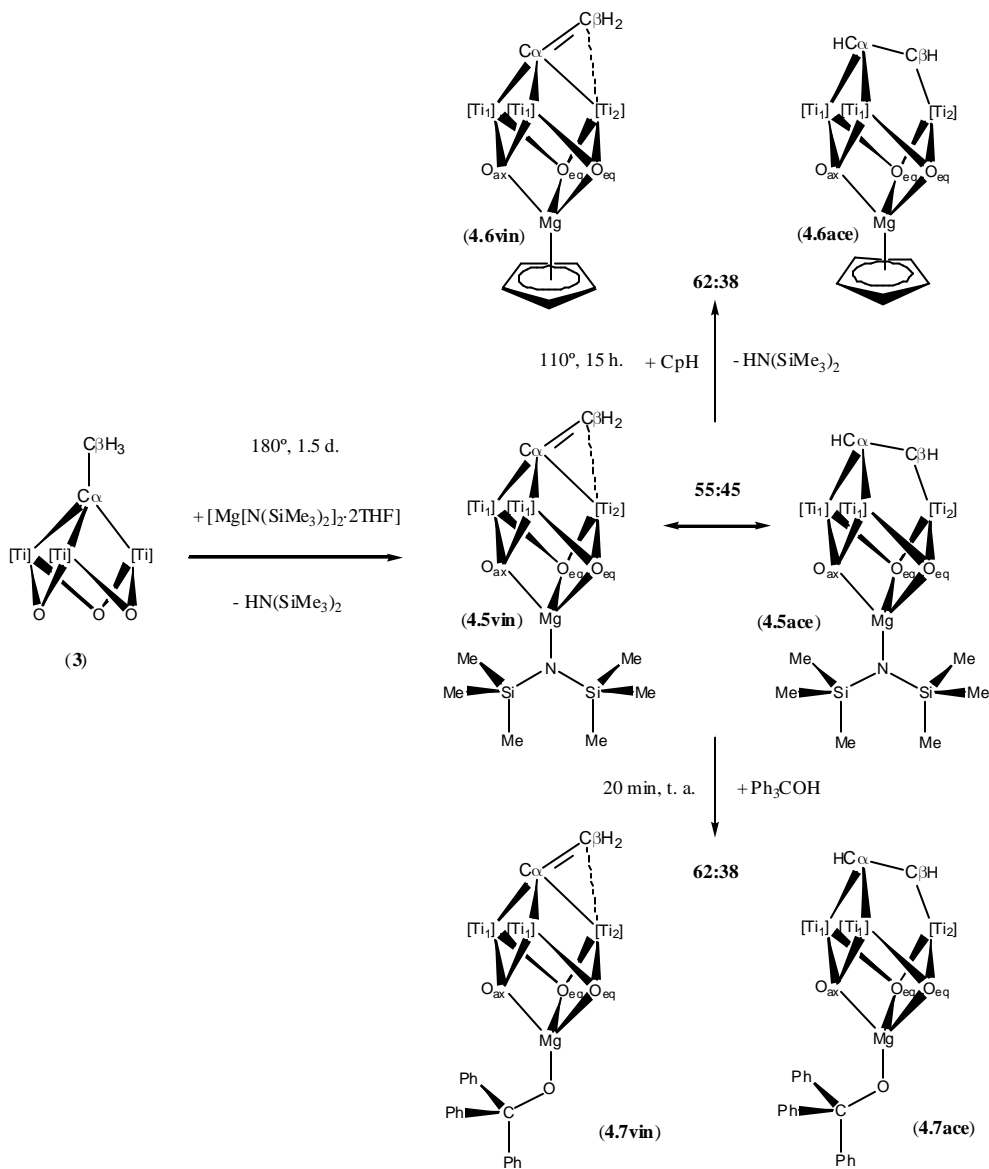
Scheme 4.4. *Reaction of 3 with magnesium bis-amides*
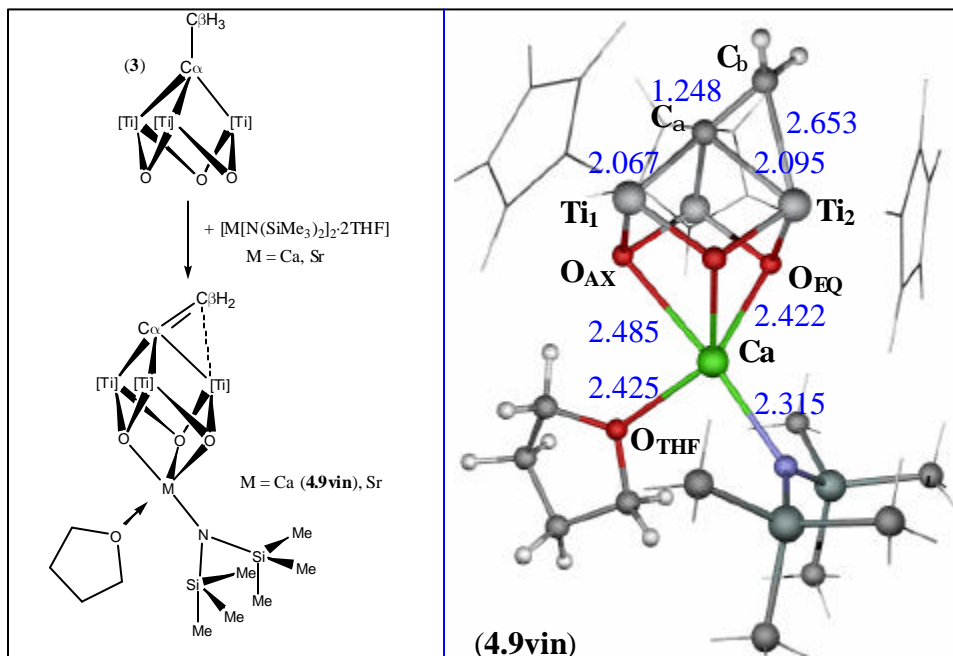
Scheme 4.5. Obtaining and X-ray structure of [{CaN(SiMe₃)₂(thf)}{TiCp*(m-O)}₃(m₃-CCH₂)] adduct, distances in Å

Vinylidene-acetylene equilibrium

DFT calculations were carried out to rationalize the presence of one or more isomers in the formation of the cubane-like complexes shown in Scheme 4.4.

Of particular interest to understand the relative amount of vinylidene and acetylene species is the dependence of the energy of the isomers with the incorporate metal fragment. The comparison of experimental and computed ^{13}C NMR chemical shifts associated to the (μ_n-C_2H_2) alkylidine unit shall allow characterizing unequivocally the structures. In the theoretical study of the series of compounds **3⁻**, and **4.5** to **4.9**, protons in all cases have substituted the methyl and phenyl ligands.

Chapter 4

Table 4.8. *Selected bond lengths (in Å) and bond angles (in degrees) computed for* **3⁻** *,* **4.5, 4.6** *and* **4.7** *vinylidene and acetylene isomers*

	C_a-C_b	C_a-Ti_1	C_a-Ti_2	C_b-Ti_1	C_b-Ti_2	Mg-O_{ax}	Mg-O_{eq}
3vin⁻	1.433	2.033	2.213	3.160	2.237	-	-
3ace-A⁻	1.415	2.130	3.273	2.250	2.060	-	-
3ace-B⁻	1.433	2.061	2.269	2.061	2.269	-	-
4.5vin	1.423	2.040	2.157	3.180	2.248	2.133	2.074
4.5ace-A	1.410	2.120	3.294	2.237	2.055	2.050	2.040
4.5ace-B	1.437	2.050	2.227	2050	2.227	2.155	2.031
4.6vin	1.424	2.039	2.161	3.177	2.250	2.191	2.135
4.6ace-A	1.415	2.109	3.279	2.242	2.053	2.082	2.099
4.7vin	1.424	2.041	2.154	3.174	2.249	2.151	2.078
4.7ace-A	1.413	2.104	3.279	2.246	2.054	2.070	2.043

	C_a-C_b-Ti_2	C_b-C_a-Ti_1	O_{ax}-Mg-O_{eq}	O_{eq}-Mg-O_{eq}
3vin⁻	72.1	130.7	-	-
3ace-A⁻	139.2	75.8	-	-
3ace-B⁻	71.6	114.4	-	-
4.5vin	67.7	132.8	81.0	85.4
4.5ace-A	143.1	75.7	81.1	81.7
4.5ace-B	71.2	114.7	79.7	81.9
4.6vin	67.8	132.7	78.7	82.1
4.6ace-A	141.2	76.2	78.5	78.8
4.7vin	67.6	132.7	79.9	84.8
4.7ace-A	141.4	75.7	80.3	80.6

In order to explore all possible configurations of the μ_n-C_2H_2 unit linked to the Ti_3 core, a preliminary study of all possible vinylidene/acetylene structures was done for anion **3⁻**. While for the vinylidene unit only one structure was found as accessible, **3vin⁻**, for the acetylene unit two coordination types are possible. In general, two types of vibrational spectra

have been observed for acetylene on metal surfaces, often referred as Type A and Type B.[32] In Type A, the molecule is absorbed in a bridge position, and the bonding formally involves four surface metal atoms. In Type B, acetylene is σ-bonded to two metal atoms of a triangle and π-bonded to a third metal (see Scheme 4.6). The relative stability of these two coordination types depends on the metal (Pd, Cu, etc.) and also of the ligand R in substituted acetylenes.[33] The same terminology was used to identify the two coordination modes in present acetylene titanium clusters.

Type A   Type B
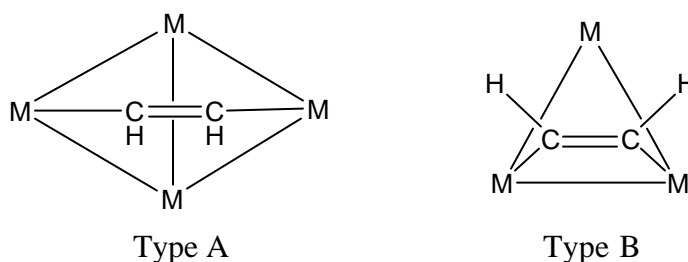
Scheme 4.6. *Acetylene structures on metal surfaces*

A 3D representation of the computed isomers **3vin⁻**, **3ace-A⁻** and **3ace-B⁻** is shown in Figure 4.6. Isomer **3ace-A⁻** has two short Ti_1-C_α bonds at 2.130 Å, while C_α-Ti_2 distance keeps as nonbonding. Instead C_β show bonding distances with the three titanium atoms. Isomer **3ace-B⁻** corresponds almost exactly with structure Type B in Scheme 4.6. Equivalent carbon atoms are middle way between Ti_1 and Ti_2 atoms, the C-Ti_2 distances are 2.061 Å and C-Ti_1 bonds are slightly longer, 2.269 Å. The CCH_2 unit in the vinylidene isomer presents typical ethene structure in which two hydrogen atoms are substituted by two Ti atoms. The relatively short σ−Ti_1-C_α bonds (2.033 Å) suggest a strong interaction between the carbon and the metal (see Table 4.8). The Ti_2-C_α and Ti_2-C_β bonds were also found to be quite short, 2.213 and 2.237 Å, indicative of a strong π interaction between the Ti_2 atom and the C-CH_2 unit. In all three species, the C_α-C_β bond is longer than 1.4 Å, fact that suggests that the formal double bond in the vinylidene and acetylene isomers is partially broken.

Chapter 4

Figure 4.7 shows a representation of the HOMO and HOMO-1 orbitals in **3vin⁻**. Interestingly, the HOMO is an orbital centered at the titanium atoms (Ti_2 30%, Ti_1 20%, C_α 10%, C_β 15%) (see Scheme 4.7). This orbital reveals the presence of a certain coupling between the Ti_2 and C_β through the π^* of the vinylidene unit. The occupation of a metal orbital suggests a partial reduction of the Ti_3 core after deprotonation. This is supported by the Mulliken population analysis that evidences a reduction of the titanium charge (see Table 4.11). This reduction is especially important for Ti_2 atoms which pass from having a nuclear charge of 1.331 in **3** to 1.081 in **3vin⁻**. A similar analysis can be performed for **3ace⁻** isomers; Figure 4.8 shows HOMO and HOMO-1 orbitals for **3ace-A⁻**, HOMO orbital is also centered in the Ti_3 core and illustrates the coupling between the π^* orbital of the acetylene unit and the titanium atoms.
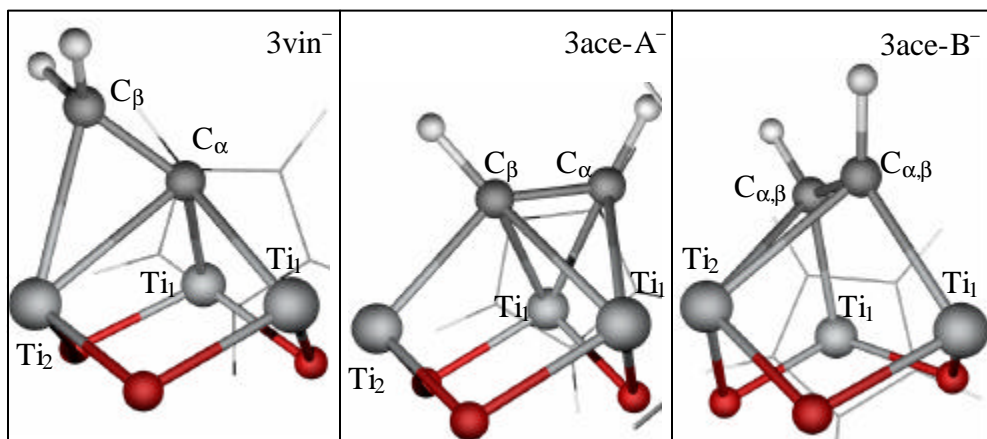
Figure 4.6. *3D representation of the vinylidene and the two rotational acetylene (Type A and B) isomers of [{TiCp*(μ₃-O)}₃(μ₃-C₂H₂)] (3⁻). The structures were optimized without symmetry restrictions and the Me groups in the Cp* ligands were replaced by H atoms*

We calculated the optimal structures for the Mg derivatives **4.5**-**4.9**. In general, the coordination of a Mg ion to the three oxo ligands does not modify significantly the geometries of the titanium cluster. The only noticeable change takes place in the vinylidene isomers. For all three Mg derivatives the formation of the tripodal (O_3-μ_3-Mg) bond is accompanied of

a shortening of the C_α-Ti_2 bond from 2.21 Å in **3**⁻ to 2.16 Å (see Table 4.8). The energy changes are much more important (see Table 4.9). In the incomplete cubane titanium complex **3**⁻, the vinylidene isomer is notably more stable than the acetylene conformers. The relative energy of the complex, when the acetylene is bonded as in type B, is 66.2 kJ mol⁻¹; whereas when the acetylene is coordinated according type A, its relative energy is 85.7 kJ mol⁻¹. In the pseudo-cubane complexes **4.5**-**4.9**, the vinylidene isomers are still the most stable, but the energy differences with the acetylene species are very small (< 5 kJ mol⁻¹). These small energy differences explain that the two species appear with similar ratios as final products in the reactions.
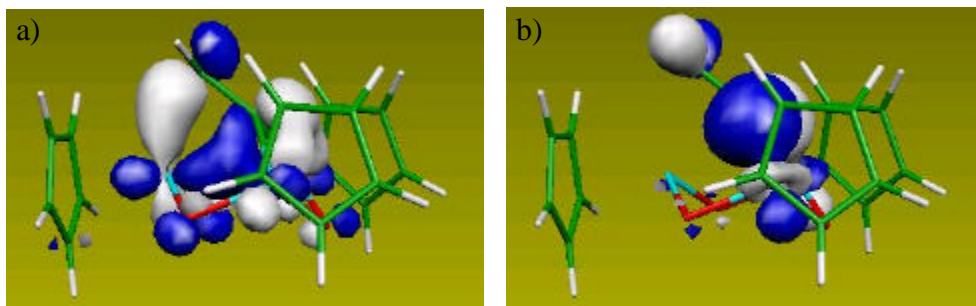
Figure 4.7. *Last occupied orbitals in the vinylidene anion [{TiCp*(m_3-O)}$_3$(m_3-CCH$_2$)]. Left HOMO (70) orbital and right HOMO-1 (69) orbital. Representation made with Molekel program, for a 0.05 contour value*[34]

Table 4.9. *Relative energies in kJ mol⁻¹ for vinylidene and acetylene isomers for 3⁻, 4.5-4.7 compounds*

Compound	Vinylidene	Acetylene (ace-A)	Acetylene (ace-B)
3⁻	0.0	85.7	66.2
4.5	0.0	3.2	23.6
4.6	0.0	4.9	-
4.7	0.0	2.2	-

DFT calculation and analysis of the ^{13}C NMR chemical shifts for C_a and C_b carbons

GIAO-DFT calculations were carried out to unambiguously characterise the chemical shifts in the ^{13}C NMR spectra for the structures given in Schemes 4.4 and 4.5. We start the analysis from the methylidyne complex $[\{TiCp*(\mu_3\text{-}O)\}_3((\mu_3\text{-}CH)]$ (**2**). The apical carbon in **2** shows a signal at 383.2 ppm. As it was discussed in section 4.2, the DFT method is able to reproduce very well this value. In fact, the discrepancy between the experimental and theoretical values is *only* 2.1 ppm. The substitution of the proton by a methyl yields $[\{TiCp*(\mu_3-O)\}_3((\mu_3\text{-}CCH_3)]$ (**3**), and shifts the signal of the $C\alpha$, bonded to the three metal atoms, to 401.7 ppm; whereas the chemical shift for the methyl carbon (C_β) appears at 39.1 ppm. The values computed for **3** match perfectly with the experimental ones. The signals were found at 404.7 and 47.8 ppm, respectively.

The decomposition of the shielding tensor for compound **3** is shown in Table 4.10. We observe how the difference of 356.9 ppm in the chemical shift for α and β carbons arises mainly from a change of -386.4 ppm in the paramagnetic contribution; while diamagnetic contribution experiment a moderate decrease of 29.5 ppm, from C_α to C_β. Strong variations in the charge of the central nucleus (Table 4.11) only produce variations of the order of few ppm in the diamagnetic term, and consequently in the chemical shift. In order to show more in detail this effect, Table 4.12 shows for **3vin⁻** and **3ace-A⁻** anions a detailed analysis of the diamagnetic tensor. This term is divided in a contribution from the core electrons and another form the valence electrons. In **3vin⁻** adduct, C_α with a charge of -0.555 shows a contribution from the valence orbitals of 47.2 ppm, instead C_β with a positive charge of 0.081 has 32.6 ppm; while the core contribution keeps invariant. This example clearly exposes the changes in the diamagnetic term in function of the atom charge. Variations are exclusively due to changes in the valence electrons, and for nuclei different than hydrogen differences are only of few ppm respect the whole range of the nucleus chemical shift, even for strong variations in the nuclear charge.

To explain the increment in the paramagnetic term in C_α respect C_β for the neutral ligand **3** is necessary to analyse the electronic structure of the

compound. Paramagnetic contribution arises from a coupling between occupied and virtual orbitals. The value is inversely proportional to energy gap of the orbitals and it depends on an appropriate symmetry of the implicated orbitals. In this sense, strong paramagnetic contributions require the participation of central atom in the highest occupied orbitals and in the low laying vacant orbitals. In our particular case, those carbon atoms linked to the fully oxidised titanium atoms participate in the first unoccupied orbitals by the interaction with the empty bonding metallic d-orbitals, and also in the last occupied orbitals in carbon metal bonds. Therefore, for structure **3**, C_α, directly bond to the Ti_3 core, experiments a considerable increment in its paramagnetic contribution respect C_β, far from metal atoms; and that no present significant carbon – metal orbital mixing.

The most striking features in the ^{13}C NMR spectra of anions **3**$^-$ are the resonances of the vinylidene moiety ($\mu_3-C_\alpha C_\beta H_2$) at $\delta = 368$ and 76.5 ppm for C_α and C_β, respectively. Again, the theoretical chemical shifts (364 and 70 ppm) are very close to the observed ones. The chemical shifts of the two possible acetylene isomers μ_3-CHCH were also calculated. The values for C_α and C_β are 170 and 139 ppm in isomer ace-A, and near 190 ppm for both carbons in isomer ace-B. The computed chemical shifts are significantly different from those of the vinylidene isomer. These results for the NMR spectra together with the highest instability of the acetylene forms (see Table 4.9) confirm that the deprotonation of **3** yields the vinylidene isomer (μ_3-CCH_2) **3vin**$^-$ as the most abundant product.

At this point it should be useful to halt a moment the analysis of anions **3**$^-$, to show the change in the chemical shift for C_α in compounds **2**, **3** and **3vin**$^-$. For compounds **2** and **3** we compute similar chemical shifts with comparable paramagnetic contributions of -444.2 ppm and -476.5 ppm, respectively. In both cases C_α has similar carbon-titanium distances (2.1 Å) for the three metals atoms and a σ bond with an alkyl unit. We introduce the idea that the slight increase in the paramagnetic term for compound **3** can be understood by the presence of slightly lower vacant orbitals with participation of the C_α for methyl than for proton substituent. Anion **3vin**$^-$ has a paramagnetic contribution of -428.2 ppm lower than both neutral compounds; in this case C_α shows short bonds with two titanium atoms (2.033 Å) and one slightly longer with the other metal (2.213 Å). In this case the diminution in the interaction with the metal atoms is directly

Chapter 4

responsible of the decrease in the paramagnetic contribution. A more detailed analysis, in these terms will be presented hereinafter for the variations in the paramagnetic contributions in the studied compounds.

Table 4.10. ^{13}C *NMR experimental and computed chemical shift and absolute shielding for selected compounds*

| | Experimental Shift | | Computed Shielding | | | | | | | |
| | C_α | C_β | C_α | | | | C_β | | | |
			Para	Dia	Total	Shift	Para	Dia	Total	Shift
3	401.7	39.1	-476.5	254.2	-222.3	**404.7**	-90.1	224.7	134.6	**47.8**
3vin⁻	368	76.5	-428.2	247.0	-181.2	**363.6**	-119.6	232.1	112.5	**69.9**
3ace-A⁻			-223.5	236.2	12.7	**169.7**	-189.8	233.4	43.6	**138.8**
3ace-B⁻			-248.8	237.7	-11.1	**193.5**	-245.0	237.3	-7.7	**190.1**
4.5vin	385.5	84.9	-453.1	248.5	-204.6	**387.0**	-133.1	230.5	97.4	**85.0**
4.5ace-A	206	200	-276.1	236.1	-40.0	**222.4**	-216.4	233.9	17.5	**164.9**
4.5ace-B			-275.5	238.0	-37.5	**219.9**	-275.5	238	-37.5	**219.9**
4.9vin	380	82	-447.1	249.1	-198.0	**380.4**	-131.1	230.4	99.1	**83.3**

Comparing chemical shifts for most stable **3vin⁻** and **3ace-A⁻** structures, we pass from having well differentiated C_α (364 ppm) and C_β (70 ppm) atoms in **3vin⁻** to have more similar and mediated C_α (170 ppm) and C_β (130 ppm) atoms in **3ace-A⁻**. The analysis of the occ-vir paramagnetic term in both cases shows a big delocalization from all occupied and virtual orbitals, otherwise most important contributions arises from couplings between the two last occupied with close vacant orbitals. Table 4.12 shows main occ-vir couplings in **3vin⁻** and **3ace-A⁻** structures; additionally, a schematic diagram of the frontier orbitals is in Scheme 4.7.

C_β in anion **3vin⁻** shows a low paramagnetic term (see Table 4.12); in fact, none coupling between occupied and virtual orbitals exceeds -7 ppm. In correspondence, as show Scheme 4.7, the participation of C_β in the frontier orbitals is small. As we explained for compound **3**, the π interaction of C_β with titanium d-orbitals, reflected in the HOMO orbital (Figure 4.7a), yields small occ-vir couplings. On the other hand, C_α, σ bond to titanium metal as reflect HOMO-1 orbital (Figure 4.7b), shows significant paramagnetic terms from couplings of this orbital with close virtuals. In addition, the

participation of C_α in both occupied and virtual orbitals is evident from Scheme 4.7. These differences in the interactions with the metal atoms explain the separation of the chemical shifts for the carbon atoms.

Paramagnetic contribution for C_α and C_β in **3ace-A**[-] adduct shows an analogous picture. Both carbon atoms appear middle way between C_α and C_β in **3vin**[-] adduct, and small occupied-virtual couplings are observed. Most important terms arises from the coupling between the two last occupied orbitals (Figure 4.8) with close vacant orbitals. In this case both carbon atoms maintain a similar interaction with the Ti_3 core, only as Table 4.11 shows a significant paramagnetic contribution appears for C_α as results of the presence of closer Ti_2 atoms. Last occupied orbitals in **3ace-A**[-] adduct (see Figure 4.8) reflect the lack of clear σ bonding interaction in C_β and the presence of important π interactions for both carbon atoms, which resumes our conclusions for observed chemical shift values.
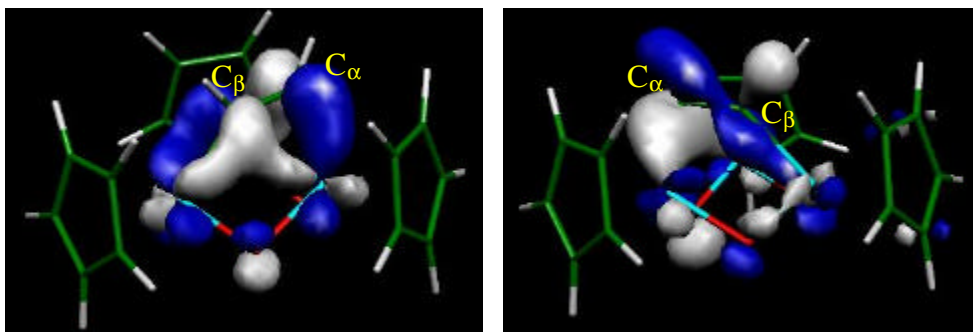
Figure 4.8. *Last occupied orbitals in acetylidene anion [{TiCp*(m_3-O)}$_3$(m_3-CHCH)] (3[-]). Left HOMO (70) orbital and right HOMO-1 (69) orbital*

Table 4.11. *Mulliken charges for **3**, **3vin**[-], **3ace-A**[-], **3ace-B**[-] and **4.5vin***

	C_α	C_β	Ti_1	Ti_2
3	-0.740	0.376	1.331	1.331
3vin[-]	-0.555	0.081	1.289	1.081
3ace-A[-]	-0.305	-0.155	1.259	1.260
3ace-B[-]	-0.222	-0.222	1.357	1.074
4.5vin	-0.573	0.135	1.260	0.984

Chapter 4

Table 4.12. *NMR shielding contributions for adducts* **3vin$^-$** *and* **3ace-A$^-$**

		3vin$^-$				3ace-A$^-$		
		C$_\alpha$		C$_\beta$		C$_\alpha$		C$_\beta$
Total		-181.6		112.3		12.7		43.6
Dia		246.7		232.0		236.1		233.4
	Valence	47.2		32.6		36.7		33.9
	Core	199.4		199.4		199.4		199.4
Para		-428.3		-119.7		-223.5		-189.8
	Occ-Vir	-574.2	Occ-Vir	-339.1	Occ-Vir	-400.9	Occ-Vir	-394.4
	69-71	-21.7	69-71	-7.2	69-72	-11.4		
	69-73	-20.4			69-75	-12.6		
	69-89	-19.1						
	70-74	-10.3						
	70-82	-13.5						
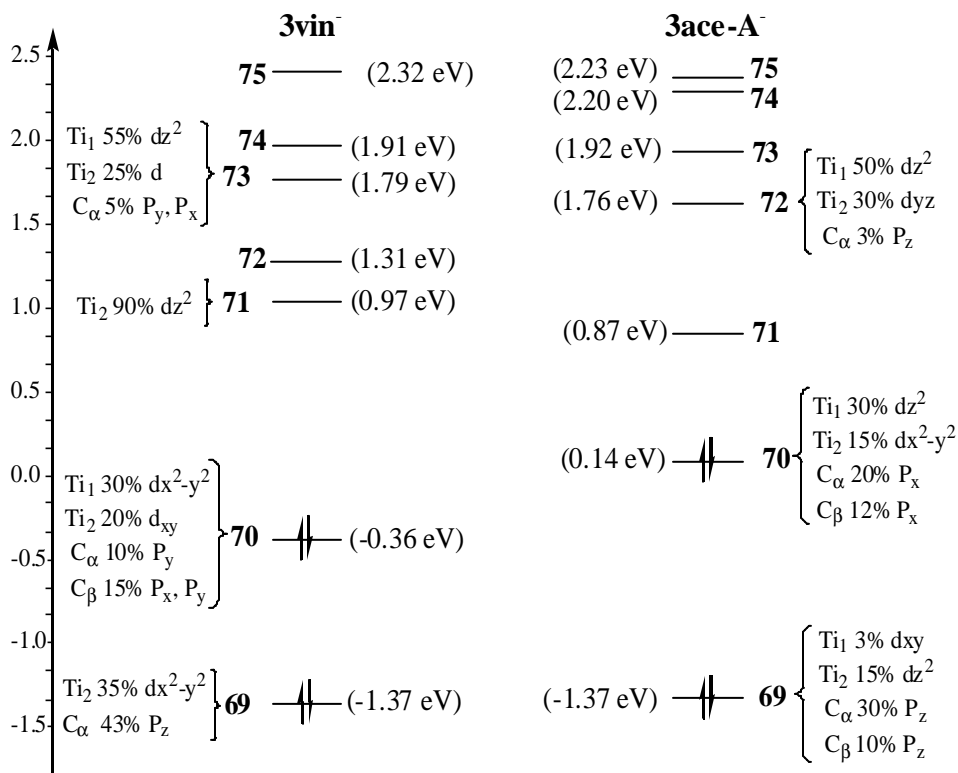
Scheme 4.7. *Schematic orbital's structure for* **3vin$^-$** *and* **3ace-A$^-$** *adducts*

212

Let us now to discuss the effect of the coordination of a metal group to 3^-. As shown above, the group of Alcalà de Henares has characterised some cubane clusters corresponding to the formal union of anion 3^- with different M^+L_n cations. Complex **3** reacts with $Mg\{N(SiMe_3)_2\}_2.thf_2$ yielding a mixture of vinylidene and acetylene complexes in a ratio 45:55, complexes **4.5** in Scheme 4.4. The ^{13}C NMR spectra are different for 3^- and **4.5**. In the latter, two series of lines are observed: one corresponding to the vinylidene isomer with values of δ of 385.5 (C_α) and 84.9 ppm (C_β); and a unique line close to 200 ppm that was associated to the acetylene tautomer. The ^{13}C NMR chemical shifts of 387 and 85 ppm computed for the vinylidene structure **4.5vin** almost coincide with the observed spectra. However, for the most stable (**ace-A**) acetylene structure **4.5ace-A**, we computed two different chemical shifts; for the carbon atom linked to two Ti atoms, C_α, δ is 222 ppm and for the carbon atom linked to only one Ti atom, C_β, $\delta = 162$ ppm. The discrepancy between experimental and theoretical values may be easily rationalised if we consider that the carbons alpha and beta may exchange through the rotation mechanism shown in Figure 4.9. In fact, this corresponds to the transformation of coordination type A (isomer **ace-A**) into coordination type B (isomer **ace-B**). The small energy difference of 23.6 kJ between the two rotational isomers yields an equivalence of C_α and C_β atoms, with different chemical shifts that collapses in a common signal at high temperatures. Note that the average of the two computed values of 222 and 162 ppm for isomer **ace-A** in complex **4.5** is 192 ppm, only 10 ppm smaller than the experimental value of 202 ppm. In isomer **ace-B**, the two carbon atoms are equivalent by symmetry and the resonance occurs at 220 ppm.
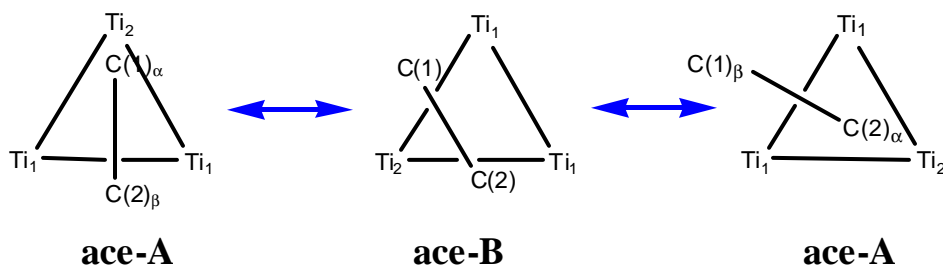
Figure 4.9. *Fluxionally of the Acetylene unit in complexes* **4.5**

Chapter 4

From the analysis of the theoretical shielding tensor (Table 4.10), we observe that the pass from **3vin⁻** to **4.5vin** adduct only implicate a small displacement of the chemical shifts. The metal fragment addition does not suppose significant changes in the carbon titanium interactions that maintain a similar electronic structure and oxidation states, fact reflected by similar diamagnetic and paramagnetic contributions to the shielding tensor.

For the calcium adduct $[\{CaN(SiH_3)_2(thf)\}\{TiCp^*(\mu-O)\}_3(\mu_3-CCH_2)]$ (**4.9**) the ^{13}C NMR spectra suggest the unique presence of the (μ_3-CCH$_2$) vinylidene isomer, in contrast with the related **4.5**-**4.7** species. For complex **4.9**, the (μ_3-CHCH) acetylene isomer type A resulted clearly disfavored by 22 kJ mol^{-1}. This different conduct in relation to the Mg derivatives seems related to the presence of the **thf** molecule in the coordination sphere of the Ca metal. In fact, after removing this extra ligand, the energy gap between the vinylidene and acetylene isomer is reduced to 10 kJ mol^{-1}. So, the acetylene/vinylidene equilibrium is clearly influenced by the metal and its coordination. We can observe in Table 4.8 that the vinylidene isomers present longer alkaline earth metal - oxygen distances, this bond enlargement is which clearly favors the introduction of additional ligands in the vinylidene adducts.

Once more, the ^{13}C NMR chemical shifts computed for C_α and C_β in complex **4.9vin** (Table 4.10) almost coincide with the observed values. This fact is very significant if we take in consideration that the X-ray and the DFT geometries for the vinylidene isomer of **4.9** present important discrepancies (see Figure 4.10). We computed a C_α–C_β bond length of 1.429Å (similar distances were found for all the Mg derivatives, Table 4.8), while the X-ray value is 1.25Å (see Scheme 4.5). This discrepancy is been reanalyzed in the laboratory and also theoretically, nevertheless two facts suggest that the theoretical value is probably correct: 1) a bond distance shorter than a typical C-C double bond and 2) the good coincidence between the observed and computed ^{13}C chemical shifts. Indeed, the chemical shifts are, in general, very sensitive with the bond distances,[35] and therefore it is not easy to explain how a DFT calculation is able to reproduce the chemical shifts from a very incorrect geometry.
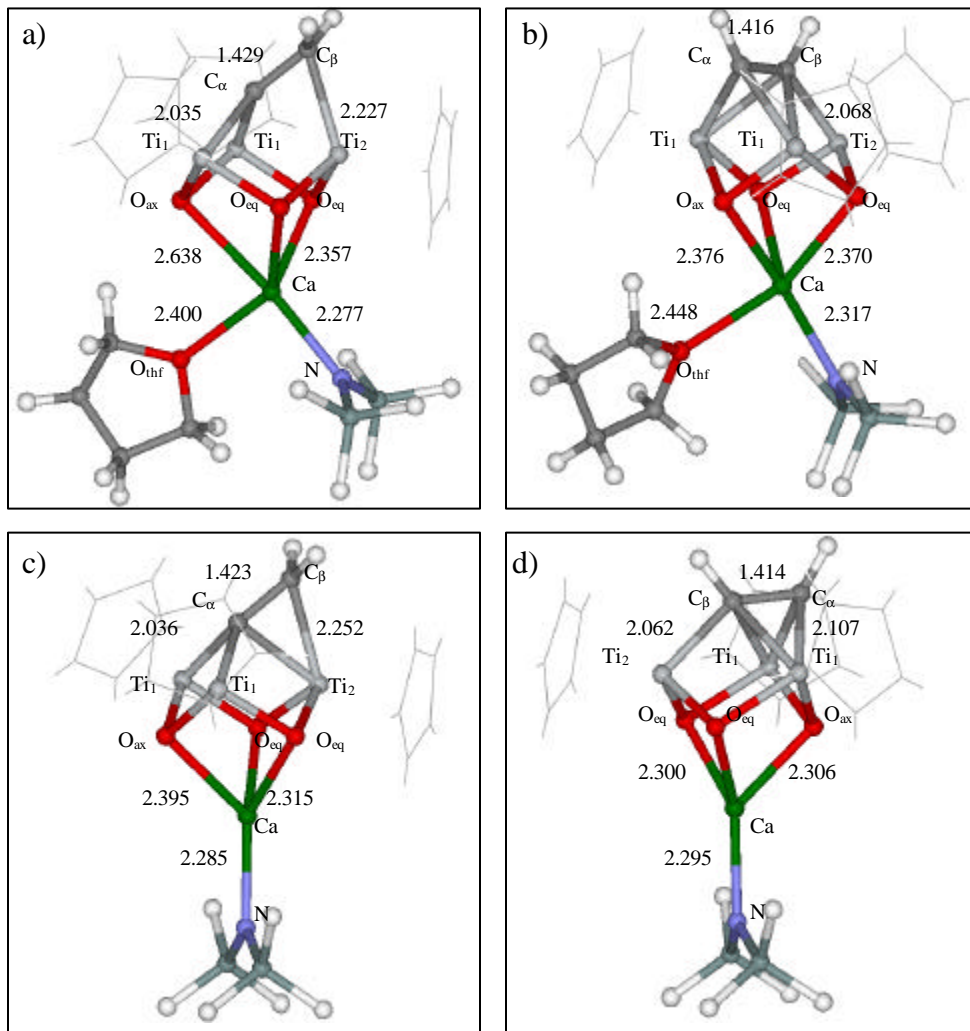
Figure 4.10. *DFT structures for complexes: [{CaN(SiMe$_3$)$_2$(thf)}{TiCp(μ-O)}$_3$(μ_3-CCH$_2$)] (a), [{CaN(SiMe$_3$)$_2$(thf)}{TiCp(μ-O)}$_3$(μ_3-CHCH)] (b), [{CaN(SiMe$_3$)$_2$}{TiCp(μ-O)}$_3$(μ_3-CCH$_2$)] (c) and [{CaN(SiMe$_3$)$_2$}{TiCp(μ-O)}$_3$(μ_3-CHCH)] (d). Distances in Å*

215

Chapter 4

References and notes

1 a) R. C. Haushalter, *J. Chem. Soc., Chem. Commun.* **1987**, 1566.
   b) K. H. Lii, R. C. Haushalter, C. J. O´Connor, *Angew. Chem., Int. Ed. Engl.* **1987**, *26*, 549.

2 a) G. Süss-Fink, L. Plasseraud, V. Ferrand, S. Stanislas, A. Neels, H. Stockli-Evans, M. Henry, G. Laurenczy, R. Roulet, *Polyhedron* **1998**, *17*, 2817.
   b) M. Ichikawa, W. Pan, Y. Imada, M. Yamaguchi, K. Isobe, T. Sido, *J. Mol. Catal.* **1996**, *107*, 23.

3 R. Andrés, M. Galakhov, A. Martín, M. Mena, C. Santamaría, *Organometallics* **1994**, *13*, 2159.

4 M. H. Chisholm, D. L. Clark, J. Hampden-Smith, D. H. Hoffman, *Angew. Chem. Int. Ed. Engl.* **1989**, *28*, 432.

5 D. Seyferth, *Adv. Organomet. Chem.* **1976**, *14*, 97.

6 a) R. D. Kemmitt, D. R. Russel, *"Comprehensive Organometallic Chemistry"*, Vol. 5; Eds.: G. Wilkinson, F. G. A. Stone, E. W. Abel; Pergamon, Oxford **1982**, p. 162.
   b) M. I. Bruce, *ibid.*, Vol. 4, p. 843.
   c) J. B. Keister, *"Encyclopedia of Inorganic Chemistry"*, Ed.: R. B. King, Wiley, Chichester, **1994**, p. 3348.
   d) M. Akita, *"Comprehensive Organometallic Chemistry II"*, Vol. 7, Eds.: G. Wilkinson, F. G. A. Stone, E. W. Abel, Pergamon, Oxford **1995**, p. 259.
   f) C. E. Barnes, *ibid.* **1995**, *8*, 419.

7 D. S. Richeson, S.-W. Hsu, N. H. Fredd, G. V. Dugne, K. H. Theopold, *J. Am. Chem. Soc.* **1986**, *108*, 8273.

8 R. Andrés, P. Gómez-Sal, E de Jesús, A. Martín, M. Mena, C. Yélamos, Angew. Chem. Int. Ed. Engl. **1997**, *36*, 115.

9 R. Andrés, M. Galakhov, A. Martín, M. Mena, C. Santamaría, *J. Chem. Soc. Chem. Comun.* **1995**, 551.

10 a) G. A. Somorjai, *"Introduction to Surface Chemistry"*, Wiley, New York, **1994**, 400.
   b) B. C. Gates, *"Catalytic Chemistry"*, Wiley, New York, **1992**.
   c) F. Zaera, *Chem. Rev.* **1995**, *95*, 2651.
   d) B. E. Bent, *ibid.* **1996**, *96*, 1361.

11 a) H. H. Kung, *"Transition Metal Oxides Surface Chemistry and Catalysis"*, Elsevier, Amsterdam, **1989**.
   b) M. A. Barteau, *Chem. Rev.* **1996**, *96,* 1413.
   c) P. M. Maitlis, H. C. R. Long Quyoum, M. L. Turner, Z-Q. Wang, *J. Chem. Soc. Chem. Commun.* **1996**, 1.

12 R. Andrés, M. Galakhov, M.-P. Goméz-Sal, A. Martín, M. Mena, C. Santamaría, *Chem. Eur. J.* **1998**, *4*, 1206.

[13] a) B. C. Gates, *Chem. Rev.* **1995**, *95*, 511.

b) K. I. Hadjiivanov, D. G. Klissurski, *Chem. Soc. Rev.* **1996**, 61.

c) J. Evans, *Chem. Soc. Rev.* **1997**, 11

d) A. Hu. K. H. Neyman, M. Staufer, T. Belling, B. C. Gates, N. Rösch, J. *Am. Chem. Soc.* **1999**, *121*, 4522.

[14] A. Abarca, M. Galakhov, P. Gómez-Sal, A. Martín, M. Mena, J.-M. Poblet, C. Santamaría, J. P. Sarasa, *Angew. Chem. Int. Ed.* **2000**, *39*, 534.

[15] C. S. Bahn, A. Tan, S. Harris, *Inorg. Chem.* **1998**, *37*, 2770.

[16] R. H. Herber, A. E. Smelkinson, *Inorg. Chem.* **1978**, *17*, 1023.

[17] R. Andrés, *PhD Thesis*, Universidad de Alcalá, Madrid, **1995**.

[18] N. Poonia, A. V. Bajaj, *Chemical Reviews* **1979**, *79*, 389.

[19] M. García-Castro, J. Gracia, A. Martín, M. Mena, J. M. Poblet, J. P. Sarasa, C. Yélamos, In press.

[20] J. Gracia, A. Martín, M. Mena, M. C. Morales-Varela, J-M. Poblet, C. Santamaría, *Angew. Chem. Int. Ed.* **2003**, *42*, 927.

[21] S. C. Lawrence, M. E. G. Skinner, J. C. Green, P. Mountford, *Chem. Commun.* **2001**, 705.

[22] a) L. Cai, B. M. Segal, J. R. Long, M. J. Scott, R. H. Holm, *J. Am. Chem. Soc.* **1995**, *117*, 8863.

b) C. Goh, B. M. Segal, J. Huang, J. R. Long, R. H. Holm, *J. Am. Chem. Soc*. **1996**, *118*, 11844.

c) J. Huang, C. Goh, R. H. Holm, *Inorg. Chem.* **1997**, *36*, 356.

d) R. Hernandez-Molina, D. N. Dybtsev, V. P. Fedein, M. R. J. Elsegood, W. Clegg, A. G. Sykes, *Inorg. Chem.* **1998**, *37*, 2995.

e) R. Hernandez-Molina, M. N. Sokolov, A. G. Sykes, *Acc. Chem. Res*. **2001**, *34*, 223.

f) M. García-Castro, A. Martín, M. Mena, A. Pérez-Redondo, C. Yélamos, *Chem. Eur. J*. **2001**, *7*, 647.

[23] M. García-Castro, A. Martín, M. Mena, A. Pérez-Redondo, C. Yélamos, *Chem. Eur. J.* **2000**, *6*, 647.

[24] a) K. Morokuma, *J. Chem. Phys.* **1971**, *55*, 1236.

b) K. Kitaura, K. Morokuma, *Int. J. Quantum. Chem.* **1976**, *10*, 325.

c) T. Ziegler, A. Rauk, *Teor. Chim. Acta* **1977**, *46*, 1.

d) T. Ziegler, A. Rauk, *Inorg. Chem.* **1979**, *18*, 1558.

[25] G. Schrekenbach, T. Ziegler, *J. Phys. Chem.* **1995**, *99*, 606.

[26] T. Helgaker, M. Jaszunski, K. Ruud, *Chem. Rev.* **1999**, *99*, 293.

[27] a) G. Lessene, R. Trípoli, P. CAzeau, C. Biran, M. Bordeau, *Tetrahedron Letters* **1999**, *40*, 4037.

b) K. W. Henderson, W. J. Kerr, J. H. Moir, *Chem. Commun.* **2000**, 479.

[28] a) J. C. Peters, A. L. Odom, C. C. Cummins, *Chem. Commun.* **1997**, 1995.

b) J. B. Greco, J. C. Peters, T. A. Baker, W. M. Davis, C. C. Cummins, G. Wu, *J. Am. Chem. Soc.* **2001**, *123*, 5003.

[29] a) M. I. Bruce, *Chem. Rev.* **1998**, *98*, 2797.

b) F. Zaera, Chem. Rev. **1995**, *95*, 2651.

[30] a) R. Stegmann, G. Frenking, *Organometallics* **1998**, *17*, 2089.

b) R. L. Hayes, E. Fattal, N. Govind, E. A. Carter, *J. Am. Chem. Soc.* **2001**, *123*, 641.

c) F. De Angelis, A. Sgamellotti, N. Re, *Organometallics* **2002**, *21*, 2715.

[31] F. Minttendorfer, C. Thomazeau, P. Raybaud, H. Toulhoat, *J. Phys. Chem. B* **2003**, *107*, 12287.

[32] A. Clotet, G. Pacchioni, *Surface Science* **1996**, *346*, 91.

[33] A. Valcárcel, A. Clotet, J. M. Ricart, F. Delbecq, P. Sautet, *Surface Science* **2004**, *549*, 121.

[34] *MOLEKEL 4.0,* P. Flükiger, H.P. Lüthi, S. Portmann, J. Weber, *Swiss Center for Scientific Computing,* Manno (Switzerland), **2000**.

[35] S. K. Wolff, T. Ziegler, E. van Lenthe, E. J. Baerends, *J. Chem. Phys.* **1999**, *110*, 7689.

5

Dinuclear cyclopentadienyl molybdenum

complexes with bridging sulphide ligands

A large number of molecular transition-metal complexes with either terminal or bridging sulphide ligands have been reported. The many possible coordination modes available for sulphide ligands[1] have been utilized in the development of synthetic routes to metal-sulphur clusters with varied structural feature. The structural and electronic flexibility provided by one or more sulphide atoms ligated to a transition metal permit a large catalytic activity. The presence of sulphur ligands coordinated to molybdenum atoms in enzyme systems and in heterogeneous desulphurisation catalysts[2,3] has led to the investigation of a large range of molybdenum sulphur complexes.[4] In particular dinuclear cyclopentadienyl molybdenum complexes with bridging sulphide ligands are one of the families who posses a wide structural flexibility and the interesting property of activating molecular hydrogen. The ability of sulphide complexes to activate molecular hydrogen and catalyze substrate reduction by hydrogen is particularly relevant in the chemistry of the hydrotreating catalysts.

After a short introduction to dinuclear cyclopentadienyl molybdenum compounds, second part of this section is dedicated to the analyse the structural and electronic features of the [CpMoS$_2$]$_2$ adducts and related compounds. The last third section provides a theoretical analysis of the mechanistic for the molecular hydrogen activation and substrate reduction by molybdenum sulphide compounds.

5.1   Introduction

5.2   [(CpMo)-S$_2$]$_2$ core complexes

5.3   Hydrogen activation by cationic dinuclear (μ-sulphido) molybdenum complexes

---

Chapter 5

5.1   Introduction

Compounds with general formula $[Cp*MS_4M'Cp*]$[a] display a remarkable variety in structure; large number of bimetallic complexes of the $[Cp*MS_2]_2$ type have been synthesized and structurally characterized. These compounds are interesting for their reactivity and their structural properties. They have been used as building blocks for the synthesis of metal-sulphur clusters,[5,6] with particular interest for cubane-type complexes[7,8] owing to the relevance of the latter to metalloenzymes. As example, the surroundings for molybdenum atom in some Fe-Mo cubanes are very similar to the suggested for this element in nitrogenase enzymes.[9]

These $[Cp*MS_2]_2$ compounds exhibit a large variety of structures.[5] Depending on the nature of the metal (Ti,[10] V,[11] Cr,[12] Mo,[13] Fe,[14,15] Ru,[16] Co[15a]) the S_4 unit may involve terminal or bridged sulphide ligands, and/or disulphide bridging ligands with a μ-η^1, μ-η^2 or μ-(η^1,η^2) coordination mode; some of them are shown in Figure 5.1.[17,18] In structures (**a-c**) two Cp*Mo fragments are bridged by four S atoms, $2[\mu$-η^2-$S_2]$; two of which have undergone the μ-$\eta^2 \rightarrow \mu$-η^1 ligand reorientation in (**d**), $[\mu$-η^2-S_2, μ-η^1-$S_2]$[14b]; in isomers (**e-f**) two of the S atoms have transformed into terminal ligands, $[\mu$-$S_2]$. Finally, it appears complex (**g**) where the coordination modes of the S_2 units have been characterized as $2[\mu$-(η^2,η^1)-$S_2]$.[14c]

Conversions between these isomers use to involve formal electron transfer between the metals and ligands which is potentially relevant to biology and catalysis. Of particular interest results the dimeric complex $[Cp*MoS_2]_2$ (**5.1**), which exhibits interesting structural and reactivity patterns. Given the richness in coordination, it is not surprising that several isomers of the title compound are known. For Mo atom, isomers (**b**)[13c] and (**f**)[13a,19] have been structurally characterized, (**a**)[20] and (**e**)[19,21] have been postulated on the basis of spectroscopic data and reactivity patterns. (**c**), (**d**) and (**g**) are not yet identified, although analogues for different metals (V, Cr, Ru, Fe, Co) are known.

---

[a] Cp* ligand experimentally go from totally substituted (C_5R_5) (R = Methyl or any Alkyl in general) to (C_5H_5) ligand, computationally in spite of simplicity only (C_5H_5) ligand is treated.
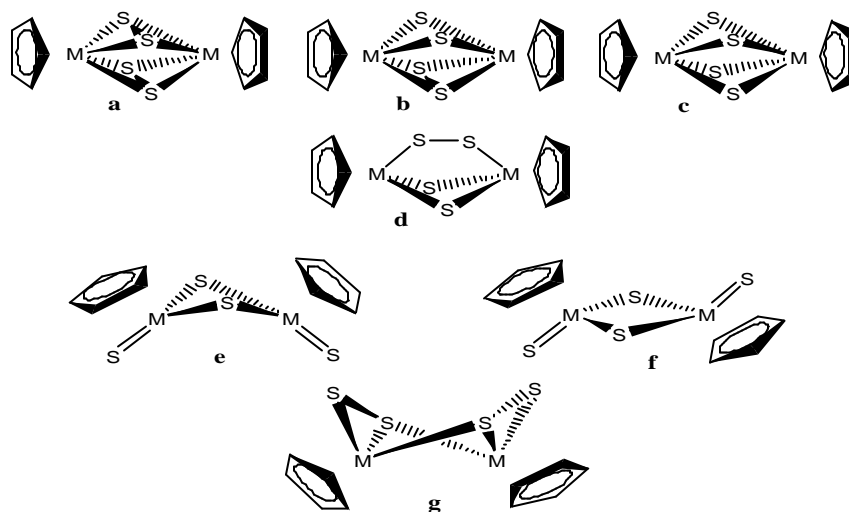
Figure 5.1. *Schematic drawing of the [Cp*MS$_2$]$_2$ adducts*

The possible structures for the [Cp*MS$_2$]$_2$ species (Figure 5.1) can be rationalized in terms of the valence electrons available to the M$_2$-S$_4$ core; in this sense, changes in the adduct charge or the addition of new ligands to the M$_2$-S$_4$ core strongly influences the molecule arrangement. Together with [Cp*MoS$_2$]$_2$ (**5.1**) specie, the [Cp*MoS$_2$]$_2^{2+}$ cation, neutral [(Cp*Mo)$_2$(S$_2$CH$_2$)S$_2$] (**5.2**), [(Cp*Mo)$_2$(S$_2$CH$_2$)SSR]$^+$ (**5.3**) (R = H, Me, C$_4$SH$_3$) cations and [(Cp*Mo)$_2$(S$_2$CH$_2$)SHSR] (**5.4**) (R = H, Me, C$_4$SH$_3$) adducts are analysed in the second part of this chapter.

The reactions of sulphide-bridged molybdenum complexes with hydrogen play a key role in the reduction of many organic substrates,[22] and they may be relevant to the hydrogen activation processes that take place on the sulphide surfaces of hydro-desulphuration catalysis;[23] the hydrodesulphurization of organosulphur compounds is an important industrial process used in the purification of petroleum feedstocks.[24] For these reasons, they have aroused the interest of scientific community in establishing the mechanism for this unusual hydrogen activation process. The mechanisms of the reactions are not well understood, although it is generally thought that a MoS$_2$ phase is the catalytic site for the hydrodesulphurization reaction. Mechanistic proposal have suggested that

the reaction proceeds through three elementary steps:[25] (1) dissociative chemisorption of H_2 on sulphide ligands to form SH ligands, (2) adsorption of the organosulphur compound at a vacant coordination site of the molybdenum, (3) hydrogen atom transfer from SH ligand to the adsorbed organosulphur compound accompanied by carbon-sulphur bond cleavage in this molecule. The synthesis and characterization of discrete hydrosulphido complexes of molybdenum provides the opportunity to obtain fundamental information on the chemical properties of S-H ligands and, in particular, on their ability to function as a source of hydrogen in substrate reduction.

Theoretical calculations can introduce new dates in this area, especially in some aspects of the reactions inaccessible by experimental techniques; and at the same time, the modelization of these systems is useful to test different theoretical methods. In the second part of present chapter DFT calculations at the pure BP general gradient approximation[26] were made to study the structure of the $[(CpMo)-S_2]_2$ core complexes. In the third part, starting from the ability of the method to reproduce the electronic structure of these bimetallic compounds, DFT calculations at the BP and hybrid B3LYP level[27] are used to elucidate some aspect points of the hydrogen activation process catalysed by these compounds.

5.2   Structures available to the $[(CpMo)-S_2]_2$ core complexes

In the experimental work reported by Brunner et al. on the reaction of S_8 with $\left[C_5Me_5(CO)_2Mo\right]_2$, three products of general formula $\left[(C_5Me_5)MoS_2\right]_2$ (**5.1**) were obtained, each of which has been isolated.[13c] After 22 h a dark blue complex, **5.1b**, is isolated together with a green-brown complex, **5.1e**. No blue product, **5.1b**, remains after 3 days, but **5.1e** together with a dark brown complex, **5.1f**, is formed.

Figure 5.2 shows the computed **5.1a-g** structures, a staggered arrangement of the unsubstituted cyclopentadienyl ligands (Cp) is used in almost all cases; but procuring to do good use of symmetry, isomers **5.1e** and **5.1g** were modelled in an eclipsed arrangement. Therefore, the three obtained complexes **5.1b**, **5.1e**, and **5.1f** were modelled within C_s, C_{2v} and C_{2h}

symmetry constraints respectively. Not observed **5.1a** C_{2h}, **5.1c** C_{2h}, **5.1d** C_{2v} and **5.1g** C_2 species were also computed for exploring and contrasting the alternatives in the $[(CpMo)-S_2]_2$ coordination sphere.
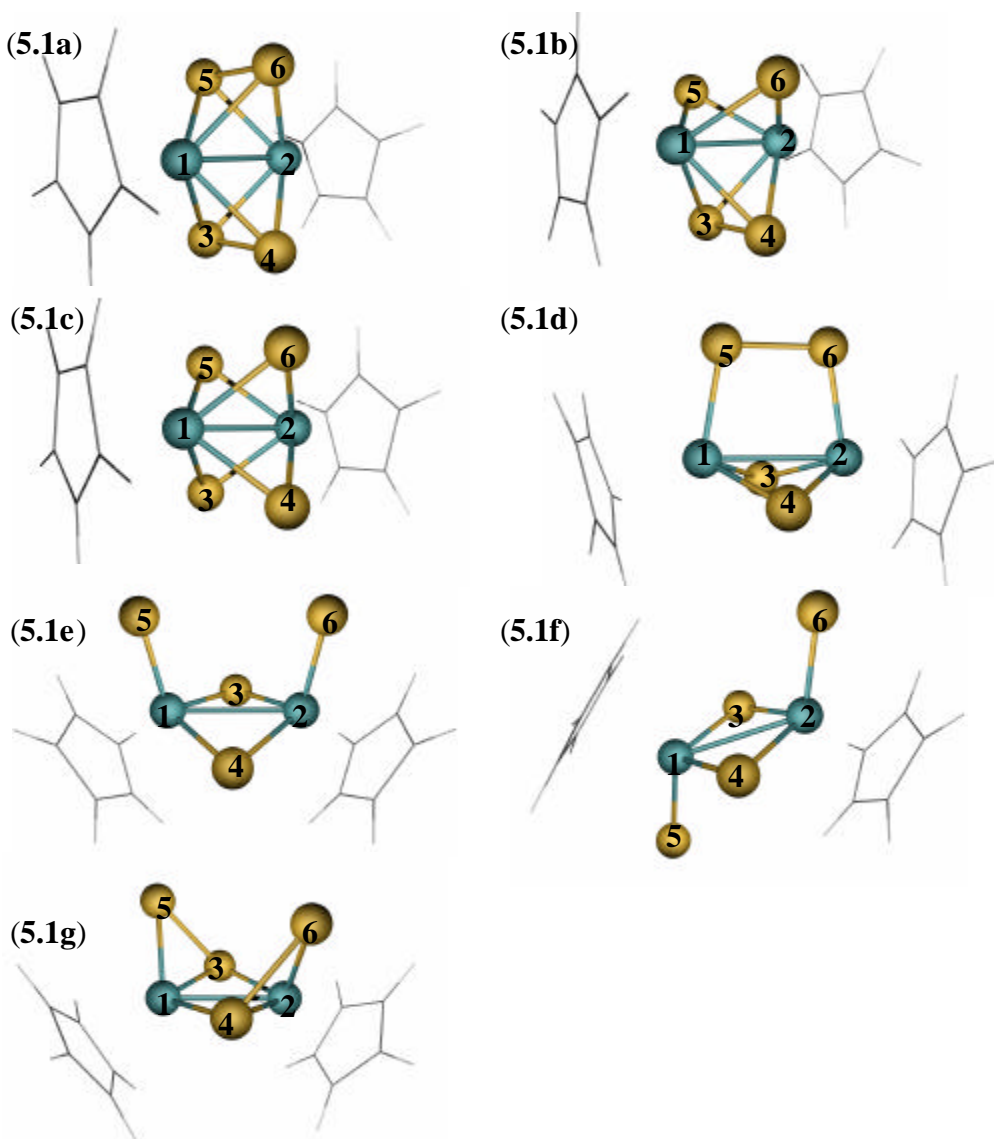

Figure 5.2. *Studied closed (**a-d**) and open (**e-g**) structures for the* $[Cp*MoS_2]_2$ *compound*

Chapter 5

Table 5.1. *Selected computed and experimental distances (Å) for* $[Cp^*Mo(m\text{-}h^2\text{-}S_2)]_2$ *(5.1a-c),* $[(Cp^*Mo)_2(m\text{-}h^2\text{-}S_2)(m\text{-}h^1\text{-}S_2)]$ *(5.1d),* $[syn\text{-}(Cp^*Mo)_2(m\text{-}S_2)(m\text{-}h^2\text{-}S_2)]$ *(5.1e),* $[trans\text{-}(Cp^*Mo)_2(m\text{-}S_2)(m\text{-}h^2\text{-}S_2)]$ *(5.1f) and* $[(Cp^*Mo)_2\{m\text{-}(h^2\text{-}h^1)\text{-}S_2\}_2]$ *(5.1g) complexes*

5.1	a	$b_{(exp)}$[a]	b	c	d
$Mo_1\text{-}Mo_2$	2.755	(2.599)	2.638	2.652	3.064
$Mo_1\text{-}S_3$	2.478	(2.447)	2.478	2.392	2.330
$Mo_1\text{-}S_5$	2.478	(2.361)	2.381	2.392	2.260
$S_3\text{-}S_4$	2.118	(2.095)	2.152	2.816	3.297
$S_5\text{-}S_6$	2.118	(3.098)*	3.152*	2.816	2.132
$S_3\text{-}S_5$	3.527*	(3.054)*	3.047*	2.816	3.433*

5.1	$e_{(exp)}$[b]	e	$f_{(exp)}$[c]	f	g
$Mo_1\text{-}Mo_2$	(2.896)	2.924	(2.911)	2.951	2.427
$Mo_1\text{-}S_3$	(2.311)	2.333	(2.309)	2.331	2.378
$Mo_1\text{-}S_5$	(2.147)	2.166	(2.145)	2.178	2.506
$S_3\text{-}S_4$	(3.528)*	3.574*	(3.576)*	3.608*	3.854*
$S_5\text{-}S_6$	(3.731)*	3.782*	-	-	3.481*
$S_3\text{-}S_5$	-	-	-	-	2.114

[a] *Experimental parameters taken from ref. 13c, eclipsed* $[(C_5Me_5)MoS_2]_2$ *compound*

[b] *Experimental parameters taken from ref. 21,* $[(Ethyltetramethyl\text{-}Cp)MoS_2]_2$ *eclipsed compound*

[c] *Experimental parameters taken from ref. 19, compound* $[(Cp)MoS_2]_2$ *staggered*

* *Nonbonded distances*

Main theoretical parameters together with available experimental ones are reported in Table 5.1. Overall, the agreement between theoretical and experimental values is very satisfactory. All the distances are overestimated; however, the differences are less than 0.040 Å. We remember that is noteworthy that the X-ray structures were characterised for complexes with different substituted $Cp*$ ligands and that they also exhibit a mixture of eclipsed and staggered conformations.

Together with the **5.1b** specie, two isomers **5.1a** and **5.1c** (for metals different from Mo) have been obtained as closed structures with $(\boldsymbol{m}\text{-}\boldsymbol{h}^2\text{-S}_2)$ coordination mode for the S_2 units. For Mo atom, isomer **5.1b** results the most stable of the closed structures by 86 kJ mol^{-1} and 27 kJ mol^{-1} respect **5.1a** and **5.1c**, in that order (see Table 5.2). These isomers differ in the nature of the $S\cdots S$ interactions of the four-bridged atoms. Complex **5.1a** posses two short $S\text{-}S$ distances of 2.118 Å and two independent S_2 units, with a separation of 3.527 Å between them. **5.1b** presents only one S_2 unit with a short distance at 2.152 Å, while lack sulphur atoms keep non-bonded between them. Finally, **5.1c** posses 4 equally long $S\text{-}S$ interactions at 2.816 Å. In addition to the changes in the $S\cdots S$ distances, it is noteworthy that there is also a significant change in the Mo-Mo distance between isomers. For example, the Mo-Mo distance in complexes **5.1b** and **5.1c** changes from 2.638 and 2.652 Å, respectively, to 2.755 Å in **5.1a** (Table 5.1).

Table 5.2. *Relative energies (kJ mol^{-1}) for [(Cp)MoS$_2$]$_2$ species respect isomer **5.1f***

Isomer	5.1a	5.1b	5.1c	5.1d	5.1e	5.1f	5.1g
BP	122.0	36.7	63.8	49.9	6.7	0.0	293.6

In order to explain the structural and energy differences between $(\boldsymbol{m}\text{-}\boldsymbol{h}^2\text{-S}_2)$ isomers, and to analyse their electronic structure, Figure 5.3 shows the frontier orbitals of the three isomers.
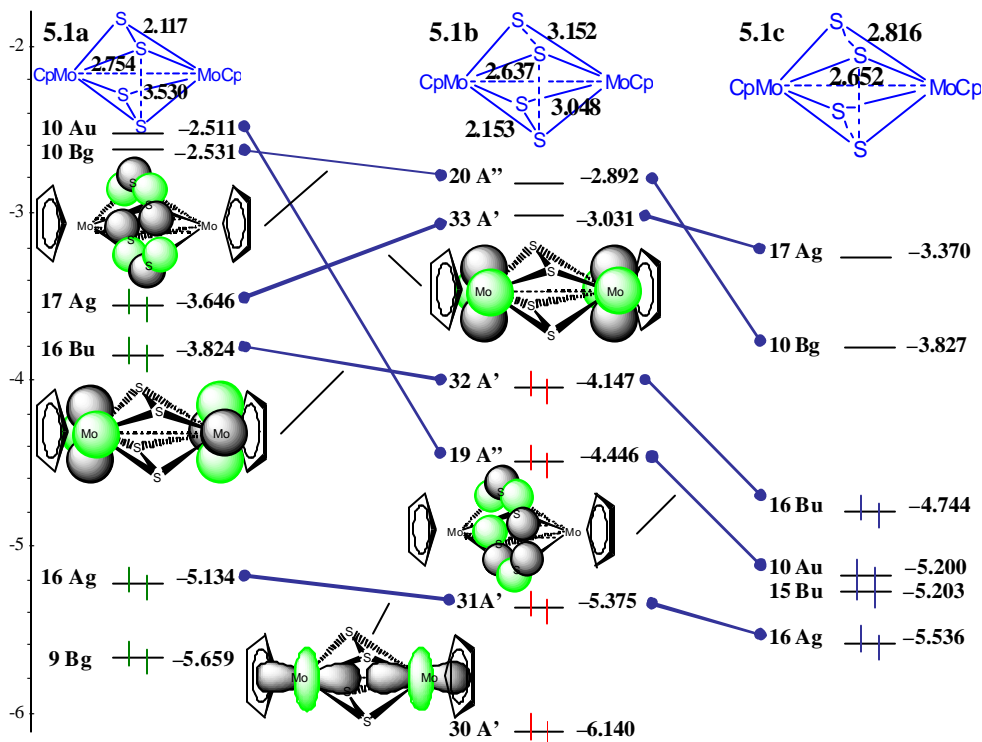
Chapter 5

Figure 5.3. *Correlation diagram for* **5.1 a-c** *isomers*

In **5.1a** isomer, the four sulphur atoms build two S_2^{2-} units, in these items S-S short distances keep disulphide bonding orbitals down in energy, while antibonding ones stay unoccupied creating a large gap between them. If we look at the frontier orbitals of **5.1a**, we see that the three highest occupied ones are mainly localised on the metals, what establishes an oxidation state (III) for the Mo atoms. If one of these S-S units is lengthened, changing from **5.1a** to **5.1b** isomer, corresponding vacant sulphur antibonding orbital (10 Au, **5.1a**) is stabilised passing to be occupied (19 A'', **5.1b**); and as a result metal-based orbital (17 Ag, **5.1a**) is shifting to be vacant (33 A', **5.1b**) by antibonding interactions with the occupied sulphur orbital. As a result, (IV) oxidation state is established for the Mo atoms in **5.1b**. At last step, if we formally open the remaining S_2^{2-} unit in **5.1b**, we change to **5.1c**; again, it will be expected that two electrons will be transferred from the metals to

an S-S antibonding orbital. However corresponding (32 A', **5.1b**) Mo orbital is not spontaneously emptied (16 Bu, **5.1c**). Actually, it is not produced a change in the Mo oxidation state, but a reorganization of the sulphur electrons, now equally distributed over the four sulphurs atoms without making a distinction between S_2^{2-} units. If however, sulphur antibonding orbital (10 Bg, **5.1c**) is forced to be occupied rather than molybdenum (16 Bu, **5.1c**) orbital, all four S-S bonds are cleaved and Mo atoms pass to be in V oxidation state; but this structure is 96.5 kJ mol^{-1} above the Mo(IV) **5.1c** structure.

5.1b adduct resulted the most stable for the (m-h^2-S_2) conformation. To examine the relative stability of the three isomers the partition of the interaction energy was perused, see Table 5.3. The analysis was made taken the atoms as fragments following the extension of the well-known decomposition scheme of Morokuma[28] that was developed by Ziegler and Rouk.[29] We observe that the **5.1a** isomer is disfavored by and increase of the *Pauli* repulsions respect **5.1b** and **5.1c** isomers, probably consequence of the six close metal electrons in Mo orbitals. At the same time **5.1b** preference respect **5.1c** isomer is consequence of a best electron distribution over the Mo_2-S_4 core what translates in a biggest electrostatic and orbital stabilizating energies.

Table 5.3. *Energy contributions in kJ mol^{-1} for* **5.1a-c**, **5.1e** *and* **5.1f** *adducts*

	(5.1a)	(5.1b)	(5.1c)	(5.1e)	(5.1f)
Pauli	57445	57216	57033	56142	56130
Electrostatic	-14661	-14478	-14388	-13913	-13916
Steric	42785	42738	42645	42230	42215
Orbital	-58349	-58388	-58267	-57909	-57901
Total	**-15564**	**-15650**	**-15623**	**-15680**	**-15687**
Relative	**122**	**37**	**64**	**7**	**0**

Chapter 5

During the modelling process, it resulted impossible to locate a minimum corresponding to $[Cp*Mo(\boldsymbol{m}\text{-}\boldsymbol{h}^2\text{-}S_2)(\boldsymbol{m}\text{-}\boldsymbol{h}^1\text{-}S_2)]$ (**5.1d**) structure on the potential energy surface. In all attempts, the optimization process yields complex **5.1e**. The aperture process responds to the electrostatic repulsion between the lone pairs over the terminal sulphur atoms. Perusing the dimeric complexes which respond to the structure **5.1d**, Fe, Ru, Cr and V,[6,7,9-11] all present a lack of electrons over the terminal sulphur atoms due to a less electron donor metal centre. This is mitigated with the formation of the corresponding S-S bonds.

The two structurally characterized open species **5.1e** and **5.1f** possess a clear distinction between the terminal sulphurs, double bonded to the metals, and the bridged-sulphur atoms; while **5.1e** and **5.1f** structures differ only in the relative positions of the terminal sulphur atoms, sync and anti respectively. Structure **5.1f** was found to be marginally more stable than **5.1e**, see Table 5.2, but with similar electronic structure; comparison between theoretical and experimental parameters reveals almost identical values for both isomers. Frontier orbitals diagram for **5.1f** compound is presented in Figure 5.4; now the two first empty orbitals belong to the metals in oxidation state (V). The formation of Mo-S double bonds stabilizes sulphurs orbitals, at the same time that antibonding interactions of the p-block orbitals of the terminal sulphurs destabilize the Mo d-orbitals. As a result there is a large gap between the stabilized occupied and the destabilized vacant orbitals, and these open structures are the more stable isomers for the $Mo_2\text{-}S_4$ core (see Table 5.2).

5.1g isomer binding mode was found in binuclear Co[15a] complexes and in a minor way in Fe complexes. Two possible structures differing in the relative positions of the S_2 units, syn or anti, can be optimised. We only computed the syn structure where the Cp ligands were kept in the staggered conformation. Comparatively, this structure keeps inaccessible for the $[CpMoS_2]_2$ adduct being quite high in energy as can be noted in Table 5.2; main theoretical parameters are reported in Table 5.1.
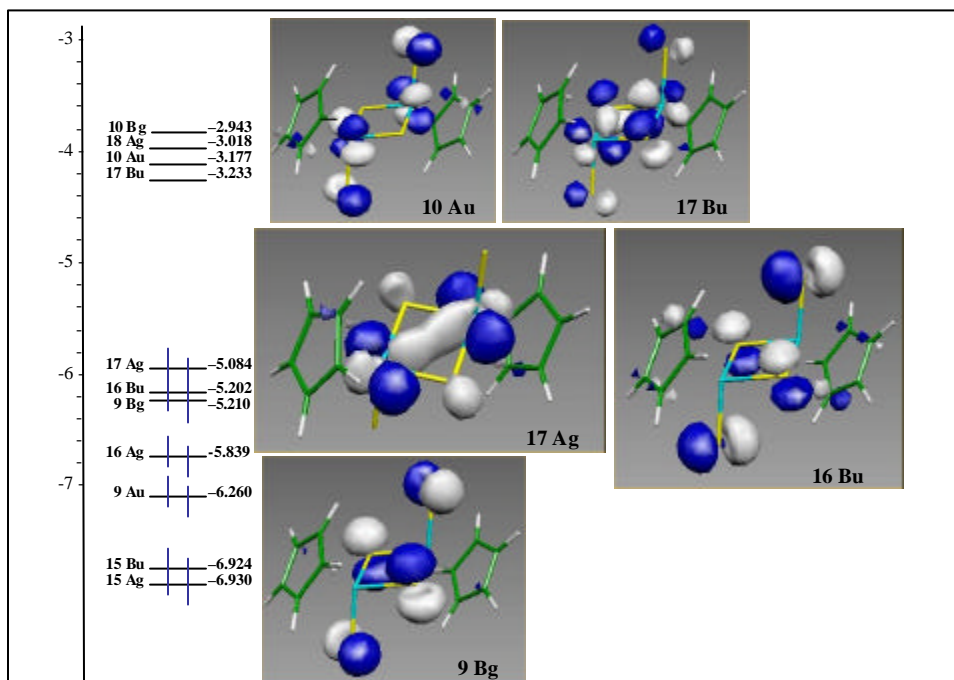
228

Figure 5.4. *Frontier orbitals for the **5.1f** isomer*

As we have observed in $[Cp*MoS_2]_2$ isomers, metal ligand electron interchange plays a key role in the molecular structure of these compounds. In order to extend our study, calculations on the $[CpMoS_2]_2^{2+}$ cations were performed for all proposed structures **5.1a-g**. In this case, an inversion in the stability of the isomers is produced, **5.1a**$^{2+}$ cation result the most stable by 2.3 kJ mol^{-1} over close **5.1c** and by 133.3 kJ mol^{-1} over open **5.1e** adduct. Isomer **5.1a**$^{2+}$ resulted slightly favoured in front of **5.1b-c**$^{2+}$ closed structures by the diminution of the Pauli repulsions over the metal atoms, and the non-presence of antibonding sulphurs interactions. At the same time **5.1e-f**$^{2+}$ open structures are clearly disfavoured by the emptied of the stabilized HOMO metal-metal bonding orbital in **5.1e-f** neutral compounds.

Additionally, we would like to include in the study the important isoelectronic catalytic compounds $[(CpMo)_2(S_2CH_2)(\mu-S)_2]$ (**5.2**) and $[(CpMo)_2(S_2CH_2)(\mu-S)(\mu-SR)]^+$ (R = H, CH$_3$, C$_4$H$_3$S) (**5.3**), which formally represent the addition of two electrons to the Mo$_2$-S$_4$ core, always talking

respect **5.1** species; and also [(CpMo)$_2$(S$_2$CH$_2$)(μ-SH)(μ-SR)] (R = H, CH$_3$, C$_4$H$_3$S) (**5.4**) adduct which represents the addition of four electrons (see Figure 5.5). In these cases, only $\left[\text{CpMo}(\boldsymbol{m}\text{-}\boldsymbol{h}^2\text{-S}_2)\right]_2$ close structure type **c**) without sulphur-sulphur bonds keeps as accessible; selected structural parameters are shown in Table 5.4.
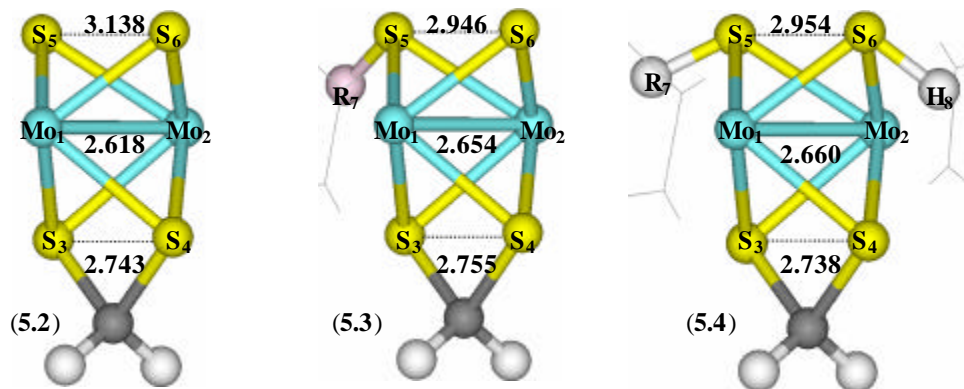

Figure 5.5. *3D view of [(CpMo)$_2$(S$_2$CH$_2$)(**m**-S)$_2$] (5.2); [(CpMo)$_2$(S$_2$CH$_2$)(**m**-S)(**m**-SH)]$^+$, R = H (5.3H); and [(CpMo)$_2$(S$_2$CH$_2$)(**m**-SH)(**m**-SR)], R =C$_4$H$_3$S (5.4TioH) compounds*

The addition of two electrons to the Mo$_2$S$_4$ core respect initial **5.1** isomers discard open structures $\left[\text{Cp}_2\text{Mo}_2(\boldsymbol{m}\text{-S}_2)(\boldsymbol{m}\text{-}\boldsymbol{h}^2\text{-S}_2)\right]$ because of the large HOMO-LUMO gap. In close $\left[\text{CpMo}(\boldsymbol{m}\text{-}\boldsymbol{h}^2\text{-S}_2)\right]_2$ structures the addition of two electrons provokes the occupation of closest antibonding sulphur-sulphur orbitals, so we only find accessible a closed structure without S_2^{2-} units. A similar situation is presented for the addition of four electrons in compounds **5.4**.

We have proved the importance of ligand metal electron transfer processes in the structural properties of Mo$_2$-S$_4$ core compounds, additionally the important catalytic abilities of these adducts can be deduced from their big electronic and structural versatility.

Table 5.4. *Selected bond distances (Å) and angles (º) for computed and experimental* **5.2**, **5.3** *and* **5.4** *species*

	Mo-Mo	Mo_1-S_5	Mo_1-S_6	S_5-S_6	Mo_1-R_7	Mo_2-H_8	S_6-H_8	S_5-R_7
5.2	2.618	2.380	2.380	3.138	-	-	-	-
(5.2)[a]	(5.580)	(2.406)	(2.408)	(3.123)	-	-	-	-
5.3Me	2.652	2.326	2.507	2.932	3.713	-	-	1.859
(5.3Me)[a]	(2.604)	(2.319)	(2.436)	(2.921)	(3.125)	-	-	(1.912)
5.3Tio	2.623	2.308	2.551	2.986	3.630	-	-	1.782
(5.3Tio)[a]	(2.608)	(2.303)	(2.476)	(2.897)	(3.590)	-	-	(1.771)
5.4H$_2$	2.658	2.500	2.500	2.970	3.116	3.121	1.373	1.373
5.4MeH	2.657	2.483	2.496	2.933	3.648	3.118	1.374	1.863
5.4TioH	2.661	2.492	2.508	2.954	3.594	3.127	1.373	1.792
(5.4(Me)$_2$)[a]	(2.596)	(2.451)	(2.451)	(2.822)	(3.604)	(3.605)	(1.823)	(1.823)

[a] *Experimental structures extracted from:* **5.2** *reference 30,* **5.3Me** *reference 31,* **5.3Tio** *reference 39 and* **5.4(CH$_3$)$_2$** *reference 38b*

In the presence of a proton adduct **5.2** evolutionates to **5.3;** and interestingly, this last compound is able to activate molecular H$_2$ to give species **5.4** with an extra proton (see Figure 5.6). From the electronic structure of **5.2** and **5.3** adducts is deduced the presence of two bare highly nucleophilic sulphur atoms, in response to the occupied antibonding sulphur orbitals. In the same way Mo (IV) atoms are also nucleophilic and they keep the option of transferring charge density to a ligand.

It is attractive for introducing the catalytic properties of these compounds to check the nucleophility of the sulphur and molybdenum atoms, and also the influence of the substituents. In compounds **5.2** and **5.3** clearly bare sulphur atoms are the most nucleophilic atoms, but in compounds **5.4** the presence of ligands in all sulphurs atoms modifies the situation. Protonation studies have provided data to suggest that in most cases the molybdenum ions are

Chapter 5

the most basic sites, while it might be expected that an electron-donating substituent would favour sulphur protonation.
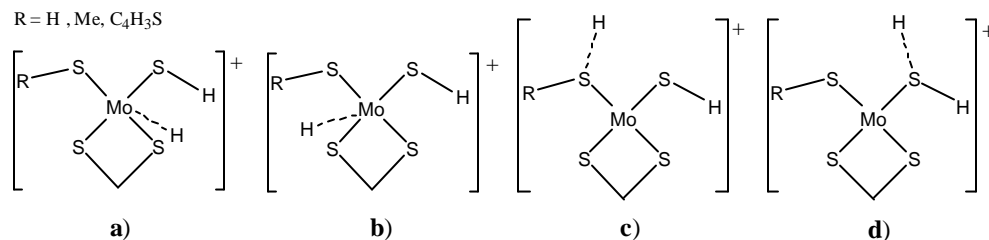

Figure 5.6. *Proposed metal and sulphur protonation sites in the neutral complexes* **5.4**

There were preformed calculations for the protonation sites in **5.4** complexes, where R = H, Me (electron-donating) and C_4H_3S (electron-withdrawing), as simplest models for different characteristic substituents (see Figure 5.6).[32] Theoretical calculations, in good accordance with experimental predictions, point to the Mo atoms as the most basic sites; but as well the addition of a proton to the sulphur atom directly bond to the electron-donating substituent keeps quite close in energy respect to the metal addition (see Table 5.5). Interesting result to start the study of the catalytic properties of these compounds.

Table 5.5. *Relative energies in kJ mol^{-1} for protonated* **5.4** *structures*

	a	b	c	d
H	0.0	0.0	38.7	38.7
Me	1.6	0.0	5.2	35.3
C_4H_3S	22.2	0.0	22.2	43.0

5.3 DFT reaction mechanisms of hydrogen activation by cationic dinuclear (μ-sulphido) molybdenum complexes

The significant work of M. Rakosky DuBois et al.[33] has shown that cationic molybdenum sulphide complexes of the general formula $[(CpMo)_2(S_2CH_2)(\mu-S)(\mu-SR)]^+$ (**5.3**) and the structurally related $[(CpMo)_2(SH)_2(\mu-S)(\mu-SR)]^+$ react with molecular hydrogen, resulting in the heterolytic cleavage of H_2. The exploration of the reduction pathways of these cations has proven valuable in understanding mechanistic features of the hydrogen activation process and of the potential substrate reduction.

In the important industrial processes of hydrodesulphurization of organosulphur compounds is generally accepted that molybdenum sulphide surface is the catalytic site for the hydrogenolysis reaction.[34] On the basis of kinetic and other studies, it has been proposed a mechanism for the hydrogenolysis of thiophene, which involves two types of sites on the catalyst surface, see Scheme 5.1.[35] One is a vacant coordination site on the molybdenum ion, which permits interaction of the organosulphur compound with the metal. The second types are the surface sulphido ligands, which are proposed to react with molecular hydrogen to form hydrosulphido ligands. The hydrogenolysis reaction involving carbon-sulphur bond rupture and hydrogen atom transfer is proposed to occur between the species absorbed on these sites. The mechanistic proposed for the hydrodesulphurisation catalysis described above may have close links into the reaction of molecular hydrogen with coordinated sulphido ligands in discrete metal complexes.

The neutral dimers $[CH_3C_5H_4MoS_2]_2$ (**5.1**), $[CH_3C_5H_4MoSHS_2]_2$, $[CH_3C_5H_4MoCH_2S_2]_2$ (**5.2**) interact with unsaturated molecules and with some organosulphur compounds, leading to the substrate reduction,[36,37] or to the formation of HD from a mixture of H_2 and D_2.[38] In the second reaction, catalytic amounts of H^+ are also required to generate the cationic $[(CpMo)_2(S_2CH_2)(\mu-S)(\mu-SR)]^+$ (**5.3**) species, which are the true catalysts. In order to understand the mechanistic aspects of these processes, DuBois et al. have studied the general process of reduction of some organic molecules catalysed by these cations (Equation 5.1).[39]

Chapter 5
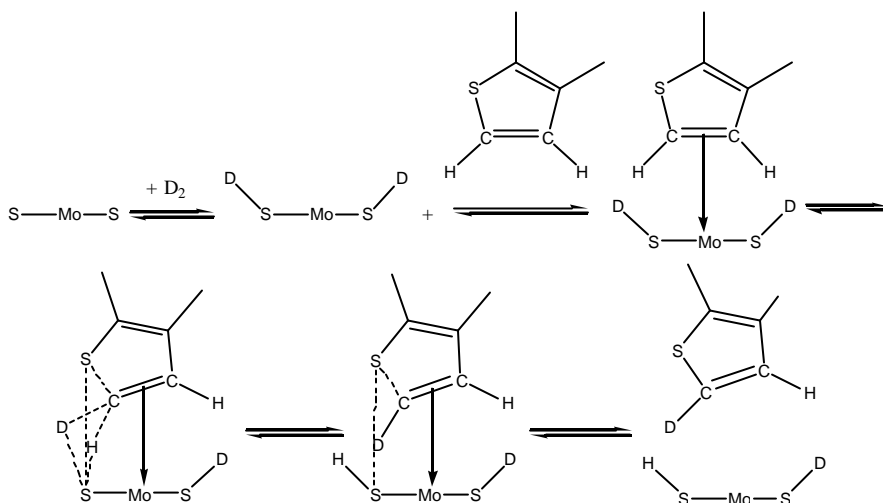
Scheme 5.1. *Details of the suggested mechanism of deuterium exchange of thiophene adsorbed according to the multipoint model*
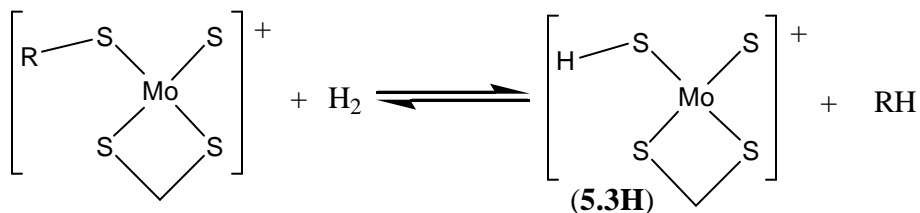

**Equation 5.1.** *Where R is an unsaturated molecule or organosulphur compound*

The process results in the function of different products depending on the identity of R. For R = H or electron-withdrawing substituents like thiophene R = C_4H_3S (**5.3Tio**), CH(Me)Ph, CH_2Ph, a rapid reduction of the substituent is observed; in contrast an alternative reaction path was observed for molybdenum thiolate complexes with electron-donating substituents. For example, where R = Me (**5.2Me**) and i-Pr, the reduction was not observed and rapid hydrogen elimination occurred instead. Attempts to monitor the course of the reaction by NMR spectroscopy were unsuccessful, but the kinetics were also followed by visible spectroscopy, the data inducting a first order dependence on hydrogen, suggesting a direct interaction of the

234

cation with hydrogen. The widely discussed mechanisms proposed for the hydro-activation and reduction are presented in Schemes 5.2 and 5.3.

DFT calculations at BP and B3LYP levels were performed for substituents type R = H, CH$_3$ (electron-donating) and C$_4$H$_3$S (electron-withdrawing), as simplest different behaviour model substituents in order to study the reaction pathway, and clarify unsure process aspects.
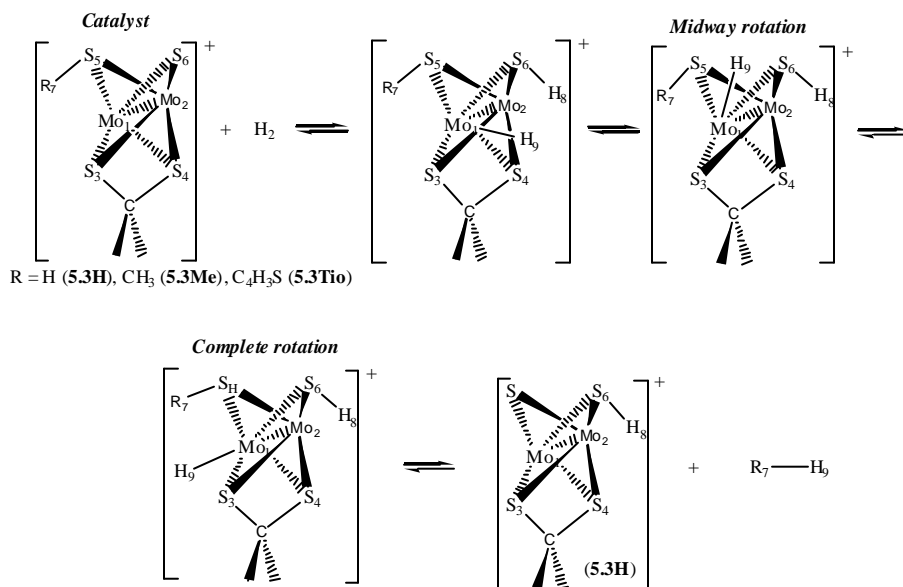

Scheme 5.2. *Suggested mechanism of hydro-activation on sulphide-bridged molybdenum complexes over sulphur-metal site*
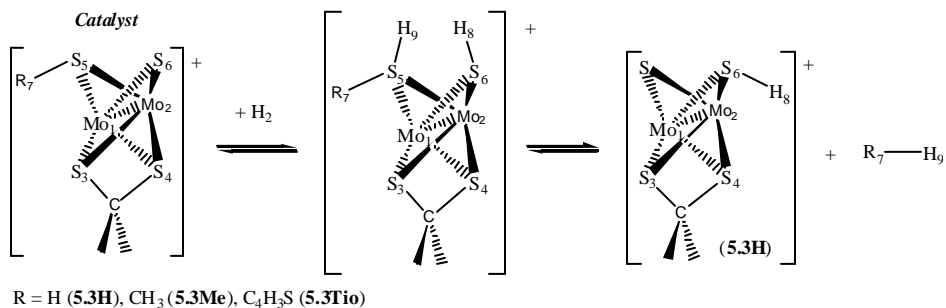
Scheme 5.3. *Suggested mechanism of hydro-activation on sulphide-bridged molybdenum complexes over sulphur sites*

Chapter 5

The addition of hydrogen molecular to **5.3** species would initially produce a cation **5.5** (R = H (**5.5H**), CH_3 (**5.5Me**), C_4H_3S (**5.5Tio**)), see Scheme 5.4. Due to the formation of paramagnetic species, NMR spectroscopy does not provide any information on the structure of intermediates. A first goal of this study is to use DFT methods to propose a structure for the intermediates formed by hydrogen addition.
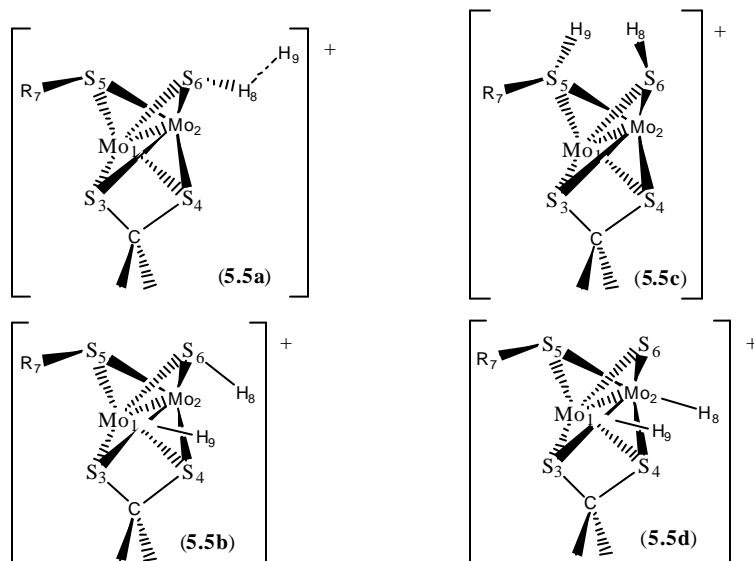
Scheme 5.4. *Proposed hydrogen addition structures*

The H_2 addition to the catalyst $[(CpMo)_2(S_2CH_2)(\mu\text{-}S)(\mu\text{-}SR)]^+$ R = H (**5.3H**), CH_3 (**5.3Me**) and C_4H_3S (**5.3Tio**) yields in all the cases to the H_2 molecule activation. Four structures were proposed as possible minima on the potential energy surface; **a**) end-on addition of hydrogen to a sulphido ligand, **b**) addition across a molybdenum-sulphide bond, **c**) addition of H_2 to the sulphurs sites and **d**) addition across a M-M bond (Scheme 5.4). Energy and main structural data are reported in Table 5.6.

The optimization process for **a**) type structures leads to H_2 elimination so end-on addition is discarded as possible way of hydrogen activation. Structures type **d**), corresponding to initial H_2 addition across a M-M

236

bond,[40] lead to the relative highest energies respect to the reactives, and we also discard them.

Table 5.6. *Relative energies in kJ mol^{-1} to reactives and main structural distances in Å (only at B3LYP level) for* **5.5R** *(R = H, Me, Tio) adducts*

Relative energies in kJ mol^{-1}

(**5.5**)	**Hb**	**Hc**	**Hd**	**Meb**	**Mec**	**Med**	**Tiob**	**Tioc**
BP	41.1	83.0	86.1	40.2	44.5	102.4	44.3	68.3
B3LYP	27.8	50.4	118.1	27.8	16.5	145.2	21.8	26.4

Main structural distances in Å (B3LYP level)

	Mo$_1$-Mo$_2$	Mo$_1$-S$_5$	Mo$_1$-S$_6$	S$_5$-S$_6$	Mo$_1$-H$_9$	Mo$_2$-H$_8$	S$_6$-H$_8$	S$_5$-H$_9$	H$_8$-H$_9$
Hb	2.679	2.548	2.574	2.905	1.670	3.142	1.360	-	2.204
Hc	2.682	2.473	2.542	3.097	3.406	3.169	1.364	1.364	2.420
Hd	2.672	2.519	2.484	2.724	1.676	1.676	2.395	-	2.956
Meb	2.676	2.544	2.575	2.869	1.668	3.136	1.361	-	2.216
Mec	2.686	2.410	2.506	2.985	3.287	3.131	1.377	1.385	2.115
Med	2.681	2.514	2.540	2.823	1.675	1.672	2.036	-	2.657
Tiob	2.673	2.598	2.545	2.868	1.662	3.139	1.362	-	2.119
Tioc	2.677	2.496	2.530	3.091	3.348	3.165	1.367	1.367	2.236

Additions type **b**) and **c**) lead to stable minima, each with a proton attached to the previously bare sulphido ligand; in **5.5c** type structures the other hydrogen is located on the RS$^-$ group, while in **5.5b** it is attached to one of the Mo centres. All the addition species are above the reactants, for R = H, **5.5Hb** structure is the most stable, by 41.9 kJ mol^{-1} at BP level and 22.6 kJ mol^{-1} at B3LYP level, suggesting that initial H$_2$ addition occurs heterolytically leading to a Mo-H bond.[41] Similar result is found for electron-withdrawing R = C$_4$H$_3$S substituent, **5.5Tiob** adduct is the most stable structure by 24 kJ mol^{-1} and 5 kJ mol^{-1} at BP and B3LYP level respectively. Instead for electron-donating R = CH$_3$ both structures are now very close in energy, at BP level **5.5Mec** is only 4 kJ mol^{-1} above **5.5Meb**

Chapter 5

and at B3LYP level **5.5Mec** is now 11 kJ mol^{-1} more stable. In general, we can conclude that short energy differences are found between both additions, especially with electron-donating methyl substituent.

Going into, transition states (T. S.) corresponding to the hydrogen molecule activation have been also identified and characterized with one negative frequency for additions type, **b**) and **c**) (see Equations 5.2 and 5.3). Table 5.7 shows computed structural and energy dates.
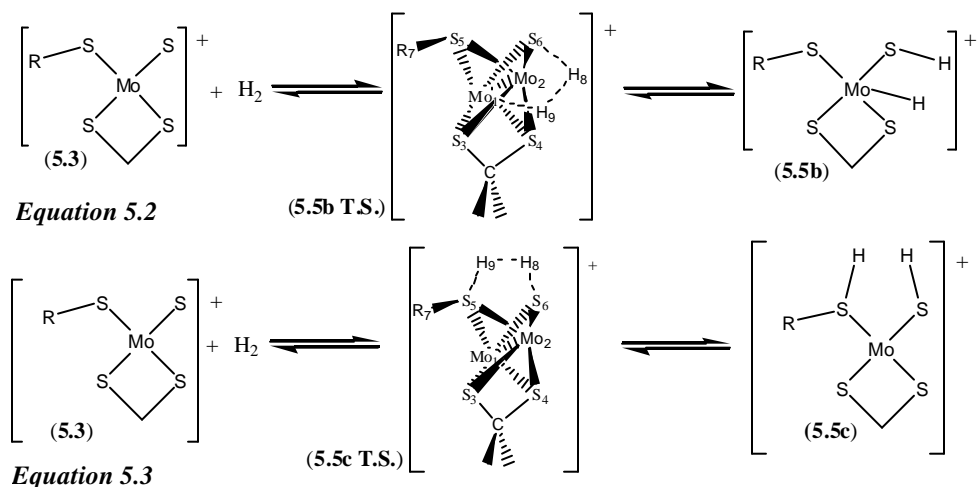

Equation 5.2   **(5.5b T.S.)**

Equation 5.3   **(5.5c T.S.)**

Table 5.7. *Relative energies in kJ mol^{-1} respect reactives, and main structural distances in Å for* **5.5-T.S.** *at B3LYP level*

	Energy	Mo$_1$-Mo$_2$	S$_5$-S$_6$	Mo$_1$-H$_9$	Mo$_2$-H$_8$	S$_6$-H$_8$	S$_5$-H$_9$	H$_8$-H$_9$
5.5H$_b^{T.S.}$	**191.1**	2.640	2.911	2.100	3.253	1.767	-	0.886
5.5H$_c^{T.S.}$	**188.5**	2.646	2.887	3.191	3.120	1.622	1.681	1.019
5.5Me$_b^{T.S.}$	**191.9**	2.636	2.864	2.108	3.258	1.774	-	0.883
5.5Me$_c^{T.S.}$	**110.3**	2.642	2.905	3.177	3.121	1.654	1.710	0.982
5.5Tio$_b^{T.S.}$	**190.1**	2.633	2.881	2.108	-	1.789	-	0.876
5.5Tio$_c^{T.S.}$	**110.3**	2.644	2.917	-	-	1.640	1.705	0.989

Computed T. S. for R = H (**5.5H$^{T.S.}$**) show a short relative energy difference lower than 3 kJ mol^{-1} in favour of sulphur - molybdenum pathway. Figure 5.6 shows both pathways.
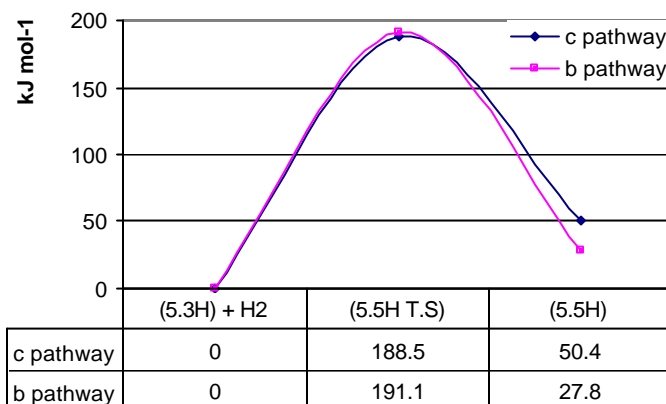

	(5.3H) + H2	(5.5H T.S)	(5.5H)
c pathway	0	188.5	50.4
b pathway	0	191.1	27.8

Figure 5.6. *Energy profile in kJ mol^{-1} for the H$_2$ activation in (5.3H) + H$_2$ → (5.5H)*

For R = CH$_3$ and C$_4$H$_3$S substrates the result is similar and show a clear influence of the substituents in the energy of the T.S. Now, the **c**) type T.S. is favoured by about 80 kJ mol^{-1}. Figure 5.7 shows the energy profile in both cases for a sulphur-sulphur addition.

	(5.3Me) + H2	(5.5Me T.S)	(5.5Me)		(5.3Tio) + H2	(5.5Tio T.S)	(5.5Tio)
c pathway	0	110.3	26.4		0	110.3	26.4
b pathway	0	190.1	21.8		0	190.1	21.8
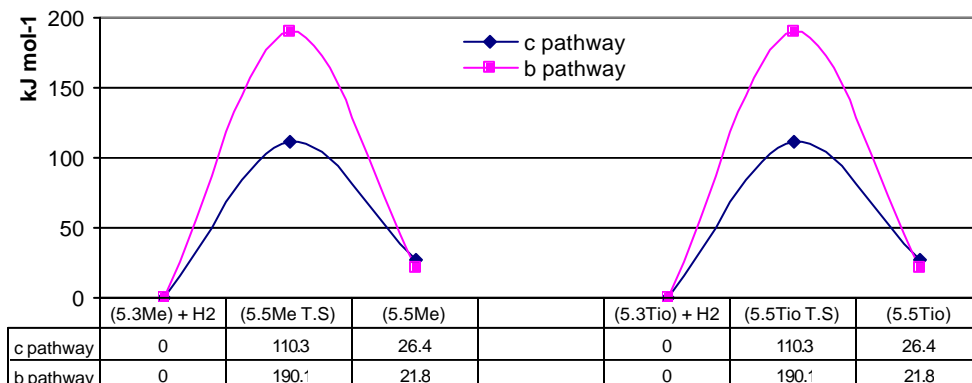
Figure 5.7. *Energy profile in kJ mol^{-1} for the H$_2$ activation from 5.3Me and 5.3Tio species*

Chapter 5

From Figure 5.6 we extract that for **5.3H** cation, R = H, sulphur-molybdenum and sulphur-sulphur molecular hydrogen absorption will occur equally. Instead both for electron-withdrawing (thiophene) and electron-donating (methyl) substituents sulphur-sulphur addition looks like favoured. Both kind of substituents do not show any noteworthy different in their behaviour, in this sense, we conclude that the different reaction behaviour for R= -CH$_3$ and -C$_4$H$_3$S substituents does not came from a distinct initial pathway in the H$_2$ activation.

Not to discard any option we follow the global reaction from both S-S and Mo-S additions. Starting from a S-Mo addition, **b**) pathway, we have resumed global reaction (Equation 5.4) in nine stages: stages 1-3 represent mentioned H$_2$ addition, stage 4-6 represent necessary proton migration over metal atom to situate the nuclei close substituent R in stage 7, and finally stage 8 represent formed T. S. for yielding the RH molecule elimination in stage 9. Starting from a S-S addition, **c**) pathway, it was only necessary to define five stages (Equation 5.5): stages 1-3 represent studied H$_2$ addition, and stage 4 represent required T. S. to yield substituent reduction in stage 5.
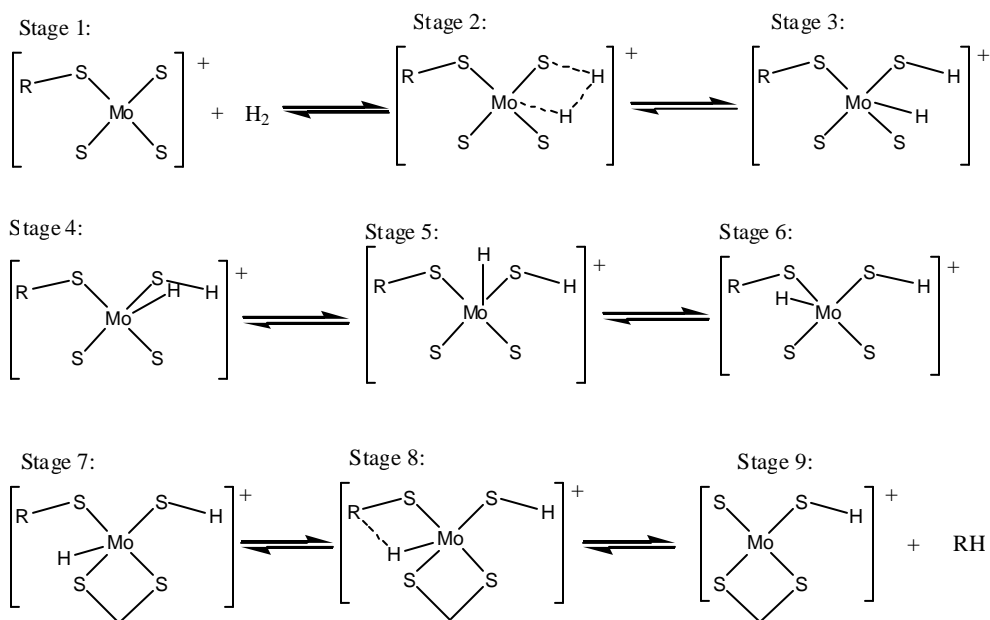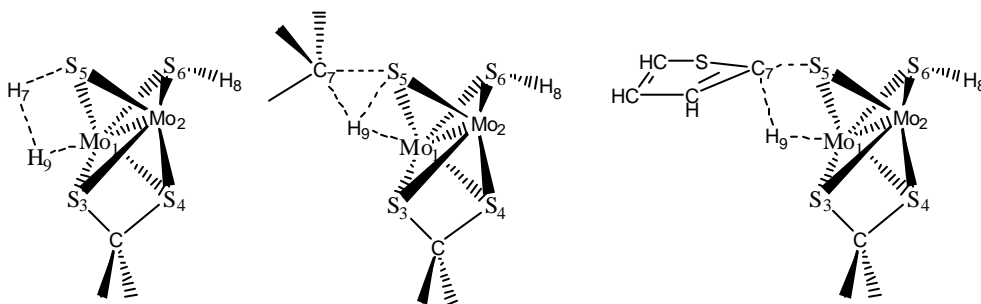

Equation 5.4. *b) pathway, sulphur-molybdenum addition*

240
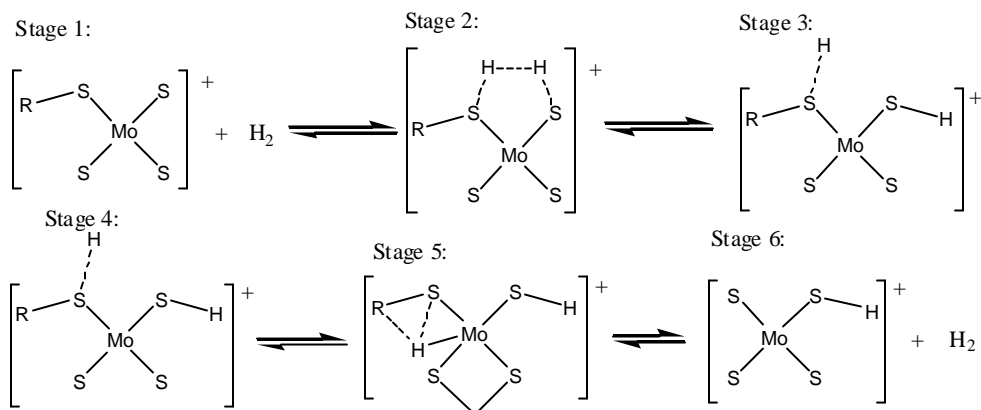
Equation 5.5 *c) pathway, sulphur-sulphur addition*

Independently of the addition pathway, a similar T.S. is found in the bond cleavage for the RH formation; what yields in both cases to a similar barrier for the RH elimination. Main structural and relative energies for the T.S. are shown in Table 5.8.

Scheme 5.5

Table 5.8. *Structural data in Å and relative energies in kJ mol^{-1} for the RH elimination T.S. respect initial reactives at B3LYP level*

R	Energy	Mo_1-Mo_2	Mo_1-S_5	Mo_1-S_6	S_5-S_6	Mo_1-H_9	S_6-H_8	S_5-A_7	S_5-H_9	A_7-H_9
H	**191.1**	2.640	2.523	2.643	2.911	2.106	1.364	1.768	2.270	0.885
Me	**196.6**	2.642	2.544	2.528	2.966	2.334	1.364	2.258	1.509	1.537
Tio	**91.6**	2.642	2.578	2.539	2.908	1.989	1.362	1.842	2.164	1.443

Chapter 5

These final T. S. show main structural and energy differences between substituents. In all cases the proton near to the substituent keep quite close to the molybdenum metal, only for R = Me this distance is enlarge until 2.334 Å, ~0.3 Å larger than when R = H and Tio. Additionally the S-H$^+$ distance for R = Me is 1.5 Å, 0.7 Å shorter than for R = H and Tio complexes. It is for R = Me where it is found the biggest barrier for the RH elimination, 179.1 kJ mol^{-1}, in front of R = C$_4$H$_3$S where a clearly short barrier of about 70 kJ mol^{-1} is found. The accessibility of the T.S. indicates the energy barrier for the RH elimination. The observed structural changes for the methyl point out biggest structural distortions, respect H$_2$ absorbed molecules, to yield the CH$_4$ elimination. In this case, the S-CH$_3$ distance is enlarged to 2.258 Å, respect the initial 1.879 Å, together with a displacement of the proton into the triangle formed by the implicated methyl carbon, the sulphur and the molybdenum atom. For alkyl substituents like CH$_3$ formally the carbon sp^3 orbitals do not favour the interaction with the proton, so an enlargement of the S-CH$_3$ bond distance and an adequate proton situation are necessaries, what translates into a big barrier. Instead, for R = Tio a shorter Mo-H distance answers to the presence of the ***p*** orbital of the aromatic ring letting an easy overlap with the proton orbitals and so a T. S. close to the reactives. Figure 5.8 shows last occupied orbitals for R = Tio T. S.
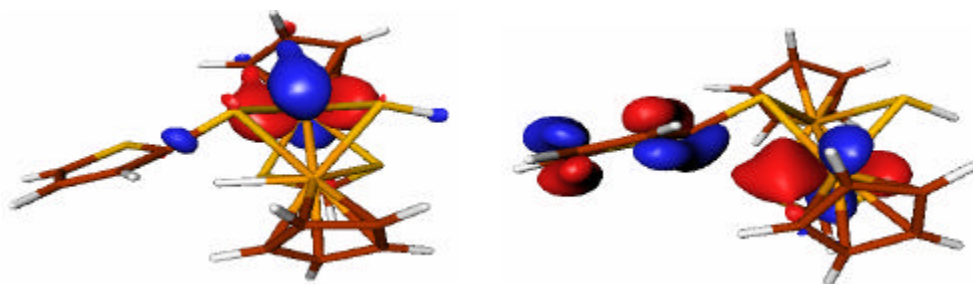

Figure 5.8. *Two last occupied molecular orbitals for R = Tio T. S. From left to right, HOMO and HOMO-1. Representation made with Molden program, for a 0.05 contour value*[42]

For the simplest R = H substituent all required species and intermediate T. S. where computed, Figure 5.9 shows b) and c) reaction profiles. Reaction profiles show that the only difference between the pathway b) and c) comes

from the necessary proton migration in sulphur-molybdenum addition that does not has associated important energy barriers.
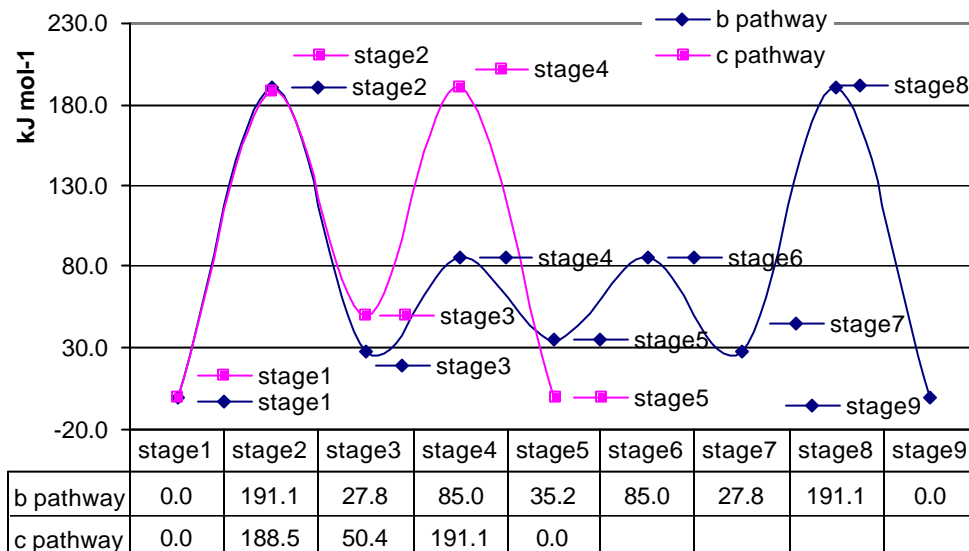

	stage1	stage2	stage3	stage4	stage5	stage6	stage7	stage8	stage9
b pathway	0.0	191.1	27.8	85.0	35.2	85.0	27.8	191.1	0.0
c pathway	0.0	188.5	50.4	191.1	0.0				

Figure 5.9. *Energy profile for global H$_2$ activation process from a S-S or a S-Mo addition for R = H*

For CH$_3$ and C$_4$H$_3$S similar reaction profiles are expected but as we can observe in Figure 5.7 sulphur-sulphur addition clearly presents a small energy barrier. In Figure 5.10 we observe the CH$_4$ formation requires 86 kJ mol^{-1} more than the H$_2$ elimination and therefore this is the main product. As contrast, the opposite is observed for thiophene, see Figure 5.11; we simply present a comparison between reaction profiles in both cases.

Figures 5.9-5.11 resume perfectly our results for studied hydrogenolysis reaction. Initial molecular hydrogen activation by **5.3R** cations can take place by two possible pathways, sulphur-sulphur or sulphur-molybdenum addition. For substituents different from hydrogen, sulphur-sulphur absorptions appear favoured in all cases. Final reaction products are indicatives of the preference of the system for a H$_2$ or RH molecule elimination. In the case of alkyl substituents like CH$_3$, their bond orientated orbitals do not favours the interaction of the CH$_3$ unit with the proton, consequently it appears a relatively high in energy T. S., so H$_2$ elimination

243

is preferred. For substituents type thiophene, the presence of π orbitals perpendicular to the molecular plane facilitates the interaction with the proton and a relatively easy hydrogenolisis take place. Finally, molybdenum metals play an important catalytic role serving as bridge for the protons in the hydrogenolisis of the substituents.
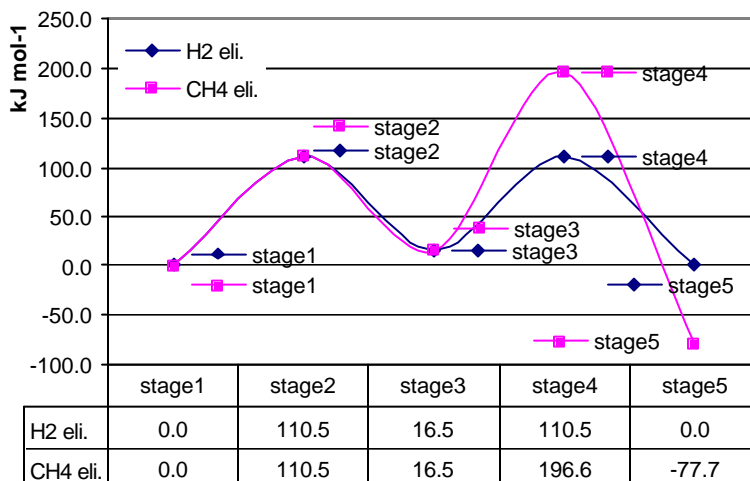

	stage1	stage2	stage3	stage4	stage5
H2 eli.	0.0	110.5	16.5	110.5	0.0
CH4 eli.	0.0	110.5	16.5	196.6	-77.7

Figure 5.10. *Energy profile for CH_4 or H_2 elimination from a S-S H_2 addition to $[(CpMo)_2(S_2CH_2)(m\text{-}S)(m\text{-}SR)]^+$ R = CH_3 (**5.3Me**)*

	stage1	stage2	stage3	stage4	stage5
H2 eli.	0.0	110.3	26.4	110.3	0.0
C4H4S eli.	0.0	110.3	26.4	91.6	-65.1
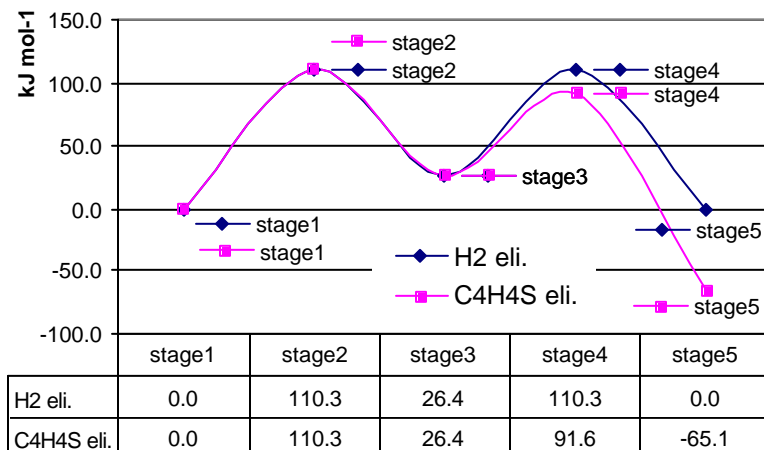
Figure 5.12. *Energy profile for C4H4S or H_2 elimination from a S-S H_2 addition to $[(CpMo)_2(S_2CH_2)(m\text{-}S)(m\text{-}SR)]^+$ R = C_4H_3S (**5.3Tio**)*

References and notes

[1] H. Vahrenkamp, *Angew. Chem., Int. Ed. Engl.* **1975**, *14*, 322**.**

[2] F. E. Massoth, *Adv. Catal.*, **1978,** *27*, 265.

[3] S. C. Schuman, H. Shalit, *Catal. Rev.* **1970**, *4*, 245.

[4] a) W. C. Newton, S. Otsuka, Eds. "Molybdenum Chemistry of Biological Significance"; Plenum Press: New York, **1980**.
b) E. I. Stiefil, *Prog. Inorg. Chem.* **1977**, *22*, 1.
c) H. F. Barry, P. C. H. Mitchell, Eds. "*Proceedings of the Climax Third International Conference on the Chemistry and Uses of Molybdenum*", Climax Molybdenum Co.: Ann arbor, MI, **1979**.

[5] J. Wachter, *Angew. Chem., Int. Ed. Engl.* **1989**, *28*, 1613.

[6] H. Ogino, S. Inomata, H. Tobita, *Chem. Rev.* **1998**, *98*, 2093.

[7] R. H. Holm, *Adv. Inorg. Chem.* **1992**, *38*, 1.

[8] M. Hidai, S. Kuwata, Y. Mizobe, *Acc. Chem. Res.* **2000**, *33*, 46.

[9] a) S. P. Cramer, K. O. Hodgson, W. O. Gillum, L. E. Mortenson, *J. Amer. Chem. Soc.* **1978**, *100*, 3398.
b) S. P. Cramer, K. O. Hodgson, W. O. Gillum, L. E. Mortenson, E. I. Stiefel, J. R. Chisnall, W. J. Brill, V. K. Shan, *J. Am. Chem. Soc.* **1978**, *100*, 3814.

[10] P. J. Lundmark, G. J. Kubas, B. L. Scott, *Organometallics* **1996**, *15*, 3631.

[11] C. M. Bolinger, T. B. Rauchfuss, A. L. Rheingold, *J. Am. Chem. Soc.*, **1983**, *105*, 6321.

[12] L. Y. Goh and T. C. W. Mak, *J. Chem. Soc., Chem. Commun.* **1986**, 1474.

[13] a) M. Rakowski DuBois, D. L. Dubois, M. C. VanDerveer, R. C. Haltiwanger, *Inorg. Chem.* **1981**, *20*, 3064.
b) A. E. Bruce, D. R. Tyler, *Inorg. Chem.* **1984**, *23*, 3433.
c) H. Brunner, W. Meier, J. Wachter, E. Guggolz, T. Zahn, M. L. Ziegler, *Organometallics* **1982**, *1*, 1107.

[14] a) H. Chaunaud, A. M. Ducourant, Giannotti, *J. Organomet. Chem.* **1980**, *190*, 201.
b) R. Weberg, R. C. Haltiwanger, M. Rakowski DuBois, *Organometallics* **1985**, *4*, 1315.
c) R. Weberg, R. C. Haltiwanger, M. Rakowski DuBois, *New. J. Chem.* **1988**, *12*, 361.

[15] a) H. Brunner, N. Janietz, W. Meier, G. Sergeson, J. Watcher, T. Zahn, M. L. Ziegler, *Angew. Chem., Int. Ed. Engl.* **1985**, *24*, 1060.
b) H. Ogino, H. Tobita, S. Inomata, M. Shimoi, *J. Chem. Soc., Chem. Commun.* **1988**, 586.
c) H. Brunner, A. Mertz, J. Pfauntsch, O. Serhadli, J. Watcher, M. L. Ziegler, *Inorg. Chem.* **1988**, *27*, 2055.

[16] T. B. Rauchfuss, D. P. S. Rodgers, S. R. Wilson, *J. Am. Chem. Soc.* **1986**, *108*, 3114.

[17] W. Tremel, R. Hoffmann, E. D. Jemmis, *Inorg. Chem.* **1989**, *28*, 1213.

[18] S. Blasco, I. Demachy, Y. Jean, A. Lledos, *New J. Chem.* **2001**, *25*, 611.

[19] W. Danzer, W. P. Fehihammer, A. T. Liu, G. Thiel, W. Beck, *Chem. Ber.* **1982**, *115*, 682.

[20] W. Beck, W. Danzer, G. Thiel, *Angew. Chem. Int. Ed. Engl.* **1973**, *12*, 582.

[21] H. Brunner, R. Grassl, W. Meier, J. Wachter, B. Nuber, M. L. Ziegler, J. Organomet. Chem. **1992**, *434*, 63.

[22] a) R. T. Weberg, R. C. Haltiwanger, J. C. V. Laurie, M. Rakowski-DuBois, *J. Am. Chem. Soc.* **1986**, *108*, 6242.

b) D. E. Coons, R. C. Haltiwanger, J. C. V. Laurie, M. Rakowski-DuBois, *Organometallics* **1987**, *6*, 2417.

c) P. Bernatis, J. C. V. Laurie, M. Rakowski-DuBois, *Organometallics* **1990**, *9*, 1607.

d) C. J. Casewit, D. E. Coons, L. L. Wright, W. K. Miller, M. Rakowski-DuBois; *Organometallics* **1986**, *5*, 951.

[23] a) B. C. Gates, J. R. Katzer, G. C. A. Schuit, *"The Chemistry Of Catalytic Processes"*; McGraw-Hill: New York, **1979**.

b) J. Barbow, K. C. Campbell, *J. Chem. Soc., Chem. Commun.* **1982**, 1371.

[24] a) F. E. Massoth, *Adv. Cat.* **1978**, *27*, 265.

b) S. C. Schuman, H. Shalit, *Cat. Rev.* **1970**, *4*, 245.

[25] B. C. Gates, J. R. Katzer, G. C. Shuit, *"Chemistry of Catalytic Processes"*, McGraw-Hill: New York, **1979**.

[26] a) A. D. Becke, *Physical Review A* **1988**, *38*, 3098.

b) J. P. Perdew, *"Density-functional approximation for the correlation energy of the inhomogeneous electron gas" Physical Review B* **1986**, *33*, 8822.

[27] a) C. Lee, W. Yang, R. G. Parr, *Phys. Rev. B*, **1988**, *37*, 785.

b) A. D. Becke, *J. Chem. Phys.*, **1993**, *98*, 5648.

[28] a) K. Morokuma, *J. Chem. Phys.* **1971**, *55*, 1236.

b) K. Kitaura, K. Morokuma, *Int. J. Quantum. Chem.* **1976**, *10*, 325.

[29] a) T. Ziegler, A. Rauk, *Teor. Chim. Acta* **1977**, *46*, 1.

b) T. Ziegler, A. Rauk, *Inorg. Chem.* **1979**, *18*, 1558.

[30] B. B. Kaul, B. Noll, S. Renshaw, M. Rakowski DuBois, *Organometallics* **1997**, *16*, 1604.

[31] C. J. Casewit, R. C. Haltiwanger, J. Noordik, M. R. DuBois, *Organometallics* **1985**, *4*, 119.

[32] P. Bernatis, R. C. Haltiwanger, M. Rakowski-DuBois, *Organometallics* **1992**, *11*, 2435.

[33] M. Rakowski-DuBois, *Chem. Rev.* **1989**, *89*, 1.

[34] D. R. Kilanowski, H. Teeuwen, V. H. J. de Beer, B. C. Gates, G. C. A. Schuit, H. Kwart, *J. Cat.* **1978**, *55*, 129.

[35] H. Kwart, G. C. A. Schuit, B. C. Gates, *J. Cat.* **1980**, *61*, 128.

[36] Y. Nishibayashi, I. Wakiji, K. Hirata, M. Rakowski-DuBois, H. Hidai, *Inorg. Chem.* **2001**, *40*, 578.

[37] D. L. DuBois, W. K. Miller, M. Rakowski-DuBois, *J. Am. Chem. Soc.* **1981**, *103*, 3429.

[38] a) M. Rakowski-DuBois, M. C. VanDerveer, D. C. Dubois, R. C. Haltiwanger, W. K. Miller, *J. Am .Chem. Soc.* **1980**, *102*, 7456.
b) M. McKenna, L. L. Wright, D. J. Miller, L. Tanner, R. C. Haltiwanger, M. Rakowski-DuBois, J. Am. Chem. Soc. **1983**, *105*, 5329.

[39] L. L. Lopez, P. Bernatis, J. Birnbaum. R. C. Haltiwanger, M. Rakowski-DuBois, *Organometallics* **1992**, *11*, 2424.

[40] B. R. James, *"In Comprehesive Organometalic Chemistry"*; G. Wilkinson, F. G. A. Stone, E. W. Abel, Eds., Pergamon: New York, **1982**; Vol. 8, Chapter 51, p 285.

[41] R. D. Adams, F. A. Cotton, *"Catalysis By Di- And Polinuclear Metal Cluster Complexes"*; Wiley-vch, Chapter 4; M. Rakowski-DuBois, p 128.

[42] G. Schaftenaar, J. H. Noordik, *"Molden: a pre- and post-processing program for molecular and electronic structures"*, *J. Comput.-Aided Mol. Design* **2000**, *14*, 123.

Chapter 5

6

Concluding remarks

6.1   Bond energies of the aza and oxo ligands. Cubane compounds have been described from the interaction of the aza and oxo precubane ligands with a wide range of metallic fragments. A correlation between the bond energies and the nature of the incorporate metal fragment can be observed (see Table 6.1).

Table 6.1. *Dissociation energy (DE_{Dis}) for azaheterometallocubane complexes $[(L_nM)(m_3\text{-}NH)_3\{Ti_3(h^5\text{-}C_5H_5)_3(m_3\text{-}N)\}]$*

[ML$_n$]	M	(ΔEdis) kJ mol^{-1}
M-F	**In**	53
	Tl	63
M-Cl	**In**	63
	Tl	61
M-I	**In**	71
	Tl	65
MI$_2$	**Sn**	106
	Pb	105
M-F	**Li**	126
	Na	100
M-Cl	**Li**	149
	Na	112
M-I	**Li**	162
	Na	118
M-I$_2$	**Ca**	241
[Cl$_2$(PhN)Ti]	**Ti(d^0)**	203
[(CO)$_3$M]	**Cr(d^6)**	376
	Mo(d^6)	351
	W(d^6)	445
M(COD)$^+$	**Rh(d^8)**	378
	Ir(d^8)	445

Chapter 6

Bond energies respond to a strong electrostatic interaction, alkaline metals are good examples of this interaction. Also the stability of the compounds is enhanced by the electronic delocalization between the metal fragment and the ligand titanium metals. Metals show a clear increase in the reaction energy with the number of d electrons.

Qualitatively there are few differences between aza- and oxo- cubane compounds. Quantitatively, there is a considerable difference in the complexation energy between the aza and oxo ligands, mainly because of the approximate 70 kJ mol^{-1} reduction in the electrostatic attractive energy due to the presence of more basic oxygen free pairs.

6.2   Solvent effects. Solvent effects play a key role in the formation of metallocubanes from solid salts. The reduction in the energy necessary to extract salt molecules from the solid in a solvent is fundamental if cubanes are to be obtained.

6.3   Ligand behavior. The aza and oxo incomplete cubane structures behave as simple ligands in most cubanes (they stabilize only the cation and not its counteranion). So the reaction energies for the compounds tend to become more stable as the nucleophilicity of the metal substituents decreases (see Table 6.1). Exceptionally, the precubanes performs as a double action ligand and stabilize the metal cation and its counteranion. In this respect, thallium fluoride is particularly stabilised by the halogen atom directly interacting with the imido proton of the ligand, so the cation and anion of the salt are simultaneously stabilized by the ligand.

6.4   Characterization of alkaline dicubanes. In the formation of the alkaline heterometallodicubanes $[M(\boldsymbol{m}_3\text{-O})_3\{Ti_3(\boldsymbol{h}^5\text{-}C_5Me_5)_3(\boldsymbol{m}_3\text{-}C)\}]_2$ (M = Li, Na, K), a deprotonation of the apical carbon, with respect to the tripodal starting material $[\{Ti(\eta^5-C_5Me_5)(\mu-O)\}_3(\mu_3-CH)]$ has been reported. For the proposed reaction mechanism (see Scheme 6.1), the overall reaction is an exothermic process consistent with the formation and the stability of the clusters.

250
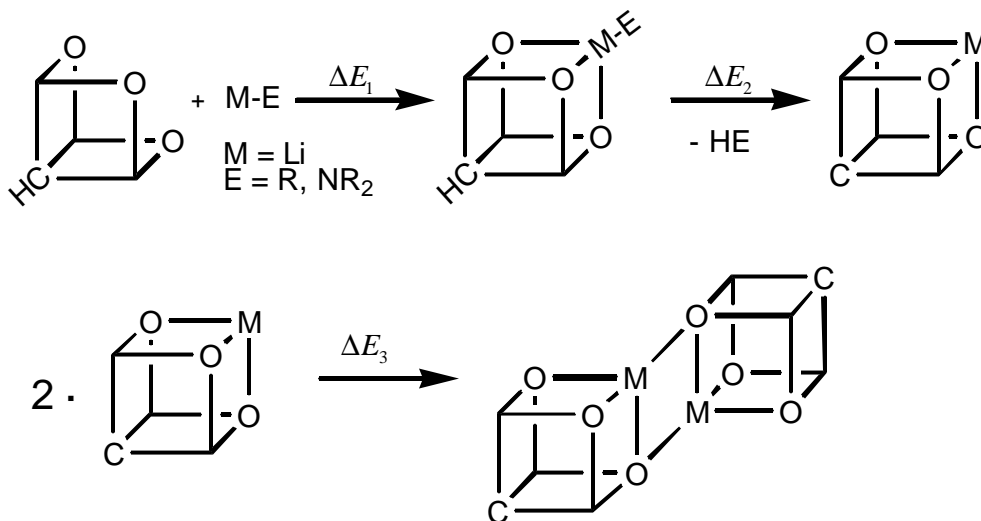
Scheme 6.1. Proposed mechanism for the formation of the heterometallic dicubane-type complexes $[M(\mathbf{m}_3\text{-}O)_3\{Ti_3(\mathbf{h}^5\text{-}C_5Me_5)_3(\mathbf{m}_3\text{-}C)\}]_2$

The observed differences in the ^{13}C NMR chemical shift for protonated and unprotonated compounds have been perfectly rationalized by the theoretical calculations. Frontier orbitals show that in unprotonated compounds the increase in energy of the occupied apical carbon p_z orbital and the stabilization of the corresponding virtual one are responsible for the increase in the chemical shifts.

6.5 $\mathbf{m}_3$-vinylidene and $\mathbf{m}_3$-acetylene isomers. DFT calculations unambiguously characterise the energy and the chemical shifts in the ^{13}C NMR spectra for the μ_3-vinylidene and the μ_3-acetylene oxometallocubane derivatives $[\{MN(SiMe_3)_2(thf)_x\}\{TiCp^*(\mu\text{-}O)\}_3(\mu_n\text{-}C_2H_2)]$ (M = Mg (x = 0), Ca (x = 1), Sr (x = 1). Slight energy differences for the magnesium metal explain the presence of both isomers in similar ratio. Instead, for Ca metal the inclusion of a thf molecule in the coordination sphere of the metal considerably favors the μ_3-vinylidene isomer, which is the only observed.

Theoretical ^{13}C NMR shielding tensors show that the metal atoms have considerable influence on the chemical shifts of the carbon atoms. The

Chapter 6

carbon atoms that closely bond to the titanium metals have the largest paramagnetic contributions.

6.6   DFT ^{13}C NMR shielding tensors. Theoretical simulation of ^{13}C NMR chemical shifts by means of DFT in studied titanium cubane compounds shows the validity of the method in computing shielding tensors for light atoms in organometallic compounds. Computed values predict almost perfectly experimental spectra, additionally the possibility of doing an analysis of the compounds in function of the structure of orbitals provides theoretical calculations an important value in order to rationalize the signals.

6.7   Substrate reduction in molybdenum sulphide catalysers. The reaction products caused by the interaction of molecular hydrogen with $[(CpMo)_2(S_2CH_2)(\mu\text{-}S)(\mu\text{-}SR)]^+$ cations change when there are modifications in the relative accessibility of the transition states for the RH or H_2 elimination. The presence of π orbitals in the substrate R favours the interaction with the proton and consequently its reduction.

6.8   DFT ^{183}W NMR shielding tensors. Theoretical simulation of the ^{183}W NMR spectra by DFT methods is quite novel, but it provides valuable information for the validation of the theoretical methods. In POTs, the appearance of unknown sources of error leads us to use similar compounds as reference molecules. Nevertheless, small chemical shift differences are difficult to reproduce and further investigations in this area are required.

List of publications

List of publications

1 "Rhodium/Iridium-Titanium Azaheterometallocubanes" *K. Freitag, J. Gracia, A. Martín, M. Mena, J. M. Poblet, J. P. Sarasa, C. Yelamos, Chem. Eur. J.* **2001**, *7*, 3644.

2 "Molecular Nitrides Containing Group 4 and 5 Metals: Single and Double Azatitanocubanes" *A. Abarca, M. V. Galakhov, J. Gracia, A. Martín, M. Mena, J. M. Poblet, J. P. Sarasa, C. Yelamos*, *Chem. Eur. J.* **2003**, *9*, 2337.

3 "Intercalation of Alkaline Metals into Layered Organotitanium Oxides" *J. Gracia, A. Martín, M. Mena, M. C. Morales-Varela, J. M. Poblet, C. Santamaría*, *Angew. Chem. Int. Ed.* **2003**, *42*, 927.

4 "Coordination of $[\{Ti(\eta^5\text{-}C_5Me_5)(\mu\text{-NH})\}_3(\mu_3\text{-N})]$ to Metal Halides: A Synthetic and Theoretical Study" *M. García-Castro, J. Gracia, A. Martín, M. Mena, J. P. Sarasa, J. M. Poblet, C. Yélamos,* submitted to Chem. Eur. J.

5 "DFT calculation of the ^{183}W and ^{17}O NMR chemical shifts in large polyoxotunhgstates" *J. Gracia, J. M. Poblet, L. Kazansky, in preparation*

6 "Titanium μ_3-Vinylidene Oxometallocubanes with Alkaline Earth Metals" *J. Gracia, A. Martín, M. Mena, M. C. Morales-Varela, J. M. Poblet, C. Santamaría, J. P. Sarasa*, *in preparation*

7 "DFT study of dinuclear molybdenum sulphide compounds" *J. Gracia, J. E. McGrady*, *in preparation*

Departament de Química Física i Inorgànica

Facultat de Química Tarragona